CRYSTALLOGRAPHIC AND MAGNETIC STUDIES OF THE ELECTRON DISTRIBUTION IN SOME TRANSITION METAL COMPLEXES

A thesis submitted for the degree of
Doctor of Philosophy of the University of London by

MALCOLM GERLOCH B.Sc. A.R.C.S.

Department of Chemistry,
Imperial College,
London S.W.7.

April 1964

ABSTRACT

A complete three-dimensional X-ray analysis of $(CF_3)_4C_5O.C_5H_5.Co$, making extensive use of Patterson and Fourier techniques and of least-squares refinement has converged to a final discrepancy index of 0.088. A system of σ - and π- bonding from the cyclopentadienone ligand to the cobalt atom is evident from the molecular configuration and is compared with the stereochemistries and bonding in several analogous organometallic complexes, showing the generality of this novel bonding scheme.

The structure of $(C_5H_5)_2MoH_2$ has also been solved by X-ray diffraction techniques, refining to a final R factor of 0.092 and confirming the stereochemistry proposed from n.m.r. spectroscopic evidence. The cyclopentadienyl rings lack perfect 5-fold symmetry and this analysis, with the above and two other recently reported structures, does suggest the distortions are significant. An explanation in terms of simple molecular orbital theory is proposed.

The temperature dependences of the paramagnetic susceptibilities of single crystals of three tetrahedral cobaltous complexes have been measured over the range 80-300°K. The results are correlated with the tetrahedron distortions known from the crystallographic literature and, in the case of Cs_3CoCl_5, the magnetic measurements prompted a new structural refinement, demonstrating how paramagnetic anisotropy measurements can be more sensitive than diffraction work. Quantitative calculations allowed estimates of electron

delocalization parameters and of anisotropic magnetic exchange integrals.

The anomalous magnetic behaviour of $K_3Fe(CN)_6$ has long been a problem and a qualitative explanation is now proposed. Complete two-dimensional X-ray analyses at $300^{\circ}K$ and $95^{\circ}K$ show that the ferricyanide octahedra are axially distorted in the same sense at both these temperatures. The magnetic behaviour and a specific heat transition at $131^{\circ}K$ may be explained, however, by a highly anisotropic superexchange mechanism.

Brief introductions to the theoretical and practical principles of the techniques of X-ray diffraction and of paramagnetic anisotropy, which have been used throughout the work, are also included.

* * *

ACKNOWLEDGEMENTS

I should like to express my warmest gratitude to Professor Ronald Mason for making the past three years' work so enjoyable. His help and direction, both as supervisor and friend, make me proud to have been his student.

I am indebted to Dr. Peter Pauling and Mr. Glen Robertson for many helpful discussions at University College and to Mr. John Avery, who has explained a wealth of theoretical matter to me with great patience. Dr. Brian Figgis has been responsible for most of the quantum mechanical theory in sections 3, 4 and 5 of Chapter 5 and has made many helpful suggestions besides.

I must record, too, the pleasure and stimulus of working with my fellow students - Hannah, Mel, Mike, John and Neil - who have also been so generous at the bar.

My thanks are due also to Miss Jenny Desmond for her hard work in typing this thesis so well.

I am grateful to the Department of Scientific and Industrial Research for their financial support.

Finally, I thank my wife, Annette, both for help in checking many tedious tables and figures and for her love and humour these last two years.

Computer Programs

I should like to acknowledge the extensive use I have made of various crystallographic computer programs written by Mrs. J. Dollimore, Drs. R.A. Sparks and J.S. Rollett and Messrs. O.S. Mills and N.A. Bailey.

PREFACE

The electron distributions in several transition metal ions, which will be described in this thesis, have been studied experimentally by the techniques of crystallography and magnetochemistry. The thesis is written in two parts, corresponding to work involving diffraction only and to work involving both of these techniques. As X-ray diffraction is common to all the investigations, studies using this technique only are discussed first, while the magneto-chemical work is left till Part II. Each Part begins with a brief introduction to the theoretical and practical principles of these physical methods.

CONTENTS

PREFACE 6

PART I - THE CRYSTALLOGRAPHY OF AND BONDING IN SOME ORGANOMETALLIC COMPOUNDS

CHAPTER 1 A survey of X-ray crystallographic methods of molecular analysis 9

CHAPTER 2 The crystal and molecular structure of π-cyclopentadienyltetrakis(trifluoromethyl)cyclopentadienonecobalt .. 27

CHAPTER 3 The crystallography of dihydridodi-π-cyclopentadienylmolybdenum .. 84

PART II - THE PARAMAGNETIC ANISOTROPIES OF SOME COBALTOUS AND FERRIC COMPLEXES

CHAPTER 4 An introduction to the principles of crystal paramagnetic anisotropies 111

CHAPTER 5 The paramagnetic anisotropies of tetrahedral cobaltous complexes 144

CHAPTER 6 The magnetism and crystallographyof potassium ferricyanide 181

CONCLUSION 221

REFERENCES 223

* * *

P A R T I

The Crystallography of and Bonding in Some Organometallic Compounds

CHAPTER 1

A Survey of X-ray Crystallographic Methods of Molecular Analysis

The general methods of X-ray crystal structure analysis are well known, so that, in this chapter, the techniques and background are only very briefly reviewed. However, detailed consideration is given to refinement techniques and the analysis of errors in molecular parameters as a good deal of the later discussions are concerned with small differences in bond lengths and their interpretation in the light of various theories of chemical bonding.

1.1 Definitions and some techniques for structure solution

Crystals are composed of groups of atoms or ions repeated in a regular way in three dimensions. For certain purposes each group of atoms can be represented by a point, the three-dimensional array of points so formed constituting the space lattice of the crystal, which can be conventionally described by the repeat units a,b,c parrallel to the axes x,y,z and with interaxial angles α,β,γ. The parallelopiped repeat unit is called the unit cell. This may contain one group of atoms or many arranged symmetrically with respect to one another, their spatial relationships being governed by the symmetry elements present. Certain symmetry elements cannot repeat indefinitely in two or three dimensions and are therefore not found in crystal structures, a restriction which limits the total possible number of symmetry combinations to 230. These comprise the space groups, detailed descriptions of some of which appear later. In the extended crystal array, many sets of regularly spaced planes may be

defined by the way they pass through lattice points or, equivalently, by the way they intersect the unit cell edges. Thus, if a set of planes divides a into h equal lengths, b into k and c into l, the set is defined by the Miller indices h,k,l and has a characteristic 'd-spacing' as the repeat along its normal. Figure 1.1 illustrates this for the planes 2,3,0.

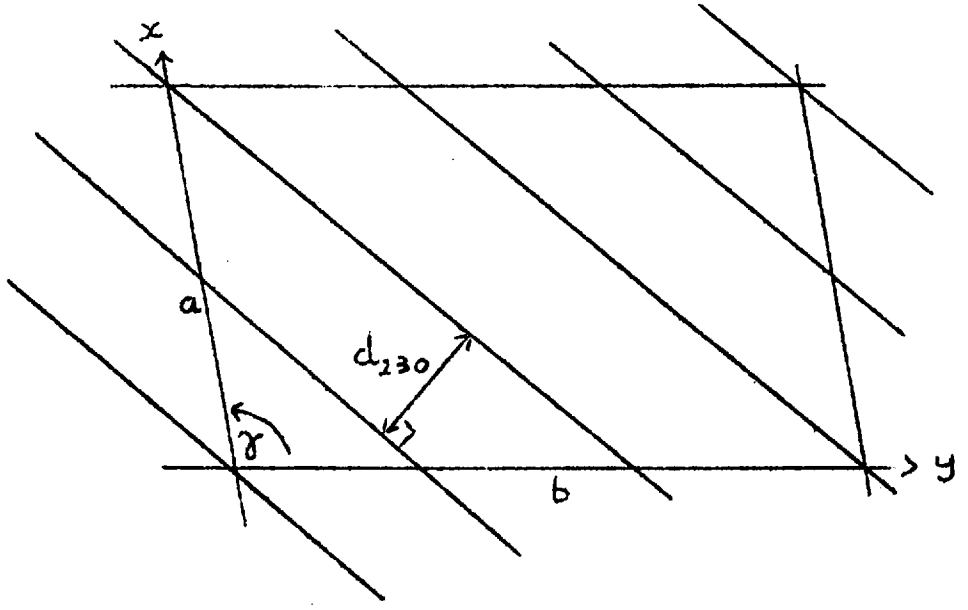


Figure 1.1

Miller indices and d-spacing

When a crystal is irradiated with X-rays, the electrons interact with the radiation acting as secondary 'point' sources. Representing the electron content of the unit cell by a single point, for the moment, the crystal may be regarded as a three-dimensional diffraction grating having repeat translations equal to all possible d-spacings of the stacks of planes defined above. Each repeat will give rise to diffraction maxima characteristic of each stack of

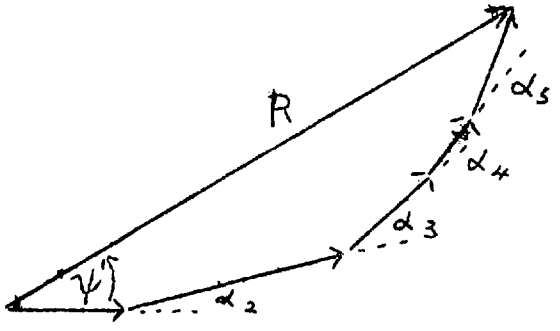
planes; thus each diffracted beam may be labelled by the indices h,k,l. The geometry of diffraction is such that the hkl planes appear to have acted as reflectors of the incident beam and so the angle of diffraction, θ (defined with respect to the normal to the planes) of the hkl diffracted ray equals the angle of incidence. The relationship $n\lambda = 2d \sin\theta$ (n is the order of diffraction and λ the incident wavelength) was first proved by W.L. Bragg and the angle θ is known as the Bragg angle and a diffraction obeying this geometry as a Bragg reflexion.

Of course, the repeat unit cell usually consists of several atoms or ions (N) and then the crystal may be seen as N interpenetrating lattices, identical in size but not in 'weight'. The weight of the lattice is its diffracting or scattering power, related to the atomic number of the Nth atom. The relationship is not simply one of proportionality as the electron in an atom occupy a finite volume and the phase differences between rays scattered from different points in this volume have to be taken into account. At increasing Bragg angles the destructive interference between rays diffracted from different points in the atom increases, resulting in a decreasing scattering factor with θ. The relationship between scattering factor, f, and θ is complex and varies a little from atom to atom: 'scattering curves' of f versus $\sin\theta/\lambda$ have been calculated for all atoms often in several valency states.

The scattering power of an atom is also related to the temperature, as all atoms vibrate to some extent, dependent upon temperature. The vibrational frequencies ($\sim 10^{13}\,\mathrm{sec}^{-1}$) are much less than the radiation frequencies

($\sim 10^{13}$ sec^{-1}) and the atoms therefore appear stationary but displaced by a greater or lesser extent from their true (that is, average) lattice positions, the total effect being to 'smear out' the electron density, somewhat. If isotropic, this effect can be allowed for by replacing f by $f \exp(-B \sin\theta/\lambda)$: the constant B, called the isotropic temperature factor, is related to the mean square displacement $\bar{u}^2$ of the atom about its mean position by $B = 8\pi^2\bar{u}^2$. Anisotropic temperature effects can be allowed for by replacing f by $f \exp\left\{-\left(b_{11}h^2 + b_{22}k^2 + b_{33}l^2 + b_{23}kl + b_{13}hl + b_{12}hk\right)\right\}$ or, as is the practice in this thesis, by an equivalent function with a binary base. This formalism assumes that the atomic vibration can be described as an elipsoid but very often this is again inadequate.

Returning to the N interpenetrating lattices with scattering powers which depend upon atom type, Bragg angle and temperature or vibration factors, let us now consider a particular diffracted beam or 'reflexion', hkl. This ray has two properties - its amplitude and its phase. The amplitude from the Nth lattice depends upon the factors enumerated above, while the phase depends upon the spatial relationships between the lattices, that is, upon the positions of the atoms in the unit cell. The resultant hkl reflexion from the whole crystal is the vectorial sum of each contribution from all N lattices. This is conveniently represented on an Argand diagram:-



α_2, α_3, α_4, α_5 represent the phases of the 2nd, 3rd, 4th and 5th lattices with respect to the 1st. The amplitudes of the five components are represented by the lengths of the shorter arrows. R is the resultant amplitude, with phase ψ.

If the components of a sufficient number of reflexions were measured it would be possible to evaluate directly all the parameters of a crystal structure - atomic co-ordinates and temperature factors. The fundamental difficulty in crystal structure determinations has always been that only the intensities (amplitude^2) of the rays are measurable: the loss of half the data - the phases ψ - constitutes the celebrated '<u>phase problem</u>' of crystallography.

The scattered rays also depend upon certain other geometric effects like polarization, absorption and so on, but that factor which is a function solely of the crystal structure is known as the <u>structure factor</u>, F. This was represented above by R and ψ: more particularly it can be shown to be:

$$F_{hkl} = \sum_{n=1}^{N} f_n \exp 2\pi i(hx_n + ky_n + lz_n)$$

(where f_n has already been corrected for vibrational effects)

One of the basic techniques in solving a crystal structure is that of trial and error, which consists of postulating an atomic arrangement and of

comparing observed structure factors with those which can be quite quickly calculated according to the above expression. A measure of the agreement is often expressed as the reliability factor or index, R:

$$R = \frac{\sum \left| |F_o| - |F_c| \right|}{\sum |F_o|}$$

If the postulated structure is approximately correct, R is low (say 0.30) and the parameters may be refined automatically by a least squares method. The initial structure may be arrived at by calling on several lines of evidence, there being many sophisticated techniques, nowadays, of quickly achieving a 'good' model. At this stage, the most generally useful way of correcting or improving a partially correct initial guess, however, has been the Fourier method.

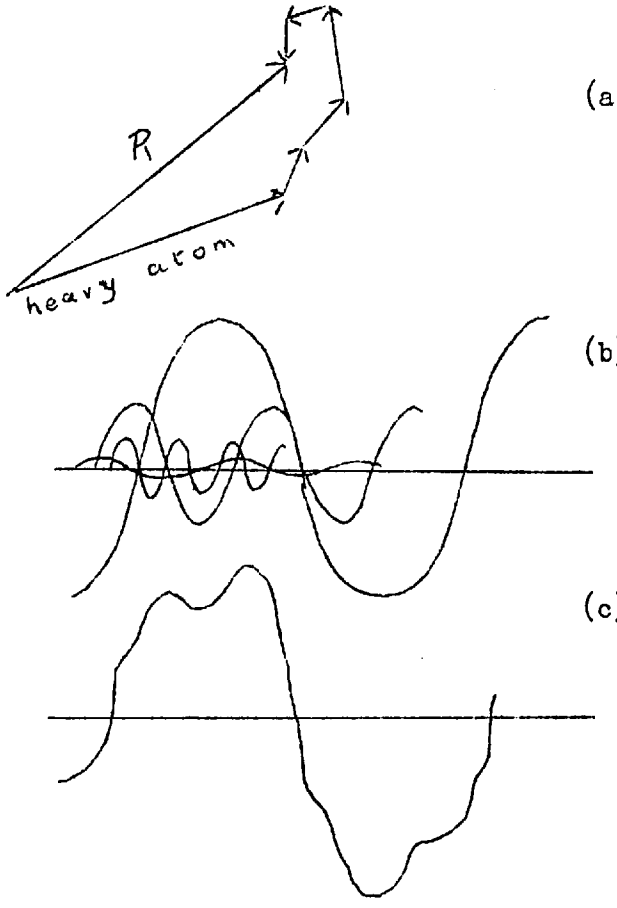
Since a crystal is periodic in three dimensions, it can be represented by a three-dimensional Fourier series and it can be shown that the electron density distribution in the unit cell can be expressed as a Fourier series whose coefficients are the structure factors:

$$\rho_{xyz} = \frac{1}{V} \sum_h \sum_k \sum_{l=-\infty} F_{hkl} \exp\left\{-2\pi i(hx + ky + lz)\right\}$$

This can be computed either as the complete three-dimensional function or as a set of two-dimensional 'projections' in which one index (h,k or l) remain constant (usually = 0). The two- or three-dimensional electron density syntheses can be plotted like contour maps, revealing peaks of height proportional to the atomic number of the atoms present. If the original guess was largely correct, most of the phases of the structure factors will have

been correctly calculated and the general outline of the molecules will be apparent in the electron density maps, even though some Fourier coefficients may have been quite wrong. Thus, the Fourier technique only requires the initial guess to phase correctly (or nearly so) a reasonable proportion of the structure factors for the whole molecule to be revealed: what constitutes a 'reasonable' proportion may be regarded as the 'sales resistance' of each individual structural problem. If the structure contains one or more 'heavy' atoms, that is, atoms with large atomic numbers and therefore large scattering power, their correct location by other means can be sufficient to phase the Fourier synthesis and reveal the lighter atoms present. In short, the 'heavy' Nth atom dominates the resultant phases for the whole crystal. Figure 1.2 serves to illustrate this. This powerful technique is known as the 'heavy atom method' and, while it is obviously of limited applicability in structure analysis as a whole, it is clearly the standard method for the analyses described in this thesis where, after the initial determination of the metal atom positions, the Fourier maps revealed several lighter atoms in the molecules and, by iterations of phasing by what was previously established, finally the complete molecules. The processes are described in detail in later chapters.

Figure 1.2



(a) shows in the Argand diagram, how R is dominated by the heavy atom

(b) shows the component Fourier terms

(c) shows the resultant Fourier wave, which was fairly well described by the heavy atom above

The heavy atom method, then, depends upon the initial determination of the heavy atom positions. This is done by use of the Patterson function, which is a Fourier series whose coefficients are the structure factors squared; as such, it may be computed directly from the observable quantities.

$$P_{uvw} = \frac{1}{V} \sum_{h} \sum_{k} \sum_{l=-\infty}^{\infty} |F_{hkl}|^2 \exp 2\pi i(hu + kv + lw)$$

where u,v,w are equivalent co-ordinates in Patterson space. A Patterson map contains a large peak at its origin and smaller peaks elsewhere. For every interatomic vector in the unit cell there exists a similar vector in the Patterson cell but displaced parallel to the cell edges so that one end lies

at the origin - at the other end is a peak. The volume of this peak is proportional to $Z_1 \times Z_2$, where Z_1 and Z_2 are the atomic numbers of the atoms at the two ends of the real-space vector concerned. There are $(N^2 - N + 1)$ peaks in the complete Patterson volume which is equal to the volume containing N atoms in real space: consequently, in the absence of an atom with a large atomic number, the Patterson is usually rather featureless and, until recently, almost if not completely impossible to interpret (see Beurger II). If heavy atoms are present, however, Patterson peaks can often be distinguished from the high background and, from the positions and number of these peaks, the positions of the corresponding atoms in the real-space unit cell can be found. This technique was successfully used throughout the analyses described in this thesis.

Having applied Patterson and the heavy-atom methods to solve the structures, accurate positional and thermal parameters can be arrived at by relatively routine refinement procedures. The method used in the work described in this thesis is now described in some detail.

* * *

1.2 Least squares refinement

The method of least squares involves finding the values of a set of variables which best satisfy a set of experimental observations. If several equally reliable measurements of a physical quantity yield the numbers $X_1, X_2, \ldots X_n$ the corresponding errors are defined by

$$x_1 = X_1 - X, \quad x_2 = X_2 - X \quad \ldots\ldots\ldots \quad x_n = X_n - X$$

where X is the true value of the quantity. In general the true value is unknown and so the residuals are defined,

$$d_1 = X_1 - \bar{X}, \quad d_2 = X_2 - \bar{X}, \quad \ldots\ldots\ldots \quad d_n = X_n - \bar{X}$$

where $\bar{X}$ is the most probable value of the quantity. It is assumed that the errors and residuals encountered are random and follow the 'normal' or 'Gaussian' distribution,

$$y = \frac{1}{\sigma\sqrt{2\pi}} \cdot e^{-x^2/2\sigma^2}$$

or, writing $h^2 = 1/2\sigma^2$,

$$y = \frac{h}{\sqrt{\pi}} \cdot e^{-h^2x^2}$$

The probability that the error of a single measurement will lie between $\pm a$ is

$$\frac{h}{\sqrt{\pi}}\int_{-a}^{a} e^{-h^2x^2}\,dx = \frac{2h}{\sqrt{\pi}}\int_{0}^{a} e^{-h^2x^2}\,dx \qquad (\equiv \text{ error function})$$

Suppose n measurements have been made, the i^{th} one having error x_i. The probability that x_i lies between x_i and $x_i + dx_i$ is

$$P_i = \frac{h}{\sqrt{\pi}} \cdot e^{-h^2x_i^2}\,dx_i$$

The probability that the n errors $x_1, x_2, \ldots\ldots x_n$ occur, is $P = \prod_{i=1}^{n} P_i$, as each measurement is independent. Therefore,

$$P = \prod_{i=1}^{n} P_i = \left(\frac{h}{\sqrt{\pi}}\right)^n \cdot e^{-h^2(x_1^2 + x_2^2 + \ldots\ldots x_n^2)}dx_1dx_2\ldots\ldots dx_n$$

As the differentials dx_i are arbitrary and as h is fixed, the probability, P is a maximum when the exponent of e is a minimum; that is

$$x_1^2 + x_2^2 + \ldots\ldots + x_n^2 = \text{a minimum}$$

is the criterion for the most probable value obtainable from n equally reliable measurements of a quantity. This result is known as the 'principle of least squares'. It can easily be shown that the most probable value of a set of measurements, $\bar{X}$ is the arithmetic mean $\sum_n X_i/n$. It can also be shown that the sum of the squares of the residuals is slightly less than the sum of the squares of the errors.

The method of least squares procedes as follows. Let q be a linear function of a set of variables x, y, z . . . . . .

$$q = ax + by + cz + \ldots\ldots \qquad \ldots\ldots(1)$$

and let there be m observations of q, each having an error E_i where $m > n$, the number of variables. Then,

$$q_i + E_i = a_i x + b_i y + c_i z + \ldots\ldots$$

giving a set of m equations:

$$\begin{aligned}
E_1 &= a_1 x + b_1 y + c_1 z + \ldots\ldots - q_1 \\
E_2 &= a_2 x + b_2 y + c_2 z + \ldots\ldots - q_2 \\
E_3 &= a_3 x + b_3 y + c_3 z + \ldots\ldots - q_3 \\
&\vdots \qquad\quad \vdots \qquad \vdots \qquad \vdots \qquad\quad \vdots \\
E_m &= a_m x + b_m y + c_m z + \ldots\ldots - q_m
\end{aligned}$$

According to the principle of least squares,

$$E_1^2 + E_2^2 + E_3^2 + \ldots\ldots + E_m^2 = \sum_i E_i^2 \quad \text{must be made a minimum.}$$

$\sum_i E_i^2 = \sum_i (a_i x + b_i y + c_i z + \ldots\ldots - q_i)^2$ is a minimum when its partial derivatives with respect to x, y, z, ... vanish; that is, when

$$\frac{\partial \sum_i E_i^2}{\partial x} = 2\sum_i (a_i x + b_i y + c_i z + \ldots\ldots - q_i) a_i = 0$$

$$\frac{\partial \sum_i E_i^2}{\partial y} = 2\sum_i (a_i x + b_i y + c_i z + \ldots\ldots - q_i) b_i = 0$$

$$\frac{\partial \sum_i E_i^2}{\partial z} = 2\sum_i (a_i x + b_i y + c_i z + \ldots\ldots - q_i) c_i = 0$$

$$\vdots \qquad\qquad \vdots \qquad\qquad \vdots$$

Rewriting the middle and R.H.S. gives:

$$\begin{aligned}
(\textstyle\sum_i a_i^2)x + (\sum_i a_i b_i)y + (\sum_i a_i c_i)z + \ldots\ldots &= \sum_i a_i q_i \\
(\textstyle\sum_i b_i a_i)x + (\sum_i b_i^2)y + (\sum_i b_i c_i)z + \ldots\ldots &= \sum_i b_i q_i \\
(\textstyle\sum_i c_i a_i)x + (\sum_i c_i b_i)y + (\sum_i c_i^2) + \ldots\ldots &= \sum_i c_i q_i \\
\vdots \qquad\qquad \vdots \qquad\qquad \vdots \qquad\qquad & \vdots
\end{aligned} \qquad \ldots\ldots(2)$$

These are the <u>normal equations</u> which when solved give the most probable values for the parameters x, y, z, ... When the observations q_i are of unequal reliability, a weighting factor ω_i can be applied and this yields the normal equations (2) multiplied by ω_i

The first step for applying the method of least squares to crystallographic refinement is to recast the structure factor, F_c,

$$F_c = \sum_r f_o e^{-(b_{11_r} h^2 + b_{22_r} k^2 + b_{33_r} l^2 + b_{12_r} hk + b_{23_r} kl + b_{31_r} lh)} \cdot e^{2\pi i (hx_r + ky_r + lz_r)} \qquad \ldots\ldots(3)$$

into a linear form.

This equation for the calculated structure factor, F_c may be made linear by expansion of the exponentials as a Taylor series and then using the first two terms. Defining ϵ_{x_r}, ϵ_{y_r}, ϵ_{z_r}; $\epsilon_{b_{11_r}}$ etc. as the corrections (or 'shifts') to be applied to the atomic parameters to give the most probable locations $x_r + \epsilon_{x_r}$ etc; $b_{11_r} + \epsilon_{b_{11_r}}$ etc, (2) reduces to

$$\Delta F_i = (F_o - F_c)_i = \sum_r \left(\epsilon_{x_r}\frac{\partial F_{c_i}}{\partial x_r} + \epsilon_{y_r}\frac{\partial F_{c_i}}{\partial y_r} + \epsilon_{z_r}\frac{\partial F_{c_i}}{\partial z_r} + \epsilon_{b_{11_r}}\frac{\partial F_{c_i}}{\partial b_{11_r}} + \ldots\right) \quad \ldots\ldots(4)$$

for the r^{th} atoms and i^{th} structure factor. Equation (4) is now in the form of (1) andthe least squares procedure may be carried out as before. The normal equations corresponding to (2) now become (omitting weights, ω):

$$\left[\sum_i \left(\frac{\partial F_{c_i}}{\partial x_1}\right)^2\right]\epsilon_{x_1} + \left[\sum_i \frac{\partial F_{c_i}}{\partial x_1}\cdot\frac{\partial F_{c_i}}{\partial y_1}\right]\epsilon_{y_1} + \left[\sum_i \frac{\partial F_{c_i}}{\partial x_1}\cdot\frac{\partial F_{c_i}}{\partial z_1}\right]\epsilon_{z_1} + \left[\sum_i \frac{\partial F_{c_i}}{\partial x_1}\cdot\frac{\partial F_{c_i}}{\partial b_{11_1}}\right]\epsilon_{b_{11_1}} + \ldots.$$

$$\ldots \text{ eto + (n atoms)} = \sum_i \frac{\partial F_{c_i}}{\partial x_1}\cdot\Delta F_i$$

$$\left[\sum_i \frac{\partial F_{c_i}}{\partial y_1}\cdot\frac{\partial F_{c_i}}{\partial x_1}\right]\epsilon_{x_1} + \quad \ldots \quad = \sum_i \frac{\partial F_{c_i}}{\partial y_1}\cdot\Delta F_i$$

$$\left[\sum_i \frac{\partial F_{c_i}}{\partial z_1}\cdot\frac{\partial F_{c_i}}{\partial x_1}\right]\epsilon_{x_1} + \quad \ldots \quad = \sum_i \frac{\partial F_{c_i}}{\partial z_1}\cdot\Delta F_i$$

$$\vdots \qquad\qquad \vdots \qquad\qquad \vdots$$

$$\ldots\ldots(5)$$

The coefficients on the left hand side may be grouped into three types:

(i) those involving positional co-ordinates, x_r etc., of one atom only,

(ii) those involving temperature coefficients, b_{11_r} etc., of one atom only, &

(iii) those involving either or both positional and temperature parameters of one or two atoms, not already described by (i) and (ii).

The normal equations (5) may be written

$$\sum_{s=1}^{K} b_{rs}\, u_s = c_r \qquad \text{.....(5a)}$$

where $b_{rs} = \sum_i \left(\frac{\partial F_{c_i}}{\partial U_r} \cdot \frac{\partial F_{c_i}}{\partial U_s}\right)$

and $c_r = \sum_i \left(\frac{\partial F_{c_i}}{\partial U_r} \cdot \Delta F_i\right)$

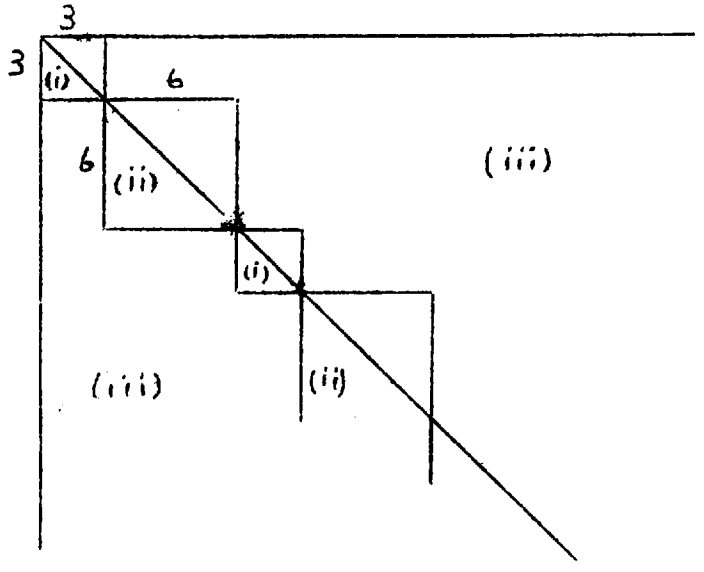
} U ≡ positional or thermal parameter

and K = number of parameters, and u is the shift

(u_r) is a column vector (written now as a row, for convenience) and may arranged by taking first the positional and then the thermal parameters for atom 1, then for atom 2 and so on:

$$(u_r) \equiv \left\{\epsilon_{x_1}\, \epsilon_{x_2}\, \epsilon_{x_3}\, \epsilon_{b_{11_1}}\, \epsilon_{b_{22_1}}\, \epsilon_{b_{33_1}}\, \epsilon_{b_{12_1}}\, \epsilon_{b_{23_1}}\, \epsilon_{b_{31_1}}, \epsilon_{x_2} \ldots\ldots \text{etc}\right\}$$

When this is done the matrix (b_{rs}) takes on the form of alternating 3 x 3 and 6 x 6 blocks about the main diagonal involving cross-terms of types (i) and (ii) respectively and with all other cross-terms (type (iii)) outside these blocks.



The matrix elements b_{rs} are computed directly from the structure factors and (u_r) obtained by inversion

$$u_r = \sum_{s=1}^{K} b^{rs} c_s$$

where b^{rs} is an element of the matrix inverse to (b_{rs}). The shifts, ϵ obtained are then used to provide a better trial set of parameters for the next least squares 'cycle'. It is convenient to derive the form of the differentials for the particular space group concerned, thereby taking advantage of symmetry properties, particularly a centre, if present.

The computation of the full matrix (b_{rs}) is very time-consuming, even for the 'Mercury' computer: for example, the full matrix cycle for the structure described in Chapter 2 would take about $6\frac{1}{2}$ hours. Sparkes (1960) points out that about $\frac{3}{4}$ of the structure factor-least squares (SFLS) cycle is taken to form the full normal equations. The 'Atlas' computer is 80 or more times faster than 'Mercury' and has a much larger store; it is, therefore, more

suitable for full-matrix calculations. 'Mercury' is not only too slow, but also too small, in general, to store a full matrix and so certain (faster) approximations to (b_{rs}) must be used. Sparkes (loc. sit.) has discussed and and compared several approximations, one of which, being used by Rollett, is described here.

Rollett neglects all cross-terms of type (iii); that is he only computes the block diagonal matrix shown above. In addition he takes account of a scale factor, k, such that $F_o = \frac{1}{k} F_c$. If k were included in the matrix like all other variables, all cross-terms between k and these 9 variables would arise. As a simplification, he considers an 'average' temperature factor, B (isotropic),

$$F_o = \frac{1}{k} \cdot F_c' e^{-B \sin^2\theta/\lambda}$$

and forms 2 x 2 matrices involving cross-terms, $\left(\frac{\partial F_{c_i}}{\partial k}\right)^2$, $\left(\frac{\partial F_{c_i}}{\partial B}\right)^2$, $\left(\frac{\partial F_{c_i}}{\partial k} \cdot \frac{\partial F_{c_i}}{\partial B}\right)$ and $\left(\frac{\partial F_{c_i}}{\partial B} \cdot \frac{\partial F_{c_i}}{\partial k}\right)$ from which is obtained ϵ_k, the shift to be applied to the scalefactor for the next SFLS cycle.

Approximately 3.2 cycles of the 'block diagonal' SFLS can be performed in the time taken for 1 cycle 'full matrix'. This speed advantage (and, of course, smaller storage space required) is partly offset by two disadvantages of the 'block diagonal' method:

(1) it is difficult or impossible to refine atoms which overlap in projection, if only one zone of data is being treated,

(2) the shifts, ϵ produced are usually too large due to neglect of the

cross-terms, (iii) and unless they are reduced by hand (by 'experience') in between refinement cycles, the convergence will be slow and, especially towards the end, oscillatory.

* * *

1.3 Errors and their statistical significance

If the errors in F_o are random and normally distributed, it can be shown that the standard deviation, σ of parameter u_r is given by

$$\sigma^2(u_r) = \frac{b^{rr} \sum_i w(\Delta F_i)^2}{n - K}$$

where n and K are the numbers of observations and parameters, respectively. If the data are subject to any systematic errors, the values of the variances b^{rr} will suffer in generally, unpredictable ways. Further, the neglect of cross-terms (iii), as in Rollett's programme will lead to a systematic underestimate of the variances to an extent dependent upon the magnitude of the omitted matrix elements. (Rollett has estimated that a 100% underestimate is possible in very unfavourable circumstances). Some idea of the magnitude of this error in any particular analysis, may be gained from the speed of the refinement (including the degree of 'half-shifting' inbetween cycles) as the faster the convergence, the closer the approximation of block-diagonal to full-matrix, the smaller the neglected cross-terms and the less the underestimate of the variances.

Having obtained standard deviations of all the parameters, and then having calculated the standard deviations of certain combinations of parameters

(eg) bond lengths and angles, the final step is to decide what significance may be attached to the results. With errors following a normal distribution, the probability, P that an observation may lie within the limits $\pm 1\sigma$ of the mean value is 68%; within the limits $\pm 2\sigma$, P = 94%; and within $\pm 3\sigma$, P = 99.8% Associated with these results, Cruickshank (see Lipson and Cochran, p.309) has suggested the following levels of significance:-

If two bonds A and B, with standard deviations $\sigma(A)$ and $\sigma(B)$, differ by an amount $\delta 1$ and if P is the probability that A could be a least $\delta 1$ greater or less than B by chance, and $\sigma_1^2 = \sigma^2(A) + \sigma^2(B)$, then,

(i) if $P > 5\%$, $\delta 1 < 1.645\sigma_1$, the difference is not significant,

(ii) if $5\% > P > 1\%$, $2.327\sigma > \delta 1 > 1.645\sigma$, the difference is possibly significant,

(iii) if $1\% > P > 0.1\%$, $3.090\sigma > \delta 1 > 2.327\sigma$, the difference is significant.

All these results assume, of course, that the standard deviations in question have allowed for systematic errors from any source.

* * *

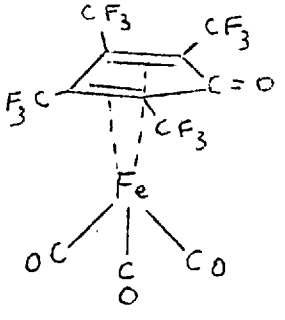
CHAPTER 2

The Crystal and Molecular Structure of π-Cyclopentadienyltetrakis(trifluoromethyl)cyclopentadienone cobalt

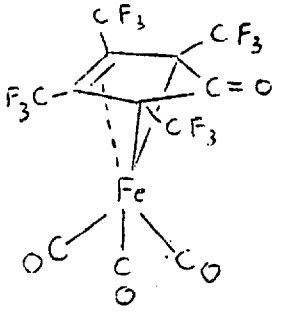
2.1 Introduction

Organometallic compounds involving donor bonds from olefins to the metal have been known for a long time, the first prepared, though not at the time structurally understood, being Zeise's salt, $PtCl_2.C_2H_4$. Recently, work has been carried out on the preparation of complexes of fluoro-olefins which were expected to be more stable than their hydrocarbon analogues; in particular Boston, Sharp and Wilkinson (1962) have investigated the reactions of hexafluorobut-2-yne with complexes of iron, cobalt and nickel.

The interaction of hexafluorobut-2-yne and pentacarbonyliron yields, at 100-200°C and autogenous pressure, a product which gives orange-yellow crystals, $C_9F_{12}OFe(CO)_3$. The chemical and spectroscopic properties of the compound are consistent with its formulation as (A) or (B):



(A)



(B)

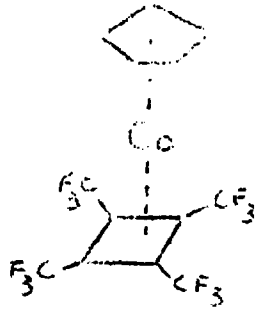
The infra-red spectrum shows strong CF_3 group absorptions in the region 1000 - 1300 cm^{-1} and there are strong metal-carbonyl stretching frequencies at 2133, 2083 and 2040 cm^{-1}. There are also strong bands at 1742 and 1729 cm^{-1} one of which disappears on protonation in concentrated sulphuric acid. It is impossible to decide which band is the ketonic stretch and which the olefinic, C=C, however, as the remaining band is solvent-dependent. The high resolution ^{19}F resonance spectrum show two bands of equal intensity at 6.8 and 10.7 p.p.m. on the low field side of benzotrifluoride reference line, indicating the prescence of two different types of $-CF_3$ groups.

Neither this complex nor its phenyl analogue tricarbonyltetraphenyl-cyclopentadienoneiron give any of the usual reactions of ketones, probably owing to the deactivating effects of the substituent groups on the cyclopentadienone ring. The carbonyl groups can be replaced, however, for example, by triphenylphosphine to give $C_9F_{12}OFe(CO)_2PPh_3$.

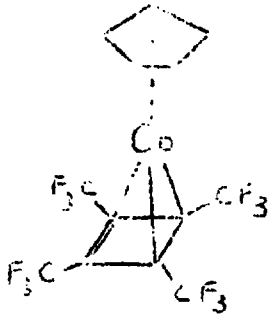
Boston et al. (loc. cit.) have also reported that the interaction of hexafluorobut-2-yne and π-cyclopentadienyldicarbonylcobalt gives high yields of a red crystalline compound π-$C_5H_5.CoC_8F_{12}$. The compound, which sublimes in vacuum above 100°, is moderately soluble in cold non-polar solvents, and in both the solid state and in solution is stable to air and extremely resistant to chemical attack. The π-C_5H_5 ring appears to be strongly deactivated by the fluorocarbon ligand, and the compound does not undergo Friedel-Crafts acylation, metallation with butyl-lithium, nitration with fuming nitric and concentrated sulphuric acid at 50°, sulphonation

with boiling concentrated sulphuric acid or chlorosulphuric acid, or halogenation with bromine in a sealed tube at 110°, and it can be recovered unchanged from the mixtures. Boiling the fuming nitric-concentrated sulphuric acid solution causes decomposition, and a white insoluble fluorine containing polymer is obtained which is incompletely attacked by either sodium or oxygen at 850°C.

The infra-red spectrum of the compound shows bands characteristic for the π-C_5H_5 compounds and for $-CF_3$ groups. There is also a strong band at 1697 cm^{-1} which appeared to be the C=C stretching frequency of a co-ordinated double bond. The p.m.r. spectrum shows only one very sharp band (τ = 4.4) for the π-C_5H_5 group. The ^{19}F resonance spectrum shows two bands of equal intensity on the low field side of benzotrifluoride at 7.1 and 11.3 p.p.m., each band having complicated fine structure. Two structures were considered possible:



(C)



(D)

The structure (C) is similar to that found for $(C_6H_5)_4C_4.Fe(CO)_3$ and $\left[(CH_3)_4C_4NiCl_2\right]_2$ and has been proposed for π-$C_5H_5CoC_4(C_6H_5)_4$.

This last compound was prepared for comparison with the fluorine complex and it was noted that although the reaction of perfluorobut-2-yne with $(\pi\text{-}C_5H_5)_2Co$ yields only traces of $\pi\text{-}C_5H_5CoC_8F_{12}$, the corresponding reaction with diphenylacetylene gives high yields. The infra-red spectrum of $\pi\text{-}C_5H_5CoC_4(C_6H_5)_4$ shows bands characteristic of $\pi\text{-}C_5H_5$ and C_6H_5 groups and since the p.m.r. spectrum had only one phenyl group line (τ = 2.6) it appears that this compound has a symmetrical structure like (C). The nickel compound also has only one proton line in its resonance spectrum. By contrast, the $\pi\text{-}C_5H_5CoC_4(CF_3)_4$ clearly has two types of $-CF_3$ groups present. Models showed that the non-equivalence of the $-CF_3$ groups could not be attributed to intramolecular steric effects and so the structure was presumed to be (D). It thus appeared that there are two modes of bonding from a cyclobutadiene ring to the metal, one <u>via</u> a completely delocalized system and the other <u>via</u> one π - and two σ - bonds: it seemed that σ -bond formation could be favoured by the highly electronegative substituent groups.

This unusual form of bonding proposed stimulated the present X-ray analysis.

* * *

2.2 <u>Crystal data</u>

Deep red monoclinic crystals with well developed 001 and 00$\bar{1}$ faces were obtained by slow evaporation of a light (40/60) petroleum ether

solution. The unit cell dimensions determined from a least-squares analysis of the high angle precession data, are:

$a = 25.39 \pm 0.03\text{Å}$, $b = 8.68 \pm 0.01\text{Å}$, $c = 14.40 \pm 0.02\text{Å}$, $\beta = 94.8 \pm 0.2^{\circ}$.

The observed density of the crystals, measured by flotation in Rohrbach's solution, is $\rho_{obs}^{20^{\circ}C} = 1.82$ gm./cc. The density may be calculated from the volume, V, of the unit cell containing n molecules of molecular weight M, from the expression:

$$\rho = \frac{n.M}{V.N}$$

where N is the Avogadro number. Assuming 8 molecules $C_5H_5CoC_8F_{12}CO$ per unit cell of volume $V = 3163\text{Å}$ gives $\rho_{calc.} = 1.92$ gm/cc. The low observed value seems to indicate solvent inclusion in the lattice (see 2.7)

Systematic absences are observed for $\{hkl\}$ reflexions when $h + k = 2n + 1$ and for $\{h0l\}$ reflexions when $l = 2n + 1$, indicating, respectively, C face-centering and the prescence of a c-glide plane perpendicular to 'b'. The spacegroup may, therefore, be Cc, C2/c or $C2_1/c$, the last two being identical. Systematic absences are unable to distinguish these, a two-fold rotation axis giving rise to no systematic absences at all and a two-fold screw producing absences ($\{0k0\}$: $k = 2n + 1$) which are already a condition of the face-centering. There are 8 equipoints in the centrosymmetric space group C2/c ($N^{\circ}15$, C_{2h}^6) and 4 in the non-centrosymmetric Cc ($N^{\circ}9$, C_5^4). The 8 molecules in the unit cell therefore require the asymmetric unit in the former case to be a single molecule but in the latter, a pair of crystallographically unrelated molecules. A detailed

study of the Patterson synthesis (see 2.3) and the ultimate solution of the structure show that the spacegroup is C2/c.

All intensity data were collected by precession photography, at first, only 610 independent reflexions being collected from 6 zones - $\{hk0\}$, $\{0k\ell\}$, $\{1k\ell\}$, $\{h0\ell\}$, $\{h1\ell\}$, $\{h2\ell\}$ - but later a further 292 intensities from $\{hk1\}$, $\{hk2\}$, $\{hk3\}$ and $\{hk4\}$ zones. (see 2.4). These 902 intensities were measured initially with a Joyce-Loebl microdensitometer, but the final refinement is completely based upon visually-estimated data (see 2.5). The intensities were corrected for Lorentz and polarization factors (Beurger,A) with a computer program written by J. Dollimore. However, no correction for absorption effects have been made, the crystals used in the analysis having approximately spherical habit ($\pm$ 20%) of diameter $\sim$0.1 mm. and the absorption cross-section for Mo Kα radiation (used in all the crystallographic work described in this thesis) being small.

* * *

2.3 The Patterson Synthesis

The Patterson function

$$P_{uvw} = \frac{1}{V} \sum_{h} \sum_{k} \sum_{l=-\infty}^{\infty} |F_{hkl}|^2 \exp 2\pi i (hu + kv + lw)$$

was computed directly from the observed intensities after correction for Lorenz and polarization factors. The Patterson was used only to locate the heavy atom position: the results obtained from the first synthesis (610 reflexions) were confirmed by the second (902 reflexions), which,

because of its greater resolution, is the one described in detail here. Table 2.1 lists the higher vector peaks found in the three-dimensional Patterson, together with their heights - due account being taken of the deepest negative value of P_{uvw} caused by omitting $F^2(0,0,0)$ from the series.

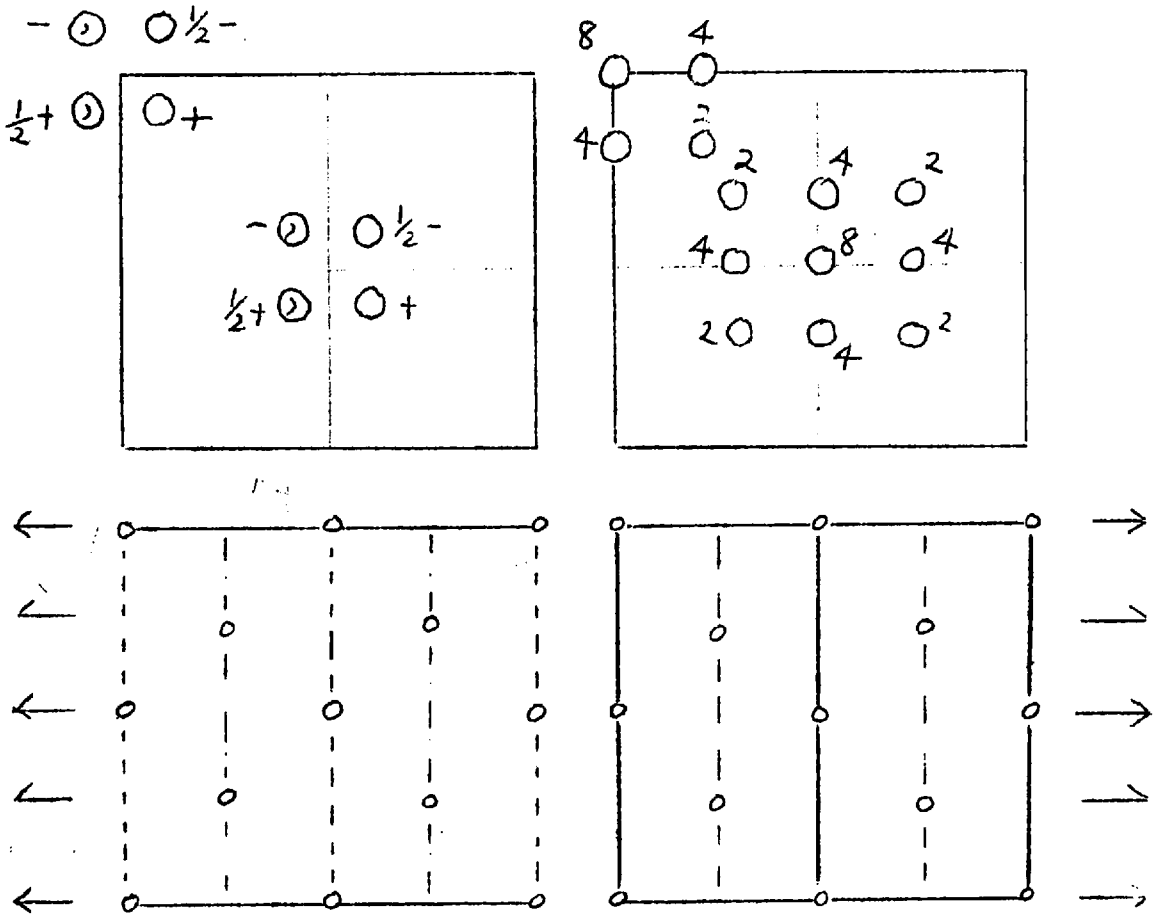
Table 2.1

Cobalt-cobalt vector peaks in the ranges $^u/_a$ 0 - 1, $^v/_b$ 0 - $\frac{1}{2}$, $^w/_c$ 0 - $\frac{1}{2}$

Peak	$^u/_a$	$^v/_b$	$^w/_c$	Peak Height	Assignment
1	0	0	0	9420	0 , 0 , 0 ,
2	$\frac{1}{2}$	$\frac{1}{2}$	$\frac{1}{2}$	9420	$\frac{1}{2}$, $\frac{1}{2}$, $\frac{1}{2}$,
3	0.2975	0.4125	0.267	1950	1 - 2x , 2y , -2z ,
4	0.7975	0.0875	0.267	1950	$1\frac{1}{2}$ - 2x, $\frac{1}{2}$ - 2y, -2z ,
5	0	0.4125	$\frac{1}{2}$	3730	0 , 2y , $\frac{1}{2}$,
6	$\frac{1}{2}$	0.0875	$\frac{1}{2}$	3730	$\frac{1}{2}$, $\frac{1}{2}$ - 2y, $\frac{1}{2}$,
7	0.2025	$\frac{1}{2}$	0.233	2800	$-\frac{1}{2}$ + 2x, $\frac{1}{2}$, $\frac{1}{2}$ + 2z,
8	0.7025	0	0.233	2800	2x , 0 , $\frac{1}{2}$ + 2z,

What are the positions and heights of the vector peaks produced by the eight equipoints of spacegroup C2/c?

The symmetry of a Patterson is that of the Laue group plus Bravais lattice of the spacegroup; thus C2/c has Patterson symmetry C2/m. In the diagram below, the symmetry elements and equipoints for C2/c are shown on the left while the symmetry of C2/m and the Patterson peaks are shown on the right.



C2/c

Direct Space

C2/m

Patterson Space

The relative peak heights (assumed to be approximately proportional to their volumes) may be summarized as follows. The origin peak which

null-vectors from the eight spacegroup equipoints will contain 8 Co-Co vectors, and, because of its identical environment, the centre peaks at $\frac{1}{2}$, $\frac{1}{2}$, 0 will also be 8-fold. All other peaks are at least double as a result of the face-centering and, in addition, those peaks which lie on the mirror planes or diads in the Patterson cell will be doubled again. These multiplicities are summarized in the top right of the diagram. The co-ordinates U,V,W of the vector peaks are:

Double peaks, general positions	$2x , \pm 2y , 2z$ $-2x , \pm 2y , -2z$	+ $\frac{1}{2}, \frac{1}{2}, 0$
Four-fold peaks, on diads	$0 , \pm 2y , \frac{1}{2}$	
Four-fold peaks, on mirror planes	$\pm 2x , 0 , \frac{1}{2} \pm 2z$	

These may be compared with the co-ordinates of the observed peaks and the assignments are shown in the last column of Table 2.1. It can be seen that the array of vectors is consistent with cobalt atom co-ordinates, $^{x}/_{a} = 0.351$, $^{y}/_{b} = 0.2063$, $^{z}/_{c} = -0.133$. The multiplicities of the observed peaks are now considered.

The volume of a Patterson peak representing the vector from atom A (with Z_A electrons) to atom B (with Z_B electrons) is $Z_A.Z_B$: the peak height is roughly proportional to $Z_A.Z_B$. The origin peak contains all self-self vectors in the unit cell which, for C2/c, means $8\sum_n Z_i^2$ for the n atoms in the molecule. For $C_5H_5.(CF_3)_4C_5O.Co$, $8\sum Z_i^2 = 17{,}808$ and a single Co-Co

vector peak will have a volume 729. The observed peak height is 9420, from which double and four-fold Co-Co vectors can be expected to have peak heights of 770 and 1540 respectively. Table 2.1 shows that the observed peak heights are, in fact, much greater than these values. The reasons for this are: (i) inevitably, in a structure of this size, there is considerable overlap of vector peaks, for example from Co-F or F-F vectors which accidentally coincide approximately with the symmetry-bound Co-Co vectors (a Patterson synthesis contains $n^2 - n + 1$ peaks in the same volume occupied by n atoms),

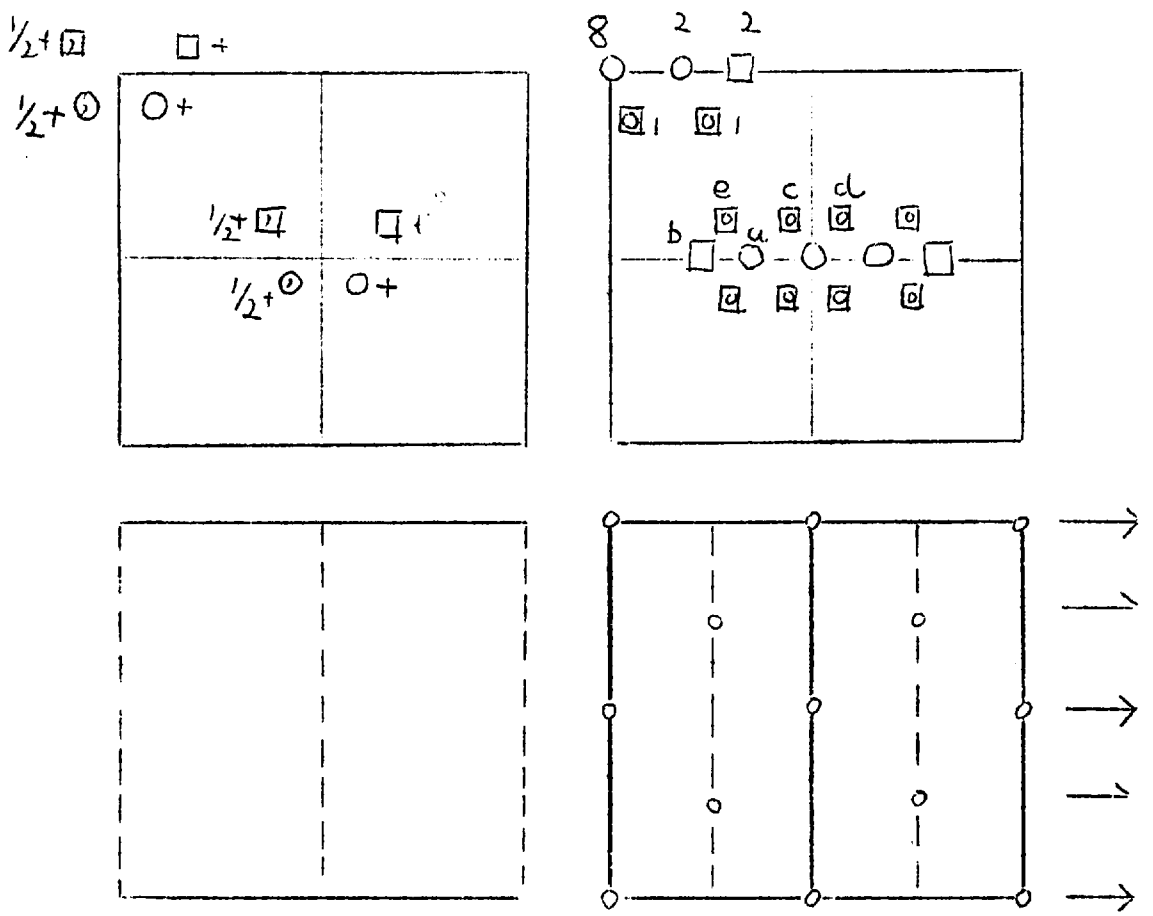
(ii) there is more chance of such overlap on Harker sections, which explains the greater discrepancy between observation and theory for peaks 5 and 6 in Table 2.1,

(iii) as will be shown later (see Table 2.3), the light atoms, most particularly the fluorines, have large thermal factors which serve to increase the spread of the origin peak which, being calibrated by peak height rather than volume, appears too low relative to the Co-Co vector peaks obtained from the heavier, less mobile atom,

(iv) the effects of series termination will modulate the Patterson density in a small and non-uniform way.

In view of these reasons, which are valid to some extent in all 'heavy atom' structures, it is hardly surprising that good agreement between observed and predicted peak heights is lacking.

As discussed in section 2.2, systematic absences were unable to distinguish between spacegroups C2/c and Cc. In the latter case the asymmetric unit will contain two crystallographically unequivalent molecules which will give rise to a set of 'cross-vectors' as shown below:



Cc

Direct Space

Cm (≡ C2/m)

Patterson Space

The two independent molecules are represented by a circle and a square as are the symmetry related peaks for each: cross-vectors are represented by the symbol, ⊡ . In general, C2/c and Cc will easily be distinguishable by the additional cross-vector peaks. While the absence of such peaks in the observed Patterson map strongly suggests the former spacegroup, the latter cannot be rigidly excluded as the two independent molecules could lie close to the eight equipoints of C2/c. In this unlikely event, peaks a and b tend to merge as do c and d and peaks e, adjusting to give the Patterson representation shown for C2/c. The correct strategy in the absence of cross-vectors is to assume the centrosymmetric spacegroup in the first instance: in fact, the structure was solved and refined successfully with this spacegroup.

* * *

2.4 Solution of the structure

The cobalt atom position obtained from the Patterson was now used to phase electron density projections $\rho(xy0)$ and $\rho(x0z)$ which could not, however, be interpreted, owing to considerable atomic overlap. Three dimensional work was begun with only 610 intensities. The first round of structure factors calculated from a Co position $^{x}/_{a} = 0.351$, $^{y}/_{b} = 0.206$, $^{z}/_{c} = -0.133$ and isotropic temperature factor B = 4.5 produced a reliability factor $R \approx 0.60$, where

$$R = \frac{\sum \left| |F_o| - |F_c| \right|^2}{\sum |F_o|}$$

A second cycle, based upon a refinement of the cobalt positional and thermal parameters, reduced R to $\sim$0.48 and was used to compute the first three-dimensional Fourier synthesis $\rho(x,y,z)$. Despite some confusion caused by the diffraction effects of series termination, the cyclopentadienyl ring could be located with some certainty and three carbon atoms of the supposed cyclobutadiene ring were fairly well resolved, two particularly so. While the general positioning of the fluoromethyl groups seemed clear, only four peaks could be confidently assigned to fluorine atoms. Several attempts to improve the phasing were now made, by inclusion of diffraction contributions from the cyclopentadienyl ring, the three 'cyclobutadiene' carbon atoms and between 4 and 12 fluorine atoms with their fluormethyl carbons. The reliability factors produced by these models varied from $\sim$0.38 with only 4 fluorine atoms to $\sim$0.30 for the complete molecule. Both 'observed' and 'difference' Fourier syntheses were computed for each model, but apart from the features already mentioned, no firm conclusions could be reached. Least squares refinement converged at R $\sim$0.29. A particularly puzzling feature was a long peak (about 3.0 Å by 1.5 Å), near the cyclobutadiene ring, which persisted in all 'observed' and 'difference' Fourier maps of all models.

It was assumed at this time that the chemical evidence for a substituted cyclobutadiene ring was correct and that the Fouriers, based on insufficient data, were wrong! Three further zones of reflexions were therefore collected and with the now 902 reflexions (see 2.2) a new attempt to determine

the structure was begun. For the sake of completeness, a second three-dimensional Patterson was first computed, which, besides confirming the conclusion of the earlier synthesis, demonstrated the much greater resolution to be had from the more representative data coverage. The cobalt and cyclopentadienyl carbon atoms were now used to phase the next round of structure factors ($R \sim 0.45$) and the 'observed' and 'difference' Fourier syntheses. Several features were clearly apparent while generally confirming the results of the earlier 600 reflexion Fourier maps. Confidence could now be placed in an additional ten peaks corresponding to an $F_3C\text{-}C\text{-}C\text{-}CF_3$ chain and a second round of structure factors and Fourier syntheses revealed the whole of the molecule. The structure was, in fact, π-cyclopentadienyltetrakis(trifluoromethyl)cyclopentadienonecobalt rather than π-cyclopentadienyltetrakis(trifluoromethyl)cyclobutadienecobalt. Inclusion of all atoms (Figure 2.1) reduced the reliability factor to 0.31 and all the peaks of the early and later Fourier maps were explained: in particular, the puzzling peak referred to above, was an unresolved carbonyl group and explains why the early cyclobutadiene models invariably required a very long C-C bond (~ 2 Å) in that region!

* * *

2.5 Refinement of atomic positional and thermal parameters

Refinement of the structure was initially based on a least squares adjustment of all position parameters, together with anisotropic and .

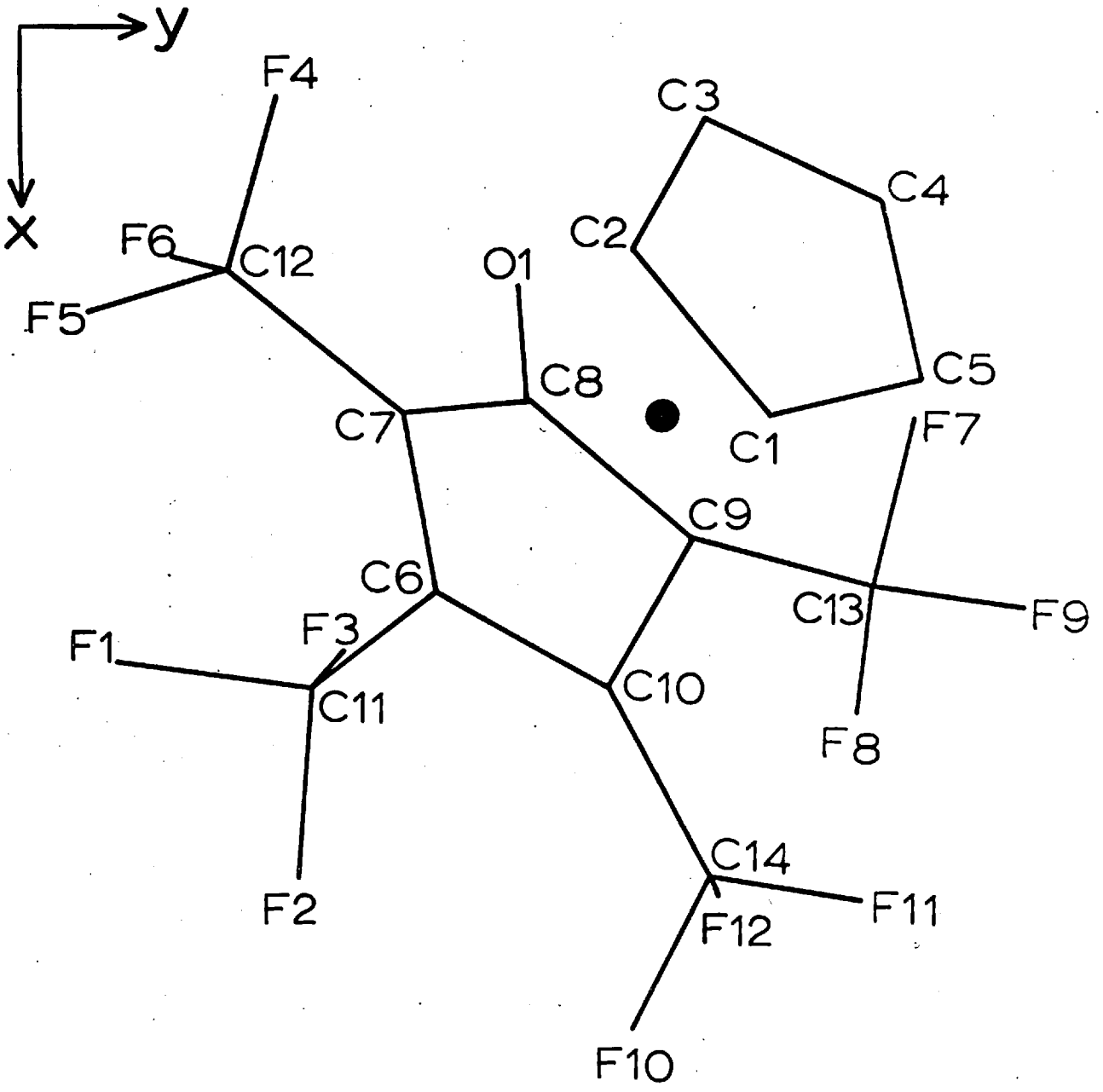


Figure 2.1

$(CF_3)_4C_5O.C_5H_5.Co$. Numbering of Atoms.

isotropic temperature factors for the cobalt and light atoms respectively. After four cycles of such refinement, when R had been reduced from 0.31 to 0.21, convergence was virtually complete. The Fourier and 'difference' Fourier maps had already indicated large librational motions for the fluorines, particularly those denoted F1 - F3 and F10 - F12 inclusive, so that a halt in the refinement at the relatively high R value of 0.21 was expected when the vibrations of all light atoms were constrained to be isotropic. Inclusion of anisotropic temperature factors for all 28 atoms, however, required six cycles of least squares refinement to converge at R = 0.138. The following record of reliability factors demonstrates how slow this convergence was:

cycle 1, R = 0.188 cycle 2, R = 0.166 cycle 3, R = 0.153

cycle 4, R = 0.145 cycle 5, R = 0.140 cycle 6, R = 0.138

Only small changes in positional parameters were involved in these cycles, $\sum w(\Delta F)^2$ being minimised by large anisotropic increases in temperature factors.

While the thermal parameters of the carbon and fluorine atoms were not altogether physically unreasonable (being, at most, about nine times larger than the Co b_{ij}'s -for two fluorines), a careful comparison of observed and calculated structure factors revealed trends which suggested that the temperature factor refinement had served to refine away systematic errors in the data, in addition to the real anisotropy of thermal vibration. Thus all 'strong' reflexions were calculating too strong and reflexions close to the

the minimum $|F_{obs}|$ were calculating too weak. With some lack of enthusiasm, all data were re-estimated visually by calibration against an incrementally exposed 'wedge'. These data did indeed serve to emphasise the systematic errors which were present in the densitometer estimated amplitudes. When using the microdensitometer, care had been taken not to measure film spots where the deposition of silver was too great and therefore not logarithmic so that errors arising from neglect of this well-known source are excluded. However, only peak heights were measured - a method which assumes that spot intensity is proportional to peak height . The proportionality constant is assumed to be the same all over the film, which is only true if the spot shapes are similar throughout the film area. Unfortunately, this is less likely to be true on precession photographs than on Weissenberg which are, of course, less suitable for this semi-automatic method of measurement. If the areas under the microdensitometer traces are measured, variation in spot shapes and sizes would be properly allowed for, but this method is more tedious and no more accurate than conventional visual estimation (see, for example, Mason and Phillips' analysis of acridine). While our results may also demonstrate shortcomings of the particular microdensitometer used, it seems clear that some check of microdensitometer data would be generally worth while.

With the previously determined position and thermal parameters the reliability factor between F_{calc} and the new visually estimated data was 0.205. Two least squares cycles, however, reduced this to 0.17 and 0.106

and convergence was reached after three further cycles when R was 0.088. Both the value of the final reliability index and the rate of convergence justify our preference for the visual data compared with that determined by densitometer methods; again, no systematic dependence of $\Delta F = \left| |F_o| - |F_c| \right|$ on $|F_{obs}|$ was obvious.

Throughout the above refinement all reflexions were given unit weight: Rollett's least squares programme was used to weight reflexions by,

$$w = \sqrt{\frac{1}{1 + \left\{(|F_o| - b)/a\right\}^2}}$$

With b = 0, a = 10,000 a close approximation to unit weighting is achieved. This weighting scheme was now replaced by b = 0, a = 100, that is F^{-1} weighting of all reflexions, as strongest reflexions are most likely to suffer from extinction effects and are therefore somewhat less reliable. With the above positional and thermal parameters and the new weighting scheme, R increased to 0.091 after the first cycle: after a second cycle convergence was complete when R = 0.089. The net result of the changed weighting was to lower some temperature factors by a few percent.

Final atomic parameters together with their e.s.d's are collected in Tables 2.2 and 2.3 while the output observed and calculated structure factors from the last cycle of refinement are listed in Table 2.4 (contribution to F_c from the five hydrogen atoms of the cyclopentadienyl ring have not been included, there being no significant indication of these atoms in the final 'difference' Fourier maps. Figure 2.2 shows the final three-dimensional

Table 2.2 $(CF_3)_4C_5O.C_5H_5Co$.

Atomic Co-ordinates and Estimated Standard Deviations.

Atom	x/a	y/b	z/c	(X) Å	(Y) Å	(Z) Å
Co	0.3518	0.20395	-0.12804	0.0023	0.0027	0.0022
C1	0.3509	0.2899	-0.2634	0.025	0.029	0.022
C2	0.3088	0.1823	-0.2538	0.024	0.026	0.020
C3	0.2738	0.2414	-0.1866	0.022	0.024	0.020
C4	0.2953	0.3778	-0.1519	0.022	0.026	0.025
C5	0.3446	0.4105	-0.1980	0.027	0.021	0.022
C6	0.3994	0.0261	-0.0989	0.017	0.021	0.019
C7	0.3522	0.0022	-0.0567	0.016	0.021	0.018
C8	0.3495	0.1016	0.0277	0.018	0.023	0.019
C9	0.3877	0.2267	0.0068	0.018	0.021	0.019
C10	0.4231	0.1676	-0.0632	0.017	0.021	0.021
C11	0.4242	-0.0724	-0.1725	0.023	0.029	0.028
C12	0.3143	-0.1300	-0.0724	0.025	0.026	0.025
C13	0.3940	0.3732	0.0627	0.025	0.024	0.019
C14	0.4734	0.2436	-0.0876	0.021	0.031	0.026
F1	0.4195	-0.2204	-0.1480	0.022	0.019	0.024
F2	0.4768	-0.0760	-0.1542	0.018	0.023	0.021
F3	0.4161	-0.0459	-0.2552	0.024	0.028	0.015
F4	0.2678	-0.0894	-0.0540	0.014	0.015	0.024
F5	0.3273	-0.2490	-0.0223	0.018	0.015	0.021
F6	0.3111	-0.1768	-0.1619	0.018	0.019	0.019
F7	0.3515	0.4054	0.1006	0.020	0.021	0.022
F8	0.4323	0.3620	0.1267	0.019	0.018	0.014
F9	0.4042	0.4913	0.0141	0.017	0.015	0.016
F10	0.5131	0.1779	-0.0467	0.015	0.031	0.022
F11	0.4832	0.3623	-0.0437	0.021	0.024	0.034
F12	0.4793	0.2459	-0.1695	0.020	0.030	0.017
O1	0.3197	0.0969	0.0861	0.013	0.019	0.014

Table 2.3 $(CF_3)_4C_5O.C_5H_5Co$. Atomic Vibration Parameters.

Temperature factor $T = 2^{-(b_{11}h^2 + b_{22}k^2 + b_{33}l^2 + b_{23}kl + b_{13}hl + b_{12}hk)}$

Atom	b_{11}	b_{22}	b_{33}	b_{23}	b_{13}	b_{12}
Co	0.0024	0.01761	0.00559	0.00112	0.00078	-0.00053
C1	0.0049	0.0425	0.0092	0.0245	-0.0005	0.0071
C2	0.0045	0.0371	0.0082	0.0024	-0.0015	-0.0022
C3	0.0047	0.0280	0.0078	0.0036	-0.0035	0.0078
C4	0.0040	0.0344	0.0140	0.0243	-0.0054	0.0125
C5	0.0065	0.0167	0.0113	0.0142	-0.0086	0.0098
C6	0.0029	0.0224	0.0068	-0.0003	0.0003	0.0031
C7	0.0023	0.0148	0.0080	-0.0074	0.0000	-0.0041
C8	0.0024	0.0277	0.0088	0.0052	-0.0024	-0.0001
C9	0.0028	0.0213	0.0067	0.0103	0.0011	-0.0016
C10	0.0019	0.0236	0.0115	-0.0005	0.0013	-0.0042
C11	0.0031	0.0394	0.0156	-0.0233	-0.0053	0.0033
C12	0.0051	0.0209	0.0146	0.0012	-0.0019	-0.0074
C13	0.0058	0.0250	0.0056	-0.0128	0.0033	-0.0046
C14	0.0028	0.0472	0.0105	-0.0020	-0.0006	-0.0070
F1	0.0110	0.0398	0.0262	-0.0380	0.0166	0.0001
F2	0.0059	0.0776	0.0225	-0.0062	0.0052	0.0134
F3	0.0118	0.1067	0.0100	-0.0185	-0.0004	0.0476
F4	0.0034	0.0320	0.0407	0.0114	0.0070	-0.0060
F5	0.0065	0.0298	0.0242	0.0180	-0.0018	-0.0139
F6	0.0072	0.0447	0.0242	-0.0122	-0.0056	-0.0110
F7	0.0068	0.0597	0.0253	-0.0461	0.0107	-0.0078
F8	0.0089	0.0373	0.0127	-0.0093	-0.0106	-0.0094
F9	0.0089	0.0198	0.0160	-0.0079	0.0013	-0.0029
F10	0.0028	0.1315	0.0309	0.0472	0.0017	-0.0101
F11	0.0087	0.0764	0.0597	-0.0727	0.0292	-0.0367
F12	0.0058	0.1240	0.0120	0.0172	0.0056	-0.0237
O1	0.0035	0.0403	0.0092	-0.0008	0.0045	-0.0019

Table 2·4

Figure 2.2

Final three-dimensional electron density synthesis

Contours are drawn at $1e\text{Å}^{-3}$ intervals

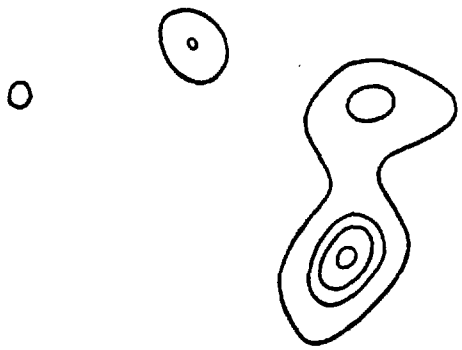
Z=42/240



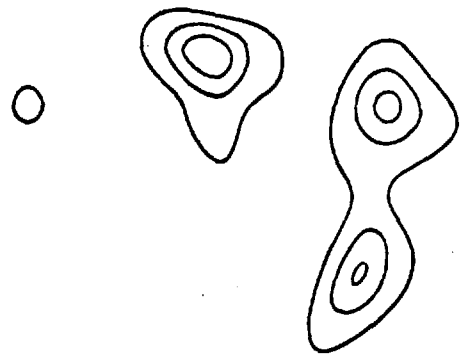
Z=36/240



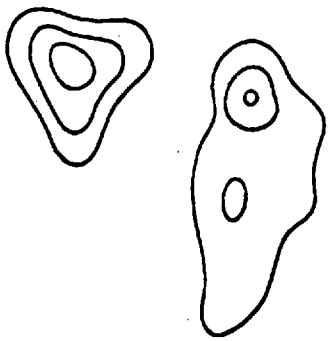
Z=30/240



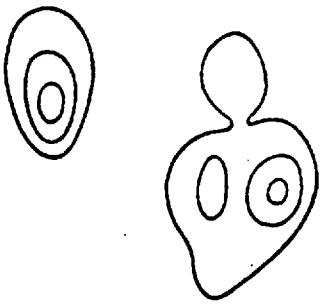
Z=24/240



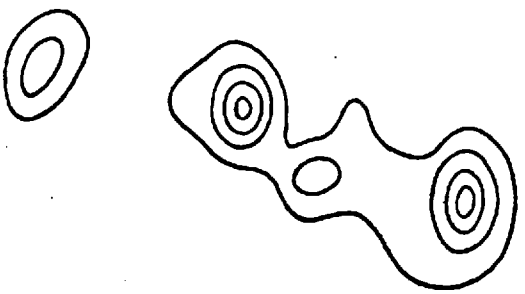
Z=18/240



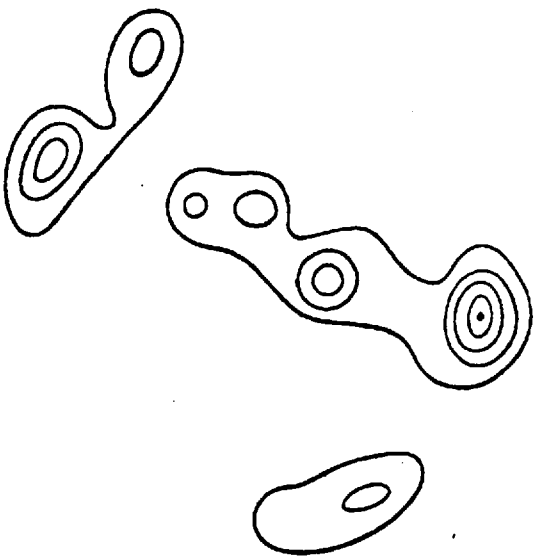
Z=12/240

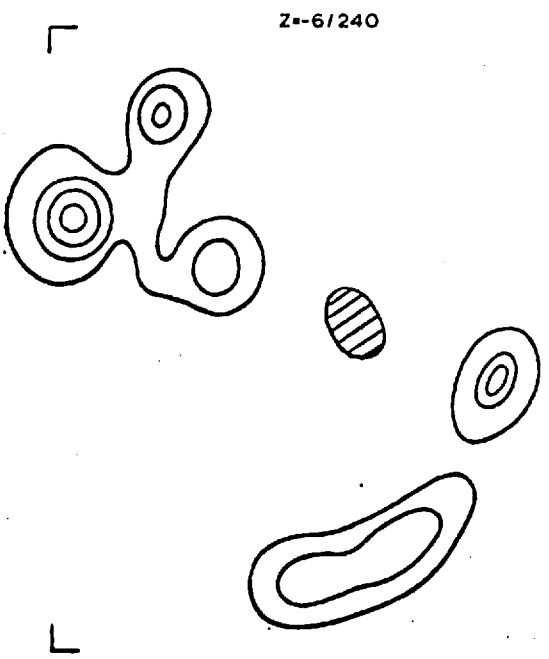


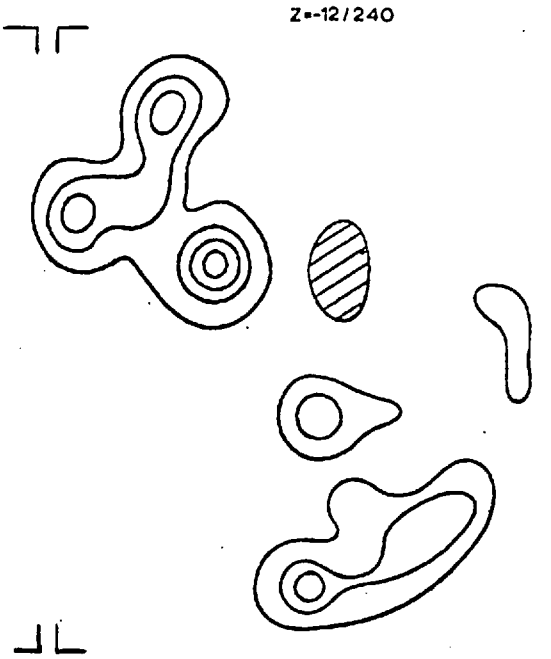
Z=6/240

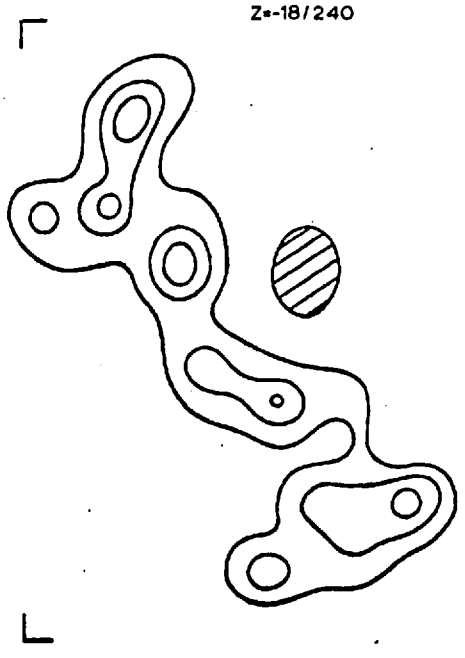


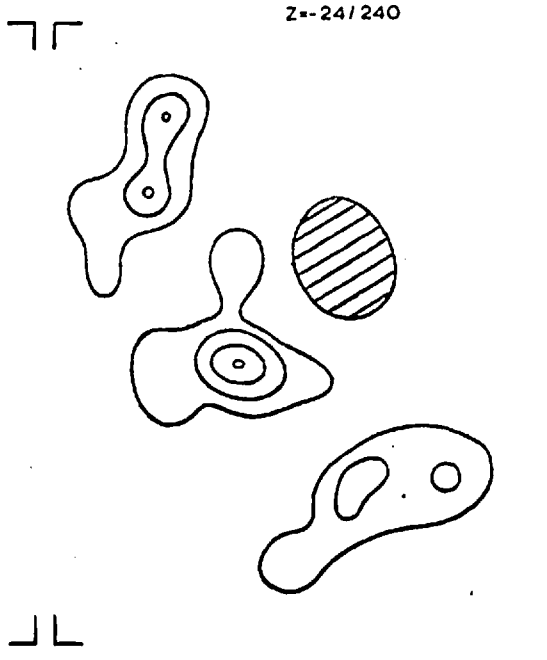
Z=0/240

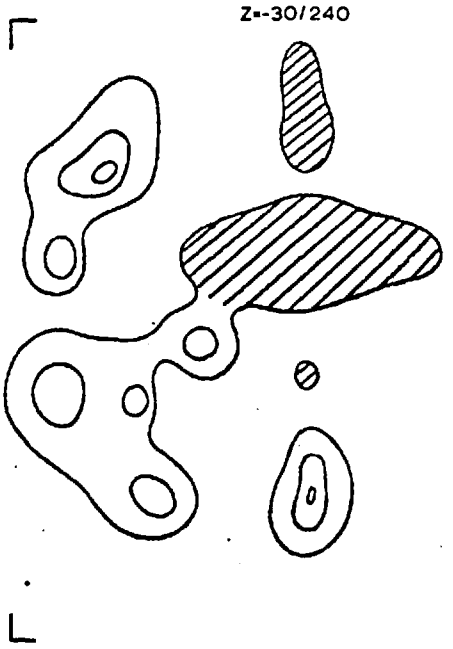


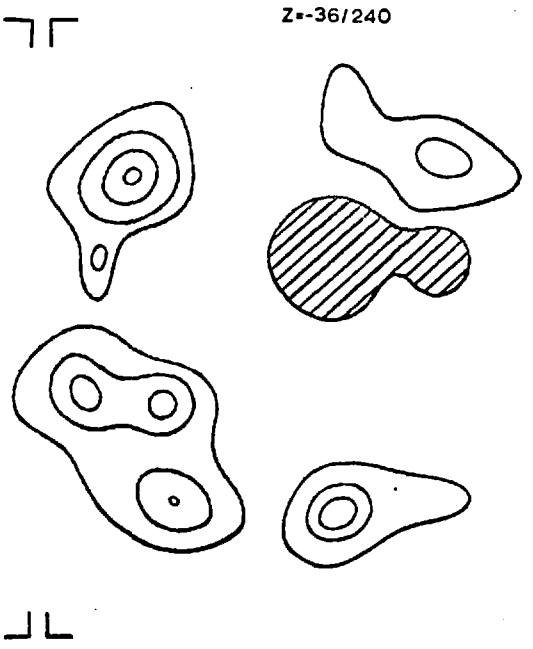

Z=-6/240

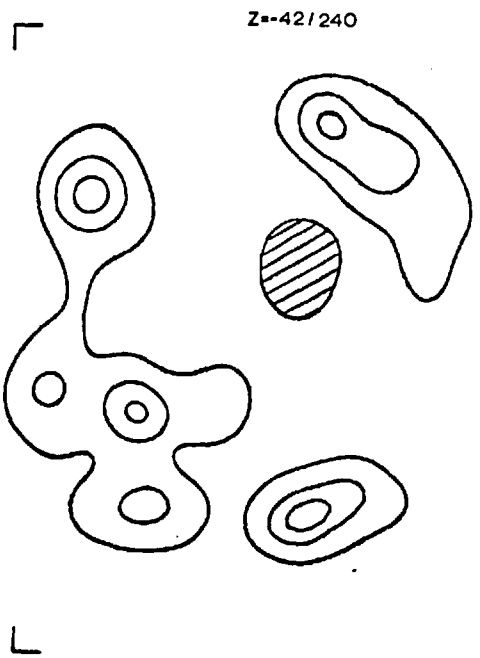

Z=-12/240

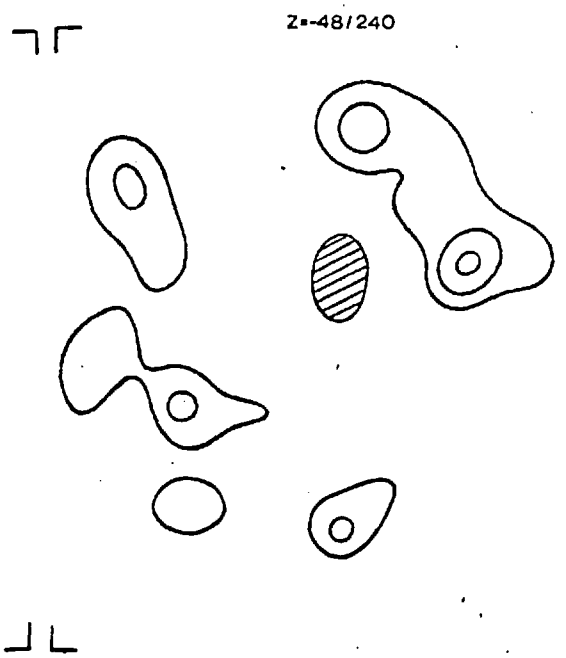

Z=-18/240

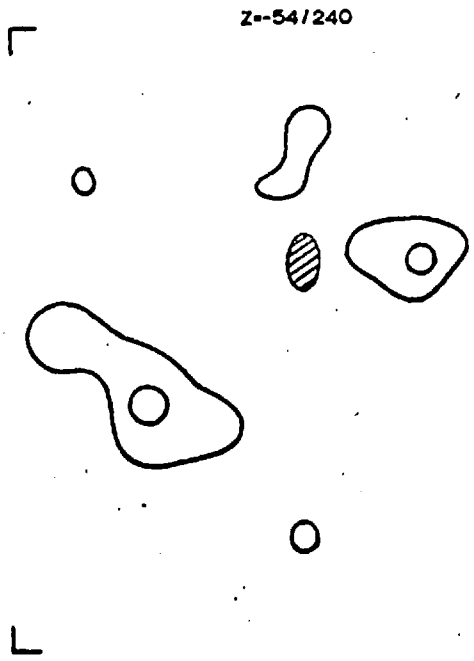

Z=-24/240

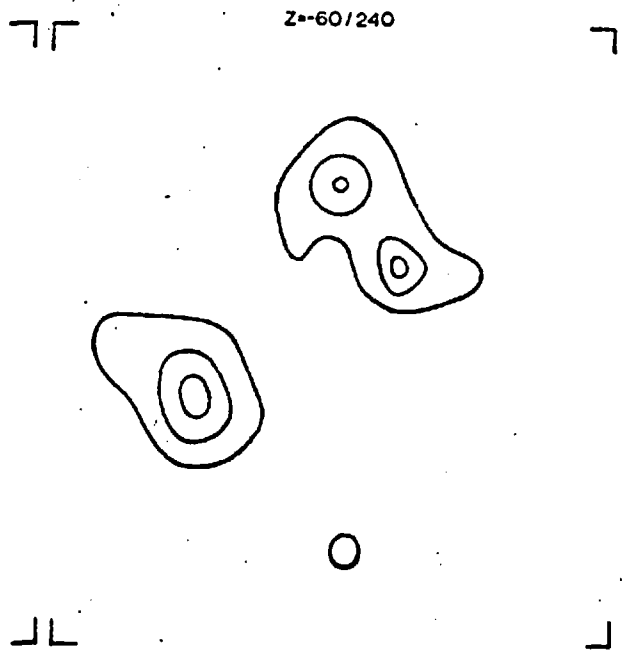

Z=-30/240

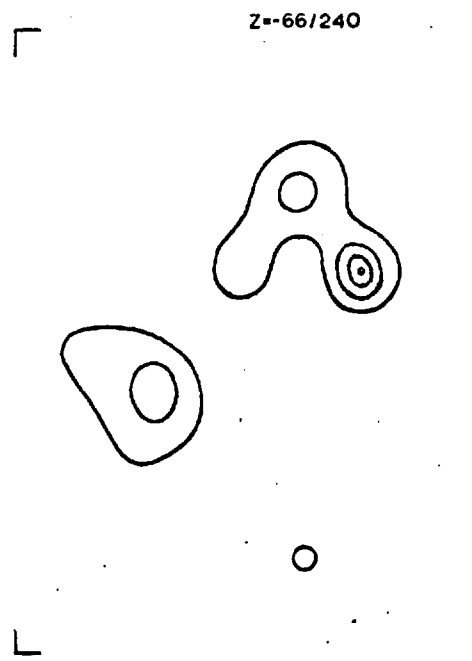

Z=-36/240

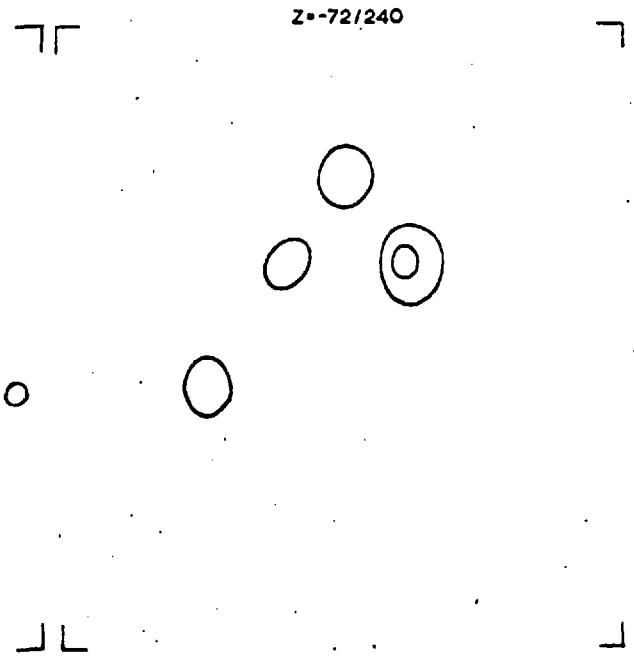

Z=-42/240


Z=-48/240


Z=-54/240


Z=-60/240


Z=-66/240


Z=-72/240

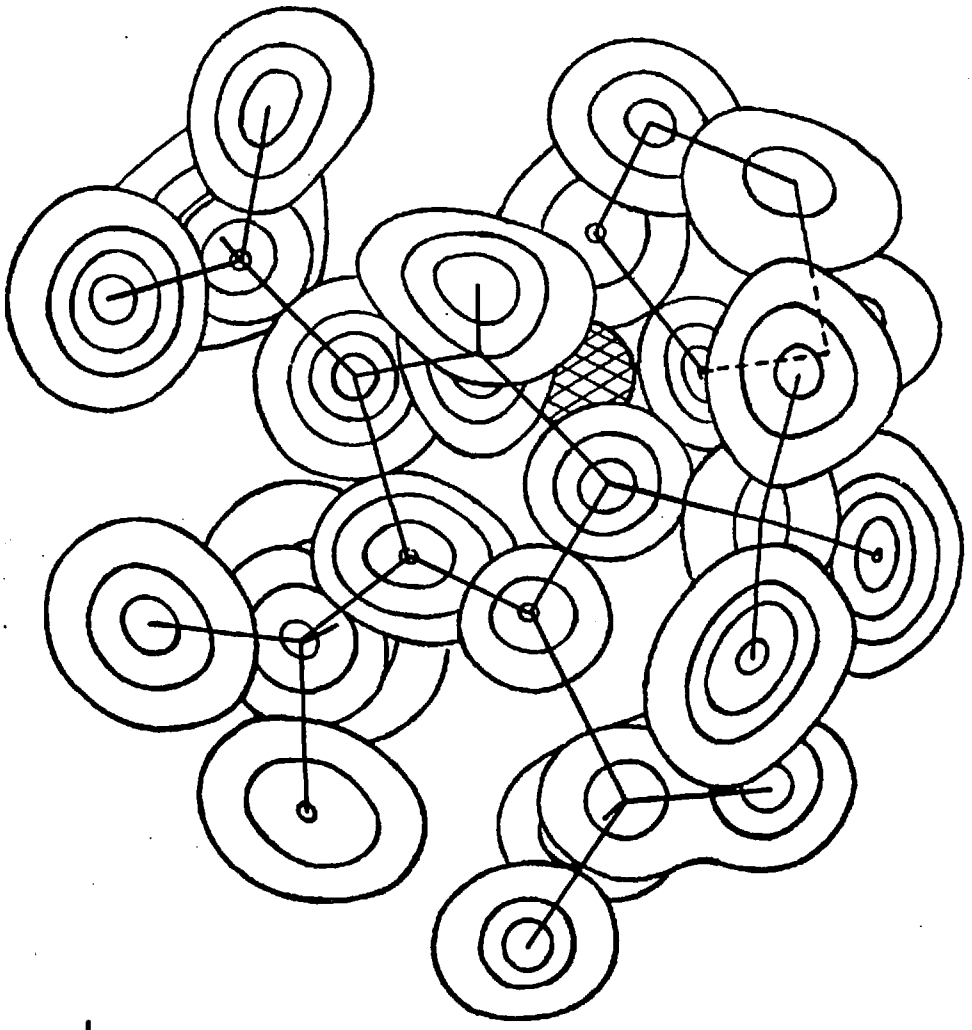


Figure 2.3

The composite molecular electron density projected down 'c'. The contours are drawn at 1 e $\mathring{A}^{-3}$ intervals.

electron density synthesis section by section, while Figure 2.3 is a composite representation of the electron distribution in a single molecule.

* * *

Discussion

2.6 The molecular structure

While the fact that the compound contains a cyclopentadienone ring rather than a cyclobutadiene ring invalidates the bonding scheme which had been proposed, it does make some puzzling chemical features much clearer. For example, the non-equivalence of the CF_3 groups shown by n.m.r. can now be understood in terms of aliphatic and olefinic groupings, as discussed below. It turns out unfortunate that the ketone stretch should be virtually coincident with the C=C stretching frequency, as the close parallel between the cobalt and iron complexes would otherwise have been apparent.

Intramolecular bond lengths and bond angles are given in Tables 2.5 and 2.6 together with their e.s.d.'s; some of the more significant results are shown in Figure 2.4(a)

The most unexpected feature of the molecular structure is, perhaps, the considerable non-planarity of the cyclopentadienone ring, C8 being tilted by an angle of 21.3° ($\pm 0.5^{\circ}$) away from the metal atom about the axis C7–C9. C6, C7, C9 and C10 are essentially co-planar, the r.m.s. deviation of atoms from a plane defined by the direction cosines 0.4453, -0.5190, 0.7296 (referred to the orthogonal axes a,b and c′) being 0.007 Å. The fluoromethyl

Table 2.5 $(CF_3)_4C_5O.C_5H_5Co$. Intramolecular Bond Lengths

Bond	Bond length, Å	e.s.d.
Co - C1	2.084	0.027
Co - C2	2.044	0.025
Co - C3	2.113	0.023
Co - C4	2.085	0.026
Co - C5	2.050	0.025
Co - C6	1.978	0.021
Co - C7	2.023	0.020
Co - C8	2.416	0.021
Co - C9	2.084	0.021
Co - C10	1.991	0.021
C1 - C2	1.431	0.035
C2 - C3	1.460	0.032
C3 - C4	1.376	0.033
C4 - C5	1.491	0.034
C5 - C1	1.422	0.035
C6 - C7	1.403	0.027
C7 - C8	1.494	0.028
C8 - C9	1.500	0.028
C9 - C10	1.494	0.027
C10 - C6	1.439	0.027
C6 - C11	1.535	0.033
C7 - C12	1.499	0.031
C9 - C13	1.502	0.030
C10 - C14	1.540	0.033
C8 - O1	1.177	0.025
C11 - F1	1.334	0.035
C11 - F2	1.341	0.035
C11 - F3	1.213	0.035
C12 - F4	1.278	0.031
C12 - F5	1.283	0 032
C12 - F6	1.347	0.032
C13 - F7	1.280	0.031
C13 - F8	1.286	0.029
C13 - F9	1.276	0.028
C14 - F10	1.259	0.035
C14 - F11	1.216	0.038
C14 - F12	1.202	0.035

Table 2.6 $(CF_3)_4C_5O.C_5H_5Co$. Bond Angles

Bonds	Angle °	e.s.d
C2 - C1 - C5	106.6	2.0
C3 - C2 - C1	109.8	1.9
C4 - C3 - C2	107.1	2.0
C5 - C4 - C3	108.9	1.8
C1 - C5 - C4	107.5	2.0
C7 - C6 - C10	108.5	1.6
C8 - C7 - C6	111.6	1.6
C9 - C8 - C7	100.1	1.4
C10 - C9 - C8	109.0	1.5
C6 - C10 - C9	105.9	1.5
C7 - C6 - C11	129.2	1.7
C10 - C6 - C11	122.3	1.8
C6 - C7 - C12	127.4	1.8
C8 - C7 - C12	119.2	1.8
C7 - C8 - O1	129.6	1.4
C9 - C8 - O1	129.3	1.4
C8 - C9 - C13	122.7	1.6
C10 - C9 - C13	127.3	1.6
C9 - C10 - C14	125.4	1.8
C6 - C10 - C14	128.7	1.8
C6 - C11 - F1	107.3	1.7
C6 - C11 - F2	109.7	1.7
C6 - C11 - F3	121.8	1.8
F1 - C11 - F2	92.0	1.8
F2 - C11 - F3	106.4	1.8
F3 - C11 - F1	115.4	1.8
C7 - C12 - F4	110.6	1.6
C7 - C11 - F5	113.2	1.6
C7 - C12 - F6	111.1	1.6
F4 - C11 - F5	107.6	1.6
F5 - C12 - F6	106.8	1.6
F6 - C12 - F4	107.3	1.6
C9 - C13 - F7	110.9	1.6
C9 - C13 - F9	113.4	1.4
F7 - C13 - F8	108.9	1.6
F8 - C13 - F9	106.1	1.4
F9 - C13 - F7	106.1	1.5
C10 - C14 - F10	110.8	1.8
C10 - C14 - F11	111.7	1.9
C10 - C14 - F12	114.5	1.7
F10 - C14 - F11	91.8	2.2
F11 - C14 - F12	117.7	2.2
F12 - C14 - F10	107.9	2.0

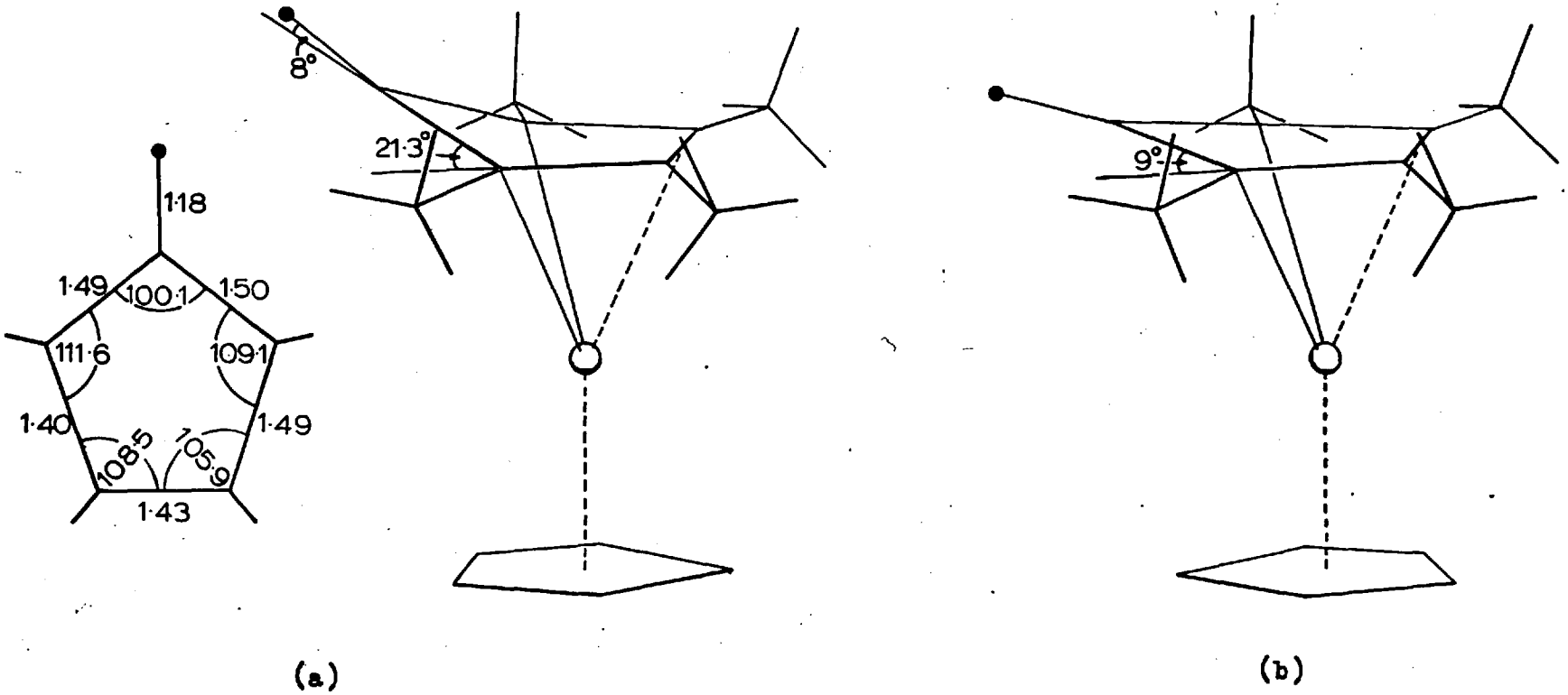


Figure 2.4

(a) $(CF_3)_4.C_5O.C_5H_5.Co$. Molecular dimensions and conformation.

(b) $(CH_3)_4.C_5O.C_5H_5.Co$. Molecular conformation.

carbon atoms C12 (+ 0.011 Å), C13 (+0.014 Å), C11 (-0.040 Å) and C14 (-0.037 Å) are also, within experimental error, co-planar with the 'butadiene' part of the cyclopentadienone ligand (see also section 2.7). The metal to centre-of-ring distance is 1.62 Å and 1.68 Å for the dienone and cyclopentadienyl respectively; these rings are in a staggered configuration with respect to one another and are closely parallel (2.7°).

The non-planarity of the dienone ring is shown in Figure 2.4(a), which also illustrates the essential tetrahedral symmetry of atoms C7 and C9. The conformation is entirely similar to that found for hhe substituted cyclopentadiene ring in π-cyclopentadienyl-1-phenylcyclopentadienecobalt (Churchill and Mason, 1963) and for the cyclopentadienone ring in tetrakis-(trifluoromethyl)cyclopentadienonetricarbonyliron (Bailey and Mason, 1963). Two σ- and one π - bonds form three bonds from the -diene or -dienone, in these two structures, to the metal, rather than a delocalized system (formally two π-bonds) as may have been expected. (see section 2.1). Unlike these structures, the bond lengths in the cyclopentadienone ring here are not of sufficient clarity to deduce a high π-bond order for C6-C10, but the molecular conformation is itself sufficiently strong evidence for postulating a σ- and π- bonding description of the metal ligand interaction. The statistical accuracy of these and other parameters will be discussed in section 2.8.

A single crystal analysis of the closely related π-cyclopentadienyl-tetramethylcyclopentadienone cobalt (Figure 2.4(b)) has been briefly

described (Dahl and Smith, 1961). These authors report that complete delocalization of the π-electrons in the cyclopentadienone is now evidenced by virtually equal carbon-carbon bond lengths in the ligand; the ketonic group is tilted by 9° away from the metal, a feature ascribed to crystal packing effects. It seems more reasonable to believe, in view of our present results, that the origin of this non-planarity is electronic and intramolecular. Thus bonding to the cobalt ion from a cyclopentadienone ring may occur in an identical way to that found for the bis-π-cyclopentadienyl complexes of transition metals or via σ-bonding centres at C7 and C9 and one π-bond from C6-C10. In the former case the dienone ligand shares 4 electrons with the cobalt ion (from 2 π-bonds) and in the latter 6 electrons (from 2 σ and 1 π-bonds): the cobalt ion also shares 6 electrons with the cyclopentadienyl ring. The 18 electron inert gas structure is, therefore, completed in the first system by Co(I),d^8 and in the second by Co(III),d^6. Nucleophilic substituents, such as $-CH_3$, on the cyclopentadienone ring will favour ring aromaticity and hence π-bonding from delocalized molecular orbitals of the ligand to the metal (Co^{1+}), whereas electophilic substituents, such as $-CF_3$ groups, will favour a Diels-Adler type addition of the ligand to the Co^{3+} ion.

The assignment of a formal oxidation state to the metal ion in these complexes is, of course, scarcely meaningful, as we should expect intermediate states between these two extreme types of bonding. Indeed, the ring conformation of the tetramethyl cyclopentadienone complex is consistent with a small amount of σ-bond donation to the metal.

The degree of localized bonding is not only a function of the ligand substituents in these complexes, but also of the relative stabilities of the possible oxidation states of the metal. To elaborate this point, we consider the compounds, tetrakis(trifluoromethyl) π -cyclopentadienyl cobalt and tetrakis(trifluoromethyl) tricarbonyliron (Bailey and Mason, loc.cit.). The relative stability of Co(III) over Co(I) is commonly greater than that of Fe(II) over Fe(0) and, in these complexes, this relationship is amplified by the stabilization of Fe(0) by the 3 carbonyl groups which have a greater power to 'back-bond' than the cyclopentadienyl ion. There is, therefore, a greater tendency for the cobalt ion to assume its higher oxidation state than for the iron and this would be reflected by a greater degree of localized σ -bonding to the cyclopentadienone ligand in the cobalt complex. This prediction has been verified - the tilt angles in the cobalt and iron complexes being 21° and 16° respectively (Bailey, Gerloch and Mason, 1963). Qualitatively, the bonding in these complexes may be summarized as follows: the degree of localized bonding is a product of (a) the tendency of the metal to assume that oxidation syate which causes it to complete its inert gas structure by sharing 6 electrons with the cyclopentadienone (or similar ligand) - which depends upon both the metal and the other ligands attached, and (b) the facility of localization of the cyclic ligand which depends upon the degree of aromaticity in the ring which, in turn, depends upon the ring substituents. This kind of bonding is important not only in the three compounds discussed immediately above, but also in π -cyclopentadienyl-1-phenylcyclopentadiene

cobalt (Churchill and Mason, loc.cit.), in hexakis(trifluoromethyl)benzene-tricarbonylrhodium (Churchill and Mason (2), 1963) and in 2.4.6 triphenyl-troponetricarbonyliron (Dahl and Smith, 1961): these and other relevant complexes will be discussed in greater detail elsewhere (Churchill, 1964).

Some idea of the strength of the metal-cyclopentadienone bonding can be gained from the metal → centre-of-ring distances in these compounds: these are given in Table 2.6 together with metal-cyclopentadienyl distances where appropriate.

Table 2.7

Metal to ring distances

Compound	Metal → cyclopentadienone (or cyclopentadiene) centre, Å	Metal → cyclopentadienyl centre, Å
π-$C_5H_5.(CH_3)_4C_5O.Co$	1.63	1.67
π-$C_5H_5.(CF_3)_4C_5O.Co$	1.62	1.68
π-$C_5H_5.C_6H_5(H_5)C_5.Co$	1.61	1.66

It might appear surprising that Co-C σ-bonds are shorter than Co-C π-bonds, but this result presumably reflects the larger orbital overlap produced by (a) the 'cyclic' σ- and π - back-bonding scheme, when localized bonding is relatively important, or (b) 'the back-donation of an electron from the metal to the ring which, with its four π-electrons, forms part of a delocalized

system similar to that of the cyclopentadienyl ligand' (taken from Dahl and Smith's molecular orbital description of the bonding in tetramethylcyclopentadienone π-cyclopentadienyl cobalt, loc.cit.).

This increased orbital overlap in the localized metal-ligand bond is also reflected in the internal angles of the cyclopentadienone ring (Figure 2.4(a)). Strain energy of the ring would be minimised if the internal angles at the formally sp^2 hybridized C6, C10 and C8 atoms were greater than the regular pentagon value of 108°, while those at the sp^3 hybridized C7 and C9 should be less than this value. The mean observed bond angle at C6 and C10 is actually 107.3°, that at C7 and C9 is 110.3°, while that at C8 is remarkably small (100.1°); that is, the ring is 'squashed' from 'side-to-side' rather than 'top-to-bottom'. A similar angular distortion is found in the cyclopentadienone and cyclopentadiene rings of $(CO)_3.(CF_3)_4C_5O.Fe$ and π-$C_5H_5.C_6H_5(H_5)C_5.Co$ respectively, and in an analogous manner in $(CF_3)C_6(CO)_3.Rh$: no values are presently available for π-$C_5H_5.(CH_3)_4C_5O.Co$. As C7 and C9 are squeezed together the implied increase in ring strain energy must be offset by an increased orbital overlap between the metal orbitals and the bonding sp^3 orbital of these atoms. The relatively strong metal-dienone bonding in this complex is, therefore, demonstrated by <u>both</u> the shorter Co-ring distance and the angular strain in the ring.

The co-ordination of the cobalt ion can be regarded, within the framework of the unsophisticated valence-bond theory, as octahedral. This configuration is based on a set of distorted d^2sp^3 hybrid orbitals directed towards an

arbitrary set of three bonding centres in the cyclopentadienyl ring while the metal hybrid orbitals also form two σ- and one π-bond to the dienone, thereby completing its inert gas configuration. Valence bond theory is scarcely a valuable description of the electron distribution in these complexes; for example, the angle subtended at the cobalt atom by C7 and C9 is only 68° rather than the 90° of a perfect octahedron. In passing, it can be seen that this small angle 'works with the cyclopentadienone ring strain' and is therefore another indication of the strong Co-dienone bonding described above.

There seems to be no a priori reason why the bonding from the metal to the cyclopentadienyl should be perfectly cylindrically symmetric in view of the asymmetric bonding to the cyclopentadienone. Some degree of localized bonding to the cyclopentadienyl ring may be responsible for the staggered conformation of the rings (see 2.7). Figure 2.5 shows that the bond C3-C4 diametrically opposite the double bond of the dienone, through the cobalt atom, is the shortest bond in the cyclopentadienyl ring, while C5-C1-C2 is the smallest angle. The average distance (2.05 Å) from the cobalt to C2 and C5 is less than that to both C3 and C4 (2.10 Å) and C1 (2.08 Å). Thus the ring is not quite planar, C1 being bent 3.8° away from the metal about the axis C2-C5 in a manner similar to that found in the dienone ligand (Figure 2.5(a)). The differences are close to the level of statistical significance but the overall pattern of distortions clearly suggests the scheme outlined above. The possibility of such a delocalised scheme as this seems even greater, in the light of our work on dihydridodi-π-cyclopentadienylmolybdenum. (Chapter 3)

* * *

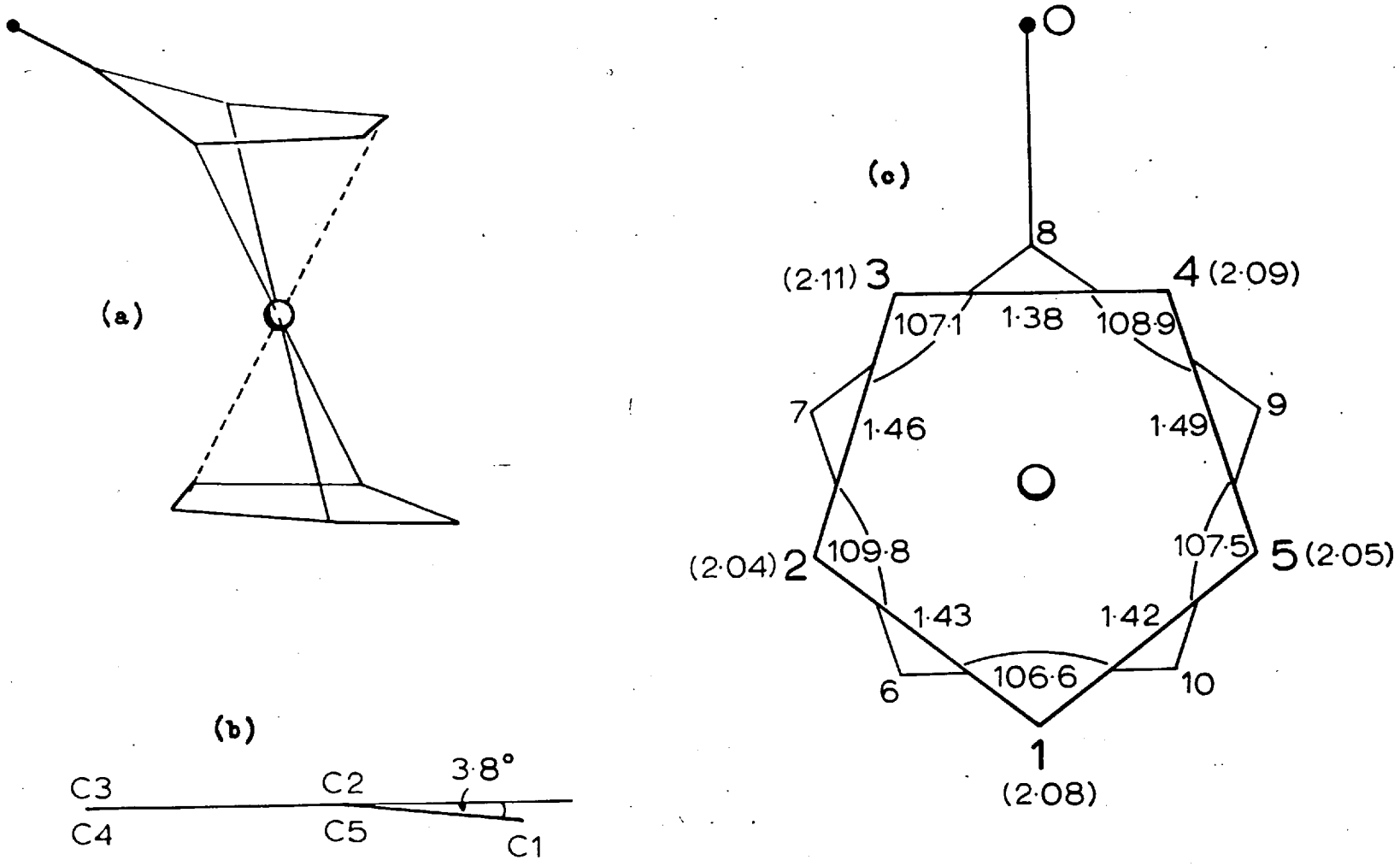


Figure 2.5. $(CF_3)_4C_5O.C_5H_5.Co$.

(a) Arrangement of bonds about the cobalt ion. (b) Non-planarity of the cyclopentadienyl ring.
(c) Staggered configuration of cyclopentadienyl and cyclopentadienone rings: metal-carbon (cyclopentadienyl) bond lengths are given in parentheses.

2.7 Thermal vibrations and crystal packing

The large librational motions of the fluoromethyl groups are evident from the results of Table 2.8 which lists the principal axes of the atomic vibration ellipsoids derived from the atomic Debye parameters (Table 2.3). Figure 2.6 - the Fourier sections of the electron density in the planes of the four groups of fluorine atoms - show directly the non-circular symmetry of the fluorine electron densities. While some elongation of Fourier peaks may result from lattice disordering rather than from librational motions, the above qualitative observations can be explained through considerations of the intramolecular packing of th fluoromethyl groups around the cyclopentadienyl ring.

Assuming Van der Waals' radii of 1.35 Å and 1.40 Å for fluorine and oxygen atoms respectively (Pauling, 1961) the equilibrium separation between two fluorines should be 2.70 Å and between fluorine and oxygen, 2.75 Å. Figure 2.7 illustrates the orientation of and contacts between the four $-CF_3$ groups and the oxygen atom round the cyclopentadienone ring. The close contacts between the fluorine atoms prevent free rotation of the $-CF_3$ group and the proximity of the oxygen atom, preventing excessive movement of the outer pair of $-CF_3$ groups, provides a barrier to coupled rotation of the groups round the ring. Greater freedom of libration will be allowed to the two middle groups (F1-3; F10-12), however, and some degree of coupled oscillations seems likely. Evidence for these motions is to be found in Figure 2.6 which shows a greater spread of electron density for these two groups vis à vis the remaining

Table 2.8 The Principal Axes of the Atomic Vibration Ellipsoids

Atom	$\sqrt{\overline{u^2}}$ max (Å)			$\sqrt{\overline{u^2}}$ med (Å)			$\sqrt{\overline{u^2}}$ min (Å)		
Co		0.233			0.217			0.198	
	0.9635	-0.2600	0.0639	-0.2171	-0.8983	-0.3820	-0.1567	-0.3541	0.9220
C1		0.39			0.33			0.17	
	0.358	0.813	0.460	0.904	-0.177	-0.389	0.234	-0.555	0.798
C2		0.34			0.30			0.23	
	0.811	-0.521	-0.265	0.516	0.851	-0.095	-0.275	0.060	-0.960
C3		0.36			0.27			0.19	
	0.872	0.408	-0.272	-0.169	0.770	0.615	-0.460	0.490	-0.740
C4		0.39			0.37			0.06	
	-0.155	0.595	0.788	0.826	0.516	-0.22	-0.543	0.616	-0.572
C5		0.44			0.30			0.02	
	0.883	0.113	0.455	0.263	0.684	0.680	-0.388	0.720	-0.575
C6		0.27			0.22			0.22	
	0.782	0.618	-0.077	-0.490	0.687	0.536	0.384	-0.382	0.841
C7		0.26			0.24			0.15	
	-0.321	0.582	-0.747	0.837	-0.194	-0.511	-0.493	-0.790	-0.425
C8		0.30			0.26			0.20	
	0.475	-0.566	-0.673	0.50	0.803	-0.322	0.723	-0.184	0.666
C9		028			0.25			0.17	
	0.331	-0.758	-0.563	0.920	0.127	0.370	-0.208	-0.640	0.739
C10		0.29			0.27			0.18	
	-0.072	0.106	-0.992	0.480	-0.868	-0.127	0.874	0.485	-0.011
C11		0.42			0.27			0.21	
	0.402	0.577	-0.711	-0.649	0.727	0.223	0.646	0.372	0.667
C12		0.38			0.31			0.21	
	0.821	-0.290	-0.493	-0.428	0.261	-0.86	-0.379	-0.921	-0.090
C13		0.37			0.27			0.07	
	0.919	-0.299	0.256	-0.387	-0.803	0.452	0.070	-0.515	-0.854
C14		0.37			0.28			0.22	
	0.352	-0.936	0.007	0.372	0.133	-0.919	0.859	0.324	0.395

Table 2.8 (continued)

Atom	$\sqrt{\bar{u}^2}$ max Å			$\sqrt{\bar{u}^2}$ mid Å			$\sqrt{\bar{u}^2}$ min Å		
F1		0.56			0.42			0.19	
	0.708	-0.239	0.664	-0.641	-0.614	0.461	0.298	-0.752	-0.588
F2		0.48			0.41			0.31	
	0.447	0.893	-0.049	0.311	-0.103	0.945	0.839	-0.438	-0.324
F3		0.68			0.32			0.23	
	0.687	0.721	-0.089	0.638	-0.540	0.550	-0.348	0.435	0.831
F4		0.55			0.32			0.22	
	-0.075	-0.106	-0.991	0.629	-0.776	0.036	0.774	0.621	-0.125
F5		0.47			0.37			0.21	
	0.588	-0.424	-0.689	-0.686	0.190	-0.703	-0.429	-0.886	0.179
F6		0.47			0.41			0.27	
	0.719	-0.101	-0.687	-0.451	0.685	-0.572	-0.528	-0.722	-0.447
F7		0.54			0.36			0.25	
	0.346	-0.599	0.722	0.899	0.432	-0.073	0.268	-0.674	-0.688
F8		0.50			0.34			0.19	
	0.902	-0.149	-0.405	-0.085	0.858	-0.506	-0.423	-0.491	-0.762
F9		0.45			0.35			0.22	
	0.998	-0.065	0.000	0.016	0.245	-0.969	-0.063	-0.967	-0.246
F10		0.64			0.41			0.23	
	0.129	-0.868	-0.480	-0.148	0.462	-0.875	0.981	0.184	-0.069
F11		0.77			0.38			0.24	
	0.411	-0.450	0.793	0.480	-0.633	-0.608	0.775	0.630	-0.044
F12		0.61			0.36			0.21	
	0.354	-0.931	-0.088	-0.698	-0.200	-0.688	-0.622	-0.305	0.721
O1		0.33			0.30			0.22	
	0.334	-0.918	0.214	0.689	0.393	0.609	-0.643	-0.056	0.764

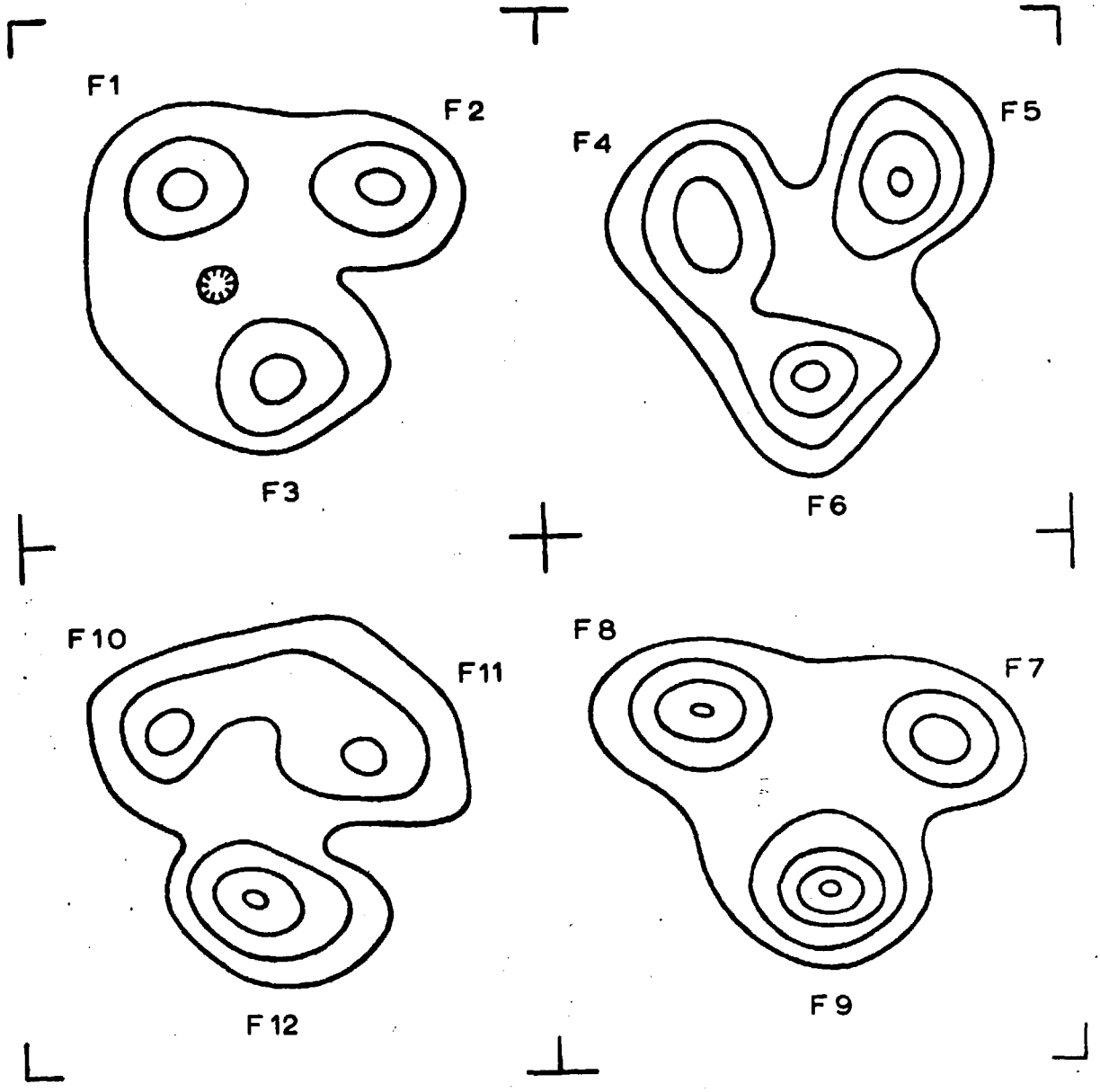


Figure 2.6

Electron density sections through the planes containing the fluorine atoms for each respective fluoromethyl group (contours at equal intervals of 1 e $Å^{-3}$.)

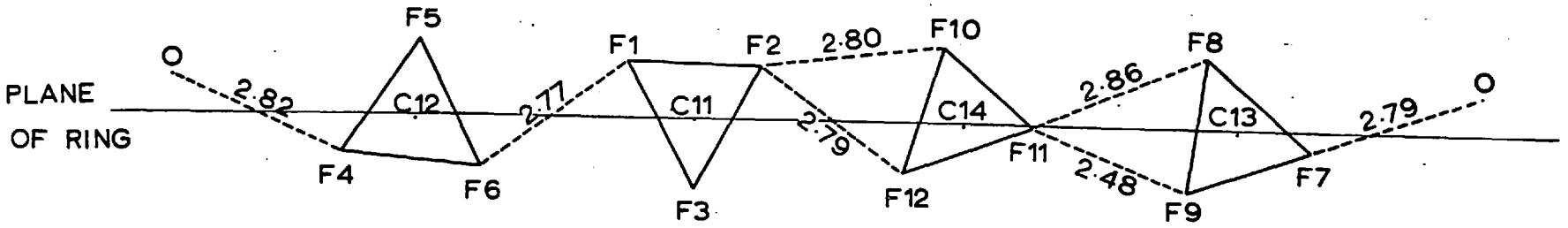


Figure 2.7

Intramolecular fluorine-fluorine contacts around the cyclopentadienone ligand.

fluoromethyl groups, and in Table 2.8. The C-O bond is bent 8° further away from the metal atom than the C7, C8, C9 plane, an explanation of this fact in terms of the intramolecular packing again following from Figure 2.7:- A closer approach of O1 to the plane of the ring would require the group F7, 8, 9 to rotate clockwise to minimise the Van der Waals' repulsive interactions; in turn F10, 11, 12 and F1, 2, 3 would be required to rotate anticlockwise and F4, 5, 6 clockwise. F4 would then be very close to the oxygen atom. In a similar way we can understand the details of the oxygen vibration scheme and of its appearance in the composite Fourier projection (Figure 2.3); all the data are consistent with the hypothesis that a bending vibration of the oxygen atom (out of the plane of Figure 2.7) is more facile than a vertical mode, a vibrational displacement which would bring the oxygen into contact with fluorine atoms F4 and F7. The deviations of C11 and C14 from the C6, 7, 9, 10 plane may also result from intramolecular over-crowding, but are too small to be statistically significant.

A similar, steric, explanation of the non-planarity of the tetramethyl cyclopentadienone ligand may be precluded by the small Van der Waals' radius of hydrogen (1.05 Å - 1.20 Å) relative to fluorine (cf. the free rotation of methyl groups in hexamethylbenzene, which is sterically more crowded than the substituted 5-membered ring, compared with the hexakis(trifluoromethyl)benzene which has been calculated to be non-planar due to fluorine over-crowding (Harris et al., 1960; Pauling, 1930).

It is interesting to compare the geometrics of the fluorine-substituted

cyclopentadienone rings in this cobalt complex and in the compound with $-Fe(CO)_3$ (Bailey et al., loc.cit.). In the latter case the fluoromethyl groups are by no means co-planar with the butadiene part of the ring, and the oxygen atom is not tilted further away from the metal. In both structures there are intermolecular F-F contacts (see Table 2.10) which are as short as the present intramolecular contacts, in some cases. The molecular packing is different for the two compounds, however, the iron complex having space group $P2_1/c$. Thus it appears that the packing energy of the cobalt compound is minimised when the $-CF_3$ groups are co-planar with the ring, causing the incidental oxygen tilt, while that of the iron complex is minimised with non-coplanar $-CF_3$ groups, which do not then interfere with the oxygen atom.

Large librations of the cyclopentadienyl ring about the five-fold axis are indicated by Figure 2.8, which shows an electron density section in the plane of the ring. (see also the relevant $\sqrt{\overline{u^2}}$ of Table 2.8)

The cyclopentadienyl ring is staggered with respect to the cyclopentadienone ring (Figure 2.9) and this can be partly understood in terms of minimising the C-F and H-F non-bonded interactions between the two rings. Figure 2.9(b) [illegible] C-F interactions which are only a little greater than the Van der Waals' contact of 3.15 Å; if an eclipsed form is assumed, the calculated contacts C1-F3 and C4-F9 both become 3.22 Å. The smallest H-F contact observed is 2.91 Å (Van der Waals' contact 2.55 Å) whereas an eclipsed ring produces one of 2.60 Å. For convenience, Table 2.9 compares observed intermolecular contacts with those which have been calculated on

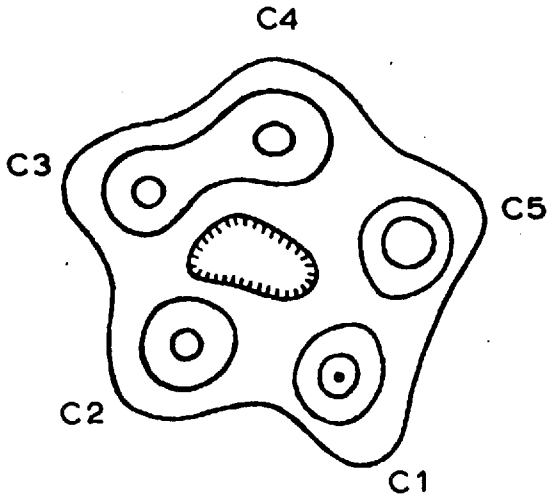
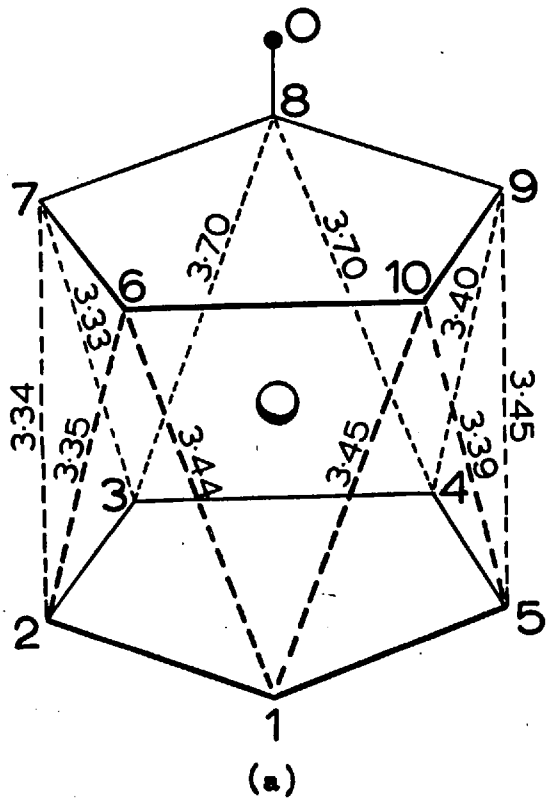
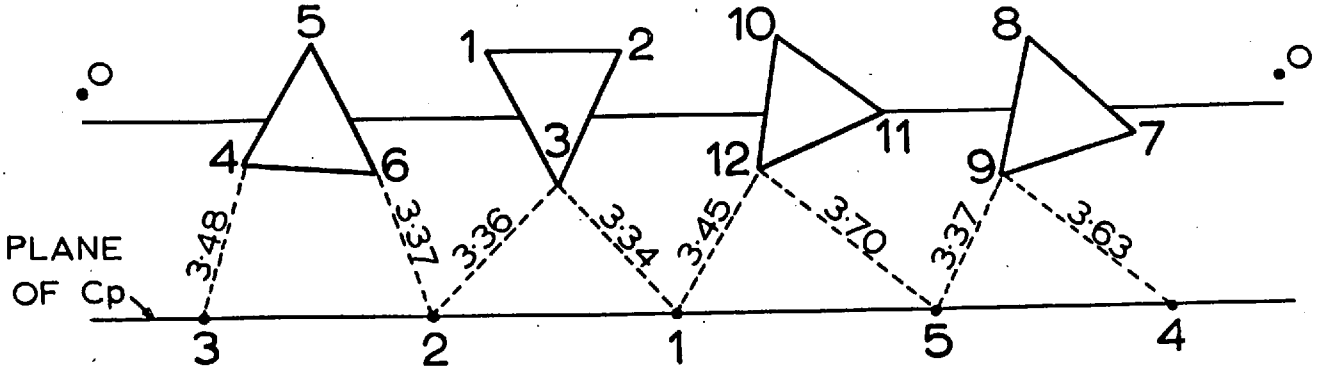


Figure 2.8

The electron density in the mean plane of the cyclopentadienyl ring (contours at equal intervals of 1 e Å^{-3}).



(a)



(b)

Figure 2.9. Intramolecular non-bonded distances between (a) carbon atoms of both ligands, and (b) cyclopentadienyl carbon and cyclopentadienone fluorine atoms.

Table 2.9 The Shorter Intermolecular Contacts between Hydrogen Atoms for the Staggered and Eclipsed Configurations.

Contact		Staggered Configuration (observed) Å	Eclipsed Configuration (not observed) Å
H1 ⟶ H4	$(\frac{1}{2} - x, -\frac{1}{2} + y, -\frac{1}{2} - z)$	2.52	2.86
H2 ⟶ C3	$(\frac{1}{2} - x, -\frac{1}{2} + y, -\frac{1}{2} - z)$	3.32	2.87
⟶ C4	$(\frac{1}{2} - x, -\frac{1}{2} + y, -\frac{1}{2} - z)$	2.84	2.73
H3 ⟶ C8	$(\frac{1}{2} - x, \frac{1}{2} - y, -z)$	3.59	2.71
H1 ⟶ F5	$(x, -y, -\frac{1}{2} + z)$	3.28	3.03
H2 ⟶ F6	$(\frac{1}{2} - x, \frac{1}{2} + y, -\frac{1}{2} - z)$	3.39	2.88
H3 ⟶ F6	$(\frac{1}{2} - x, \frac{1}{2} + y, -\frac{1}{2} - z)$	2.92	3.46
⟶ F7	$(\frac{1}{2} - x, \frac{1}{2} - y, -z)$	2.63	3.08
H4 ⟶ F4	$(\frac{1}{2} - x, \frac{1}{2} - y, -z)$	2.87	3.79
⟶ F5	$(x, 1 + y, z)$	3.03	2.46
⟶ F6	$(x, 1 + y, z)$	3.46	2.70
H5 ⟶ F1	$(x, 1 + y, z)$	2.64	3.62
⟶ F7	$(x, 1 - y, -\frac{1}{2} + z)$	3.16	2.77
⟶ F8	$(x, 1 - y, -\frac{1}{2} + z)$	>4	2.95
H1 ⟶ O1	$(x, -y, -\frac{1}{2} + z)$	3.89	2.58
H2 ⟶ O1	$(x, -y, -\frac{1}{2} + z)$	2.43	3.60
H3 ⟶ O1	$(\frac{1}{2} - x, \frac{1}{2} - y, -z)$	2.68	1.71
H4 ⟶ O1	$(\frac{1}{2} - x, \frac{1}{2} - y, -z)$	2.59	>4

the basis of an eclipsed conformation of the two rings. In contrast to ferrocene (Edwards, Kington and Mason, 1960) a rationale for the staggered arrangement cannot be derived from considering H-H interactions, as the shorter of these - 2.52 Å - becomes larger (2.86 Å) when the eclipsed form is assumed (Table 2.9). However, a number of H-C. H-F and H-O intermolecular contacts do seem relevant, particularly one H-O interaction of 2.68 Å which becomes 1.71 Å in the eclipsed model. It is interesting that three H-O contacts in the (observed) staggered model are short enough (2.43 Å, 2.68 Å, 2.59 Å) to suggest some degree of hydrogen bonding in the crystal. (Sutor, 1963) Thus, the staggered conformation of the ring may derive from intramolecular C-F and H-F interactions and from O-H, hydrogen-bonded or non-bonded intermolecular interactions, or both. These considerations complement the possibility of some localized Co-C bonding to the cyclopentadienyl ring, outlined above.

Observed intermolecular contacts less than 3.8 Å between carbon, fluorine and oxygen atoms are given in Table 2.10. There are several F-F contacts, as mentioned previously, which are as short as the intramolecular interactions in Figure 2.8: these may indicate the possibility of coupled oscillations throughout the crystal.

The molecular arrangement in the unit cell is shown in Figure 2.10 & 2.11 The relatively open structure does suggest that solvent inclusion by addition or substitution may not be too difficult and this hypothesis is borne out by the low observed crystal density. Solvent substitution may be responsible,

Table 2.10 Intermolecular Contacts less than 3.8 Å between Carbon, Fluorine, and Oxygen Atoms.

Contact	Å	Contact	Å
C2 → O1 (x, -y, $-\frac{1}{2}$ + z)	3.36	F1 → F8 (x, -y, $-\frac{1}{2}$ + z)	3.51
C3 → O1 ($\frac{1}{2}$ - x, $\frac{1}{2}$ - y, -z)	3.20	→ F9 (x, -1 + y, z)	3.46
C4 → O1 ($\frac{1}{2}$ -x, $\frac{1}{2}$ - y, -z)	3.15	→ F10 (1 - x, -y, -z)	3.18
C1 → F5 (x, -y, $-\frac{1}{2}$ + z)	3.74	→ F11 (1 - x, -y, -z)	3.77
→ F7 (x, 1 - y, $-\frac{1}{2}$ + z)	3.28	F2 → F2 (1 - x, y, $-\frac{1}{2}$ - z)	3.09
C2 → F6 ($\frac{1}{2}$ - x, $\frac{1}{2}$ + y, $-\frac{1}{2}$ - z)	3.41	→ F3 (1 - x, y, $-\frac{1}{2}$ - z)	3.12
C3 → F6 ($\frac{1}{2}$ - x, $\frac{1}{2}$ + y, $-\frac{1}{2}$ - z)	3.02	→ F8 (1 - x, -y, -z)	3.38
C4 → F5 (x, 1 + y, z)	3.78	→ F10 (1 - x, -y, -z)	3.01
→ F6 ($\frac{1}{2}$ - x, $\frac{1}{2}$ + y, $-\frac{1}{2}$ - z)	3.67	F3 → F8 (x, -y, $-\frac{1}{2}$ + z)	3.20
C5 → F1 (x, 1 + y, z)	3.75	F4 → F4 ($\frac{1}{2}$ - x, $-\frac{1}{2}$ - y, -z)	3.34
→ F6 (x, 1 + y, z)	3.71	→ F5 ($\frac{1}{2}$ - x, $-\frac{1}{2}$ - y, -z)	3.07
→ F7 (x, 1 - y, $-\frac{1}{2}$ + z)	3.32	→ F7 ($\frac{1}{2}$ - x, $\frac{1}{2}$ - y, -z)	3.44
C6 → F10 (1 - x, -y, -z)	3.42	F5 → F7 (x, -1 + y, z)	3.50
C8 → F3 (x, -y, $\frac{1}{2}$ + z)	3.46	→ F9 (x, 1 + y, z)	2.89
C9 → F3 (x, -y, $\frac{1}{2}$ + z)	3.78	F8 → F11 (1 - x, 1 - y, -z)	3.50
C10 → F10 (1 - x, -y, -z)	3.69	F9 → F10 (1 - x, 1 - y, -z)	3.56
C11 → F2 (1 - x, y, $-\frac{1}{2}$ - z)	3.69	→ F11 (1 - x, 1 - y, -z)	3.15
→ F10 (1 - x, -y, -z)	3.53	F10 → F10 (1 - x, -y, -z)	3.44
C12 → F4 ($\frac{1}{2}$ - x, $-\frac{1}{2}$ - y, -z)	3.76	F11 → F11 (1 - x, 1 - y, -z)	2.81
F3 → O1 (x, -y, $-\frac{1}{2}$ + z)	3.23	F12 → F12 (1 - x, y, $-\frac{1}{2}$ - z)	2.62
F6 → O1 (x, -y, $-\frac{1}{2}$ + z)	3.72		

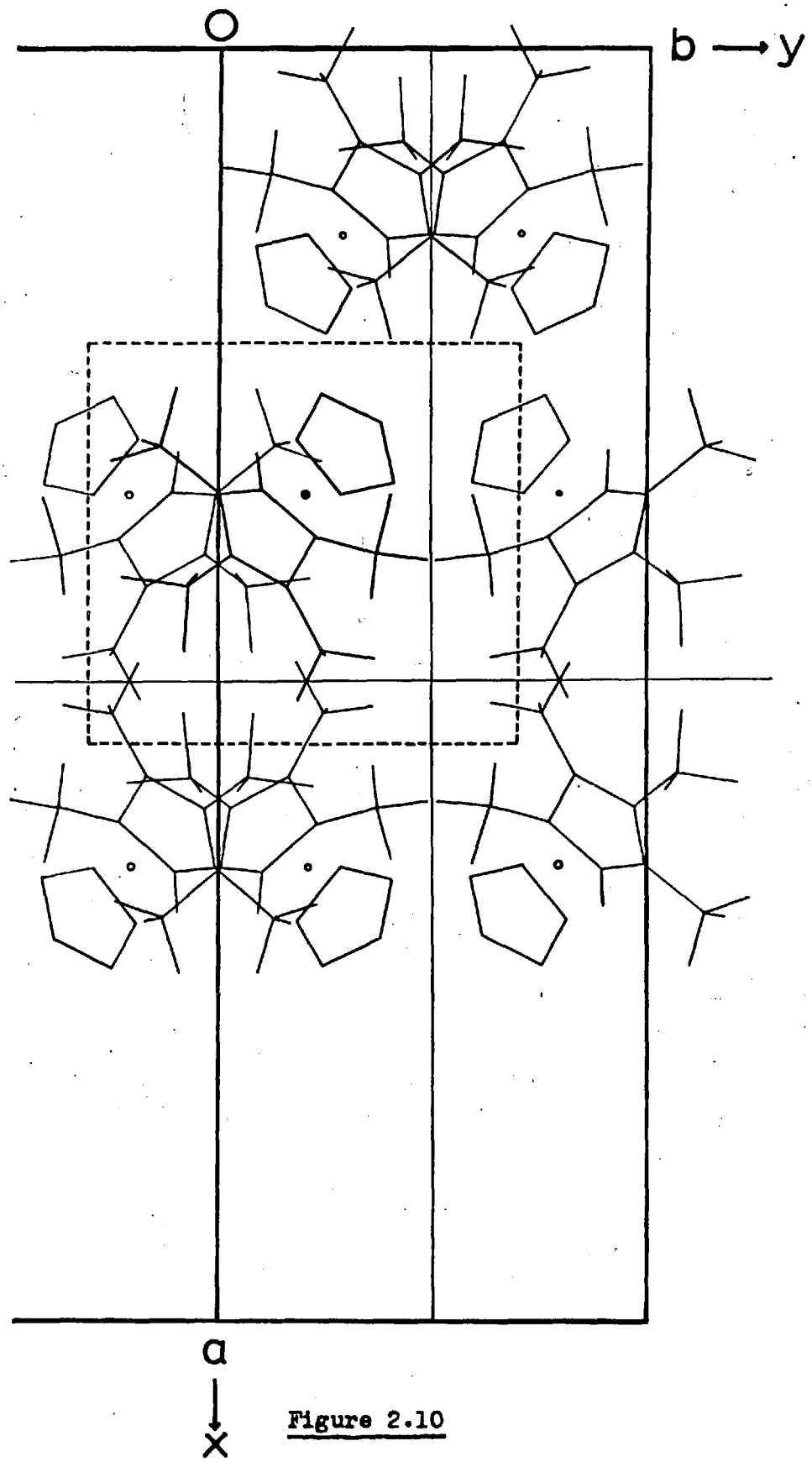
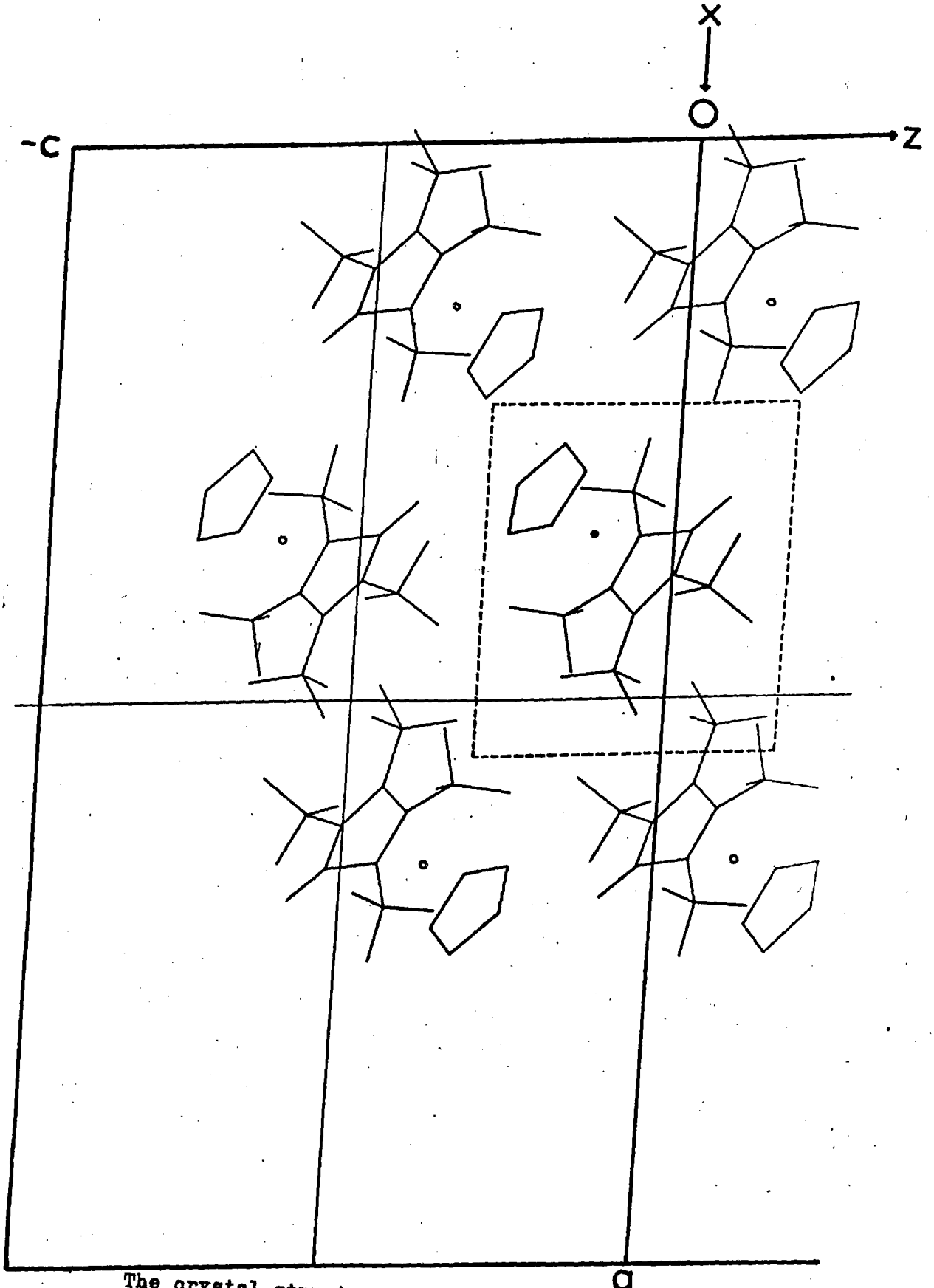


Figure 2.10

The crystal structure projected along 'c'.

Figure 2.11



The crystal structure projected along 'b'.

in part at least, for the rather low electron density found in the Fourier map (Figure 2.3), although the effect of high thermal vibrations and series termination must also play a part.

* * *

2.8 Accuracy

Some observed dimensions in the molecule appear to be in error: one F-F contact is less than the double fluorine Van der Waals' radius; the C-F bond lengths show much scatter and are rather far from the C-F bond length 1.41 Å calculated from Pauling's covalent radii (Pauling, 1960); and the C-C bond lengths in the cyclopentadienone ring do not appear convincing, perhaps, in view of the proposed bonding and ring localization scheme.

While some inaccuracies must result from the relatively low reciprocal lattice coverage (ca. 25% of the limiting sphere, approximately one half of which reflexions were systematically absent), this would serve to increase standard deviations in a systematic manner: the standard deviations listed in Table 2.1 and 2.2 are calculated from Rollet's program assuming random errors in the data and their small anisotropies reflect the differing extents of data coverage in the three principal directions. However, systematic errors will result from describing the large fluorine atom vibrations by simple ellipsoids. Such gross approximations will affect the results of the least squares refinement in two ways: the unrealistic model will cause 'errors' in F_o to be taken up by other parameter shifts in a non-random way; and the

cross-terms involving thermal parameters of the fluorine atoms and the positional and thermal parameters of other atoms (type (iii) in Chapter I) can no longer be assumed negligible. Of course, bond lengths can be corrected for the effects of the ellipsoidal vibration scheme (Cox, Cruickshank and Smith, 1955) but, in view of the large uncertainty in the calculated librational motions, we have not felt justified in carrying out these calculations.

Bearing in mind the remarks made in 1.2, consider the bonds C6-C7 (1.40 Å) and C9-C10 (1.49 Å) which, on chemical grounds may be expected to be of equal length. Following the notation in Chapter 1.2, the standard deviation, σ_1 associated with the probability, P that these bonds could differ by chance equals the r.m.s. of the standard deviations of the bonds; thus

$$\sigma_1 = \sqrt{0.027^2 + 0.027^2} = 0.038 \text{ Å}$$

The difference, $\delta 1$ between the bond lengths = 0.09 Å ≡ 2.36 and, according to the relations (ii) and (iii) in 1.2, this difference is just significant. However, even apart from the chemical unreasonableness of this result, two factors throw doubt on this significance. Even assuming random errors, Rollett's program actually tends to underestimate standard deviations (see 1.2) - a fault which here can be even greater by neglect of the model's systematic errors known to be present. Obviously, the arguments used here to discount the difference between bond lengths C6-C7 and C9-C10 can also be used with equal weight to explain 'anomalous' results elsewhere in the molecule. In defence, it must be said that the standard deviations found

here are quite typical of crystallographic analyses of compounds like the present one, and in addition, this analysis has been very much complicated by the large fluorine atome librations.

The inexactness of this structure determination, does not invalidate the proposed bonding system, however, which rests firmly upon the conformation of the cyclopentadienone ring and, to a lesser extent, upon the analogous compounds quoted. Similarly, although the statistical significance of the suggested asymmetric bonding to the cyclopentadienyl ring is questionable, the overall pattern of distortions, complemented by chemical feasability, suggested that the figures obtained were worth some attention.

* * *

CHAPTER 3

The Crystallography of Dihydridodi-π-cyclopentadienylmolybdenum

3.1 Introduction

Recent studies of transition metal hydrides have led to the preparation of a number of di-π-cyclopentadienyl hydrides of general formula $(\pi\text{-}C_5H_5)_2MH_x$, (x = 1, 2 or 3) (Green, Pratt and Wilkinson, 1958). The hydride complexes are prepared in high yields by the interaction of the anhydrous metal chlorides with a solution of sodium cyclopentadienide in tetrahydrofuran containing an excess of sodium borohydride. The complex hydrides with one or two hydride atoms behave as bases and are soluble in dilute aqueous acids and in trifluoroacetic acid to give the ions $(\pi\text{-}C_5H_5)_2MH_2^+$ or $(\pi\text{-}C_5H_5)_2MH_3^+$; with gaseous hydrogen chloride or bromide the deliquescent halide salts are formed. The tantalum hydride, $(\pi\text{-}C_5H_5)_2TaH_3$ does not appear to behave as a base, even in trifluoroacetic acid, and is decomposed by aqueous acids.

The stereochemistry of these molecules was originally suggested as being a trigonal bipyramid in which parallel cyclopentadienyl rings occupy axial positions; if the cyclopentadienyl anions are formally considered to be tridentate ligands, the proposed structure would be similar to that of $Nd(H_2O)_9^{3+}$. The three hydrogen atoms in the trihydride species $(\pi\text{-}C_5H_5)_2TaH_3$ and $(\pi\text{-}C_5H_5)_2WH_3^+$, are then required to occupy the equivalent equatorial positions, but the high resolution proton magnetic resonance spectra of these complexes indicate only two equivalent hydrogen atoms in an A_2B grouping. The non-

equivalence of the third proton was therefore interpreted as favouring a distorted trigonal bipyramidal structure in which the metal-to-ring axes are non-colinear, the structures of the dihydrido- and monohydrido- complexes being described in a similar way (Green, McCleverty, Pratt and Wilkinson, 1961). Dipole moment and infra-red studies are unable to distinguish unequivocally whether the cyclopentadienyl rings are parallel (Fritz, Hristidu, Hummel and Schneider, 1959) the present X-ray analysis being thus undertaken to determine the relative conformation of the π-cyclopentadienyl ligands.

* * *

3.2 Crystal data

The complex was prepared, in high yield, by the reaction of the anhydrous metal chloride $MoCl_5$ with a solution of sodium cyclopentadienide in tetrahydrofuran containing an excess of sodium borohydride (Green et al., loc.cit.). Pale yellow crystals, of acicular habit, were grown from the reaction mixture by slow sublimination in vacuo, selected crystals being sealed, under nitrogen, in a Lindemann glass capillary. Weissenberg and precession data (Mo $K\alpha$ radiation $\bar{\lambda}$ = 0.7107 Å) gave the monoclinic unit cell dimensions as,
$a = 14.30 \pm 0.04$ Å, $b = 5.90 \pm 0.02$ Å, $c = 10.41 \pm 0.03$ Å, $\beta = 104.0 \pm 0.2^\circ$
$V = 852$ Å^3. With four molecules per unit cell, $\rho_{calc} = 1.78$ gm/cc, the high reactivity of the complex preventing any accurate determination of the density of the crystals. The systematic absences $h0\ell$ for $\ell = 2n + 1$ and $hk0$ for $h + k = 2n + 1$ indicate the space group as either $C2/c$ (C_{2h}^6) or Cc (C_5^4).

In C2/c, the molybdenum atom must lie in a special position – either at a centre of symmetry or on the diad axis. In the first case, reflexions with $\{k+\ell\}$ even should be systematically weak and this is not observed. With the molybdenum at 0, y, $\frac{1}{4}$, the reflexions $\{00\ell\}$ should be systematically strong; this condition is observed but does not, of course, preclude a choice of the non-centrosymmetric space group. The structure was thus initially determined on the basis of Cc so as to avoid any a priori assumption of the molecular symmetry but the final refinement suggests that the molecule may possess exact C_2 symmetry.

Relative intensities of the Weissenberg $\{h0\ell\}$ and $\{h1\ell\}$ data were estimated visually by standard methods; the $\{hk0\}$ and $\{0k\ell\}$ precession data were initially measured by a Joyce-Loebl microdensitometer but, since these data appeared to contain systematic errors, these zones were later re-estimated visually. These 274 intensities have not been corrected for absorption, being derived from a crystal of 0.2 mm average cross-section.

* * *

3.3 Determination and refinement of the structure

The Patterson symmetries for spacegroups C2/c and Cc have been discussed in general terms in the preceding chapter. With only four molecules in the unit cell, they are unable to distinguish the spacegroups, only the heavy atom y-coordinate being determined. The Patterson series $P(\overline{u}v0)$ gave the y-co-ordinate of molybdenum as 0.33, the x and z co-ordinates being fixed as 0 in

the spacegroup Cc.

The electron density synthesis ρ (xy0), phased by the molybdenum atom showed peaks consistent with a cyclopentadienyl ring together with a mirror-related series of peaks generated by the symmetry of the heavy-atom-phased Fourier series. The origin of this extra symmetry is as follows:
The Fourier series representing a repeat unit containing only one atom may be considered as a series of Fourier 'waves' each of which has its crest at the atom. In general, each wave will have a phase ϕ at the origin of the repeat unit: however, if the unit cell contains two atoms related by a centre of symmetry at the origin, the phase ϕ must, for all waves, be 0 or π. Thus, in this centrosymmetric case the phase of each Fourier wave at the atom must be general and the atom will be located at the resultant crest of all the Fourier waves in that region. In the non-centrosymmetric case, the atom lies simultaneously at the crests of all Fourier waves and thus defines a centre of symmetry - this has been observed for the h0ℓ projection which lacks all but spacegroup translational symmetry. Both the hk0 and 0k ℓ projections, hoeever, have mirror spacegroup symmetry and therefore, any Fourier waves which pass through the mirror planes cannot, in general, have crests at the atom: those waves which 'propogate' parallel to the symmetry planes are unrestricted by such considerations and, therefore, do have crests at the atom. Accordingly, the hk0 and 0kℓ projections phased only by the molybdenum atom have a 'false' mirror plane perpendicular to that produced by the space-group.

The false additional symmetry in $\rho(xy0)$ was removed when the contribution of one cyclopentadienyl ring were included in the structure factor calculations, the subsequent Fourier map suggesting two possible positions for the second cyclopentadienyl ring. Of these, one allowed the reliability factor R(hk0) to be reduced from 0.23 to 0.07 in three cycles of least squares refinement of molybdenum positional and anisotropic thermal parameters and carbon coordinates and isotropic B factors. Approximate z-coordinates for all atoms were obtained from a model combined with the previously determined x and y parameters, these values giving $R(h0\ell) = 0.19$ and $R(0k\ell) = 0.17$, respectively. The final scaling together of the three zones was via the calculated structure factors, least squares refinement of the 201 observed reflexions progressing smoothly from 0.17 to 0.098 in eight cycles. The Difference density syntheses D(xy0) and D(x0z) computed at this stage showed significant peaks near the molybdenum atom in positions where the two hydride atoms might be expected.

It was now clear that the molecule was wedgelike (Figure 3.1), having essentially two-fold symmetry. A new refinement was begun, placing the molybdenum at 0, y, $\frac{1}{4}$, that is on a diad axis in C2/c, the least squares analysis being based, now, on the visually estimated intensities for all 274 reflexions from the $\{hk0\}$, $\{h0\ell\}$, $\{0k\ell\}$ and $\{h1\ell\}$ zones. Successive adjustment of the positional and anisotropic thermal parameters of the crystallographically non-equivalent molybdenum and five carbon atoms slowly reduced the reliability index from 0.098 to 0.087 in 5 cycles, all hydrogen atom contributions to the structure factors being included. The final atomic

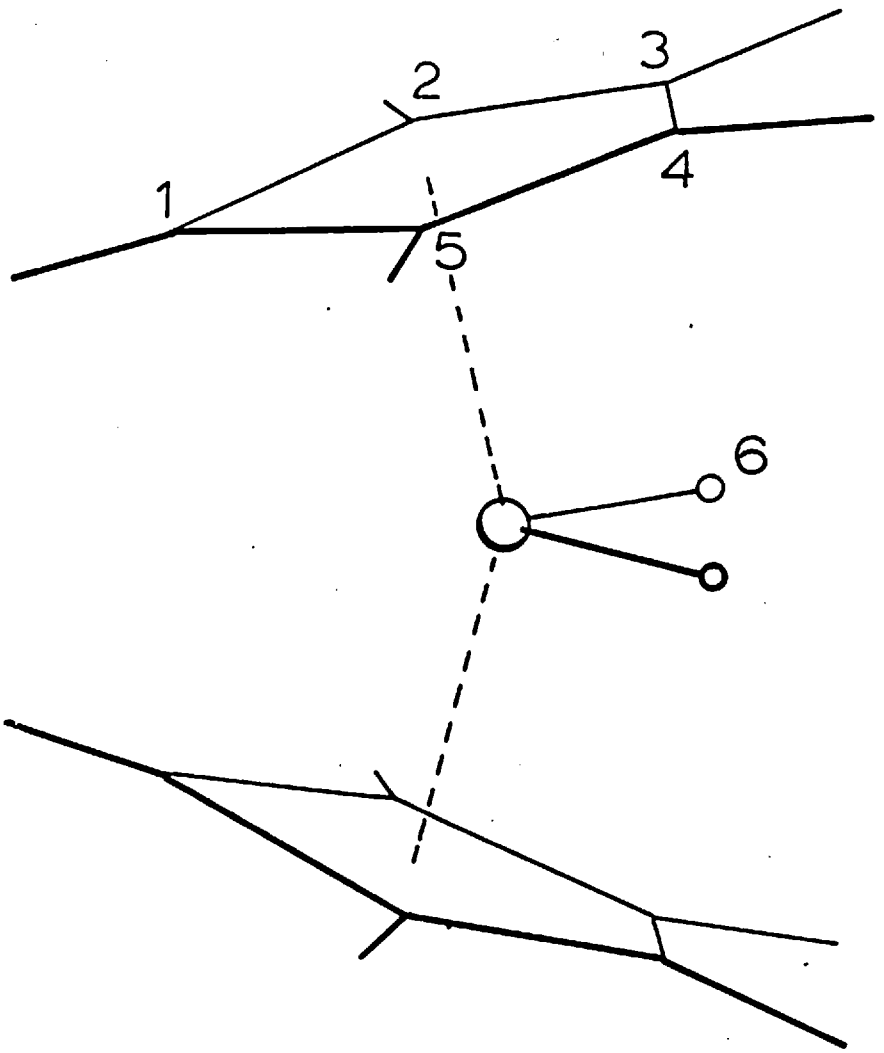


Figure 3.1

$(\pi\text{-}C_5H_5)_2MoH_2$. Molecular Configuration and Numbering of Atoms

co-ordinates are shown together with their e.s.d.'s in Table 3.1, while the thermal coefficients, b_{ij}, are listed in Table 3.2: observed and calculated structure factors are given in Table 3.3.

Several Difference density syntheses were finally calculated, at this stage, subtracting all Mo + 5C + 5H atoms. D(x0z) and D(xy0) again show peaks in the hydride atom positions (Figures 3.2 (a) and (b)), severe overlap preventing a simple interpretation of D(0yz). The peak heights of 0.3 - 0.6 $e\text{Å}^{-2}$ are certainly close to the level of significance ($\sim 2 - 3\sigma$) but their appearance in chemically reasonable positions adds some weight to the argument for regarding them as genuine rather than as anomalous 'ghost' peaks produced by the molybdenum atom. Some check of this was made by constructing the Difference map (xy0) using only those contributions from reflexions with $\sin\theta \lesssim 0.5$, a procedure which minimises Fourier features produced predominantly by any inexact temperature factor of the heavy molybdenum atom. The resulting map (Figure 3.2(c)) clearly shows marginal attenuation of the peaks ascribed to the hydride atoms while all other peaks, especially the large negative feature at (0,0,0), have been greatly diminished. Perhaps the principal reason why the hydrogens have been apparently located lies in the very small thermal vibrations which these bonded atoms would, in all probability, execute; the marked dependence of ρ_{obs}(hydrogen) on temperature factor is well known. (McDonald, 1956).

* * *

Table 3.1 Atomic co-ordinates and e.s.d.'s

Atom	x/a	y/b	z/c	(X) Å	(Y) Å	(Z) Å
Mol	0	0.33188	¼	-	0.0039	-
C1	-0.1027	0.0610	0.2712	0.020	0.025	0.029
C2	-0.1459	0.1796	0.1634	0.019	0.038	0.037
C3	-0.1667	0.4145	0.2027	0.019	0.037	0.032
C4	-0.1290	0.4187	0 3423	0.021	0.039	0.027
C5	-0.0897	0.1906	0.3849	0.023	0.031	0.026
H1	-0.080	-0.113	0.270			
H2	-0.167	0.111	0.058			
H3	-0.200	0.548	0.140			
H4	-0.131	0.563	0.405			
H5	-0.054	0.140	0.485			
H6*	-0.033	0.500	0.200			

Values, not refined, were obtained by geometrical calculation

* Value obtained from Difference Fourier maps - see text

Table 3.2 Atomic Debye Factors

$$T = 2^{-(b_{11}h^2 + b_{22}k^2 + b_{33}l^2 + b_{23}kl + b_{13}hl + b_{12}hk)}$$

Atom	b_{11}	b_{22}	b_{33}	b_{23}	b_{13}	b_{12}
Mo1	0.00448	0.02685	0.01180	0	0.00407	0
C1	0.0046	0.0236	0.0264	0.0181	0.0058	-0.0048
C2	0.0031	0.0590	0.0427	-0.0068	0.0094	-0.0149
C3	0.0034	0.0791	0.0353	0.0810	0.0040	0.0046
C4	0.0063	0.0648	0.0239	-0.0167	0.0176	0.0071
C5	0.0036	0.0249	0.0216	0.0133	0.0177	-0.0045

H1 - 5 calculated with b_{ij}'s of C1 - 5

Table 3.4 (a) Bond lengths and e.s.d.'s

Bond	Length Å	e.s.d. Å	Bond	Length Å	e.s.d. Å
Mo - C1	2.22	0.021	C1 - C2	1.34	0.041
Mo - C2	2.25	0.022	C2 - C3	1.51	0.052
Mo - C3	2.37	0.022	C3 - C4	1.42	0.042
Mo - C4	2.34	0.023	C4 - C5	1.49	0.050
Mo - C5	2.28	0.024	C5 - C1	1.39	0.037

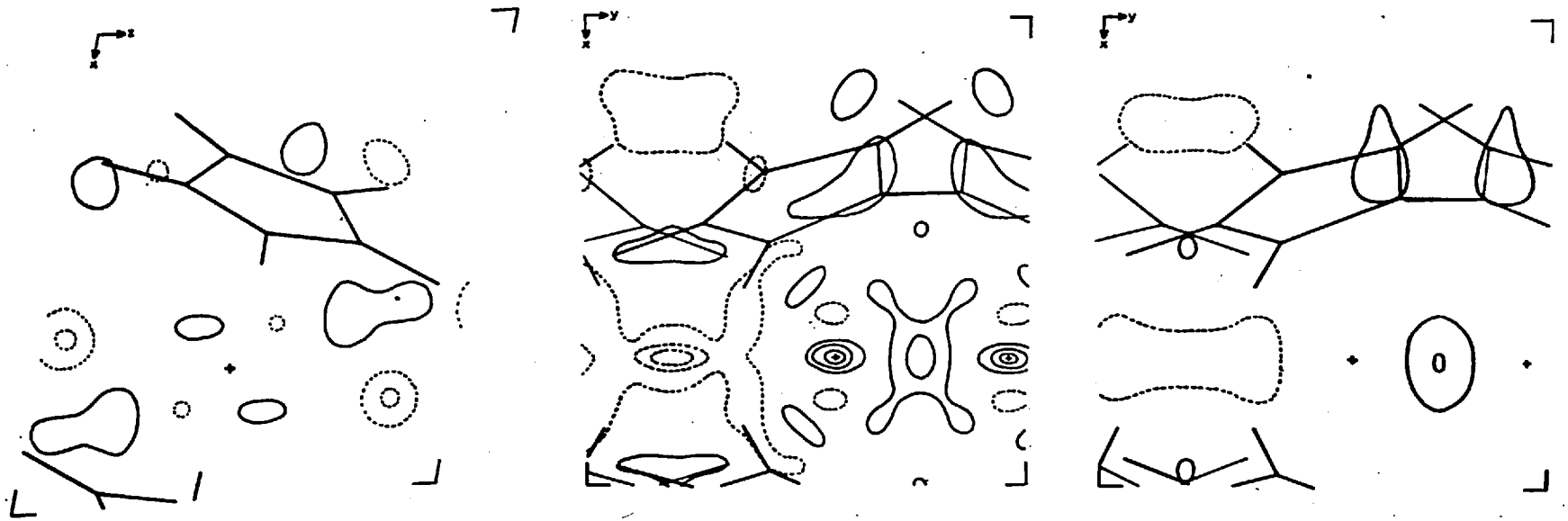
(b) Bond angles and e.s.d.'s

Bonds	Angle (o)	e.s.d. (o)	Bonds	Angle (o)	e.s.d (o)
C1 - Mo - C2	34.8	1.1	C5 - C1 - C2	111.9	2.7
C2 - Mo - C3	38.1	1.3	C1 - C2 - C3	109.3	2.5
C3 - Mo - C4	35.1	1.1	C2 - C3 - C4	104.3	2.7
C4 - Mo - C5	37.8	1.2	C3 - C4 - C5	108.1	2.5
C5 - Mo - C1	35.9	1.0	C4 - C5 - C1	106.4	2.5

h	k	l	$\|F_o\|$	F_c
1	1	1	4019	-4267
3	1	1	5060	-4713
5	1	1	8326	-2589
9	1	1	3083	-2827
11	1	1	8263	-2347
13	1	1	2349	-2335
15	1	1	854	-988
17	1	1	938	1572
1	1	-1	8372	8807
3	1	-1	6942	6104
5	1	-1	4001	3972
7	1	-1	3326	2405
9	1	-1	2276	2413
11	1	-1	1530	1603
13	1	-1	888	948
15	1	-1	963	981
17	1	-1	2887	3274
1	1	2	2359	2510
3	1	2	2946	2934
5	1	2	2060	2225
7	1	2	1597	1618
9	1	2	1174	1357
11	1	2	538	714
13	1	2	2339	2750
1	1	-2	1914	2094
3	1	-2	3450	3407
7	1	-2	1010	1146
11	1	-2	2164	2374
13	1	-2	1144	1062
15	1	-2	1082	-1627
1	1	4	2460	-2500
3	1	4	2419	-2594
5	1	4	1108	-1435
7	1	4	888	-1146
9	1	4	1144	-1158
11	1	4	1988	-2278
1	1	-4	2450	-2745
3	1	-4	3020	-3367
5	1	-4	2431	-2479
7	1	-4	1269	-1454
11	1	-4	2096	-2480
13	1	-4	590	-818
15	1	-4	2419	-2719
1	1	5	3955	-3690
3	1	5	3575	-3313
5	1	5	1836	-2088
7	1	5	2025	-2204
9	1	5	1889	-1910
11	1	5	761	-992
13	1	5	664	-792
15	1	5	3785	3954
1	1	-5	5502	5391
3	1	-5	3728	4124
5	1	-5	2622	2849
7	1	-5	2757	2700
9	1	-5	2326	2446
11	1	-5	2025	2037
13	1	-5	1597	1727
15	1	-5	1428	1424
17	1	-5	2704	2691
1	1	7	3010	2607
3	1	7	1756	1905
5	1	7	1323	1481
7	1	7	1038	1218
11	1	7	798	798
13	1	7	3010	-3142
1	1	-7	3244	-3399
3	1	-7	2371	-2364
5	1	-7	1874	-1961
7	1	-7	2326	-2699
9	1	-7	2509	-2631
11	1	-7	1597	-1661
13	1	-7	854	-1104
15	1	-7	1144	-1105
17	1	-7	938	-942
1	1	8	2292	-1284
3	1	8	706	-912
5	1	8	664	-445
7	1	8	1756	-1550
11	1	8	2040	-1295
1	1	-8	1038	-1210
3	1	-8	1144	-1053
5	1	-8	1144	-1275
7	1	-8	888	-767
9	1	-8	1108	1091
15	1	-8	2082	2139
1	1	-10	761	725
3	1	-10	1010	931
5	1	-10	1082	1188
9	1	-10	963	1019
1	1	11	798	855
3	1	11	798	734
7	1	11	1144	-1106
1	1	-11	1144	-1218
3	1	-11	1232	-1461
5	1	-11	1428	-1585
7	1	-11	1208	-1153
9	1	-11	761	-732
11	1	-11	798	-816
13	1	-11	2413	-2457
0	2	0	2280	-2382
0	4	0	1754	1892
0	6	0	1000	-987
0	8	0	3567	-2769
1	1	0	4068	3735
1	3	0	1027	-932
1	5	0	943	-855
1	7	0	3274	-3395
2	2	0	2892	-2626
2	4	0	1848	2049
2	6	0	695	-644
2	8	0	2138	-1777
3	1	0	5099	5265
3	3	0	2104	-1945
3	5	0	695	-543
3	7	0	646	-192
4	0	0	3364	-3304
4	2	0	1254	-1266
4	4	0	2041	2007
4	6	0	277	-180
4	8	0	5347	-4601
5	1	0	4592	4607
5	3	0	1569	-1545
5	5	0	524	-543
5	7	0	5844	5921
6	0	0	2535	-2319
6	2	0	1719	-1687
6	4	0	1622	1638
6	6	0	3854	-3439
7	1	0	3215	3352
7	3	0	1059	-1009
7	5	0	393	-378
7	7	0	5637	5340
8	0	0	1624	-1692
8	2	0	1318	-1352
8	4	0	1482	1348
8	6	0	1305	-1164
9	1	0	3219	3153
9	3	0	1232	-1206
9	5	0	671	-621
9	7	0	3241	3418
10	0	0	1363	-1270
10	2	0	960	-816
10	4	0	1651	1132
10	6	0	1048	-1144
11	1	0	2469	2653
11	3	0	1148	-806
11	5	0	3270	3309
12	0	0	1579	-1490
12	2	0	877	-713
12	4	0	1363	1123
12	6	0	1204	-1214
13	1	0	1586	1538
13	3	0	584	-357
13	5	0	2051	2141
14	0	0	1530	-1430
14	2	0	1059	-731
14	4	0	1266	-995
15	1	0	1589	1278
15	3	0	770	-554
15	5	0	1558	1267
16	0	0	1084	-619
16	2	0	1318	-1016
17	1	0	1460	1389
17	3	0	1445	1256
18	0	0	756	-294
18	2	0	770	-384
19	1	0	12229	-11970
0	0	2	4274	4597
0	0	4	4243	-3693
0	0	6	3010	2977
0	0	8	2828	-1788
0	0	10	1546	1065
0	0	12	723	-633
0	0	14	3602	4596
0	2	1	1372	1431
0	2	2	4993	-5044
0	2	3	1029	-1038
0	2	4	3158	3476
0	2	5	2248	1582
0	2	6	1926	-2001
0	2	7	2886	-2319
0	2	8	1588	1585
0	2	9	981	706
0	2	10	1174	-1139
0	2	11	732	-464
0	2	12	772	649
0	2	13	2128	-2321
0	4	1	1703	1851
0	4	2	3623	3639
0	4	3	1133	-1189
0	4	4	2574	-3112
0	4	5	1023	651
0	4	6	1700	1853
0	4	7	607	-606
0	4	8	1696	-1294
0	4	9	755	497
0	4	10	919	911
0	4	11	654	-298
0	4	12	763	-399
0	6	1	1503	-1622
0	6	2	1495	1350
0	6	4	1591	-1335
0	6	6	588	86
0	6	7	969	1175
0	6	8	627	721
0	8	1	723	722
0	8	2	801	-642
0	8	3	7650	-7493
2	0	2	5957	-5818
4	0	2	6889	-7237
6	0	-2	7025	-7183
8	0	-2	5021	5793
4	0	4	5741	6165
2	0	-4	5073	-4538
6	0	2	2784	-2916
8	0	2	3585	-3460
10	0	2	3215	-3170
12	0	2	1310	-1383
14	0	2	1049	-1098
16	0	2	1223	-1328
18	0	2	0	-307
4	0	-2	3188	-3208
10	0	-2	2685	-2594
12	0	-2	2284	-2417
14	0	-2	1534	-1485
16	0	-2	1164	-1256
18	0	-2	1139	-1196
20	0	-2	4785	4841
2	0	4	3256	3506
6	0	4	2085	2206
8	0	4	2659	3120
10	0	4	2068	2312
12	0	4	1049	999
16	0	4	998	517
20	0	4	5804	5495
4	0	-4	6139	5433
6	0	-4	4999	4559
8	0	-4	3139	2929
10	0	-4	2944	2624
12	0	-4	2153	2235
14	0	-4	1688	1691
16	0	-4	1432	1545
18	0	-4	1072	1102
20	0	-4	3253	2805
2	0	8	2390	2327
4	0	8	1424	1551
6	0	8	1353	1384
8	0	8	1251	1350
10	0	8	784	972
12	0	8	827	716
14	0	8	3320	3056
2	0	-8	2654	2358
4	0	-8	1982	2045
6	0	-8	1339	2999
8	0	-8	3215	3142
10	0	-8	1874	1921
12	0	-8	1114	1032
14	0	-8	1114	1119
16	0	-8	1154	1376
18	0	-8	827	894
20	0	-8	2017	-1740
2	0	10	1353	-1466
4	0	10	1049	-1133
6	0	10	1103	-951
8	0	10	1664	-1658
10	0	-10	1472	-1599
2	0	-10	2118	-2050
4	0	-10	2230	-2416
6	0	-10	1545	-1700
8	0	-10	706	-833
10	0	-10	1103	-990
12	0	-10	1154	-1318
14	0	-10	1038	-1006
16	0	-10		
18	0	-10		

Table 3.3 $(\pi\text{-}C_5H_5)_2MoH_2$. Observed and Calculated Structure Factors (x50)

Figure 3.2



(a) (b) (c)

Difference Fourier Projections : zero contours not shown

(a) D(x0z) with all terms included : contours at $0.3e\text{Å}^{-2}$ intervals

(b) D(xy0) with all terms included : contours at $0.5e\text{Å}^{-2}$ intervals

(c) D(xy0) including only terms for which $\sin\theta \leq 0.5e\text{Å}^{-2}$ contour intervals

3.4 Discussion

The first feature of chemical interest - the mutual orientation of the cyclopentadienyl rings - confirms the suggestions of Wilkinson et al. (loc.cit.) and rules out configurations similar to those of the $Nd(H_2O)_9^{3+}$ and $(TaF_7)^{2-}$ ions. The cyclopentadienyl rings are essentially planar (r.m.s. deviation, 0.007 Å), the direction cosines of the normal to the mean plane of the reference ring being -0.9486, -0.2932, 0.1190, referred to the orthogonal axes a, b and c'. The angle between the π-cyclopentadienyl rings of one molecule is, therefore, $34.1^{\circ} \pm 1^{\circ}$.

Molecular orbital calculations on protonated sandwich compounds have been reported by Ballhausen and Dahl (1961) who showed that the angle of tilt between the rings could not exceed 45°; within this limit, overlap between the ring molecular orbitals and metal hybrid orbitals was not reduced a great deal, that is, there is little loss in metal-ligand bond strength. With these angular bonds, it followed, without recourse to f-orbitals, that in addition to the six metal bonding orbitals, there remained three strongly space-directed orbitals on the metal, orientated in the plane bisecting the angle between the π-cyclopentadienyl rings (Figure 3.3). Two orbitals, ψ_y and ψ_{-y}, are equivalent ($spd_{x^2-y^2}$, d_{z^2} hybrids) and different from the third, ψ_o (an sp hybrid), and together with the six bonding orbitals directed at the rings, make up a new form of nine co-ordination (see also Bennett and Mason, 1963). In the dihydride species, the non-bonding pairs of electrons occupy ψ_o, a configuration which is more stable than that of the $(TaF_7)^{2-}$ ion. It is,

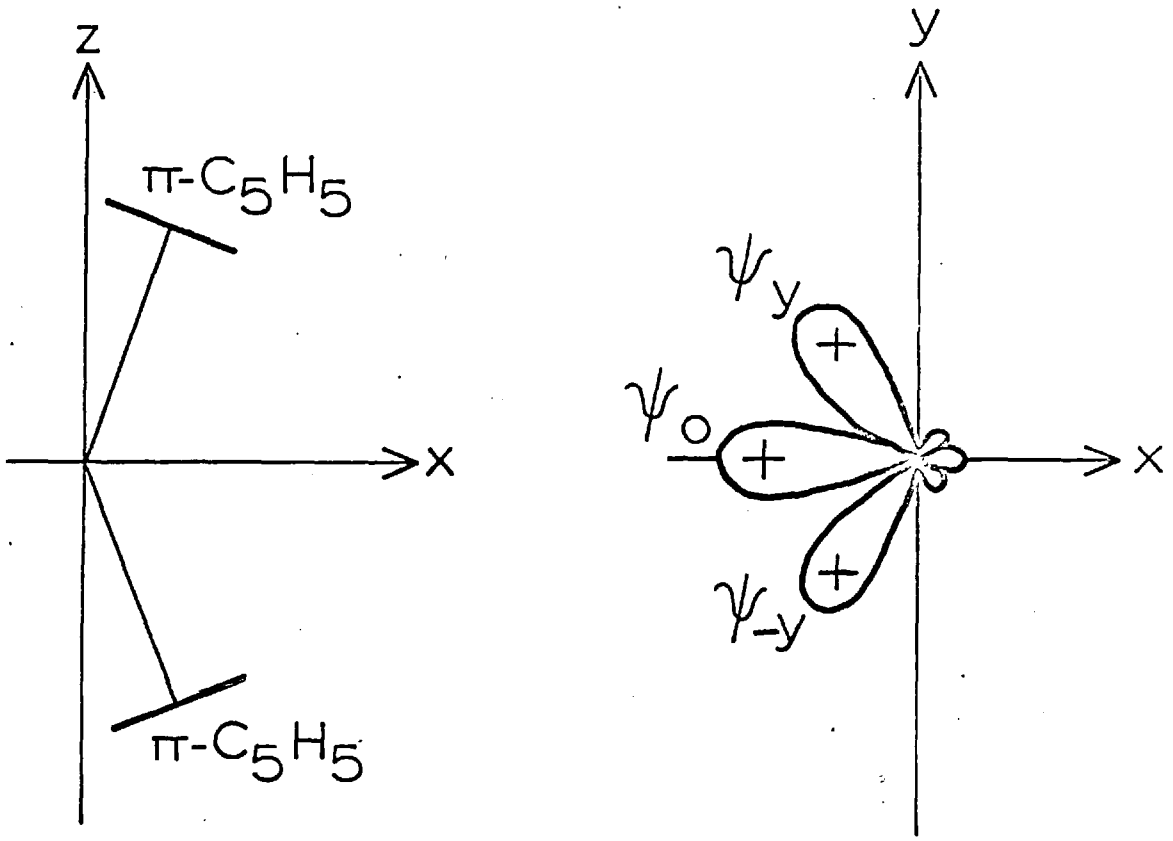


Figure 3.3

The disposition of the cyclopentadienyl rings and available metal orbitals (after Ballhausen and Dahl, 1961)

however, difficult to understand why the trihydrides share this asymmetric geometry; it may be that the $Nd(H_2O)_9^{3+}$ ion finds the Ballhausen-Dahl geometry unfavourable because of the greater steric effects between the H_2O ligands compared with those between the hydride atoms and thus adopts what might otherwise be the more unstable, symmetrical structure.

Perhaps the most important result of the present analysis is the lack of five-fold symmetry in the cyclopentadienyl rings. Bond lengths and angles, together with their e.s.d.'s have been collected in Table 3.4 and some are shown in Figure 3.4 to illustrate the point. The idea is not quite new.

Since the discovery of ferrocene, bis-π-cyclopentadienyliron, the cyclopentadienyl ligand has been used in the preparation of a large number of organometallic compounds. Its π-bonded complexes have often been described by fairly sophisticated theories although one difficulty in assessing the value of the various structural models has been the lack of precise values of molecular parameters; even in ferrocene, disorder in the crystal makes an accurate determination of carbon-carbon bond lengths somewhat difficult. (Edwards, Kington and Mason, 1960). Figure 3.5 compares the cyclopentadienyl bond lengths found in the structures reported in this and the preceding chapter together with two other recent analyses.

It is assumed, and generally accepted, that in the bis-π-cyclopentadienyls or any other π-cyclopentadienyl complex possessing essentially

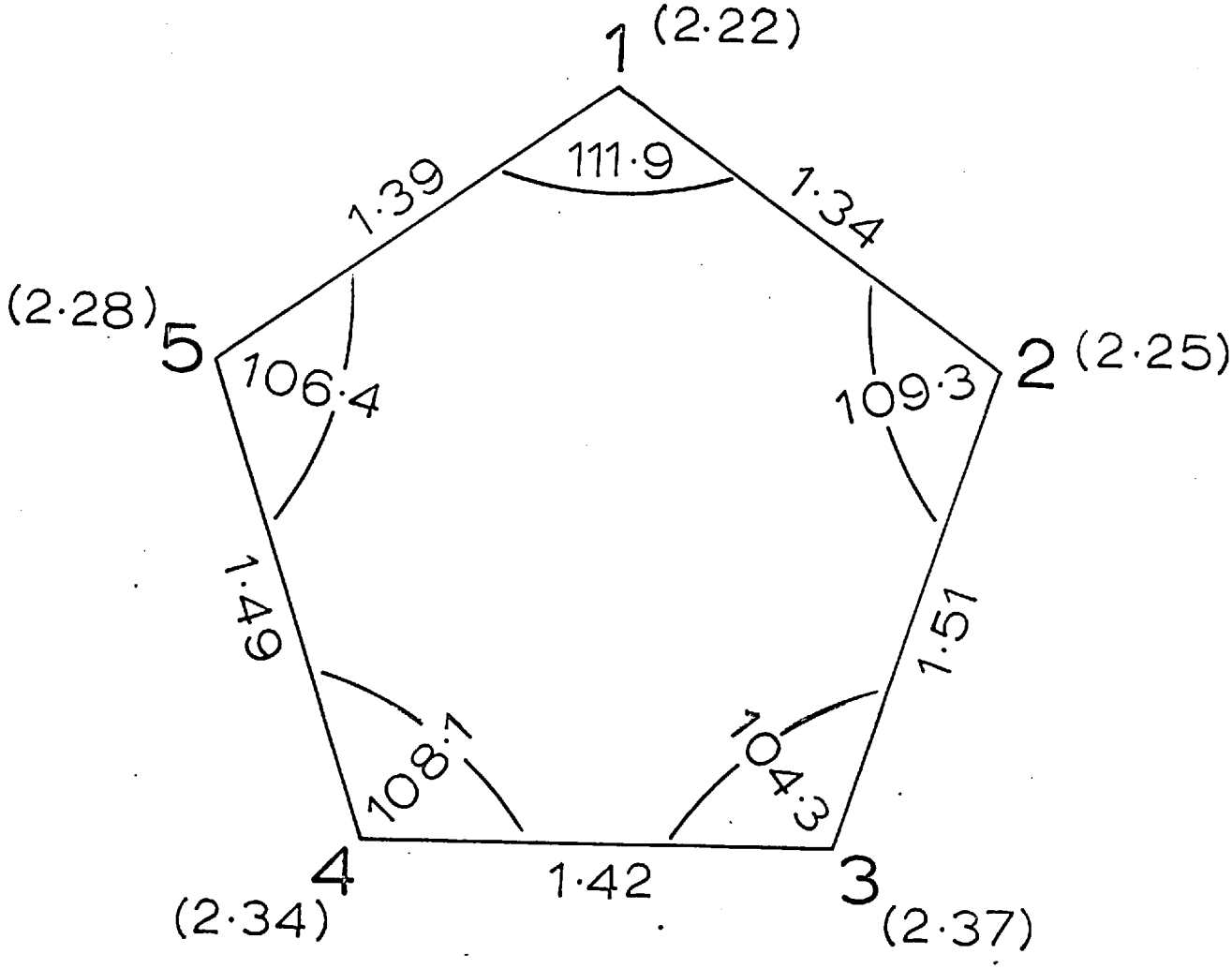
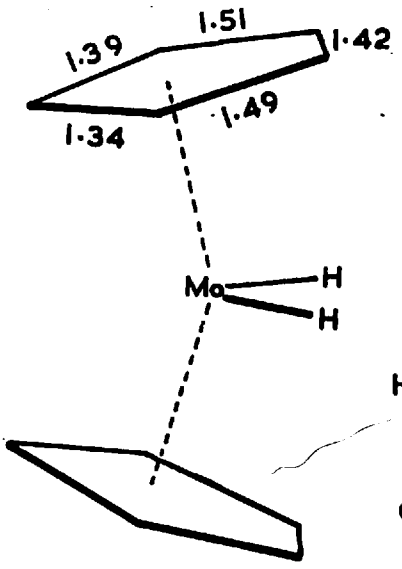


Figure 3.4

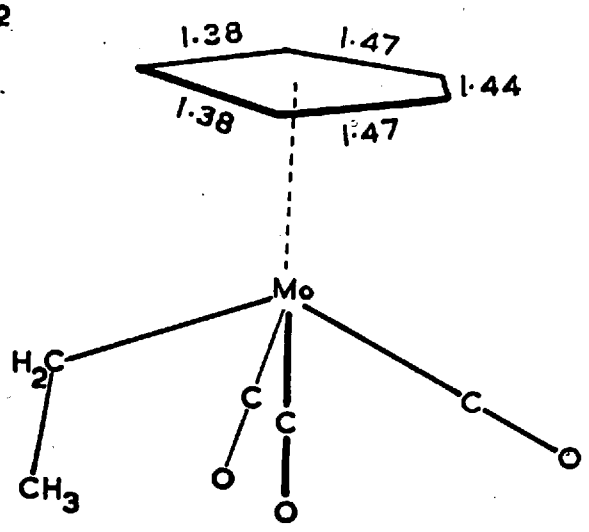
$(\pi\text{-}C_5H_5)_2MoH_2$. Dimensions in the cyclopentadienyl ring: molybdenum-carbon bond lengths are shown in parentheses

Figure 3.5 The lack of 5-fold symmetry in the cyclopentadienyl ligand



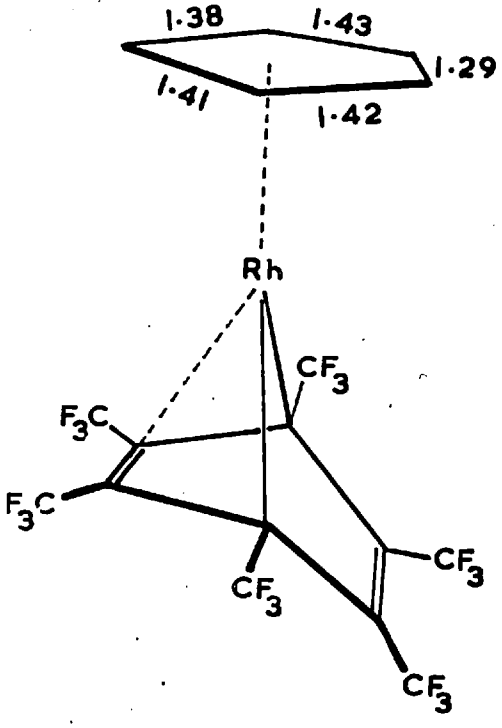
a

(This chapter)



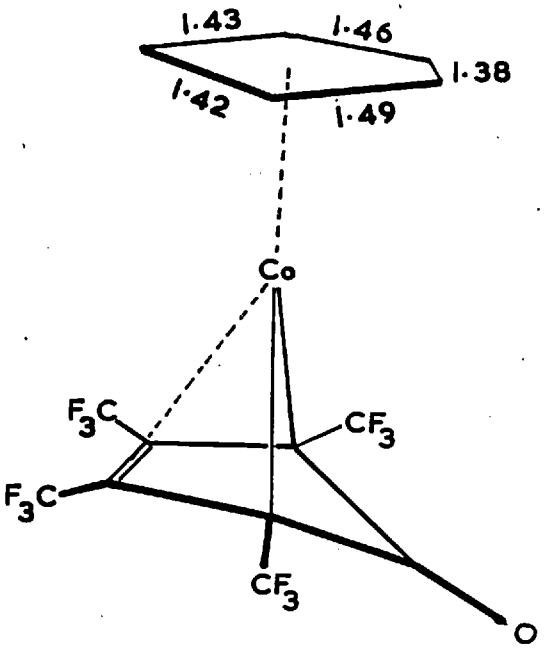
b

(Bennett and Mason, 1963)



c

(Churchill and Mason, 1964)



d

(Previous chapter)

cylindrical symmetry around the metal ion (for example, π-cyclopentadienyl manganese tricarbonyl), the carbon-carbon bond lengths in the cyclopentadienyl ligand are all, within experimental error, identical. The molecular geometries summarised here are constant in their pattern and distinguished by (i) the lack of cylindrical symmetry around the metal ion and, as we suggest, as a consequence (ii) localisation of electron density in the cyclopentadienyl ring; the standard deviations of the carbon-carbon band lengths range up to 0.04 Å so that significance can be attached to a number of the bond length differences of Figure 3.5.

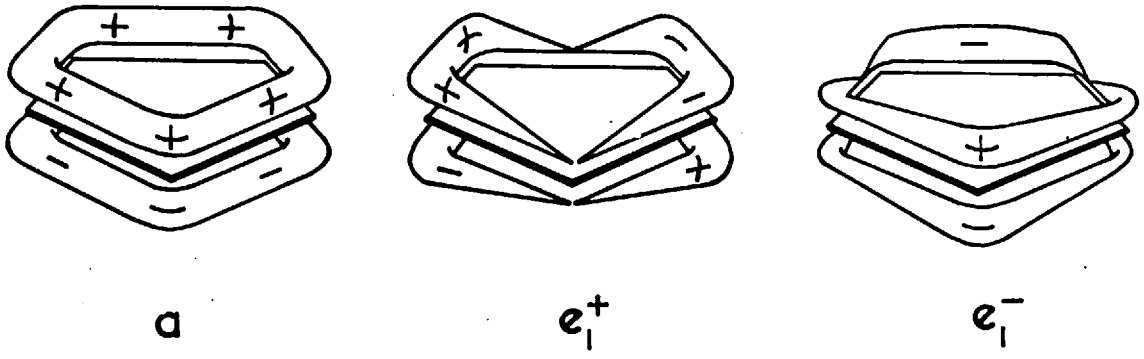
The first discussion of the possibility of localised metal-cyclopentadienyl bonding is that of Dahl and Wei (1963) relating to the structure of [2,3-bis-(methoxycarbonyl)-2π, 5-norbonadien-7-yl] π-cyclopentadienylnickel. The bond lengths in the cyclopentadienyl ring vary from 1.39 Å to 1.47 Å (σ = 0.02 Å) and like the present values are probably within the borderline of statistical significance. The variation in nickel-carbon bond lengths led Dahl and Wei to provide an explanation in essentially valence bond terms in so far as they suggest that the results originate from the tendency of the nickel (II) ion to acheive a square planar configuration using dsp^2 hybrids. These authors therefore predicted that localised metal-cyclopentadienyl interactions might be found in complexes of the closely related Rh(I) and Ir(I). Our results suggest that it is more useful to examine the bonding within the framework of the molecular orbital approximation.

In the cyclopentadienyl anion, the six π - electrons are distributed

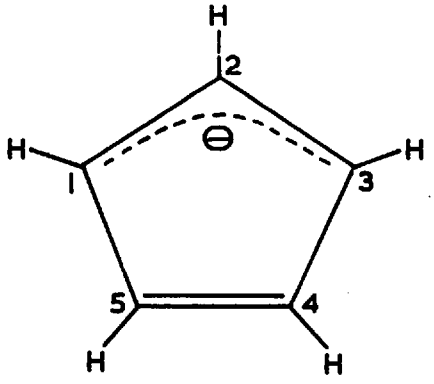
amongst the three molecular orbitals designated in the usual way as the a, e_1^+ and e_1^- orbitals (Figure 3.6(a)).

Provided the doubly degenerate e orbitals are equally occupied, there is uniformity of electron density around the ring and therefore identity of carbon-carbon bond lengths. A considerable proportion of the metal ligand bonding arises from overlap of the degenerate d_{yz} and d_{xz} orbitals of the metal with the e molecular orbitals of the cyclopentadienyl ring. If now the degeneracy of these 'd' orbitals is lifted through the field around the metal ion having less than cylindrical symmetry, there seems no a priori reason why the respective metal orbitals should combine equally (in terms of overlap integral) with e_1^+ and e_1^- molecular orbitals. In other words, the removal of metal orbital degeneracy also serves to remove the degeneracy of the bonding orbitals on the cyclopentadienyl ring. Examination of all the observed bond lengths together with those of Dahl and Wei shows a consistent scheme which can be readily understood. If one formally writes the structure as in Figure 3.6(b) as representing the bond lengths in the cyclopentadienyl ligand then one finds that the 'allyl' group is always trans to the relatively strong field ligands on the opposite side of the molecule - for example, the hydride ions of (a), one of the carbonyl groups of (b) and the unconjugated olefinic group of the norbonadiene ligand (Dahl et al., loc.cit.). Thus by either electrostatic effects, π -bonding or both we obtain a perturbation of the 'd' orbitals which serves to remove their degeneracy over and above the normal crystal field splitting effects. We thus obtain the situation that

Figure 3.6



(a) The lowest lying molecular orbitals of the cyclopentadienyl ring



(b) 'Allyl' type of bonding resulting from deflection of electron density in the e_1^+ molecular orbitals.

donation of electrons from the two degenerate e orbitals of the cyclopentadienyl ligand into metal 'd' orbitals is unequal, the net result being unequal population of the ring orbitals with a concomitant loss of five-fold symmetry in the ligand.

We should point out that if we follow Dahl and Wei in postulating bonds to the central atom of the 'allyl' group and the centre of the carbon-carbon bond opposite, we should arrive at a co-ordination number of six for molybdenum in (a) and (b). But there seems little value in doing so. We would predict, however, that more detailed examination of the bond lengths in complexes, where crystal structures have been reported, would be valuable. Thus some asymmetry in the cyclopentadienyl ligands would be expected, for example, in the structure of $\left[TiCl_2\ (C_5H_5)\right]_2\ O$ and $Ti(C_5H_5)_2Cl_2Al(C_2H_5)_2$. It will, of course, be impossible to draw conclusions from such data as the nuclear magnetic resonance spectra for reasons which have been discussed previously (Dickens and Lipscomb, 1962), but careful comparisons of the infra-red spectra of these and other complexes in the solid state and in solution would offer some independent check that the results of Figure 3.5 do not arise from some unknown systematic errors in the X-ray data which would invalidate estimates of the accuracy of the bond lengths. In particular, while the differences between the carbon-carbon bond lengths in the present complex are on the borderline of statistical significance ($\sim 3\sigma$), the overall pattern of distortions and the large C_2-C_1-C_5 angle clearly suggest the scheme outlined above. The differences between the molybdenum-carbon bond

lengths do appear to be significant, however (5-6σ), having the regular pattern around the ring shown in Figure 3.4. This seems to be consistent with the observation above that the 'allyl'-type group of the cyclopentadienyl ring is trans to the relatively strong field ligands on the opposite side of the molecule in all of the above complexes.

The nature of the metal-hydrogen bonding in transition metal hydrides has been discussed by a number of authors. Several (Cotton, 1958; Bishop, Down, Eastage, Richards and Wilkinson, 1959) assumed that the characteristic high field lines in the high resolution nuclear magnetic resonance spectra of these complexes can be explained by a model involving the embedding of the hydride atoms in the electron density of the metal ion. Bishop et al. (loc.cit.) have studied the wide line n.m.r. spectrum of $H_2Fe(CO)_4$ and found a proton-proton distance of 1.56 ± 0.05 Å from which a most probable Fe-H distance of 1.1 Å can be calculated assuming a value of 110° for the H-Fe-H bond angle. Stevens, Kern and Lipscomb (1962) considered that the simple view of an embedded proton involves a "drastic assumption" and attempt an explanation of the anomalous magnetic resonance shift without involving a particularly short metal-hydrogen bond, showing that when the large diffuse 4s and 4p levels of the metal are occupied by back-donation from such ligands as CO, the proton can be sufficiently shielded so as to achieve the observed shift to high fields, even when the M-H distance is a normal covalent bond length of 1.4 to

1.6 Å. Some support is given to these calculations by Ibers and LaPlaca (1963) who report a RH-H distance of 1.71 Å, determined by X-ray crystallography. The present Mo-H distance, estimated from the Difference (xy0) and (x0z) maps, is 1.23 Å, the angle H-Mo-H being 75°. The agreement of these values with the nuclear magnetic resonance data on $H_2Fe(CO)_4$ must be nothing more than fortuitous, both from the standpoint of the large likely error in the present result and because there is no a priori justification for believing that the proton will coincide with the centroid of the electron density of the bonded hydrogen atom. A complete three-dimensional analysis would, of course, have improved the e.s.d.'s of the observed bond lengths but we have felt that the problem is more amenable to an accurate neutron diffraction analysis, and this is now being carried out (Brown, 1963).

The packing of the molecules in the crystal is illustrated by three principal crystal projections (Figures 3.7 (a), (b) and (c)). The wedge-like shape of the molecule allows a dovetailing together in the lattice thus forming close packed chains parallel to 'b'. These chains are quite well separated (Figures 3.7 (b) and (c); cf. the relatively few short intermolecular contacts of Table 3.5), the high volatitlity of the crystals presumably resulting from this mode of packing which originates from the asymmetric shape.

* * *

Table 3.5 Inter-ring H-H contacts less than 3.0 Å

	Contact		Å
1	H1 → H1′		2.42
2	H3	(x,-1 + y, z)	2.77
3	H4	(x, -1 + y, z)	2.58
4	H5	(-x, -y, 1 - z)	2.80
5	H2 → H2	$(-\frac{1}{2} - x, \frac{1}{2} - y, -z)$	2.90
6	H3	$(-\frac{1}{2} - x, \frac{1}{2} - y, -z)$	2.62
7	H4	$(x, 1 - y, -\frac{1}{2} + z)$	2.63
8	H5	$(x, -y, -\frac{1}{2} + z)$	2.45
9	H3 → H4	$(x, 1 -y, -\frac{1}{2} + z)$	2.93
10	H5 → H5	(-x, -y, 1 - z)	2.23

The primed symbol refers to the second cyclopentadienyl ring in the reference molecule, related to the first by the diad at $z = \frac{1}{4}$.

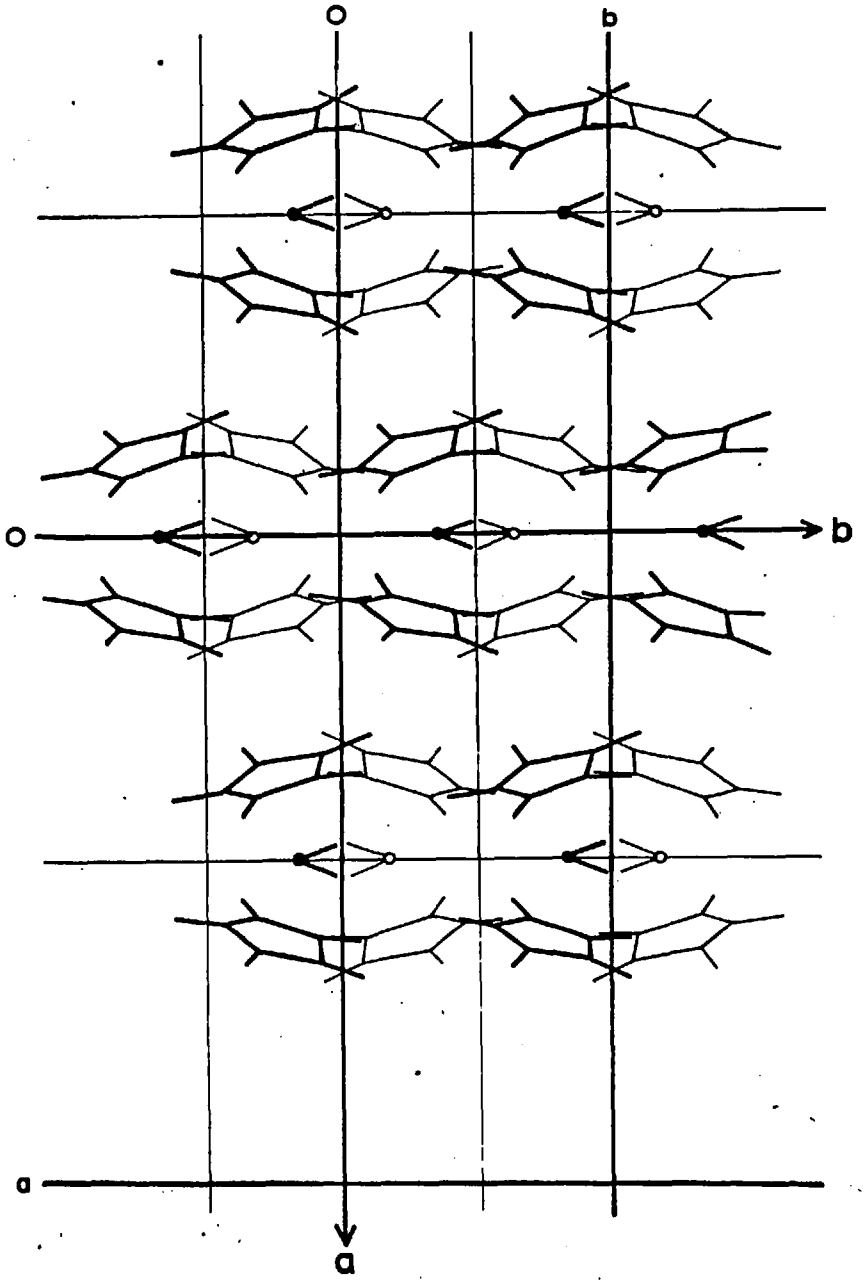


Figure 3.7

Molecular Packing Projections

(a) down 'c'

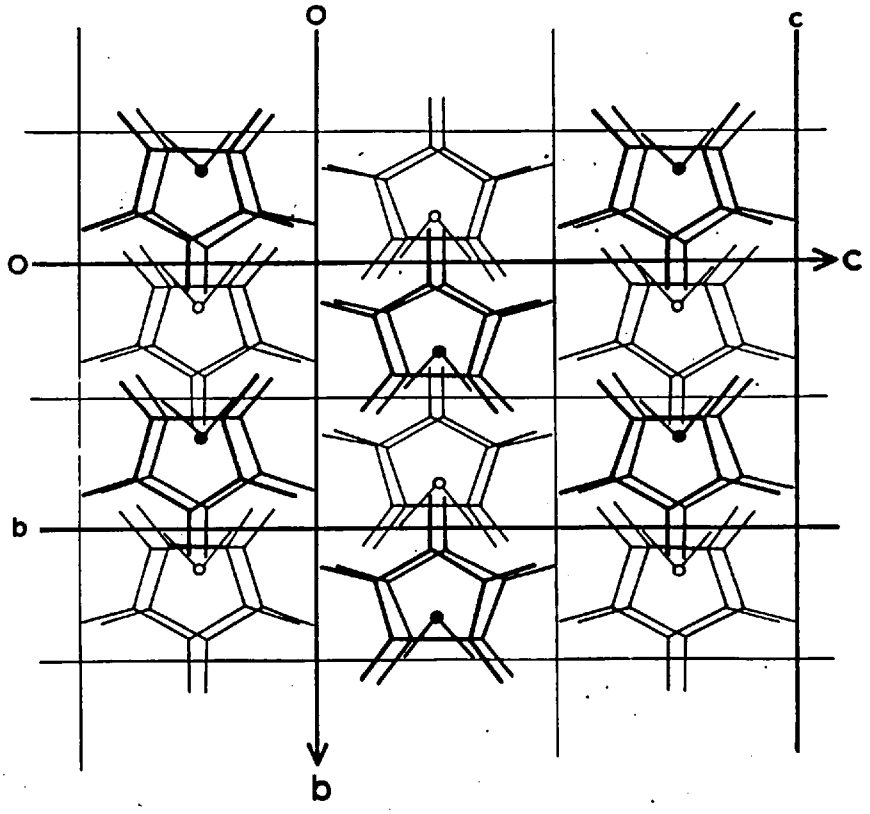


Figure 3.7

(b) down 'a'

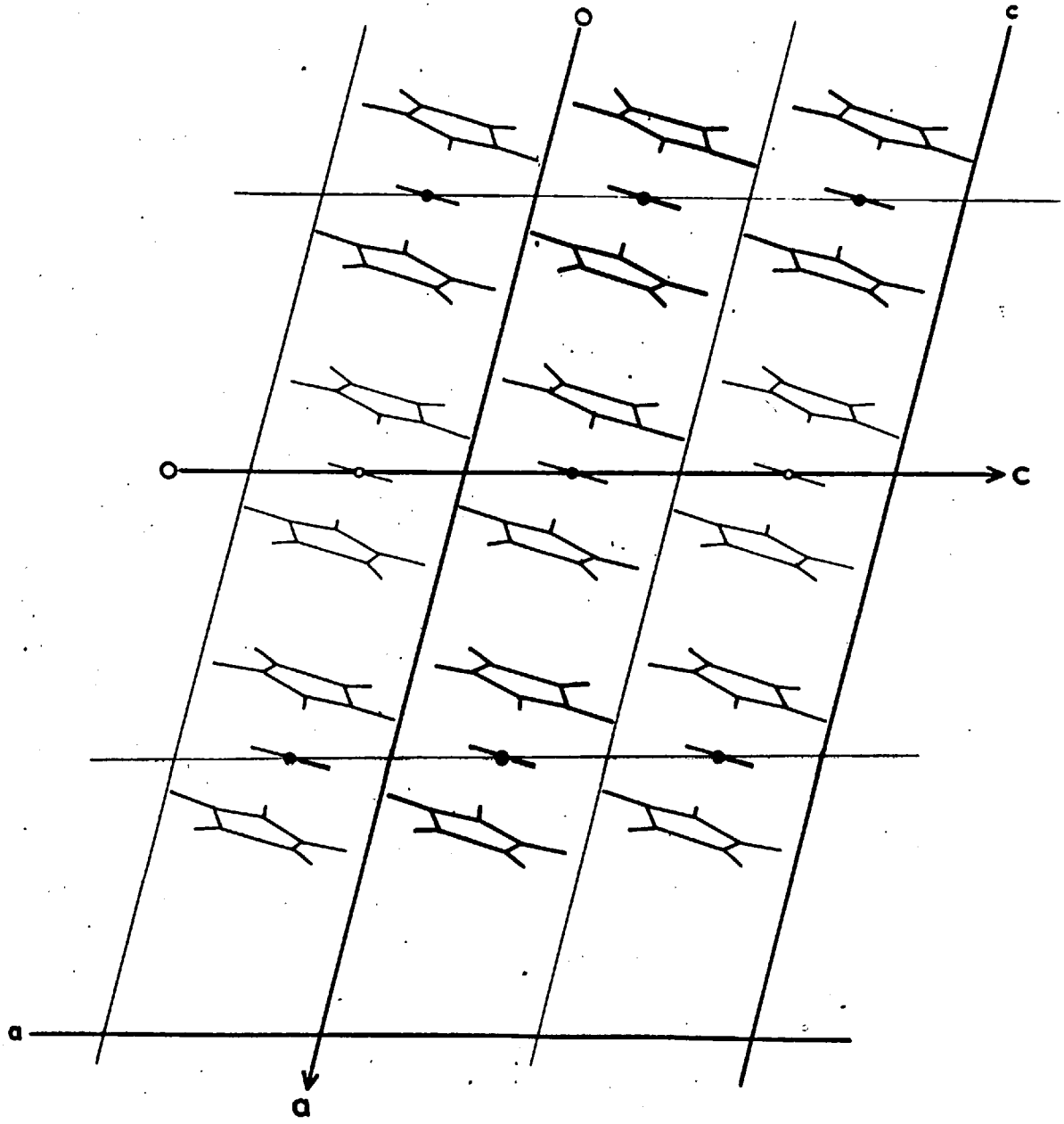


Figure 3.7

(c) down 'b'

P A R T II

The Paramagnetic Anisotropies of Some Cobaltous and Ferric Complexes

CHAPTER 4

An Introduction to the Principles of Crystal Paramagnetic Anisotropies

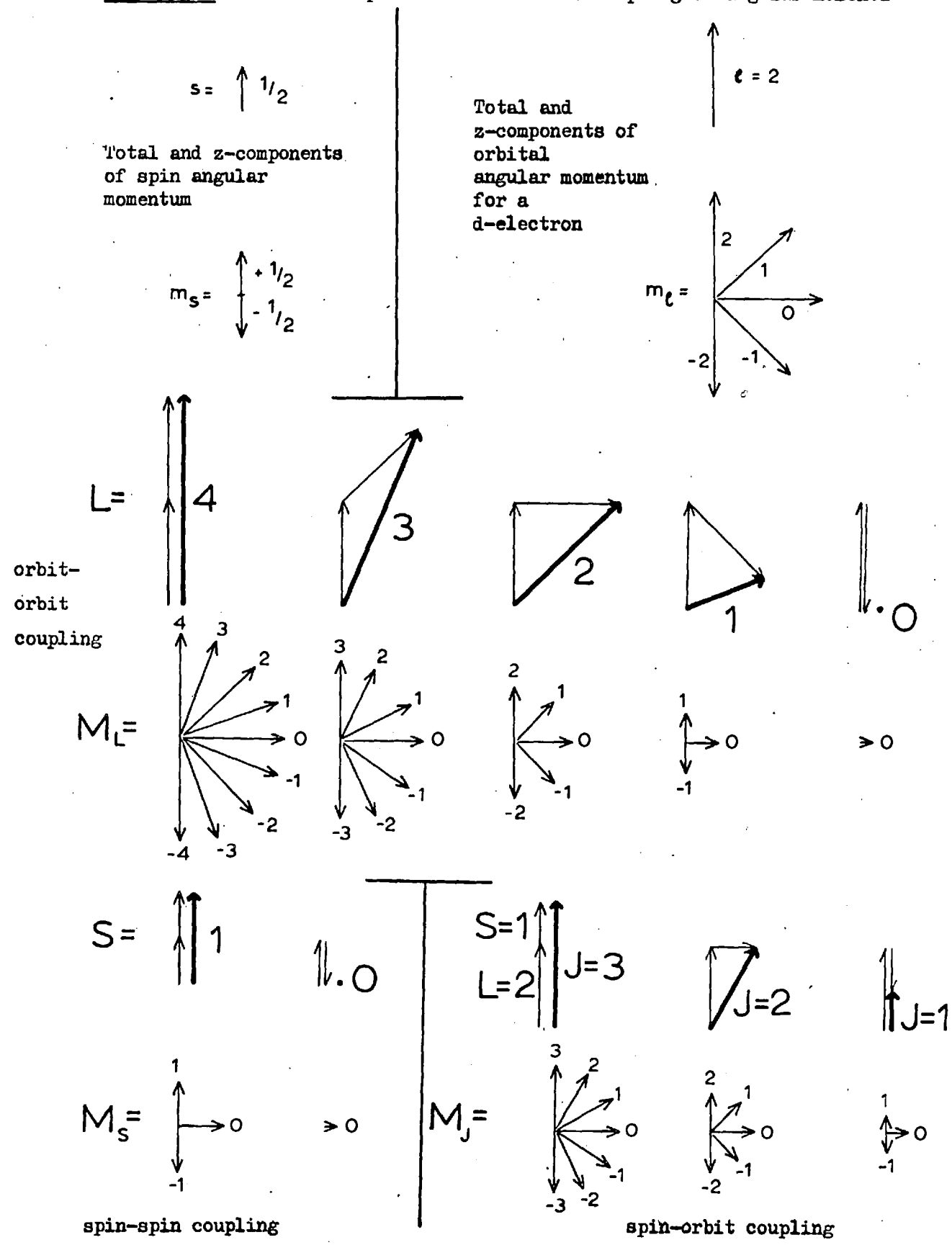
Part II of the thesis describes studies of the paramagnetic anisotropies of several crystals of first-row transition metal ions, and in this chapter an attempt is made to outline the principles involved in the theoretical and practical aspects of the subject. At first the concepts of electronic angular momentum and coupling are discussed, followed by a description of the Russell-Saunders coupling scheme in free ions. The explanation of the origin of paramagnetic anisotropy follows a brief section on the influence of cubic ligand fields on term splittings, while the latter half of the chapter describes the formal relationships between molecular and crystal anisotropies and the experimental methods which have been used to measure them.

4.1 The free ion : Russell-Saunders coupling

The quantum mechanical treatment of the hydrogen atom is, today, well understood and has led to a degree of familiarity with 'the' quantum numbers n, l, m and s. The primary quantum number, n, labels an eigenvalue (allowed value) of the radial part of the Hamiltonian describing any atom with a spherically symmetric central field: l is associated with an eigenvalue of the total orbital angular momentum operator, while m_l labels an eigenvalue of the operator associated with the z-component of orbital angular momentum: similarly, s ($= \pm\frac{1}{2}$) describes the spin angular momentum of an electron, m_s

being, again, the 'z-component' of $\underline{s}$. These definitions are also meaningful for hydrogen-like atoms, having a single electron in the outermost shell, experiencing a spherically symmetric electric field from the completed shells within - the quantum numbers of the hydrogen atom, then, are still 'good' for hydrogen-like atoms. However, when more electrons are introduced into the outer shell (but without completion), the field they experience is far from spherically symmetric, with the result that $\underline{l}$, $\underline{m}_l$, $\underline{s}$, $\underline{m}_s$ no longer form a good set of quantum numbers. The properties of the individual electrons in an incomplete shell are dependent upon one another because their angular momenta 'couple' together: this has often been described by the 'quantized' vectorial addition of the individual $\underline{l}$, $\underline{s}$, $\underline{m}_l$, $\underline{m}_s$'s to give resultant L, S, M_L, and M_S values as shown in Figure 4.1, a description which has certain conceptual advantages. What is important, is that the coupling together of several angular momenta causes the meanings of their <u>individual</u> z-components to be lost, being replaced by other <u>collective</u> quantities. For example, the coupling of two electrons with angular momentum quantum numbers (l_1,l_2, m_{l_1},m_{l_2}, s_1, s_2, m_{s_1}, m_{s_2}) produces a new set (l_1, l_2, L, M_L, s_1, s_2. S, M_S). When the states described by l_i and s_i differ widely in energy, the coupling is small and the individual m_{l_i}'s and m_{s_i}'s retain their original significance. This situation holds for the negligible coupling between electrons from different subshells. Within any subshell, the coupling energies between different quantities are, in general, unequal and it is necessary to consider them in order of magnitude: for the first half of the periodic table,

Figure 4.1 Vectorial representations of the coupling of angular momenta



approximately, the order of coupling energies is spin-spin $>$ orbit-orbit $>$ spin-orbit and the systematic description of atomic states following this order is known as the Russell-Saunders coupling scheme.

States having particular L values are called terms, being labelled S, P, D, F, G, H.... when L = 0, 1, 2, 3, 4, 5..... Just as m_l can have all quantised values from +l to -l, so M_L can take values from +L to -L - that is, there are 2L + 1 M_L values for any term L, referred to as the orbital multiplicity of the term. Each term may have several different values of S representing the different modes of coupling individual electronic spins: again, S may be orientated with respect to the z-direction in 2S + 1 ways - the spin multiplicity. Thus, a fuller description of a term may be given by a term letter (S, P, D etc) with a left superscript, 2S + 1: for example, ^3D, triplet D, labels the state with L = 2 and S = 1.

Only certain terms arise from a given configuration: for example, the maximum possible value of L is obtained when all $\underline{l}$'s are parallel to the z-direction and there is a similar restriction upon S (see Figure 4.1). In addition to these obvious constraints is the Pauli Exclusion Principle which states, in effect, that no two electrons in the same atom can have all quantum numbers equal. This rule becomes relevant in the present discussion only when electrons from the same subshell are considered, for if two electrons differ in their $\underline{n}$ or $\underline{l}$ values there is no further restriction upon other quantum numbers. Thus the terms arising from the coupling of a 2p and a 3p electron (this being small anyway) will be ^3D, ^1D, ^3P, ^1P, ^3S, ^1S. The

application of the Pauli Exclusion Principle to determine which terms can arise in configurations within the same subshell is involved but, for the sake of completeness, is described in detail here for the d^2 configuration.

We construct Table 4.1 which represents the ways individual electronic spin and orbital angular momenta may be coupled to give the total z-components, M_L and M_S, spin-orbit coupling being completely neglected at this stage. The values of m_l are represented as 2, 1, 0, -1, -2 and of m_s by + and -: these symbols refer to the individual electronic wave functions. We have two d electrons, so that S has a maximum value of 1, with spin multiplicity, $2S + 1 = 3$; that is, there are, at most, three orientations of the total spin with respect to the z-direction and these are represented by the last three columns of the table. Similarly, the maximum value of L is 4, orbital multiplicity, $2L + 1 = 9$, represented by the nine rows in Table 4.1. We now form linear combinations of the individual electronic wave functions, denoting those being combined inside parentheses. We invoke Ehrenfest's Adiabatic Law which states that for an infinitely slow adiabatic change of coupling conditions, the quantum numbers of the system will not change. When completing the table, we assume zero coupling, when $M_L = \sum m_l$ and $M_S = \sum m_s$, in order to arrive at the number of ways of achieving any given 'total' state. When coupling is finite, the combined wave functions no longer lead to the same quantum numbers as before, as described above, and it must be emphasised that the symbols in Table 4.1 refer only to the ways in which the individual wave functions may be combined to produce final combinations with the appropriate

Table 4.1 Linear combinations for the d^2 configuration

M_L \ M_S	1	0	-1
4		$(2^+ \; 2^-)$	
3	$(2^+ \; 1^+)$	$(2^+ \; 1^-)(2^- \; 1^+)$	$(2^- \; 1^-)$
2	$(2^+ \; 0^+)$	$(2^+ \; 0^-)(2^- \; 0^+)$ $(1^+ \; 1^-)$	$(2^- \; 0^-)$
1	$(2^+ \; -1^+)$ $(1^+ \; 0^+)$	$(2^+ \; -1^-)(2^- \; -1^+)$ $(1^+ \; 0^-)(1^- \; 0^+)$	$(2^- \; -1^-)$ $(1^- \; 0^-)$
0	$(2^+ \; -2^+)$ $(1^+ \; -1^+)$	$(2^+ \; -2^-)(2^- \; -2^+)$ $(1^+ \; -1^-)(1^- \; -1^+)$ $(0^+ \; 0^-)$	$(2^- \; -2^-)$ $(1^- \; -1^-)$
-1	$(-2^+ \; 1^+)$ $(-1^+ \; 0^+)$	$(-2^+ \; 1^-)(-2^- \; 1^+)$ $(-1^+ \; 0^-)(-1^- \; 0^+)$	$(-2^- \; 1^-)$ $(-1^- \; 0^-)$
-2	$(-2^+ \; 0^+)$	$(-2^+ \; 0^-)(-2^- \; 0^+)$ $(-1^+ \; -1^-)$	$(-2^- \; 0^-)$
-3	$(-2^+ \; -1^+)$	$(-2^+ \; -1^-)(-2^- \; -1^+)$	$(-2^- \; -1^-)$
-4		$(-2^+ \; -2^-)$	

M_L and M_S values, no description of energy levels being directly implied. The table is completed, then, as follows. We first consider the combination $(2^+\ 2^+)$ to give $M_S = 1$, $M_L = 4$, but this is forbidden by the Pauli Exclusion Principle (as too, are $1^+\ 1^+$ etc., etc.,) and so does not appear in the table. Also, the table does not contain pairs of combinations like $(1^+\ 0^+)(0^+\ 1^+)$ as these are identical descriptions by virtue of the impossibility to distinguish electrons other than by their quantum numbers. Routine application of these rules produces the complete Table 4.1. We now wish to derive a set of terms described uniquely by the combinations in the table and begin with the term having the greatest multiplicity - ^3G. This must have a component in each column ($M_S = 1$, 0, and -1) and in each row ($M_L = 4 \rightarrow -4$) but, as there are no components with $M_S = \pm 1$, $M_L = \pm 4$, a ^3G is not formed. Consider next a ^1G, having a component in each row of the middle column ($M_S = 0$): we allocate one combination from each 'box', which one, being immaterial as, for finite coupling, the individual electronic quantum numbers are without meaning. We now have a ^1G term and no remaining combinations with $M_L = \pm 4$. Next, we take the ^3F term, allocating one component from each column and each row (from $M_L = 3 \rightarrow -3$) when there remain no further combinations with $M_L = \pm 3$. We now consider a ^3D term... and so on. The final group of terms for the d^2 configuration is ^1G, ^3F, ^1D, ^3P, ^1S.

Terms arising from other configurations may be derived in a similar way, Table 4.2 listing those from d^2 configurations. The calculation of the energy splittings of these terms is beyond the scope of this thesis but the order by

energy is summarised in Hund's rules: (1) terms with the greatest spin multiplicity lie lowest and (2) of these, those with greatest orbital multiplicity lie lowest. The splitting diagram for the d^2 configuration is set out in Figure 4.2.

Table 4.2

Configuration	Terms Arising
d^1 d^9	^2D
d^2 d^8	^3F ^3P ^1G ^1D ^1S
d^3 d^7	^4F ^4P ^2H ^2G ^2F $^2D(2)$ ^2P
d^4 d^6	^5D ^3H ^3G $^3F(2)$ ^3D $^3P(2)$ ^1I $^1G(2)$ ^1F $^1D(2)$ $^1S(2)$
d^5	^6S ^4G ^4F ^4D ^4P ^2I ^2H $^2G(2)$ $^2F(2)$ $^2D(3)$ ^2P ^2S

When a configuration (like d^3) gives rise to two separate terms with the same designation, these do not, in general, have the same energy, being derived from different linear combinations of the individual electronic wave functions. A set of terms, such as that for d^2, form a group of energy levels for one particular configuration only, the lowest term being the ground state, occupation of higher terms constituting the excited states.

The preceding discussion has neglected spin-orbit coupling. If taken into account, this effect may be treated analogously to s-s and l-l coupling. Thus if the spin and orbital angular momenta, $\underline{s}$ and $\underline{l}$, of any given electron

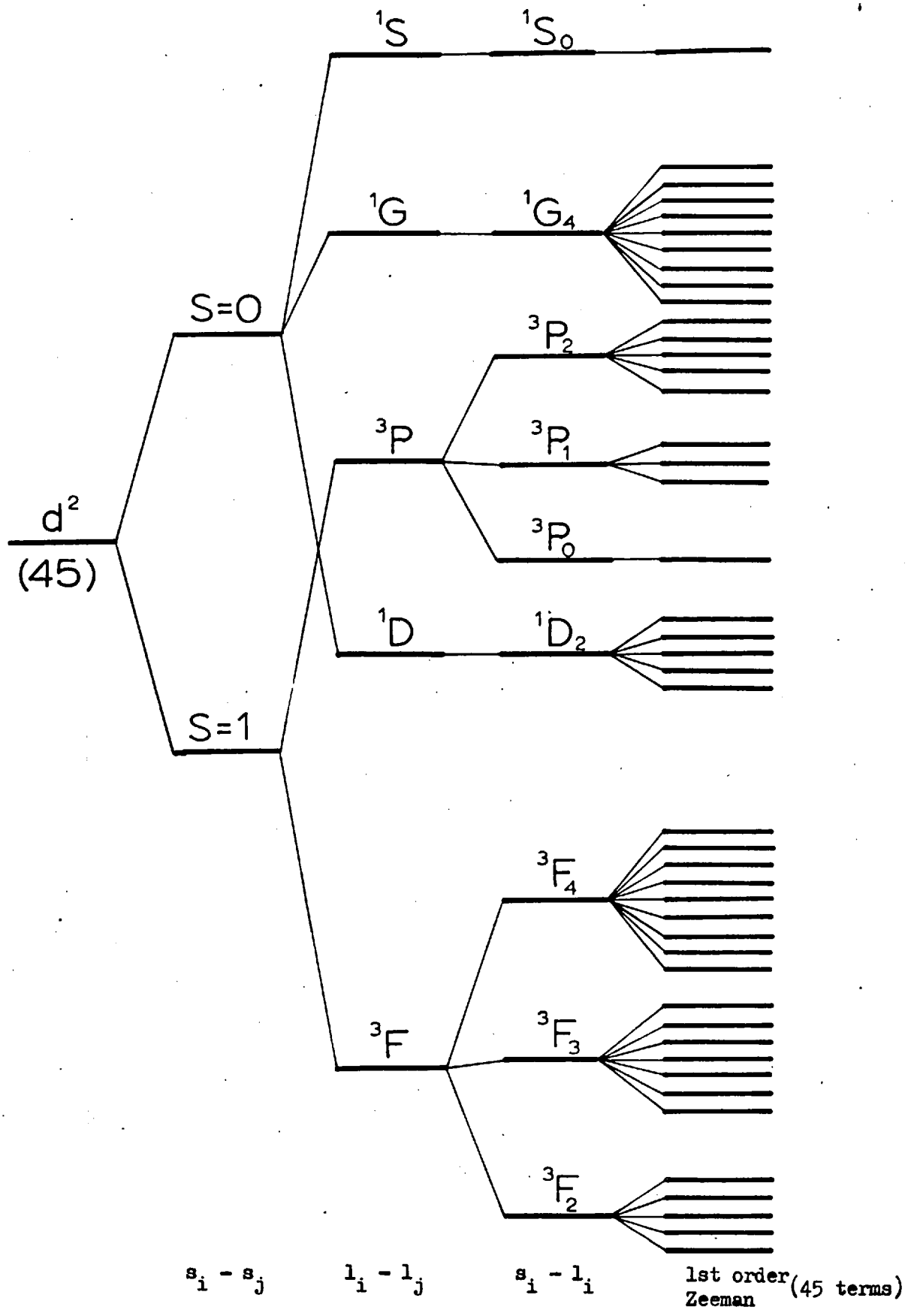


Figure 4.2 Russell-Saunders coupling for the d^2 configuration

interact we must introduce the new 'total' quantum numbers J and M_J to represent the total angular momentum. For two electons, say, we replace (l_1, l_2, m_{l_1}, m_{l_2}, s_1, s_2, m_{s_1}, m_{s_2}) by (l_1, l_2, L, s_1, s_2, S, J, M_J). The energy separation of terms differing only in their J (and M_J) values is small in the Russell-Saunders scheme and they group together to form a multiplet, each component now being labelled $^{2S+1}L_J$ where J can take all values from $L + S \rightarrow L - S$ giving 2L + 1 or 2S + 1 components, whichever is the smaller. Each component has a total multiplicity with respect to the z-direction of 2J + 1, labelled by the M_J values. The spin-orbit coupling stages for the d^2 configuration has been included in Figure 4.2. The energy splittings of the multiples is governed by a rule in some ways analagous to Hund's rules and, in magnitude, is proportional to the spin-orbit coupling constant, λ ; λ is positive for a shell less than half full and negative when more than half full.

* * *

4.2 The magnetic moment

In the presence of a magnetic field the degeneracy of the (2S + 1) M_S-states of the ion is completely removed; that is, the M_S-states will split up, the distribution of the ions among these states will become unequal and the ions will, in consequence, have a resultant magnetic moment along the field (z-) directions. This is known as the first-order Zeeman effect and accounts for the paramagnetism of ions having a ground state with $J > 0$ (or a thermally

accessible excited state with $J > 0$). The magnetic moment of the system may be obtained by computing the root mean square moment associated with each eigenfunction (describing each M_S-state), weighted by the probability of occupation of each level. The populations of the levels may be found, assuming a Boltzman distribution between the levels which are split by $g\beta H$ where H is the magnetic field strength, β the Bohr magneton and g the Landé splitting factor (or gyromagnetic ratio):

$$g = \left[1 + \frac{J(J+1) + S(S+1) - L(L+1)}{2J(J+1)} \right]$$

When the splitting is much less than kT the populations of the various levels are nearly equal and the magnetic susceptibility, $\bar{\chi}$ obeys the Curie Law:

$$\bar{\chi} = \frac{C}{T}$$

where C is the Curie constant. Empirically, the temperature dependences of paramagnetic bulk susceptibilities often follow the Curie-Weiss Law:

$$\bar{\chi} = \frac{C}{(T + \theta)}$$

where θ is the Weiss constant. While θ can sometimes be correlated with antiferromagnetic exchange effects, in general its origin is complex and usually not yet completely understood (vide infra).

Using another mechanism, even ions with a non-degenerate ground state ($J = 0$) may have a paramagnetic moment. This is called the second-order Zeeman effect and it can also augment any moment produced by the first-order effect. It describes the effect of polarizing the ion's electronic cloud by the magnetic

field when the polarised ion is more properly described by a different wave function which is formed by a suitable combination of the unpolarised ground state plus some excited state wave functions. Such a process is described as the 'mixing-in' of an excited state, the degree being inversely related to the separation between the ground and excited state of the ion. If the level 'mixed-in' is much greater than kT above the ground level, thermal distribution between the levels does not occur and the resultant contribution to the paramagnetic susceptibility is independent of temperature, being referred to as temperature-independent paramagnetism (T.I.P.)

For a free ion following the Russell-Saunders coupling scheme, the effective magnetic moment resulting from the 1^{st} order Zeeman effect is given by:

$$\mu_{eff} = g\left\{J(J+1)\right\}^{\frac{1}{2}} \quad \text{B.M.} \qquad .....(1)$$

While this is found to describe the magnetic behaviour of the lanthamide elements quite well, as they have buried d electrons experiencing virtually no external asymmetric fields, it is less useful for the first-row transition ions. In the first place, spin-orbit coupling is much smaller than for the lanthamides so that the expression,

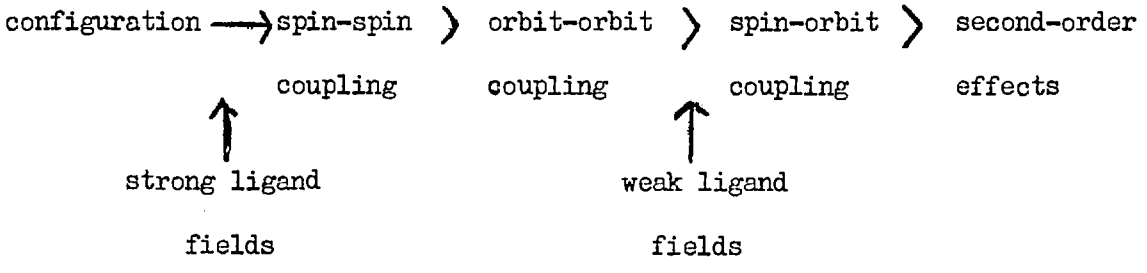
$$\mu_{eff} = \left\{L(L+1) + 4S(S+1)\right\}^{\frac{1}{2}} \quad \text{B.M.} \qquad .....(2)$$

is a closer approximation: secondly, these ions are very susceptible to the effects of the electric fields produced by the ligands which can cause a partial or complete 'quenching' of the orbital part of the magnetic moment, giving a resultant moment between that given by (2) and the 'spin-only' moment;

$$\mu_{eff} = \left\{4S(S+1)\right\}^{\frac{1}{2}} \quad \text{B.M.} \qquad .....(3)$$

4.3 Ligand fields

The description of Russell-Saunders given above is strictly valid only for free ions experiencing no external fields. In complexes, and in most real situations, the ions are surrounded by ligands whose fields perturb, to a greater or lesser degree, the potenials which the electrons experience. As a result the various coupling schemes for the free ion break down to an extent depending upon the strength of the ligand field and the weak field cases. The weak field case assumes that the ligand field is a small perturbation compared with the free ion electron repulsion effects, but large compared with spin-orbit coupling. The strong field case assumes that the ligand field perturbation is the strongest of all, causing spin-pairing, i.e. minimum spin multiplicity, to have the lowest energy. These extremes are represented in the diagram:



In the weak field approximation the free ion terms are 'sorted out' and split further, but otherwise not altered, whereas in strong ligand fields they lose their meanings completely, giving rise to new terms. Intermediate ligand fields may be represented by correlation diagrams, an example of which appears in Figure 4.3

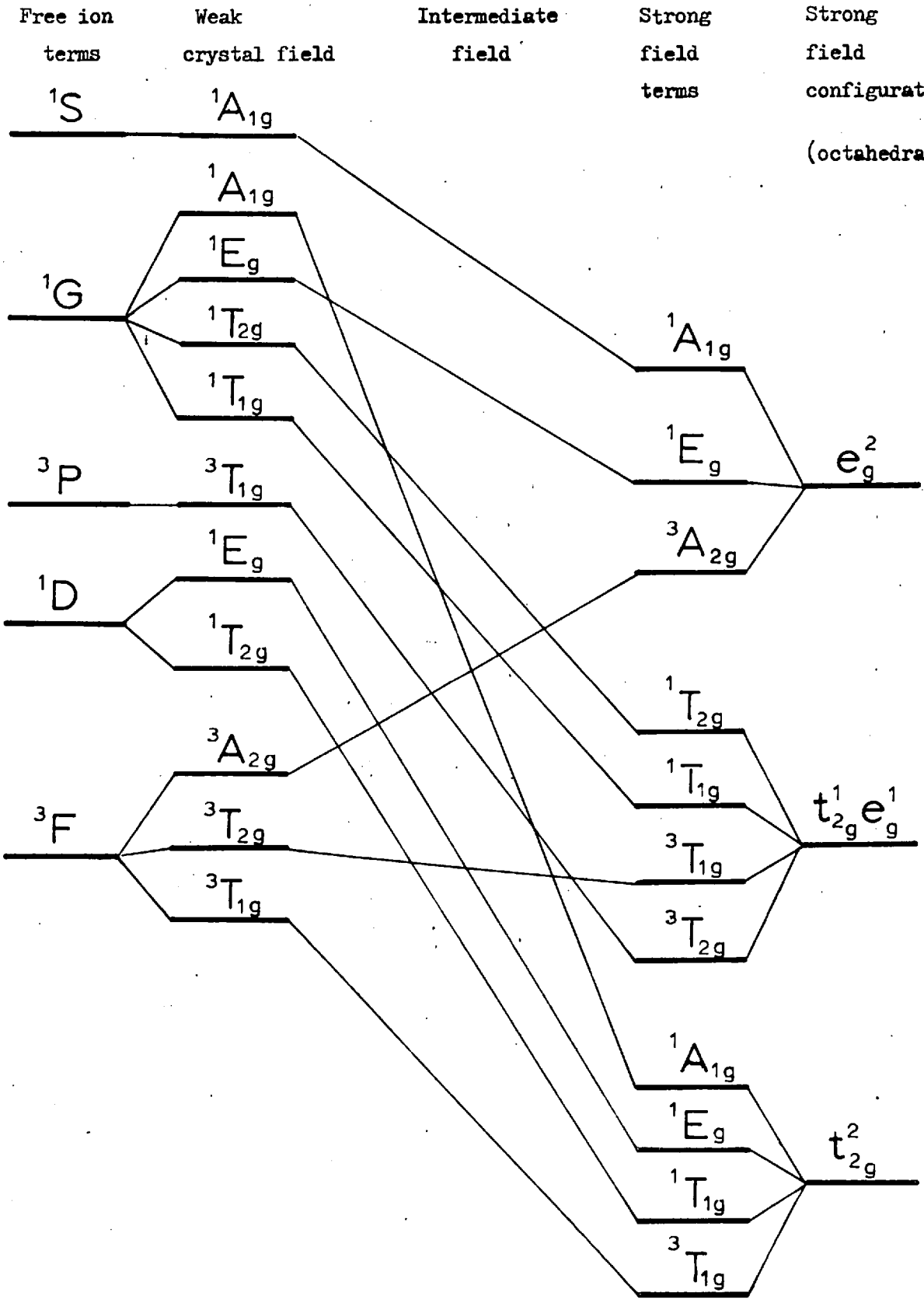


Figure 4.3 Correlation diagram for d^2 free ion → strong field configuration

The work described in the later chapters has been concerned with stereochemistries which were closely cubic. Octahedral and tetrahedral symmetries are both cubic: 'octahedral' ligands may be placed on the axes of a cube, centred on the metal atom, passing through the mid-points of each face while 'tetrahedral' ligands lie at alternate corners of the cube. The right hand side of the correlation diagram (Figure 4.3) thus describes the ground and excited states represented by putting electrons into the well-known t_{2g} and e_g orbitals. (The t_{2g}/e_g description is only strictly valid for the 'd' configuration when the strong field and weak field approximations lead to identical results). The orbital splittings of some weak field terms in a cubic potential are given in Table 4.3. The group-theoretical symbols A, E, T, describe orbitally non-degenerate, doubly degenerate and triply degenerate states, respectively. These splittings have been used to complete the correlation diagrams in Figure 4.3

Table 4.3

Free Ion Term	Terms in Cubic Fields
S	A_1
P	T_1
D	$E + T_2$
F	$A_2 + T_1 + T_2$
G	$A_1 + E + T_1 + T_2$
H	$E + 2T_1 + T_2$

We consider, now, what general effects the ligand fields may have on the paramagnetic moment. One consequence is that apart from degeneracy changes, the Zeeman splitting is different in magnitude, the splitting factor, g, now being a complex function dependent upon the ligand fields. The most important effect, however, is known as orbital 'quenching'. The loss of the free ion terms in the presence of ligand fields can only make itself felt by an alteration of the orbital degeneracy of the ground and excited states (other than the drastic change of spin multiplicity associated with strong fields, of course): this has the result of diminishing the orbital magnetic moment and sometimes of removing it completely leaving a total effective moment given closely by the 'spin-only' expression above. This can be seen by noting that, in the presence of strong asymmetric crystalline electric fields, the degeneracy in respect of the orbital moments of the ions is partially or completely removed, so that, if the separations were large compared with kT, the distribution of the ions among these levels would remain practically unaffected by the application of a magnetic field, that is, the orbital moment has been 'quenched'.

The magnetic moment may also be altered by other effects. Firstly, spin-orbit coupling may 'mix-in' an excited state with the same spin multiplicity as the ground state, to an extent dependent upon the spin-orbit coupling constant, λ, with resultant splitting of the ground term. This is merely a way of modifying the expression (2) above, for the 1^{st}-row elements, to approach expression (1). The moment is modified by a factor $(1 - \alpha . \frac{\lambda}{\Delta})$ where α is a

constant and Δ is the separation between the ground levels and the excited level being mixed in. The temperature dependences of the moments of ions in perfect cubic symmetry, corrected for this first-order spin-orbit coupling effect, have been computed by Kotani to give fair agreement with the behaviours of many ions. Secondly, orbital quenching can alter the moments when the ligand field is less than cubic, having, perhaps, a trigonal or tetragonal distortion. This effect is generally more important than spin-orbit coupling for the first row transition ions which have small values for λ. The effect is responsible, in the main, for the magnetic anisotropy shown by many complex ions.

* * *

4.4 Paramagnetic anisotropy

The spin moments are not affected directly by the crystalline fields, though indirectly they are, by their coupling, with the orbital moments. When the latter have been 'frozen' by the ligand field, the coupling of the spins with them would be equivalent to subjecting the spins to local fields which, if the ligand fields were asymmetric, would also be asymmetric. In consequence, the ion would exhibit a magnetic anisotropy and the temperature variation of its principal susceptibilities would deviate from the Curie Law.

The degree of magnetic or spectral anisotropy shown by an ion depends upon the orbital multiplicity of the ground term. For example, the D and F ground terms for several of the first row transition metal ions are split by pure

cubic ligand fields variously into A_2, E, T_1 and T_2 levels, having orbital degeneracies of 1, 2, 3 and 3, respectively. When a triply degenerate level (T_1 or T_2) is deepest, a high amount of magnetic anisotropy is expected if a small trigonal or tetragonal distortion is present, as the triplet is decomposed by the non-cubic components of the field into A and E terms which will be associated with particular directions. However, if the singlet, A_2, or the so called 'non-magnetic' doublet, E, terms lie lowest, only feeble anisotropy can result. The reason why any anisotropy is observed in these cases at all is due to second-order spin-orbit coupling which mixes in the low-symmetry-split triplet components of higher energy: this effects features in Chapter 5 for the d^7 tetrahedral Co^{2+} ion. The actual orders of splitting in octahedral and tetrahedral fields for the D and F terms can be predicted by quantum mechanical arguments and are shown in Figure 4.4. The implications of the diagrams agree well with experiment and, for example, explain, nicely, why octahedral Co^{2+} complexes have large magnetic anisotropies and tetrahedral Co^{2+}, small. The splitting diagrams furnish another method of investigating stereochemistry.

Further, more detailed, discussion of paramagnetic anisotropy is left for Chapters 5 and 6. We now consider the relevance of crystal physics to magnetic anisotropies.

* * *

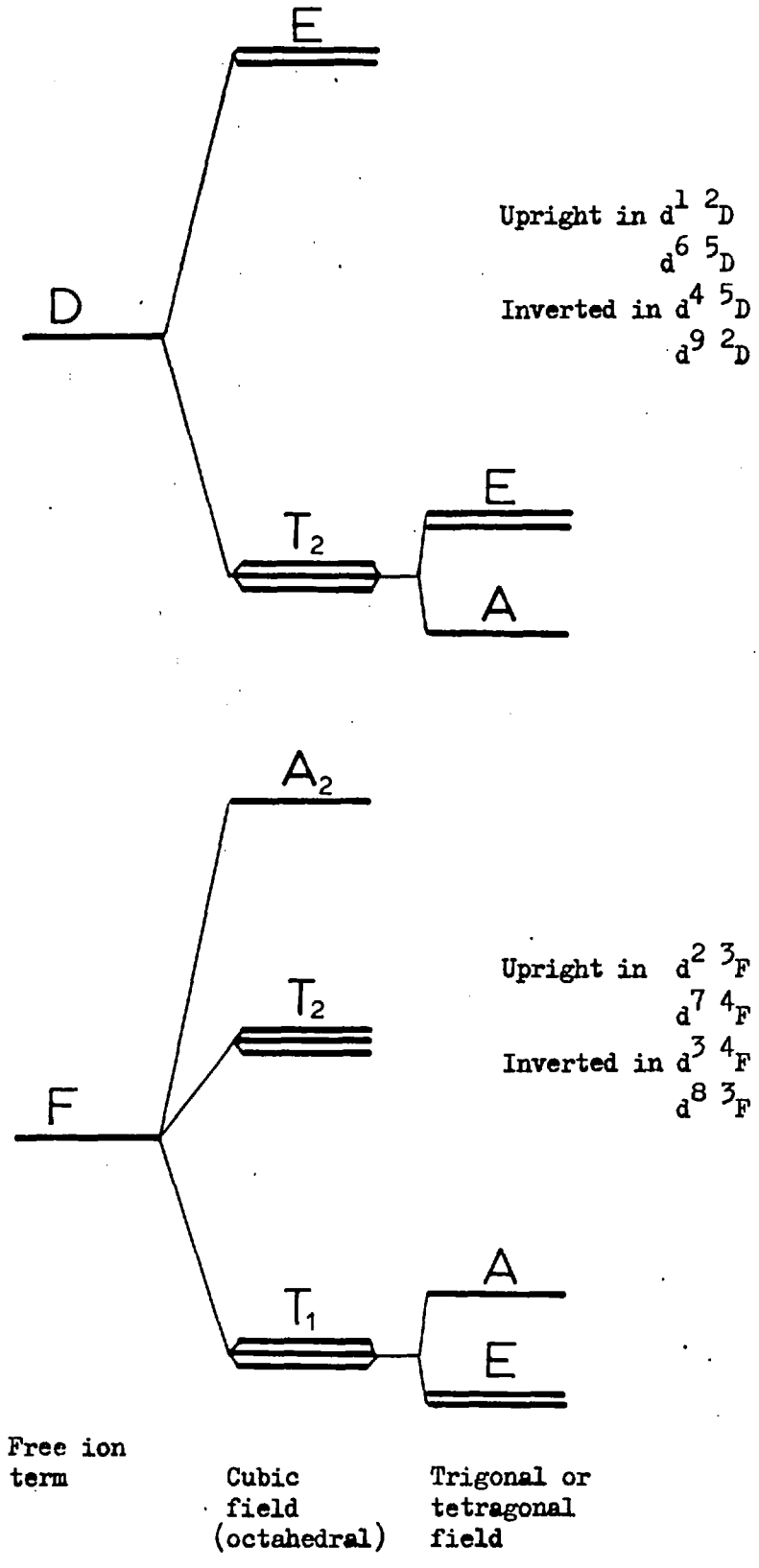


Figure 4.4 Splitting of D and F terms by asymmetric ligand fields. Levels inverted for tetrahedral symmetry (after Van Vleck, 1959)

4.5 Some general relationships in crystal physics

Scalars, vectors and tensors, which may describe physical quantities, are entities defined by their transformation rules. A property, like temperature, which is invariant on transformation, being a function only of the co-ordinates, x_i, of the point to which it refers, is called a scalar quantity. Other properties, like temperature gradient or electric field strength, are represent-presented by vectors, which are arrays of k quantities, A_k, where k is the number of dimensions, transforming according to (1).

$$\left.\begin{array}{ll} \text{covariant vector} & : \quad A'_k = \dfrac{\partial x_l}{\partial x'_k} A_l \\ \text{contravariant vector (or reverse transformation)} & : \quad A'^k = \dfrac{\partial x'_k}{\partial x_l} A^l \end{array}\right\} \qquad \ldots\ldots(1)$$

The primed symbols refer to the quantity in the new frame, that is after transformation, and, by convention, the appearance of the same index twice in a product implies the sum over all such terms (i.e. one for each dimension). Again, other kinds of properties, like thermoelasticity or electrical conductivity, are described by tensors, which, in general, are arrays of n^s quantities, where n is the number of dimensions and s, the rank of the tensor. We are concerned only with those properties which may be represented by a three-dimensional second-rank tensor, T^{kl}, having the transformation rule,

$$T'^{kl} = \frac{\partial x'_k}{\partial x_r} \frac{\partial x'_l}{\partial x_s} T^{rs} \qquad \ldots\ldots(2)$$

Further, the only transformation we need consider here is that of rotation. We construct two sets of Cartesian axes $X_1X_2X_3$ and $X_1'X_2'X_3'$ (Figure 4.5) representing the original and rotated co-ordinate frames, respectively. Their mutual orientation may be represented by the angles which each axis of one set makes with each axis of the other, or better, by the cosines of these angles. The resulting array of <u>direction cosines</u>,

	X_1'	X_2'	X_3'
X_1	c_{11}	c_{12}	c_{13}
X_2	c_{21}	c_{22}	c_{23}
X_3	c_{31}	c_{32}	c_{33}

.....(3)

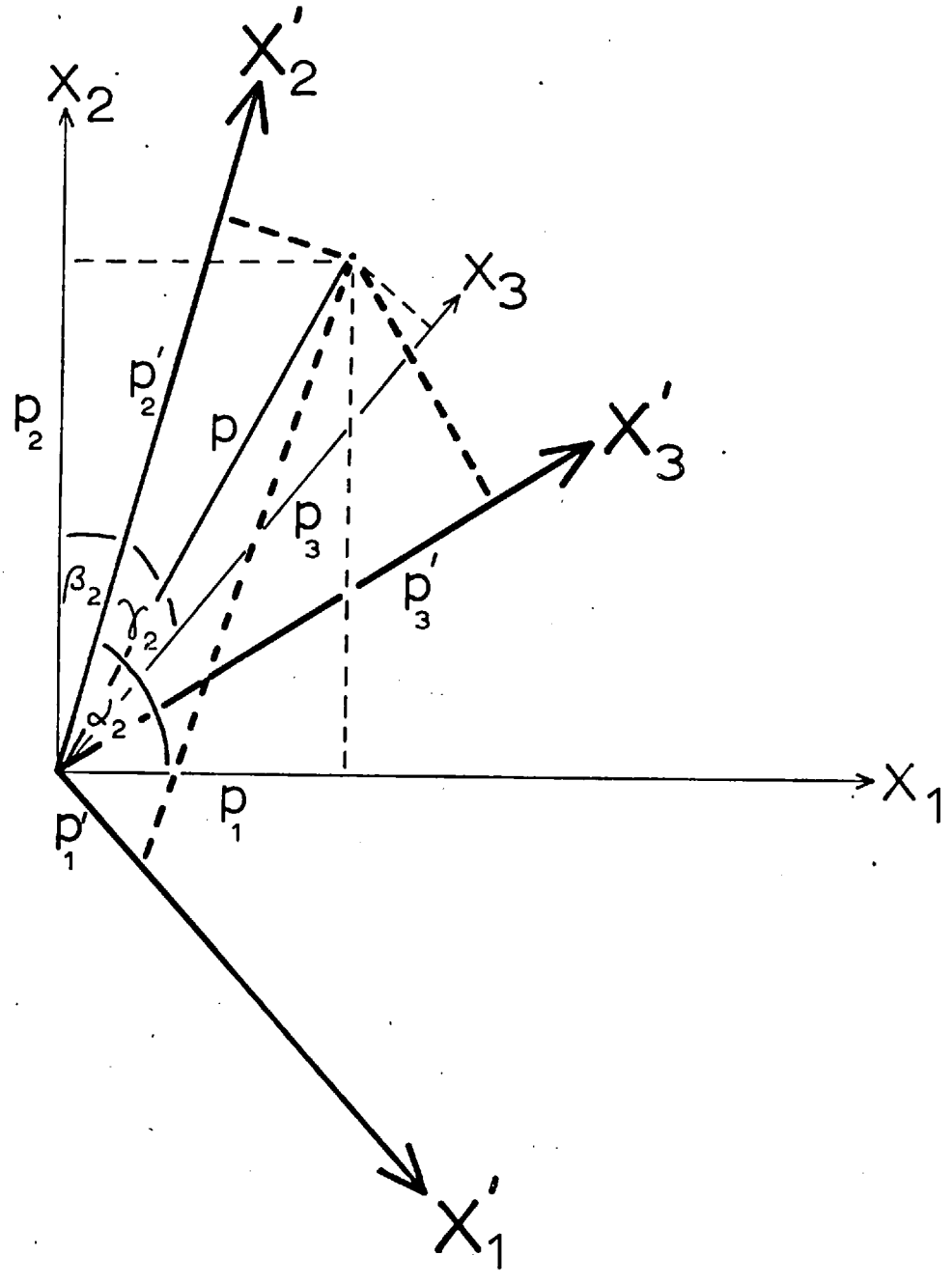
may be represented by the tensor C_{ik}. A vector, p, in the original frame, with components p_1, p_2, p_3 parallel to X_1, X_2, X_3 may be transformed into p' with components p_1', p_2', p_3' parallel to X_1', X_2', X_3' (Figure 4.5) giving:

$$\begin{aligned} p_1' &= c_{11}p_1 + c_{21}p_2 + c_{31}p_3 \\ p_2' &= c_{12}p_1 + c_{22}p_2 + c_{32}p_3 \\ p_3' &= c_{13}p_1 + c_{23}p_2 + c_{33}p_3 \end{aligned} \qquad \text{.....(4a)}$$

or, in tensor notation,

$$\left.\begin{aligned} p_i' &= c_{ki}p_k \\ \text{and, for the reverse transformation,} \\ p_i &= c_{ik}p_k' \end{aligned}\right\} \qquad \text{.....(4b)}$$

Figure 4.5 Vectorial transformation on rotation of Cartesian axes



$$\cos\alpha_2 \equiv c_{12}$$

$$\cos\beta_2 \equiv c_{22}$$

$$\cos\gamma_2 \equiv c_{32}$$

Equations (4b) are equivalent to the special case of equations (1) when the differentials of the general transformation are substituted by the direction cosines in (3).

Two vector quantities, p and q, associated with some point and related by a physical property, a, of that point, may be described by the equation,

$$P_i = a_{ki}\, q_i \qquad \text{.....(5)}$$

This equation implies that each component of p is a linear function of all the components of q. The physical property, a, is a second-rank tensor, having nine components, a_{ki}. The transformation of a upon rotation of the co-ordinate system is of great importance in the studies of many physical properties. The general transformation of a second-rank tensor has been given in equation (2); for this, particular, transformation, the differentials are replaced by the direction cosines, giving:

$$\left.\begin{aligned} a'_{ik} &= c_{li}\, c_{mk}\, a_{lm} \\ \text{or for the reverse transformation,} \\ a_{ik} &= c_{il}\, c_{km}\, a'_{lm} \end{aligned}\right\} \qquad \text{.....(6)}$$

Consider one particular term, a_{33}:

$$\begin{aligned} a'_{33} = {} & c_{13}\, c_{13}\, a_{11} + c_{13}\, c_{23}\, a_{12} + c_{13}\, c_{33}\, a_{13} \\ & + c_{23}\, c_{13}\, a_{21} + c_{23}\, c_{23}\, a_{22} + c_{23}\, c_{33}\, a_{23} \\ & + c_{33}\, c_{13}\, a_{31} + c_{33}\, c_{23}\, a_{32} + c_{33}\, c_{33}\, a_{33} \end{aligned} \qquad \text{.....(7a)}$$

For all real, physical properties which may be represented by a second rank tensor, it is found, experimentally, that $a_{12} = a_{21}$, $a_{23} = a_{32}$, $a_{13} = a_{31}$; that is, the physical properties are centro-symmetric. Hence:

$$a'_{33} = c^2_{13}a_{11} + c^2_{23}a_{22} + c^2_{33}a_{33} + 2c_{13}c_{23}a_{12} + 2c_{13}c_{33}a_{13} + 2c_{23}c_{33}a_{23} \ldots\ldots \quad \ldots\ldots(7b)$$

which is the equation of a surface of second order, usually a triaxial ellipsoid. There are, therefore, valid, as well as conceptual, reasons for representing such physical properties as ellipsoids.

These general remarks are good for many physical properties of crystals and may serve as an introduction to the particular subject of the next section.

* * *

4.6 Molecular and crystal magnetic susceptibilities

The magnetic susceptibility, χ , at a point is the property relating the magnetic field strength vector, H, to the induced magnetic moment, M (also a vector quantity), produced by it at that point:

$$M_i = \chi_{ki} H_k \quad \ldots\ldots(8)$$

Analagous to equation (7b) we have

$$\chi'_{33} = c^2_{13}\chi_{11} + c^2_{23}\chi_{22} + c^2_{33}\chi_{33} + 2c_{13}c_{23}\chi_{12} + 2c_{13}c_{33}\chi_{13} + 2c_{23}c_{33}\chi_{23} \ldots\ldots \quad \ldots\ldots(9)$$

which, if we chose appropriate co-ordinatesaxes, reduces to

$$\chi'_{33} = c^2_{13}\chi_1 + c^2_{23}\chi_2 + c^2_{33}\chi_3 \quad \ldots\ldots(10)$$

where χ_1, χ_2, χ_3 are the principal magnetic susceptibilities, directed along the major, median and minor axes of the magnetic ellipsoid.

In general, we wish to relate the molecular magnetic ellipsoid, defined by the principal molecular susceptibilities K_1, K_2, K_3 and their direction cosines with respect to the crystal axes, to the crystal magnetic ellipsoid (χ_1, χ_2, χ_3) which we measure experimentally.

The procedure can be illustrated for the monoclinic crystal class. The maximum symmetry here is that of reflexion plus inversion, when we take into account the centrosymmetry of the magnetic ellipsoid: the co-ordinates of equivalent points are $\pm (x,y,z\ ;\ x,\bar{y},z)$. For convenience, we shall relate the ellipsoids to an orthogonal co-ordinate system defined by two of the crystal axes a, b and their mutual normal c'. (see Figure 4.6). Relative to these axes, the direction cosines of the K_1, K_2, K_3 axes of any one molecule and its inversion are,

	a	b	c
K_1^A	c_{11}	c_{12}	c_{13}
K_2^A	c_{21}	c_{22}	c_{23}
K_3^A	c_{31}	c_{32}	c_{33}

for molecules A

only three of these being independent. The direction cosines of the principal axes of the other pair of molecules will be,

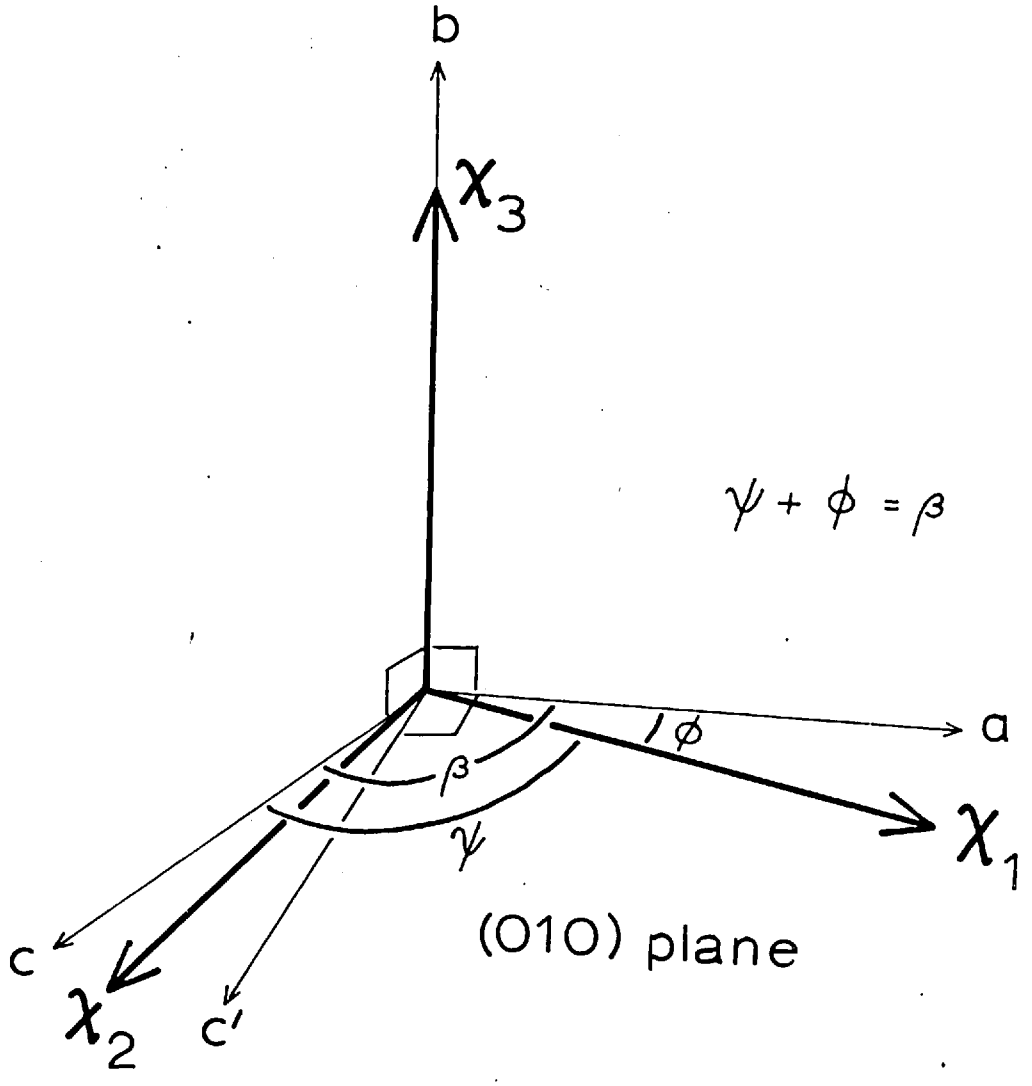


Figure 4.6 Definitions of crystal and magnetic axes for the monoclinic system

	a	b	c	
K_1^B	c_{11}	$-c_{12}$	c_{13}	
K_2^B	c_{21}	$-c_{22}$	c_{23}	for molecule B
K_3^B	c_{31}	$-c_{32}$	c_{33}	

We first transform each of these molecular magnetic ellipsoids into the orthogonal system (primed), abc′, using equation (11); compare equation (6)

$$K'_{ik} = c_{1i}\, c_{mk}\, K_{1m} \qquad \ldots\ldots(11)$$

where

$$K_{1m} = \begin{pmatrix} K_{11} & 0 & 0 \\ 0 & K_{22} & 0 \\ 0 & 0 & K_{33} \end{pmatrix};$$

to give,

$$K_{1m}^A = \begin{pmatrix} K_{11}c_{11}c_{11} + K_{22}c_{12}c_{12} + K_{33}c_{13}c_{13} & K_{11}c_{11}c_{21} + K_{22}c_{12}c_{22} + K_{33}c_{13}c_{23} & K_{11}c_{11}c_{31} + K_{22}c_{12}^2{}_{32} + K_{33}c_{13}c_{33} \\ K_{11}c_{21}c_{11} + K_{22}c_{22}c_{12} + K_{33}c_{23}c_{13} & K_{11}c_{21}c_{21} + K_{22}c_{22}c_{22} + K_{33}c_{23}c_{23} & K_{11}c_{21}c_{31} + K_{22}c_{22}c_{32} + K_{33}c_{23}c_{33} \\ K_{11}c_{31}c_{11} + K_{22}c_{32}c_{12} + K_{33}c_{33}c_{13} & K_{11}c_{31}c_{21} + K_{22}c_{32}c_{21} + K_{33}c_{33}c_{23} & K_{11}c_{31}c_{31} + K_{22}c_{32}c_{32} + K_{33}c_{33}c_{33} \end{pmatrix}$$

K^B_{lm} is numerically equal but with sign changes given by,

$$\begin{pmatrix} + & - & + \\ - & + & - \\ + & - & + \end{pmatrix}$$

We now transform the crystal magnetic ellipsoid, with direction cosines,

	a	b	c′
1	l_1	m_1	n_1
2	l_2	m_2	n_2
3	l_3	m_3	n_3

into the same co-ordinate frame. We have, therefore:-

$$\chi_{lm} = \begin{pmatrix} \sum \chi_{ii} l_i^2 & \sum \chi_{ii} l_i m_i & \sum \chi_{ii} l_i n_i \\ \sum \chi_{ii} m_i l_i & \sum \chi_{ii} m_i^2 & \sum \chi_{ii} m_i n_i \\ \sum \chi_{ii} n_i l_i & \sum \chi_{ii} n_i m_i & \sum \chi_{ii} n_i^2 \end{pmatrix}.$$

We have $\frac{1}{2}$ gm. mole each of A and of B molecules for a total of 1 gm. mole; therefore:-

$$\chi_{lm} = \tfrac{1}{2}K^A_{lm} + \tfrac{1}{2}K^B_{lm}$$

Equating, component by component,

$$\left.\begin{aligned} \sum \chi_{ii} l_i^2 &= \sum K_{ii} c_{1i}^2 & \sum \chi_{ii} l_i n_i &= \sum K_{ii} c_{1i} c_{3i} \\ \sum \chi_{ii} m_i^2 &= \sum K_{ii} c_{2i}^2 & \sum \chi_{ii} l_i m_i &= \sum K_{ii} c_{1i} c_{2i} = 0 \\ \sum \chi_{ii} n_i^2 &= \sum K_{ii} c_{3i}^2 & \sum \chi_{ii} m_i n_i &= \sum K_{ii} c_{2i} c_{3i} = 0 \end{aligned}\right\} \quad \ldots\ldots(12)$$

The crystal is monoclinic and, therefore, $m_2 = 1$; $m_1 = m_3 = 0$. Hence, we are left with one principal susceptibility along the 'b' axis,

$$\chi_3 = \chi_b = K_{11}c_{21}^2 + K_{22}c_{22}^2 + K_{33}c_{23}^2$$

the other two lying in the (010) plane. By convention, we define $|\chi_1| < |\chi_2|$ with χ_1 making an angle ϕ with a, ψ with c, where $\phi + \psi = \beta$ (the monoclinic obtuse angle), as shown in Figure 4.6. The angles ϕ and ψ are determined experimentally by noting the orientation of the crystal, suspended along the 'b' axis, in a magnetic field: all other direction cosines are calculated from structural data. Using the methods described in the following section to measure the principal crystal susceptibilities, and the relationships in (12), we can then compute the principal molecular susceptibilities. The general relationships between crystal and molecular magnetic ellipsoids for triclinic and monoclinic crystal classes and for those of higher symmetry are described in detail by Lonsdale and Krishnan (1936) and are discussed, where appropriate, in later chapters.

* * *

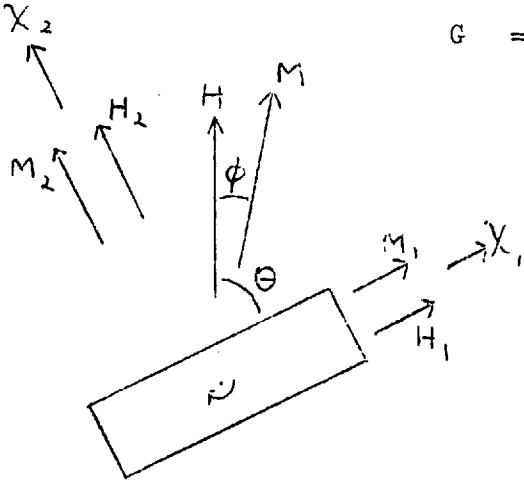
4.7 Experimental methods

Let us consider the action of a homogeneous magnetic field on a crystal of volume, v, which is free to rotate about an axis perpendicular to the field, containing one of the principal magnetic axes (say χ_3). The magnetic field, H, and the induced moment, M, will not generally have the same direction (this, of course, is why the property, χ, relating them is a tensor quantity). If the

angle between them is ϕ, then the couple, G, exerted on the crystal is given by

$$G = M \cdot H \cdot \sin\phi$$

M and H, being vector quantities, may be resolved into components M_1M_2, H_1H_2 parallel to the directions of the principal susceptibilities perpendicular to the axis of rotation of the crystal. The resultant couple, G, is equal to the difference between the two couples M_1H_2 and M_2H_1, acting in opposite senses;



$$G = M_1H_2 - M_2H_1$$

Now, $H_1 = H\cos\phi$, $H_2 = H\sin\phi$

If the principal susceptibilities are χ_1 and χ_2 then

$$M_1 = v\chi_1H_1, \quad M_2 = v\chi_2H_2$$

Hence:

$$G = v\chi_1H_1H_2 - v\chi_2H_2H_1$$

$$= vH^2 \sin\theta \cdot \cos\theta\,(\chi_1 - \chi_2)$$

$$= \tfrac{1}{2}vH^2 \sin2\theta\,(\chi_1 - \chi_2)$$

This couple is a maximum when $\sin2\theta = 1$

ie. when $\theta = \pi/4$

In practice, the crystal is suspended by a fine quartz fibre carried by a torsion head which may be rotated so that, initially, the crystal experiences no couple on application of the magnetic field; that is, the largest principal susceptibility (here χ_1) in the plane of the magnetic field is parallel to the field. With the field on, the torsion head is now rotated, causing the crystal to rotate against the field, the applied torque being balanced by the magnetic

couple, G. This reaches a maximum value ($= \frac{1}{2}vH^2(\chi_1 - \chi_2)$) when the crystal has rotated 45° from the field direction. Further rotation of the torsion head destroys the balance and the crystal 'flips' round violently. At the critical torque,

$$k\,(\alpha_c - \pi/4) = \tfrac{1}{2}vH^2\,(\chi_1 - \chi_2)$$

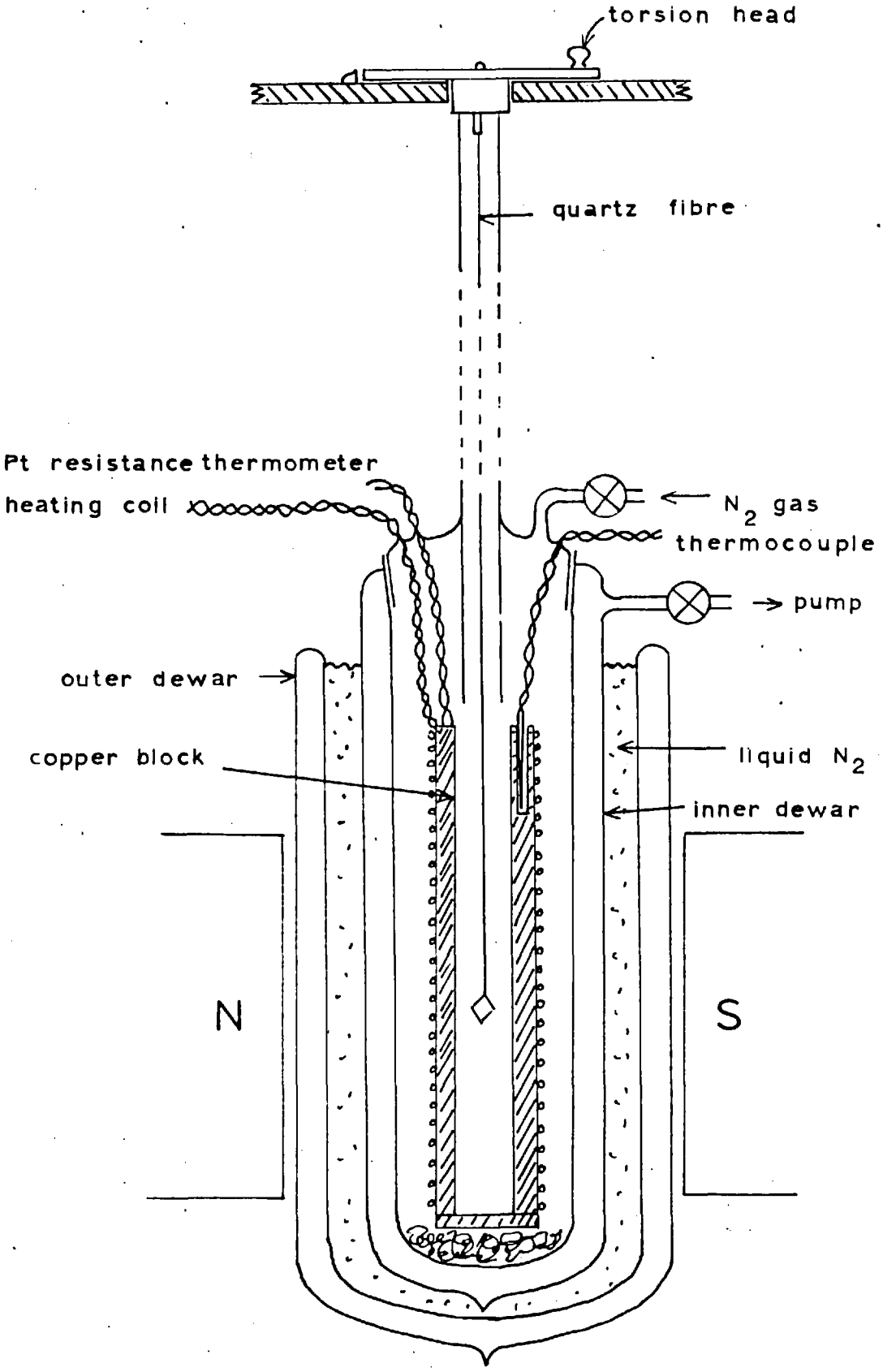
where k is the torsional constant of the fibre and α_c the critical angle through which the torsion head was rotated, which, in practice, may be anything from 1 to 50 complete revolutions. For the work described later, the torsional constant of the quartz fibres were determined by calibration using a crystal of known anisotropy. An absolute method for the determination of crystal anisotropies is given by Krishnan and Banerjee (1935). To measure all three principal susceptibilities, the crystal is also suspended along another principal direction and, for the sake of a check, along all three principal magnetic axes in turn. In addition, we require the value of $\bar{\chi}$, the average or bulk susceptibility of the substance, measured by the well-known Gory method. The relationships between $\bar{\chi}$ and the crystal anisotropies, $\Delta\chi_i$, are given for particular crystal symmetries, where appropri te, in Chapters 5 and 6.

* * *

4.8 Apparatus

The apparatus is shown in Figure 4.7 and follows the design of Figgis and Nyholm (1959). The electromagnet has 4" pole pieces with a gap of approx. 3" and is supplied with current of up to 5 amps from an unstabilized mains

Figure 4.7 Cryostat (schematic)



rectifier, producing field strengths up to $\sim$ 5000 gauss. The cryostat arrangement consists of a cylindrical copper block wound with a heating coil and surrounded by a coolant of liquid nitrogen in the outer dewar: a platinum resistance thermometer wound with the heating coil forms the fourth arm of a Wheatstone bridge network, any off-balance current, activating a Sunvic relay system controlling the heating current. The cooling effect of the liquid nitrogen may be reduced for higher block temperatures by evacuation of the inner dewar. The temperature of the copper block is measured with a thermo-couple inserted into it, calibrated using the known temperature dependence of the bulk susceptibility of cupric sulphate (Krishnan and Mookherji, 1938). The torsion head shown in the figure may be replaced by a Gouy balance for the powder measurements.

Packing inconsistancies may produce an error of $\frac{1}{2}$ - 1% in the Gouy determinations. The temperature of the block may be held constant and measured to $\pm$ 0.5° above 100°K or $\pm$ 1° from 80 - 100°K. The accuracy of the anisotropy measurements will be discussed in detail in the later chapters but, in general, the absolute values may be in error to $\pm$ 5% due to difficulties in orientating crystals on the fibres, while the relative accuracy (i.e. temperature dependence) is good to $\pm$ 1%

* * *

CHAPTER 5

The Paramagnetic Anisotropies of Tetrahedral Cobaltous Complexes

5.1 Introduction

While the anisotropy of the magnetic susceptibility of paramagnetic complexes of transition metals has been studied for some time, remarkably little attempt has been made to correlate molecular anisotropy with the stereochemical disposition of the ligands. This situation is in complete contrast with that for diamagnetic organic molecules where an extensive magnetochemical criterion of anisotropy on the one hand and structure and electron distribution on the other has been established (see, for example, Craig, Heffernan, Mason and Paddock, 1961; and references therein); Part of the explanation lies in the lack of detailed information relating to the crystal structure of complexes. The present report is concerned with the magnetic properties of three tetrahedrally co-ordinated cobaltous complexes for which some X-ray structural data already exist and for which studies of the mean magnetic susceptibilities have left the origin of the small observed Weiss constants (θ in the Curie-Weiss law) uncertain (Cotton, Goodgame and Goodgame, 1961; Figgis, 1960).

Ligand-field theory has, in general, been developed from the assumption that the immediate neighbours of a central metal ion are responsible for almost all the ligand field to which it is subject. In his original formulation of crystal field theory, Bethe (1929), however, included contributions from ions other than those forming the first co-ordination shell. A number of discussions

have since been held on the role of "long-range" contributions to the ligand field, particularly as they are reflected in magnetic properties (Van Vleck, 1958), but again have been inconclusive because of the lack of detailed structural information. With the nearest neighbours approximation, it can be assumed that the axes of the ligand field potential coincide with, or are simply related to, the axes of the system of the central ion together with its immediate neighbours. Where non-nearest neighbours are important in determining the electron distribution on the central metal ion, no such relationship may exist. The principal molecular susceptibilities of a central ion must correspond quite closely, so far as their direction is concerned, with the axes of the ligand field to which it is subject. With a field of rhombic or higher symmetry the magnetic and ligand-field axes should be coincident. Long-range contributions to the ligand field should therefore be analysable from a study of the paramagnetic molecular susceptibilities and their temperature dependence.

Subject to a crystal field from a regular tetrahedron of point charges, the ^4F free-ion ground term of Co^{2+} (d^7) is split in such a way as to make the lowest cubic-field term that which is designated $^4A_2$ (Figure 5.1); the $^4T_2$ term also arising from the free-ion ^4F term lies at about 3000 cm^{-1} above the $^4A_2$ term as may be readily determined by spectroscopic methods (Cotton et al., loc. cit.). Our first approximation assumes that it is possible to describe any departure of the ligand field from cubic symmetry by adding a tetragonal or trigonal ligand-field component to the tetrahedral field. Such a component splits the $^4T_2$ term and it has been shown (Figgis, loc.cit.) that second-order

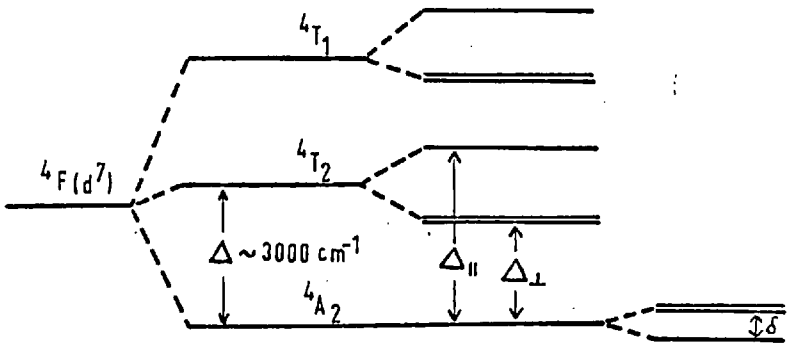


Figure 5.1

The splitting of a ^4F term (d^7) by a tetrahedral ligand field and spin-orbit coupling.

spin-orbit coupling between the $^4A_2$ and $^4T_2$ terms removes the spin degeneracy of the $^4A_2$ term. The molecular susceptibilities of the cobaltous ion are then related to the ligand field parameters by the expressions

$$K_{\parallel} = \frac{N\beta^2}{3kT}\frac{15}{}\left(1 - \frac{8k\lambda}{\Delta_{\parallel}}\right)\left(1 - \frac{2x}{5}\right) + \frac{8N\beta^2k^2}{\Delta_{\parallel}}$$

$$K_{\perp} = \frac{N\beta^2}{3kT}\frac{15}{}\left(1 - \frac{8k\lambda}{\Delta_{\perp}}\right)\left(1 + \frac{x}{5}\right) + \frac{8N\beta^2k^2}{\Delta_{\perp}} \qquad \text{.....(1)}$$

for $x = \delta/kT \ll 1$. k is the electron delocalisation factor. For $x \ll 1$, temperatures are high compared to δ. These relationships show a simple connection between the molecular magnetic susceptibilities and the ligand field parameters, and it is in this way that we may investigate the relationship between the molecular axes and the ligand field. [The assumption that the distortion of the ligand field is of tetragonal (or trigonal) symmetry may not be completely valid; however, as the experimental section will elaborate, the data available from the crystals we have studied are such that little information can be obtained on ligand-field components of symmetry lower than tetragonal. Throughout we are therefore concerned with only two molecular susceptibilities, $K_{\parallel}$ and $K_{\perp}$, which are respectively parallel and perpendicular to the axis of distortion.]

* * *

5.2 Experimental

Tricaesium pentachloro-cobalt(II), Cs_3CoCl_5

Crystals of this compound were prepared by the slow evaporation of an aqueous solution of cobaltous chloride containing several molar excess of caesium chloride. The crystals are tetragonal (Powell and Wells, 1935; Figgis, Gerloch and Mason, 1963) with well developed 001 faces surrounded by 101, 112 and 110 faces. The crystals are magnetically uniaxial, $\chi_{\parallel}$ lying along the unique four-fold axes of the crystal ('c') and $\chi_{\perp}$ in the ab plane. $\Delta\chi = \chi_{\parallel} - \chi_{\perp}$ was determined by suspending a crystal (25 mg.) with the ab plane vertical; both the temperature dependence of $\Delta\chi$ and its absolute value were determined as the mean for three separate crystals. The values of $\bar{\chi}$ and $\Delta\chi$ are listed in Table 5.1. The relation

$$\bar{\chi} = \frac{1}{3}(2\chi_{\perp} + \chi_{\parallel})$$

allows the calculation of $\chi_{\parallel}$ and $\chi_{\perp}$. $\Delta\chi_{303^{\circ}K} = 685.10^{-6}$ c.g.s.e.m.u. which compares reasonably well with the value of 650.10^{-6} c.g.s.e.m.u. reported by Krishnan and Mookherji (1938).

Dicaesium tetrachloro-cobalt(II), Cs_2CoCl_4

Suitable single crystals of Cs_2CoCl_4 were obtained by the slow evaporation of stoichiometric amounts of cobaltous and caesium chlorides in water. The crystals are orthorhombic (Porai-Koshits, 1954) with well formed 001 faces. The magnetic ellipsoid is defined by the three principal crystal susceptibilities χ_a, χ_b and χ_c lying along the orthogonal 'a', 'b', and 'c' axes of the crystal. The average susceptibility is now given by the relation

Table 5.1 Cs_3CoCl_5 - Crystal and Powder Susceptibilities

$^\circ$K	$\Delta\chi = \chi_{\parallel} - \chi_{\perp}$	$^\circ$K	$\bar{\chi}_{Co}$
80.0	4620	83.0	30185
86.6	4080	90.0	27635
89.7	3800	101.7	24685
94.9	3440	112.2	22425
100.7	3310	121.5	20765
101.8	3110	131.5	19685
104.5	3100	142.2	18155
109.5	2860	154.9	16915
116.0	2635	166.4	15645
120.9	2420.	166.6	15745
124.5	2400	178.0	14915
124.7	2360	187.3	13815
127.5	2262	192.5	13545
132.3	2145	200.6	13085
138.4	2040	211.7	12430
139.7	1971	223.1	11875
146.1	1874	232.4	11485
153.2	1711	239.1	11085
161.5	1587	244.5	10795
168.4	1500	250.8	10585
175.1	1440	260.7	10225
176.4	1389	270.8	9925
178.7	1408	282.1	9585
186.2	1300	285.5	9485
196.0	1212	292.5	9260
204.5	1146		
213.1	1092		
221.1	1050		
230.0	996		
237.4	949		
246.1	910		
253.2	867		
259.9	842		
267.5	815		
275.2	787		
282.5	759		
289.4	735		
294.9	717		

$$\bar{\chi} = \frac{1}{3}(\chi_a + \chi_b + \chi_c)$$

and the anisotropies

$$\Delta\chi_a = \left|\chi_b - \chi_c\right| \qquad \text{etc.}$$

are determined by suspension of the crystal along each of the crystal axes in turn. The crystal habit allowed an accurate determination of $\Delta\chi_a$ and $\Delta\chi_b$; $\Delta\chi_c$ may be subject to a systematic error of not more than 2% due to difficulties of crystal orientation along 'c'.

The magnetic data for Cs_2CoCl_4 are summarised in Table 5.2. Krishnan and Mookherji (loc.cit.) have again reported the values of the anisotropies at 303°K. These values are, however, referred to a non-primitive unit cell, the results of optical goniometric measurements being related to those determined by X-ray methods by a simple transformation.

	Krishnan and Mookherji (1938)	This investigation
$\Delta\chi_1 \cdot 10^4$ c.g.s.e.m.u.	254	260
$\Delta\chi_2 \cdot 10^4$ c.g.s.e.m.u.	394	415
$\Delta\chi_3 \cdot 10^4$ c.g.s.e.m.u.	146	158

Dipotassium tetrathiocyanato-cobalt(II) tetrahydrate, $K_2Co(CNS)_4 \cdot 4H_2O$

This was prepared by slowly lowering the temperature of an aqueous solution of the compound made by dissolving cobaltous thiocyanate in an appropriate amount of potassium thiocyanate; crystallisation as orthorhombic needles (Zdhanov and Zvonkova, 1950) was also from water and required several seeding procedures. The three principal anisotropies $\Delta\chi_a$, $\Delta\chi_b$ and $\Delta\chi_c$ are listed in Table 5.3.

Table 5.2 Crystal and powder susceptibilities of Cs_2CoCl_4

^{o}K	$\Delta\chi_a$	^{o}K	$\Delta\chi_b$	^{o}K	$\Delta\chi_c$	^{o}K	$\bar{\chi}_{Co}$
80.0	2837	83.5	1480	80.1	1155		
82.3	2778	85.4	1391	86.6	1069	82.5	30167
85.7	2637	93.0	1286	95.7	960	92.6	26777
89.9	2380	101.2	1122	107.2	829	106.9	24287
91.5	2350	110.9	960	117.2	745	118.0	22027
97.2	2148	120.0	854	128.7	662	135.4	19277
98.7	2054	127.6	770	140.5	596	147.6	17757
104.3	1994	137.1	685	149.1	555	159.5	16447
111.5	1805	144.4	625	158.2	516	171.4	15427
118.0	1615	156.0	545	170.0	471	183.3	14507
124.7	1505	166.9	485	177.5	446	197.0	13487
134.6	1340	175.8	438	186.1	418	200.4	13357
143.6	1211	183.6	410	197.3	390	211.3	12677
153.1	1101	192.5	361	205.0	377	223.8	12217
162.7	995	201.0	335	212.4	364	227.3	11787
170.0	928	209.8	310	222.7	342	242.6	11167
177.4	872	217.9	292	231.8	327	255.7	10647
186.5	814	225.6	272	241.1	318	267.6	10187
195.0	760	233.7	257	250.0	311	279.8	9827
202.6	713	244.4	234	260.1	299	289.1	9477
211.6	675	251.7	223	271.1	287		
221.5	630	260.2	211	280.0	277		
231.0	590	268.4	199	287.9	272		
240.8	560	276.8	190	295.3	264		
249.7	528	285.4	178				
259.3	500	293.8	165				
267.0	485						
276.5	456						
288.4	430						
297.5	418						

Table 5.3 Crystal and powder susceptibilities of $K_2Co(CNS)_4 \cdot 4H_2O$

^{o}K	$\Delta\chi_a$	^{o}K	$\Delta\chi_b$	^{o}K	$\Delta\chi_c$	^{o}K	$\bar{\chi}_{Co}$
81.3	1802	80.5	981	88.8	714	78.0	29410
82.0	1745	91.5	800	104.1	540	83.5	27370
89.6	1480	104.5	686	120.1	412	86.5	26500
95.5	1339	111.3	621	136.2	333	100.0	23270
102.4	1181	121.0	526	152.8	263	110.3	21310
116.3	996	132.4	478	174.4	190	120.0	19520
129.2	805	150.0	396	192.0	143	130.0	18070
142.5	694	151.0	382	212.0	132	143.8	16550
157.6	585	168.4	334			160.0	14960
174.3	489	174.0	292			178.2	13670
184.8	452	184.3	297			202.3	12090
198.6	389	200.9	260			220.5	11070
208.2	357	207.0	237			224.2	11170
226.4	307	220.2	233			231.7	10660
244.1	276	235.8	217			246.2	10170
264.8	251	246.0	205			260.0	9660
281.7	215	257.4	191			272.0	9350
		271.8	173			284.3	9080
		282.4	167			290.0	8740
		287.0	159			295.3	8570
		288.4	166				

They are self-consistent to only 7%. This error is due to two main sources: the crystals were acicular in habit with poorly developed 011 and $01\bar{1}$ faces. Orientation of the crystal for the measurement of $\Delta\chi_b$ and $\Delta\chi_c$ was particularly difficult and in contrast with the accurately determined $\Delta\chi_a$, these former results are accurate to only $\pm$ 2%. A larger source of error may originate from the variability in crystal composition; the crystal structure is such as to allow the free gain or loss of any of the four molecules of water of crystallisation without significant lattice distortion (Zdhanov and Zvonkova, loc.cit.), these water molecules not being associated with the co-ordination sphere about the cobalt atoms. The mean susceptibility was determined on the fully hydrated compound. This is not possible for the single crystals so that while the variability in water composition will not affect the temperature dependence of $\Delta\chi$, χ, or K, the absolute values of $\Delta\chi$ are each subject to a possible systematic error of up to 5%.

The results of the anisotropy determination for the three tetrahedral complexes are shown graphically in Figure 5.2.

Figure 5.3 shows that for each of the compounds the average susceptibility depends upon the temperature in a way which is predicted by the Curie-Weiss Law. The effective magnetic moments at room temperature defined by the equation $\mu_{eff} = 2.84\sqrt{\bar{\chi}_A T}$ are

Cs_3CoCl_5	4.66 $\pm$ 0.04 B.M.
Cs_2CoCl_4	4.71 $\pm$ 0.04 B.M.
$K_2Co(CNS)_4.4H_2O$	4.53 $\pm$ 0.04 B.M.

* * *

Figure 5.2 The temperature dependences of the principal anisotropies

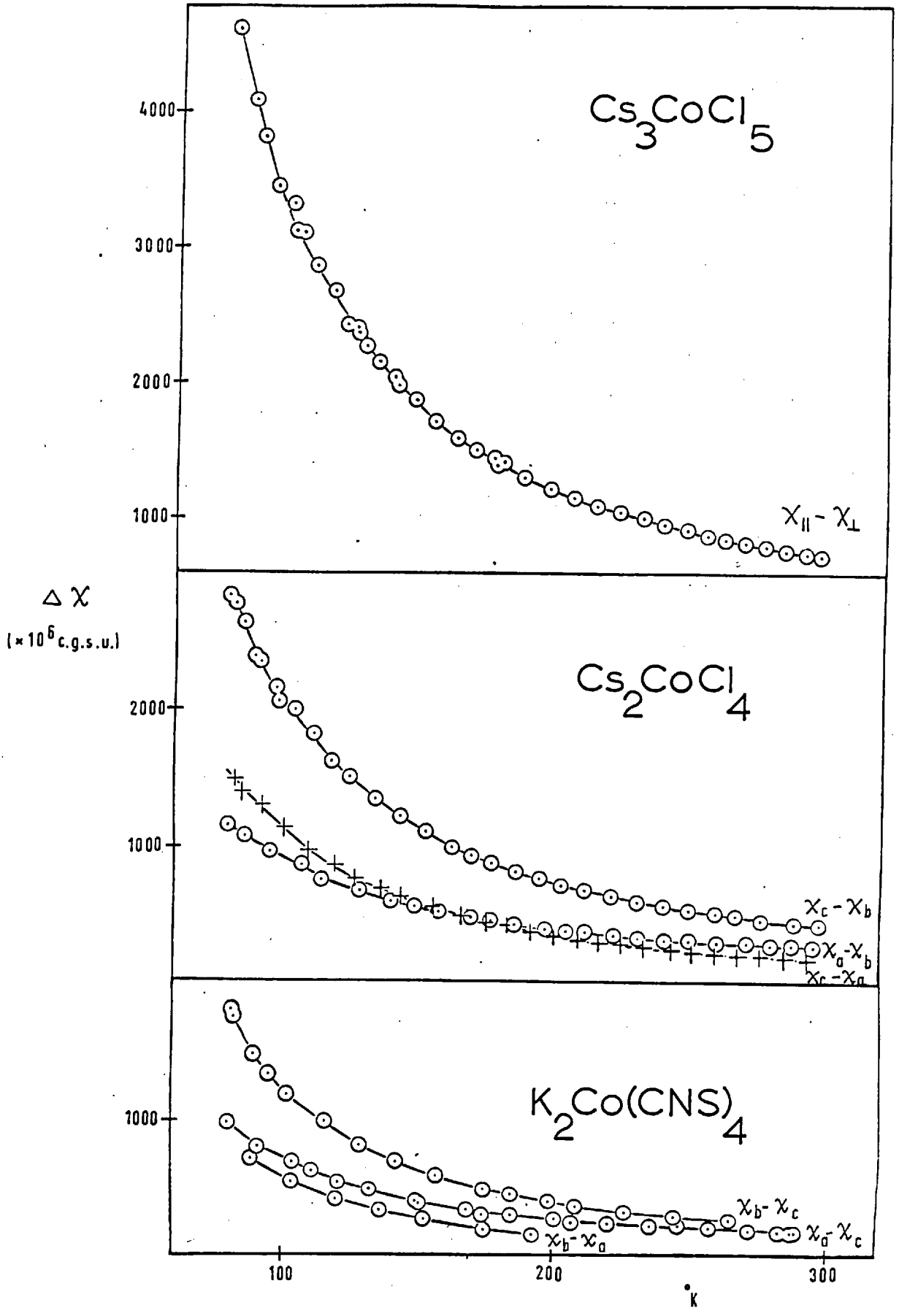
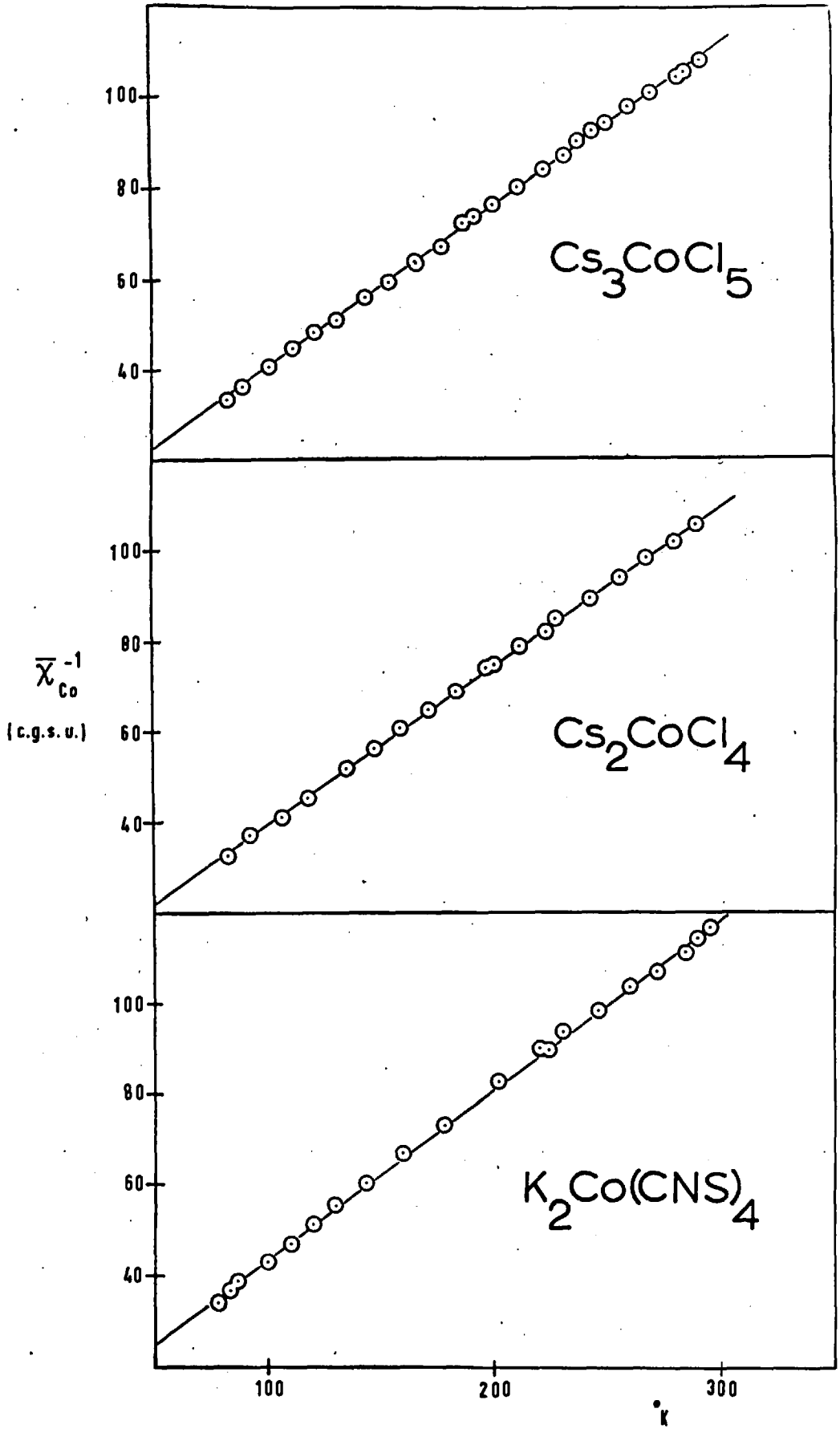


Figure 5.3 Curie-Weiss behaviour of the Powder susceptibility



5.3 The principal molecular susceptibilities and stereochemistry

The molecular susceptibilities K_i are related to the crystal susceptibilities χ_i by the expressions (compare 4.6)

$$K_1 = \sum_i \alpha_i^2 \chi_i$$

$$K_2 = \sum_i \beta_i^2 \chi_i \qquad i = 1, 2 \text{ or } 3$$

$$K_3 = \sum_i \gamma_i^2 \chi_i$$

with α_i, β_i and γ_i denoting the direction cosines of the i^{th} molecular axis referred to a set of orthogonal axes in the crystal ('a', 'b' and 'c' for the three present complexes).

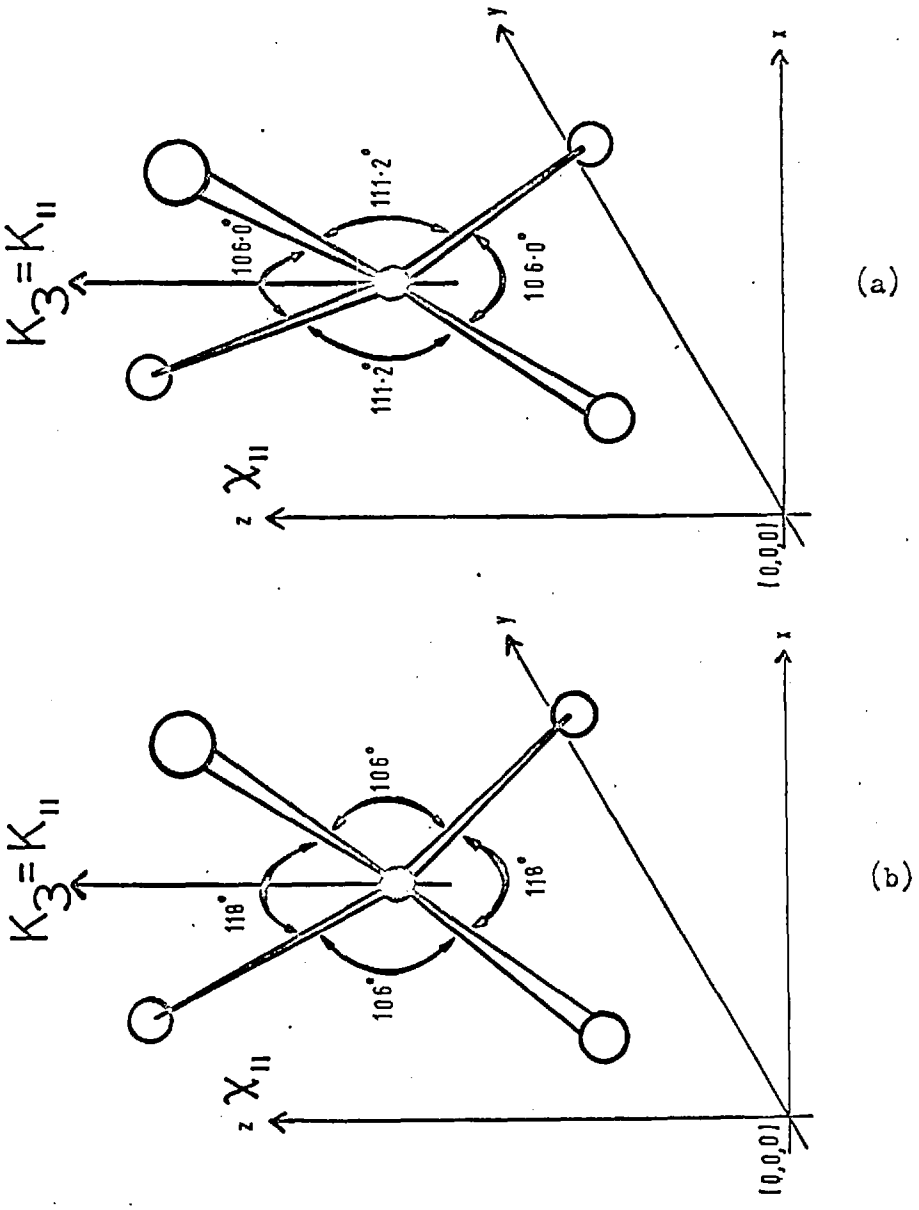
The molecular axes for all three complexes were chosen so as to coincide with the two-fold axes of the 'best' regular tetrahedron; their direction cosines can be calculated from the co-ordinates of Powell and Wells (loc.cit.), Figgis, Gerloch and Mason (loc.cit.) (Cs_3CoCl_5), Porai-Koshits (loc.cit.) (Cs_2CoCl_4), and Zdhanov and Zvonkova (loc.cit.) ($K_2Co(CNS)_4.4H_2O$).

Figure 5.4, illustrating the molecular arrangement in crystals of Cs_3CoCl_5, shows also that the molecular magnetic ellipsoid is identical with the crystal ellipsoid, that is $K_3 = \chi_{\perp}$ (χ_c) and $K_1 = (= K_2) = \chi_{\parallel}$ ($= \chi_a = \chi_b$). According to the co-ordinates given by Powell and Wells (loc.cit.), K_3 bisects the larger angle of the angularly distorted tetrahedron, whereas the later X-ray analysis shows it to bisect the smaller angle. In Cs_3CoCl_5, with its rigorous tetragonal distortion, $K_3 = K_{\parallel}$ (direction cosines 0, 0, 1, referred to the

Figure 5.4 Cs_3CoCl_5 - Molecular magnetic ellipsoid

(a) after Powell and Wells

(b) after Figgis, Gerloch and Mason



orthogonal axes a, b and c of the crystal) and $K_1 = K_2 = K_\perp$.

The chlorine co-ordination of the cobalt ions in the crystal structure of Cs_2CoCl_4 is shown in Figure 5.5; K_3 is chosen to bisect the largest angle of the distorted tetrahedron and has direction cosines -0.6442, 0.7649, 0, the direction cosines of K_1 (-0.5411, -0.4549, 0.7073) and K_2 (0.5411, 0.4549, 0.7073) being calculated to approximate to the bisectors of the angles $Cl_{(2)}$ - Co - $Cl_{(4)}$ and $Cl_{(1)}$ - Co - $Cl_{(4)}$ while maintaining the ortho-normality relation for K_1, K_2 and K_3. As K_3 approximates in direction to that of the unique axis of a tetragonally distorted tetrahedron, we define $K_\parallel = K_3$ and $K_\perp = K_1 = K_2$.

The distorted tetrahedral co-ordination of nitrogen atoms about a cobalt, at 0, $-\frac{1}{4}$, 0 in the unit cell of $K_2Co(CNS)_4.4H_2O$ is shown in Figure 5.6. The molecular susceptibility K_1 is chosen to lie along the crystallographic and molecular two-fold axis ('b'), and therefore has direction cosines 0, 1, 0 which, as above, are referred to the orthogonal crystallographic axes. By analogy with Cs_3CoCl_5 and Cs_2CoCl_4, K_3 was taken along the direction of the unique axis of distortion (direction cosines 0, 1, 0), while K_1 and K_2 were determined by the orthonormal relationship; K_1 (-0.9000, 0, 0.4360) and K_2 (0.4360, 0, 0.9000) closely bisect the angles N_1 - Co - N_2 and N_1 '- Co - N_2' respectively. Thus $K_\parallel = K_3$ $(= \chi_b)$ and $K_\perp = \frac{1}{2}(K_1 + K_2)$.

The calculated values of the principal molecular susceptibilities of the three compounds, based on these definitions, are listed in Table 5.4.

It is worth pointing out here that the geometrical distortion in all three complexes is simply angular: there is no significant difference in any of the

Figure 5.5 Cs_2CoCl_4 - Molecular magnetic ellipsoid

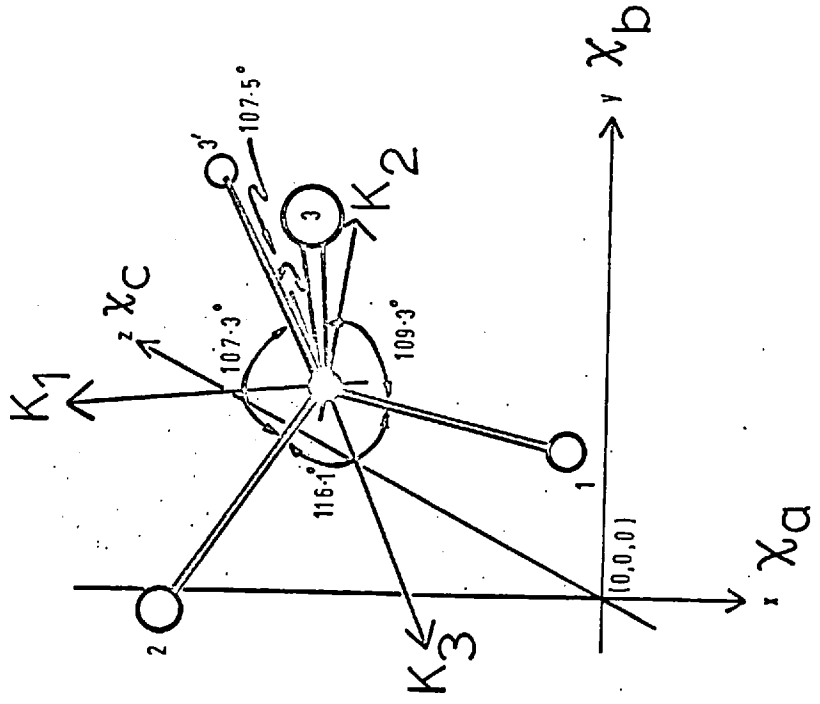


Figure 5.6 $K_2Co(CNS)_4$ - Molecular magnetic ellipsoid

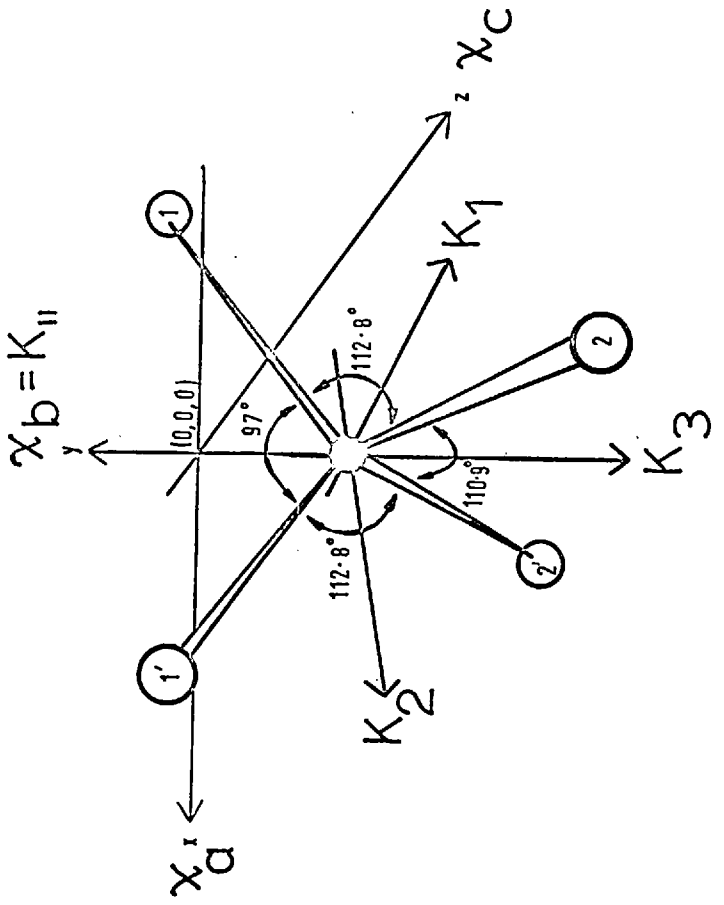


Table 5.4 Calculated principal molecular susceptibilities for Cs_3CoCl_5, Cs_2CoCl_4, and $K_2Co(CNS)_4 \cdot 4H_2O$

°K	Cs_3CoCl_5		Cs_2CoCl_4		$K_2Co(CNS)_4 \cdot 4H_2O$			
	$K_1=K_2=K_\perp$	$K_3=K_\parallel$	$K_1=K_2=K_\perp$	$K_3=K_\parallel$	K_1	K_2	$K_3=K_\parallel$	$K_\perp=\frac{1}{2}(K_1+K_2)$
80	28,743	33,413	32,174	27,412	26603	28204	28696	27403
90	26,067	29,827	28,976	24,866	24229	25602	25887	24915
100	23,810	27,020	26,319	22,825	22175	23359	23572	22762
110	21,907	24,707	24,102	21,030	20492	21501	21702	20996
120	20,287	22,757	22,229	19,554	19010	19887	20049	19448
130	18,900	21,090	20,655	18,283	17829	18599	18731	18214
140	17,693	19,663	19,251	17,140	16660	17354	17449	17007
150	16,640	18,410	18,040	16,151	15719	16345	16421	16032
160	15,683	17,293	16,974	15,267	14830	15397	15463	15113
170	14,840	16,310	16,034	14,482	14052	14580	14623	14316
180	14,077	15,437	15,185	13,765	13356	13841	13864	13598
190	13,387	14,657	14,421	13,113	12715	13160	13172	12937
200	12,785	13,970	13,718	12,508	12135	12556	12553	12345
210	12,094	13,322	13,115	11,983	11591	11989	11980	11790
220	11,701	12,748	12,533	11,495	11117	11496	11476	11306
230	11,230	12,220	12,017	11,037	10674	11028	11003	10851
240	10,799	11,734	11,532	10,602	10252	10596	10565	10424
250	10,405	11,290	11,091	10,227	9873	10198	10169	10035
260	10,029	10,871	10,688	9,856	9515	9820	9796	9667
270	9,678	10,478	10,305	9,518	9196	9483	9460	9338
280	9,351	10,116	9,955	9,207	8896	9153	9143	9025
290	9,046	9,777	9,625	8,912				
300	8,767	9,467	9,314	8,626				
310	8,503	9,175						

respective Co-Cl and Co-N bond lengths.

* * *

5.4 A qualitative correlation of susceptibilities with ligand field parameters

Before discussing the relation of the principal molecular susceptibilities and their dependence on temperature to the geometry of the ligand atoms which surround the cobalt atoms in the three complexes, the results of Table 5.4 can first be modified to allow for the temperature-independent paramagnetism term of equation (1). An accurate determination of this value is impossible from our present data although a reasonable estimate can be derived by finding what value subtracted from χ gives a Curie-Weiss Law behaviour at high temperatures, the results are 500 . 10^{-6} c.g.s.e.m.u. in Cs_2CoCl_4 and Cs_3CoCl_5 and 600 . 10^{-6} c.g.s.e.m.u. in $K_2Co(CNS)_4.4H_2O$ (all ± 100 . 10^{-6} c.g.s.e.m.u.) and are averages for $K_{||}$ and $K_{\perp}$ in each complex. The estimates, while of limited accuracy, are, at least in the case of the chlorides, consistent with the cubic ligand field parameter of 10 Dq = -3200 $cm.^{-1}$ (Cotton et al., loc.cit.) provided that a delocalisation factor $k \approx 0.9$ is used; on the other hand, a smaller result for the temperature-independent paramagnetism term for $K_2Co(CNS)_4$ would have been expected since 10 Dq is now -4550 $cm.^{-1}$ (Cotton et al., loc.cit.). Fortunately the correction is small so that its precise value is unimportant. Susceptibilities which have been corrected in this way are denoted by the primed symbols, K'.

The magnetic data are conveniently summarised by plotting the function

8 K'T/15 against T. Here, $8 = 3k/N\beta^2$ and 15 is the value of μ^2_{eff} for the "spin-only" d^7 system, so that 8K'T/15 is the ratio of the observed value of K'T to the corresponding result for the "spin-only" system. Figure 5.7 shows these data for both $K'_{||}T$ and $K'_{\perp}T$ for the three complexes.

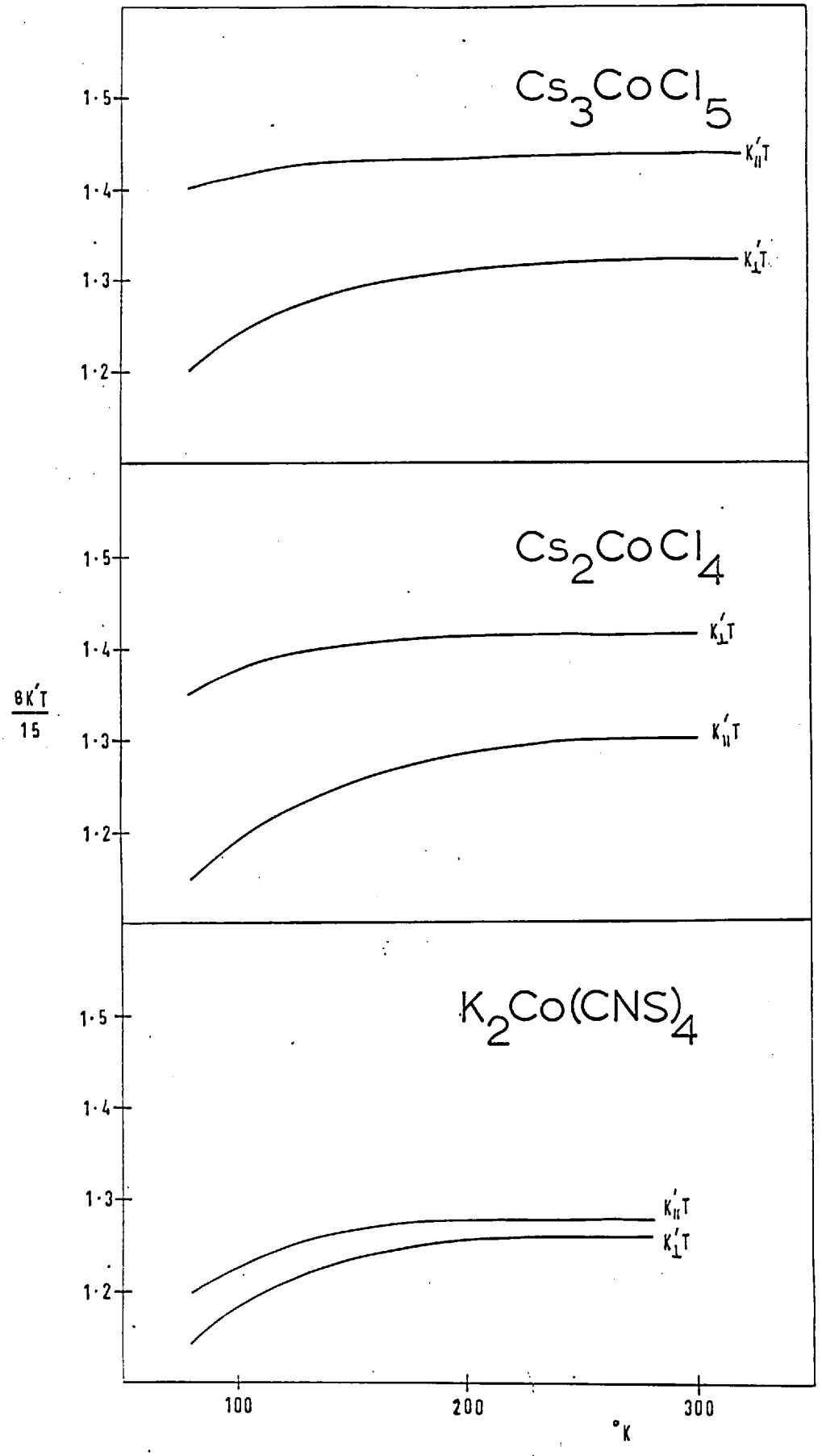
For reasons of simplicity rather than rigour, this discussion is based on three assumptions: that the symmetry of the ligand field acting on the Co^{2+} ions is approximately tetragonal; that the ligand field parameters $\Delta_{||}$ and $\Delta_{\perp}$ are essentially independent of temperature; and, finally, that the spin-orbit coupling and electron delocalisation parameters are isotropic ($\lambda_{||} = \lambda_{\perp}$, $k_{||} = k_{\perp}$).

In principle, δ of Figure 5.1 and equation (1) is related to the splitting $(\Delta_{||} - \Delta_{\perp})$ of the $^4T_2$ term, an unsophisticated calculation (Figgis, loc.cit.) giving

$$\delta = 8\lambda^2 (\Delta_{||}^{-1} - \Delta_{\perp}^{-1}) \qquad .....(2)$$

Miejen and Gernitsen (1955) have given a somewhat different relation by a more detailed treatment but in either case it should be possible to obtain estimates of $\Delta_{||}$ and $\Delta_{\perp}$ independent of those available from equation (1). It has, however, been pointed out (Kamimura, 1960; Tanabe and Sugano, 1958) that observed values of δ are not reproduced, even so far as their sign is concerned, when such calculations are performed in systems where the splitting of the excited terms by a low symmetry ligand field is known with some accuracy from spectroscopic studies. The same result is clear from the present data: in none of the three compounds is the temperature dependence predicted by the

Figure 5.7 Plots of $8K'T/15$ versus temperature



effect found. For the chloride complexes, the result is confused by the effects of magnetic exchange. Electron spin resonance measurements of Cs_3CoCl_5 have given δ as -9 cm.$^{-1}$ in the undiluted compound (Owen, unpublished work cited in Bowers and Owen, 1955) but the significance of this result is not clear because of antiferromagnetic exchange in the crystals (vide infra). The calculation of δ is one of second order so that the unsatisfactory nature of the results does not cast doubt on equation (1) which is obtained in the first order. Observed relative magnitudes of $K_{||}$ and $K_{\perp}$ are given in Table 5.5 and the relative values of $\Delta_{||}$ and $\Delta_{\perp}$ deduced from equation (1) are also listed.

The relationship of the ligand field parameters $\Delta_{||}$ and $\Delta_{\perp}$ to the detailed molecular geometry of the respective complexes can now be considered. Figure 5.8a represents the regular tetrahedron constructed from the alternate corners of a cube, through the centres of whose faces pass the Cartesian axes, X, Y and Z. In the regular tetrahedron, the d_{xy}, d_{xz} and d_{yz} orbitals are degenerate. If the tetrahedron is distorted so as to bring the tetrahedral vertices closer to the Z axis, the relationship between $\alpha_{||}$ and $\alpha_{\perp}$ (cf. Figure 5.8a) is $\alpha_{||} < \alpha_{\perp}$. In spite of the possibility of considerable covalency in the metal-ligand bond, we can use the simple crystal field theory, representing ligands as point charges, to show that the repulsion between ligand charges at the tetrahedral positions and an electron in the d_{xy} orbital is reduced while that between the charges and electrons in the d_{xz} and d_{yz} orbitals is increased. This splitting of d orbitals in a distorted tetrahedral ligand field is represented in Figure 5.8b.

Table 5.5 Relative values of molecular susceptibilities and ligand field parameters

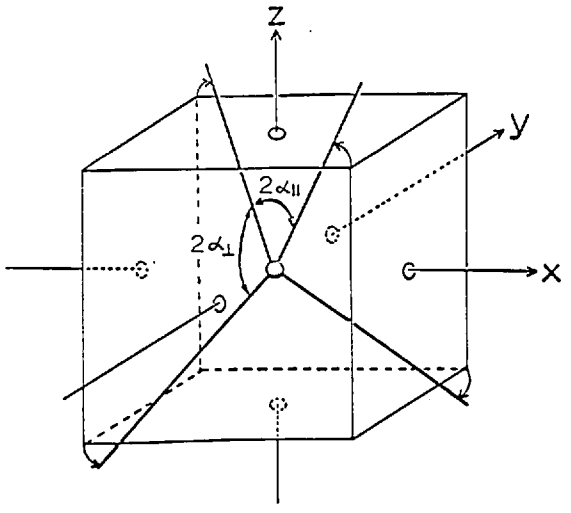
Compound	Molecular susceptibilities		
Cs_3CoCl_5	$K_{\parallel} > K_{\perp}$	$\Delta_{\parallel} < \Delta_{\perp}$	$\alpha_{\parallel} < \alpha_{\perp}$
Cs_2CoCl_4	$K_{\parallel} < K_{\perp}$	$\Delta_{\parallel} > \Delta_{\perp}$	$\alpha_{\parallel} > \alpha_{\perp}$
$K_2Co(CNS)_4.4H_2O$	$K_{\parallel} > K_{\perp}$	$\Delta_{\parallel} < \Delta_{\perp}$	$\alpha_{\parallel} < \alpha_{\perp}$

Table 5.6 $(CoCl_4)^{2-}$ and $Co(CNS)_4^{2-}$. Ligand field parameters

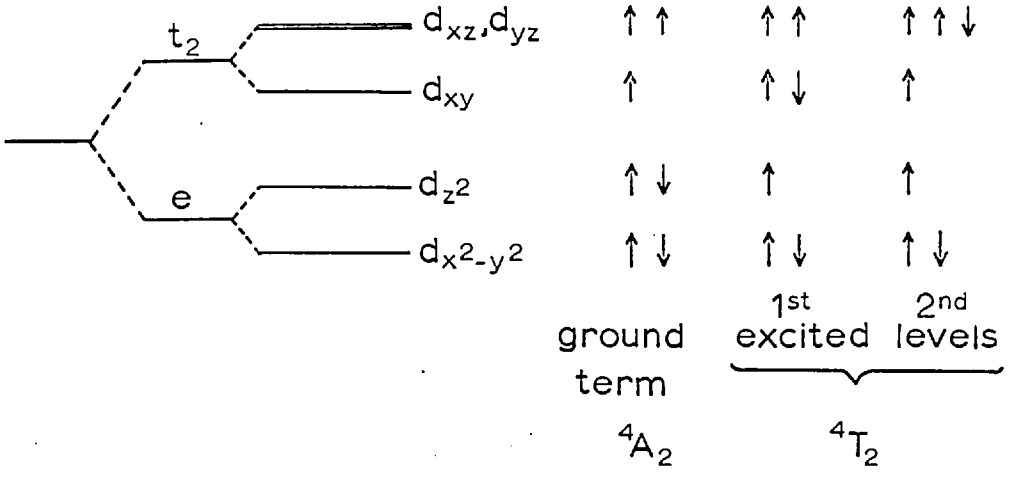
Parameter	Cs_3CoCl_5	Cs_2CoCl_4	$K_2Co(CNS)_4.4H_2O$
$8k^2\lambda_0/\Delta_{\parallel}$	-0.437	-0.303	-0.276
$8k^2\lambda_0/\Delta_{\perp}$	-0.323	-0.413	-0.258
$10\ Dq = -\frac{1}{2}(\Delta_{\parallel} + 2\Delta_{\perp})$*	-3200 $cm.^{-1}$	-3200 $cm.^{-1}$	-4550 $cm.^{-1}$
Δ	900 $cm.^{-1}$	-1000 $cm.^{-1}$	450 $cm.^{-1}$
k	0.91	0.93	0.93
$\Delta_{calc.}$	400 $cm.^{-1}$	-430 $cm.^{-1}$	600 $cm.^{-1}$

* Cotton, Goodgame and Goodgame (loc.cit)

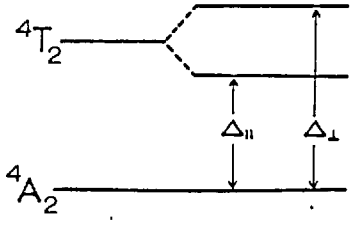
Figure 5.8 Ligand-field distortions and energy levels in tetrahedral d^7 complexes



(a)



(b) (c)



(d)

Within the approximation that electron repulsions are small although sufficient to prevent spin-pairing, we can now examine how the electrons are arranged in the d orbitals (the fact that the approximation is not strictly valid for tetrahedral Co^{2+} complexes does not affect the present argument). The distortion of the ligand field does not, of course, affect the ground $^4A_2$ term which corresponds to the configuration $d^2_{x^2-y^2} \cdot d^2_{z^2} d^1_{xy} (d_{xz}\ d_{yz})^2$. The lowest quartet excited configuration which can be written is $d^2_{x^2-y^2} \cdot d^1_{z^2} d^2_{xy} (d_{xz}\ d_{yz})^2$ and is orbitally non-degenerate (Figure 5.8c); the next highest quartet configuration is $d^2_{x^2-y^2} \cdot d^1_{z^2} \cdot d^1_{xy} (d_{xz}\ d_{yz})^3$ and is orbitally two-fold degenerate. A more rigorous treatment of the problem confirms these simple considerations and shows that for a distortion of the type shown in Figure 5.8a, the $^4T_2$ term is split according to the scheme illustrated in Figure 5.8d. The simplest form of crystal field theory therefore predicts the relationships,

$$\alpha_{\parallel} < \alpha_{\perp} \quad , \quad \Delta_{\parallel} < \Delta_{\perp}$$

$$\alpha_{\parallel} > \alpha_{\perp} \quad , \quad \Delta_{\parallel} > \Delta_{\perp}$$

which a comparison with the results of Table 5.5 shows are valid for the three complexes which we have studied. This agreement shows that in spite of some covalent character in metal-ligand bonds, a simple electrostatic model forms a reasonable basis for the discussion of distortions from cubic symmetry in tetrahedral cobaltous complexes; it also indicates that "long-range" crystal field effects are relatively unimportant.

It is interesting to note that these simple arguments were sufficient to indicate that the bond angles of the $CoCl_4^{2-}$ ion reported by Powell and Wells (loc.cit.) were incorrect and suggested to us the value of a more detailed X-ray analysis based on a least squares refinement (Figgis, Gerloch and Mason, loc.cit. - see also Appendix in this chapter.). The results of this later analysis confirm the prediction based on the magnetic anisotropy; that $2\alpha_{\parallel} < 2\alpha_{\perp}$.

* * *

5.5 Quantitative correlations

We can continue, in view of the success of the above qualitative correlations, by investigating quantitative relationships between molecular geometry and the magnitude of the low symmetry crystal field component. Combining the results of Figure 5.7 with equation (1) as $x \rightarrow \infty$ and assuming that λ is reduced below the free-ion value ($\lambda_0 = -172$ cm.$^{-1}$) by the factor k (Griffiths, 1961) it becomes possible to estimate both k and Δ (Table 5.6).

k determined in this way is in reasonable agreement with the magnitudes found for the temperature-independent paramagnetism term above and for the reduction in the interelectronic repulsion parameter B determined from the spectra of the complexes by Cotton et al. (loc.cit.).

Calculations of the energies of the five d orbital wave functions (m_l) as a function of the deviation of the ligand-metal-ligand angle in a distorted cube from the symmetrical value have recently been made by Randic (1961) and the results may be applied directly to the case of tetrahedral complexes. Their

application to the $^4T_2$ term of d^7 (Co^{2+}) requires a knowledge of the way in which the T_2 term orbital wave functions are built up from single electron wave functions. The calculations are performed first for the $^3T_{2g}$ term of d^3 in octahedral symmetry: the results for d^7 may be obtained by considering the inversion properties for 'holes' relative to electrons in the 'd' shell, and for tetrahedral ligand fields relative to octahedral fields.

The T_2 orbital wave functions can be written (cf. Penney and Schlapp, 1932) in terms of the free ion F term wave functions $\langle 3, M_L \rangle$

$$\langle \tfrac{1}{2} \rangle = 24^{-\frac{1}{2}} \left[3 \langle 3, 3 \rangle + 15^{\frac{1}{2}} \langle 3, -1 \rangle \right]$$

$$\langle - \rangle = 2^{-\frac{1}{2}} \left[\langle 3, 2 \rangle - \langle 3, -2 \rangle \right]$$

$$\langle -\tfrac{1}{2} \rangle = 24^{-\frac{1}{2}} \left[3 \langle 3, -3 \rangle + 15^{\frac{1}{2}} \langle 3, 1 \rangle \right]$$

$\langle \pm\frac{1}{2} \rangle$ obey the relationship

$$\langle\langle \pm\tfrac{1}{2} \rangle | L_z | \langle \pm\tfrac{1}{2} \rangle\rangle = \pm\tfrac{1}{2} .$$

The wave functions $\langle 3, M_L \rangle$ are themselves composed of single electron wave functions (m_ℓ),

$$\langle 3, \pm 3 \rangle = (\pm 2, \pm 1)$$

$$\langle 3, \pm 2 \rangle = (\pm 2, 0)$$

$$\langle 3, \pm 1 \rangle = (^2/_5)^{\frac{1}{2}} (\pm 1, 0) + (^3/_5)^{\frac{1}{2}} (\pm 2, \pm 1)$$

$$\langle 3, 0 \rangle = (^4/_5)^{\frac{1}{2}} (1, -1) + 5^{-\frac{1}{2}} (2, -2)$$

where, for example, (2,0) represents the Slater determinantal wave function $2^{-\frac{1}{2}} (2)(0) - (0)(2)$. The energies of $\langle \pm \tfrac{1}{2} \rangle$ and $\langle - \rangle$ may now be obtained as

$$E_{\langle \pm \frac{1}{2} \rangle} = 0.25\, H_{(0,0)} + H_{(1,1)} + 0.75\, H_{(2,2)} + 0.75\, H_{(2,-2)}$$

$$E_{\langle -1 \rangle} = H_{(2,2)} + H_{(0,0)} - H_{(2,-2)}$$

If V is the crystal field potential (Randic, loc.cit.) we have

$$H_{(i,j)} = \langle (i) \mid V \mid (j) \rangle$$

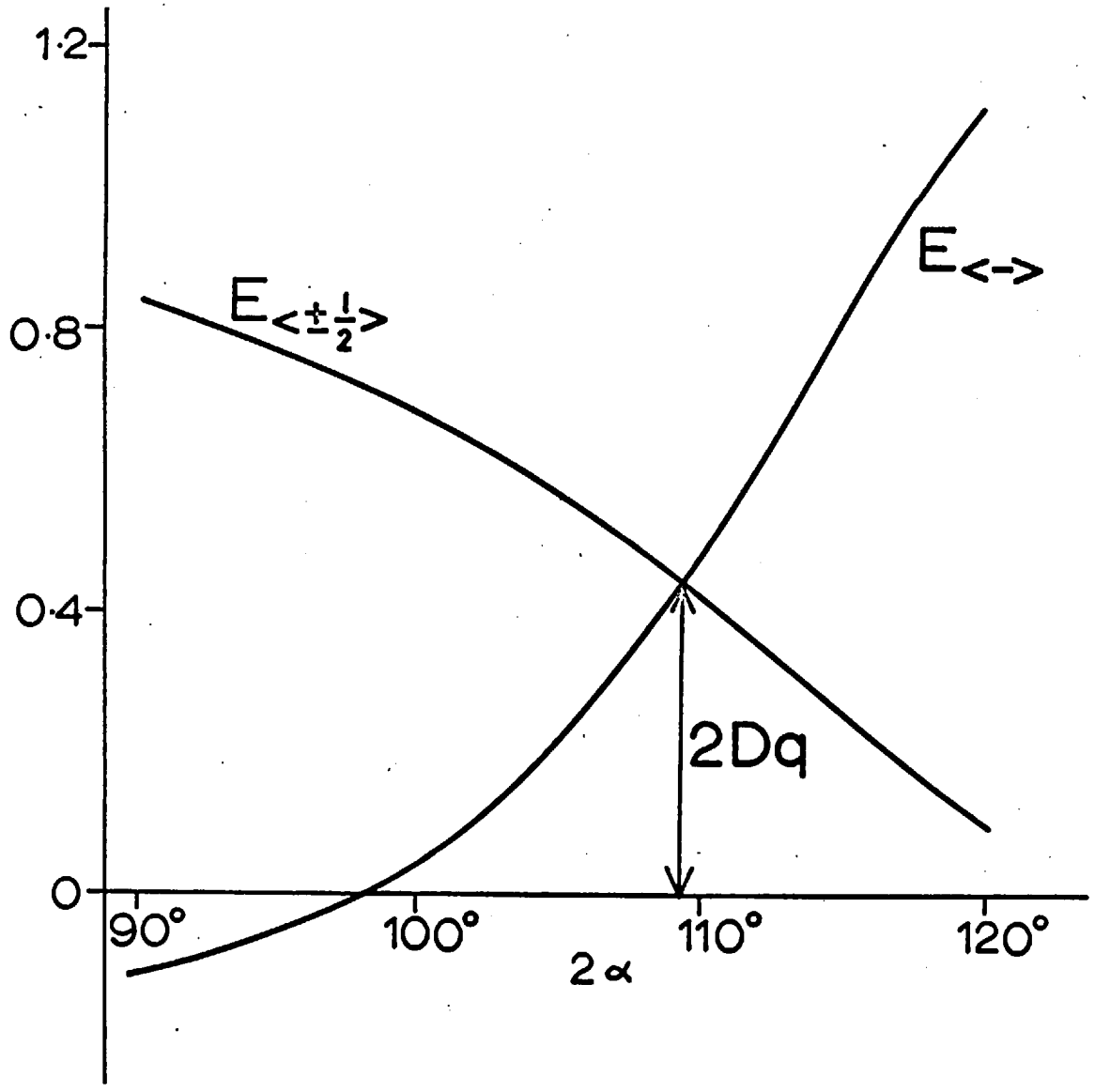
With these expressions for H_{ij} the dependence of the energies of $\langle \pm \frac{1}{2} \rangle$ $\langle - \rangle$ on the angle α between the S_4 axis and a vertex of a flattened or elongated tetrahedron can be calculated (2α is, of course, 109° 28' for a regular tetrahedron); the results are shown in Figure 5.9. This figure is constructed for $\overline{r_{3d}^4} / \overline{r_{3d}^2} = 3$ (Ballhausen, 1954); for a regular tetrahedron both levels lie at an energy 2Dq.

Throughout we have defined K_{11} as coinciding with the S_4 axis or what closely approximates to the S_4 axis (Figures 5.4 - 6). Thus for Cs_3CoCl_5 the value of 2α is 106°; the distortions Δ predicted by the theory may be obtained as

$$\Delta_{calc} = 5(E_{\langle \pm \frac{1}{2} \rangle} - E_{\langle - \rangle}) / E_0$$

where E_0 is the energy of the degenerate levels at $2\alpha = 109^\circ$ 28'. In Cs_2CoCl_4 2α has the values 107° and 117° and the mean of the energies for the levels at these two angles was used in deducing Δ_{calc}; results for all three complexes are included in Table 5.6, which shows that the calculated values of Δ are at least of the same magnitude as the experimental data. We should hardly expect better agreement in view of the gross approximations involved - the averaging of energies in Cs_2CoCl_4, the assumption that $\overline{r_{3d}^4} / \overline{r_{3d}^2} = 3$ and finally the considerable uncertainties in the experimental estimation of Δ. Certainly the

Figure 5.9 The dependence of $E\langle \pm \frac{1}{2} \rangle$ and $E\langle - \rangle$ on 2α for $\overline{r^4}/\overline{r^2} = 3$



close agreement of the ratios of the calculated to the observed distortions of Cs_3CoCl_5 and Cs_2CoCl_4, which are of opposite signs in the two compounds, must be regarded as some confirmation of the basic reliability of the local environment approximation. The change in the ratio of the calculated to observed distortion in going from the chlorides to the thiocyanate complex is again scarcely surprising in view of the change of ligand type.

* * *

5.6 Magnetic exchange phenomena

In the presence of zero field splitting, equation (1) predicts that if, say, $K'_{||}T$ increases with decreasing temperature, $K'_{\perp}T$ will decrease. Figure 5.7 shows that neither of these products increases with decrease of temperature for any of the complexes reported here. This result can be attributed to the presence of magnetic exchange, of an antiferromagnetic nature, between adjacent cobalt ions in the crystal lattice, the effect of which is to reduce K' more rapidly than the zero field splitting effect can increase it. The inequality

$$\theta > \sim \delta/5$$

expresses the condition that the magnetic exchange gives rise to a Weiss constant θ sufficiently large to override the zero field splitting effect. While equation (2) does not even predict its correct sign it may be used to give a very approximate idea of the magnitudes to be expected for δ. With the values of $\Delta_{||}$, $\Delta_{\perp}$, 10 Dq and k derived above, δ can be expected to be of the order of 10 $cm.^{-1}$; a Weiss constant from magnetic exchange of a few degrees is

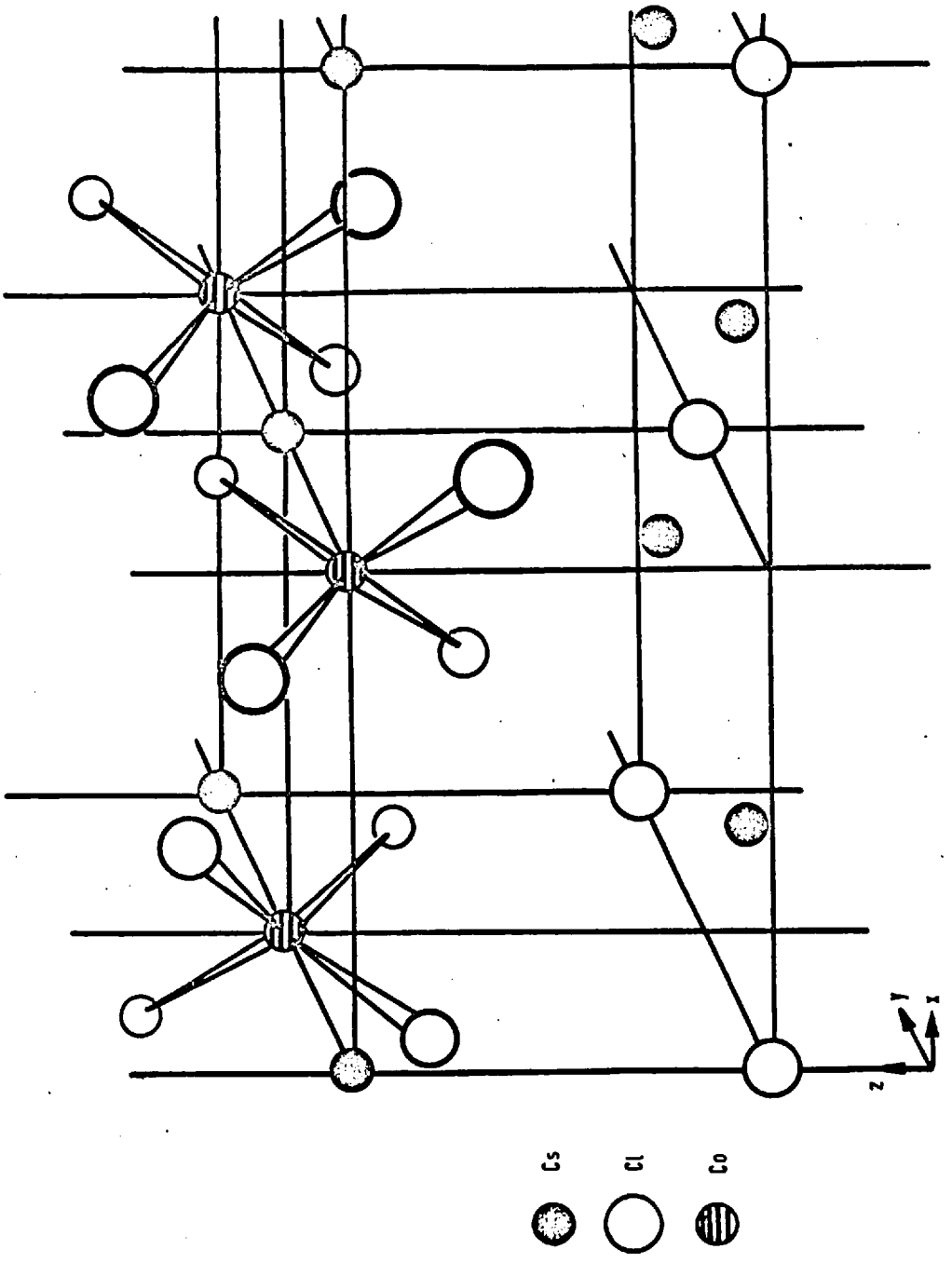
therefore sufficient to interfere with the interpretation of zero field splitting.

The mechanism for magnetic exchange in the chloro-complexes seems clear in relation to their crystal structures. Figure 5.10a shows that the crystal structure of Cs_3CoCl_5 is built up from alternate layers of Cs_2CoCl_4 and CsCl. Within each layer of Cs_2CoCl_4, the $(CoCl_4)^{2-}$ tetrahedra are arranged (Figure 5.10b and 5.10c) with chlorines above and below the 001 plane, the distance separating the + and - chlorine atoms of adjacent tetrahedra being 3.95 Å (Figgis, Gerloch and Mason, loc.cit.). Magnetic exchange in two dimensions, entirely similar to that proposed for three-dimensional interactions, by Griffiths, Owen, Park and Partridge (1959) for iridium ions in $(NH_4)_2IrCl_6$ and K_2IrCl_6, can thus be envisaged. By treating the neighbouring pairs of chlorine atoms on adjacent $(IrCl_6)^{2-}$ octahedra as extended chlorine molecules, these authors obtained a semiquantitative agreement between calculated and observed values of the exchange integral, J. Qualitatively, the concept of magnetic exchange transmitted by the proposed mechanism is consistent with the data of Cs_3CoCl_5, since it is to be expected that exchange will be much larger in the direction of $K_\perp$, which lies in the Cs_2CoCl_4 layers, than for $K_{\parallel}$, along which direction the $(CoCl_4)^{2-}$ tetrahedra are separated by layers of CsCl. The T.I.P. corrected molecular susceptibilities $K'_{\parallel}$ and $K'_\perp$ obey Curie-Weiss laws with $\theta_{\parallel} = 3^\circ$ and $\theta_\perp = 10^\circ$; the large effect of exchange on $K'_\perp$ may also be seen in Figure 5.7.

The equation

$$\theta = zJS(S + 1) / 3k$$

Figure 5.10 (a) Layer structure in Cs_3CoCl_5



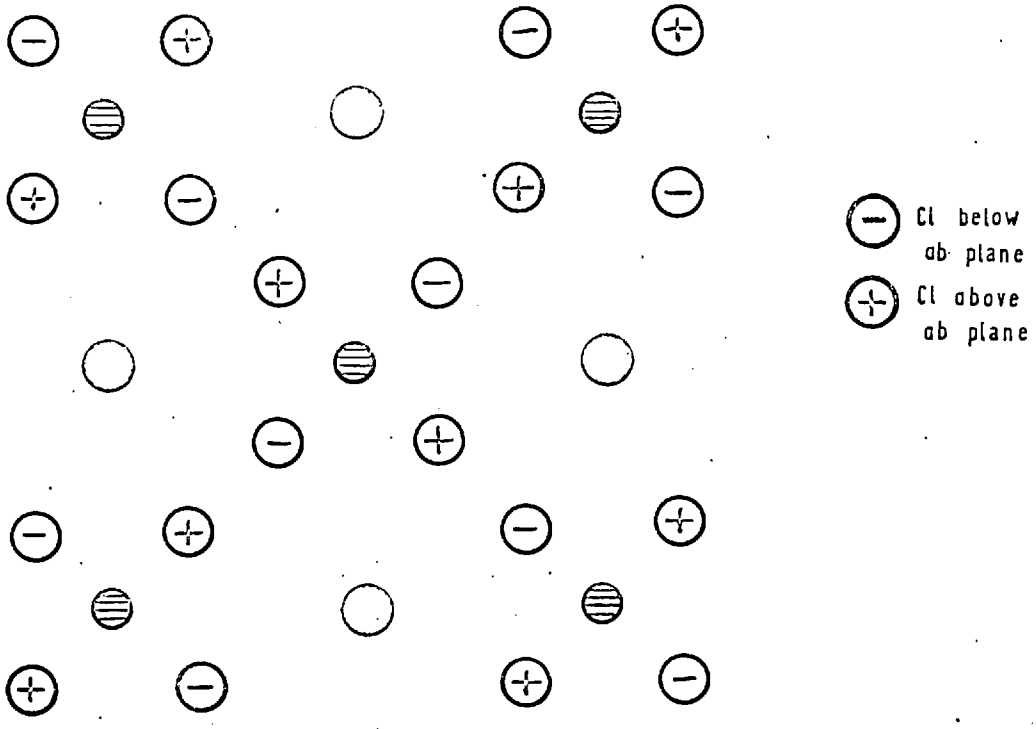


Figure 5.10 (b) Layers of $CoCl_4^{=}$ tetrahedron projected on to 001

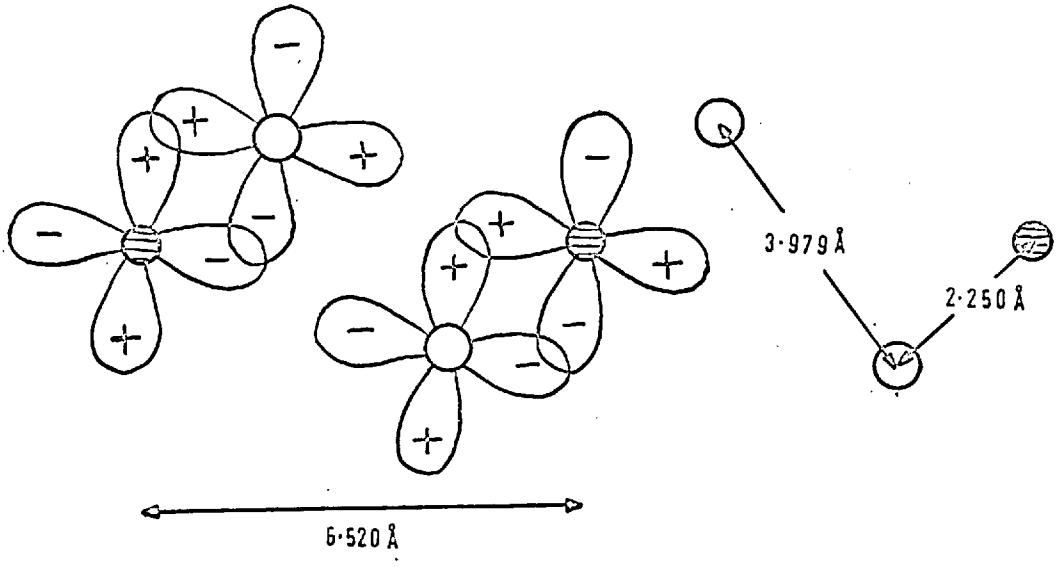


Figure 5.10 (c) Magnetic exchange mechanism in $CoCl_4^{=}$ layers

was given by Cooke,Lazenby, McKim, Owne and Wolf (1959) as relating the Weiss constant θ with the exchange intergral, J. z is now the number of neighbours with which exchange takes place from a particular ion and S is the spin quantum number for the ions. For the layers of $(CoCl_4)^{2-}$ tetrahedra in Cs_3CoCl_5, we have $z = 4$, $S = 3/2$ and

$$\theta = 5J/k \qquad .....(3)$$

For magnetic exchange in the 001 plane we can write

$$J_\perp = \theta_\perp /5 = 2^0 = 1.4 \text{ cm.}^{-1}$$

(Cooke et al. (loc.cit.) discuss the relative roles of nearest and next nearest neighbours in the exchange process; as in the iridium complexes, exchange due to non-nearest neighbour interactions can be neglected.) Griffiths et al. (loc.cit.) calculated the exchange integral by means of the expression

$$J = 2p^2D\left[1 - (1 - \exp\{-\beta(r - r_\theta)\})^2\right] \qquad .....(4)$$

where p is the probability that metal eleotrons are delocalised into the p orbitals of a chlorine ligand atom. The remainder of the expression is based on a Morse potential curve for the chlorine molecule with D = 20,000 cm.^{-1}, $\beta = 2.04$, $r_\theta = 1.99$ Å. For Cs_3Cl_5, with $r = 3.98$ Å, $p = 1 - (1 - k)/4$ and $k = 0.91$, $J_\perp(\text{calc.}) = 0.5 \text{ cm.}^{-1}$.

The result for $J_{(calc)}$ is critically dependent on the value of k and the agreement between the calculated (0.5 cm.^{-1}) and experimental (1.4 cm.^{-1}) values of $J_\perp$ can be regarded as reasonable, particularly as $\theta_\perp$ originates, in part, from zero field splitting effects. The small Weiss constant $\theta_{||}$ may be due to a small amount of magnetic exchange along 'c' or, perhaps more likely, to the

fact that δ of equation (1) is positive.

The mechanism of magnetic exchange in Cs_2CoCl_4 is not quite so easy to illustrate as in Cs_3CoCl_5. For Cs_2CoCl_4, $\theta_{\parallel} = 15^{\circ}$ and $\theta_{\perp} = 4^{\circ}$ (cf. Figure 5.7 which shows that $K'_{\parallel}T$ decreases more quickly at low temperatures than does $K'_{\perp}T$). The closest Cl-Cl interatomic distances between adjacent tetrahedra in the crystal range from 3.8 to 4.1 Å and we calculate $J_{\parallel} = 3^{\circ} = 2.1$ cm.$^{-1}$ and $J_{\perp} = 0{\cdot}6$ cm.$^{-1}$. The Weiss constant in the perpendicular direction can be quite readily accounted for by magnetic exchange but, again, may be due to zero field splitting effects. In the thiocyanate complex the values of the Weiss constants are $\theta = 10^{\circ}$ and 4°. The separation between the sulphur atoms of the (N=C=S) ligand groupings of adjacent tetrahedra now ranges from 3.45 Å and may be sufficiently small to allow intermolecular exchange interactions; no information is, however, available on how the exchange is transmitted along the N=C=S group.

* * *

5.7 Appendix

A least-squares refinement of the crystal structure of tricaesium pentachlorocobalt (II), Cs_3CoCl_5

Deep blue crystals of Cs_3CoCl_5 were obtained as described in section 5.2, a least squares analysis of high-angle precession data giving the unit cell,

$a = 9.219 \pm 0.003$ Å; $c = 14.554 \pm 0.005$ Å

ccompared with,

$a = 9.18$ Å, $c = 14.47$ Å reported by Powell and Wells (1935). The

space group is I 4/mcm (D_{4h}^{18} ; No. 140).

A least-squares refinement of the positional and vibrational atomic parameters was based on 131 $\{h0\ell\}$ and $\{hk\ell\}$ reflections, the relative intensities of which were visually estimated from non-integrated precession photographs (MoKα); no correction for absorption effects has been made, the maximum difference in path length being some 10% in a crystal of average thickness 0.1 mm. The refinement analysis, with unit weighting of all reflexions, converged to a discrepancy index, R = 0.062, after twelve cycles, the final atomic co-ordinates, their e.s.d.'s and temperature factors being listed in Table 5.7. It should be noted that the atomic co-ordinates are now referred to the origin of the standard setting of I 4/mcm rather than that of Powell and Wells (loc.cit.). Final observed and calculated structure factors are listed in Table 5.8.

The Co-Cl bond length is 2.252 ± 0.013 Å compared with the Powell and Wells value of 2.34 Å; the present result is in good agreement with that of 2.23 Å reported for the Co-Cl distance in Cs_2CoCl_4 (Porai-Koshits, loc. cit.). The bond angles of the distorted tetrahedrally-coordinated cobalt atom have been shown in Figure 5.4. They confirm our predictions based on the magnetic work that the distortion previously reported was incorrect. Other interatomic contacts are collected in Table 5.9, the results from the earlier analysis being given in parentheses.

* * *

Table 5.7 Atomic co-ordinates and temperature parameters of the Debye factor, $B = 2^{-(b_{11}h^2 + b_{22}k^2 + b_{33}l^2 + b_{23}kl + b_{31}lh + b_{12}hk)}$

Atom	x/a	y/b	z/c	b_{11}	b_{22}	b_{33}	b_{23}	b_{31}	b_{12}
Cs(1)	0	0	$\frac{1}{4}$	0.0119	0.0119	0.0038	0	0	0
Cs(2)	0.1655(4)	0.6655(4)	$\frac{1}{2}$	0.0073	0.0073	0.0037	0	0	-0.0013
Co(1)	0	$\frac{1}{2}$	$\frac{1}{4}$	0.0068	0.0068	0.0018	0	0	0
Cl(1)	0	0	0	0.0073	0.0073	0.0060	0	0	0
Cl(2)	0.1380(16)	0.6380(16)	0.1570(16)	0.0105	0.0105	0.0040	0.0031	0.0031	-0.0083

Table 5.9 Cs_3CoCl_5. Interatomic distances less than 4 Å

Reference Atom	Nearest neighbours (Å)			
Cs(1)	8	Cl(2)	at 3.820	(3.67)
	2	Cl(1)	at 3.639	(3.62)
Cs(2)	2	Cl(1)	at 3.440	(3.42)
	2	Cl(2)	at 3.433	(3.39)
	4	Cl(2)	at 3.622	(3.85)
Cl(1)	2	Cs(1)	at 3.639	(3.67)
	4	Cs(2)	at 3.440	(3.42)
Cl(2)	1	Co(1)	at 2.252	(2.34)
	2	Cs(1)	at 3.820	(3.67)
	1	Cs(2)	at 3.433	(3.39)
	2	Cs(2)	at 3.622	(3.85)
	1	Cl(2)	at 3.982	(3.45)

Table 5.8 Cs_3CoCl_5 - Observed and calculated structure factors (x 0.5)

	$\|F_o\|$	F_c
0 0		
2	78.4	69.4
4	554.3	561.6
6	279.9	286.7
8	497.3	501.8
10	18.9	-16.5
12	378.7	405.0
14	75.4	70.4
16	160.0	163.3
18	53.1	44.3
20	151.8	151.9
1 1		
0	63.8	-45.0
2	124.1	-104.0
4	127.4	112.1
6	186.9	-184.1
8	30.2	28.6
10	45.5	-47.5
12	18.8	-12.1
14	63.6	-67.0
16	15.7	25.1
18	34.0	-38.2
2 2		
0	385.9	410.4
2	167.4	-125.3
4	388.8	357.4
6	119.8	-105.9
8	280.2	263.9
10	96.2	-81.6
12	183.8	183.5
14	59.9	-60.6
16	122.5	119.3
18	39.6	-40.1
3 3		
0	305.0	-310.5
2	297.7	-294.9
4	131.8	-115.0
6	367.5	-368.5
8	145.7	-139.0
10	155.3	-155.9
12	162.3	-150.5
14	157.6	-148.9
16	40.4	-42.4
18	105.7	-100.6
4 4		
0	392.0	383.3
2	131.6	-113.6
4	196.7	186.7
6	17.2	14.1
8	201.8	204.6
10	116.2	-115.4
12	178.5	185.7
14	19.5	-22.5
16	63.6	61.3
18	25.8	-19.7
5 5		
0	39.9	35.6
2	65.5	-61.5
4	35.3	25.9
6	51.0	-51.0
8	11.8	11.1
10	39.1	-36.7
12	12.0	11.0
14	23.2	-30.3
16	9.9	0.5
6 6		
0	299.3	307.3
2	95.1	82.8
4	293.5	283.6
6	94.3	79.1
8	226.6	228.8
10	50.9	55.5
12	184.7	180.5
14	33.4	30.3
7 7		
0	57.2	-52.8
2	20.1	-17.9
4	34.8	34.4
6	77.6	-80.0
8	7.2	2.2
10	7.2	6.4
12	27.5	-31.3
8 8		
0	115.9	112.5
2	34.4	-35.8
4	77.1	68.7
6	13.2	-11.2
8	83.2	78.1
9 9		
0	67.1	-53.2
2	86.6	-85.5
2 0		
0	153.1	122.7
2	370.9	-401.4
4	180.6	151.3
6	334.5	-360.5
8	119.3	97.5
10	242.4	-230.5
12	55.9	50.0
14	164.8	-165.7
16	51.0	50.2
18	115.9	-112.3
20	35.0	25.8
1 0		
0	68.5	-54.8
2	373.8	-388.3
4	208.1	184.1
6	390.7	-399.9
8	87.7	68.5
10	162.5	-142.2
12	26.3	-2.5
14	169.5	-170.9
16	74.0	77.3
18	114.0	-113.3
3 0		
0	502.0	500.1
2	93.3	87.9
4	361.0	382.3
6	151.6	135.3
8	322.3	320.8
10	40.0	39.4
12	267.8	265.9
14	43.4	41.8
16	131.3	141.2
18	40.6	34.5
5 0		
0	114.7	117.8
2	203.0	-198.7
4	14.8	9.5
6	125.3	-107.7
8	53.7	46.7
10	169.6	-165.7
12	57.3	56.0
14	71.7	-76.3
10 0		
0	22.5	-19.6
2	119.0	-121.1
4	45.0	42.2
6	148.6	-157.3
8	26.9	21.8
10	67.2	-77.5
12	17.1	-8.9
12 0		
0	143.3	140.9
2	50.6	62.4
4	151.5	166.4
6	34.8	34.3

CHAPTER 6

The Magnetism and Crystallography of Potassium Ferricyanide

6.1 Early work

It has been described in section 4.4 how the coupling together of spin angular momenta with orbital angular momenta which have been 'frozen' by asymmetric ligand fields resulted in paramagnetic anisotropy. It follows from this theory (Van Vleck, 1932) that when the orbital moment of the ground state is zero, there will be no resultant anisotropy, a prediction which has been tested many times. For example, Jackson (1933) measured the crystal paramagnetic anisotropies of several manganous and ferric ions which have an S ground state and found that their principal susceptibilities differed by no more than 1-2%, in good agreement with theory. Further, the observed magnetic moments agreed well with the spin-only value expected for the five unpaired electrons of the $^6S_{5/2}$ ground state of these ions. An exception, however, was found in $K_3Fe(CN)_6$ which has an effective magnetic moment corresponding to between 1 and 2 unpaired electrons and an anisotropy as great as 100% at low temperatures. The first explanation of the decreased moment was given by Pauling (1931) who deduced a pairing up of electrons on the basis of the structure $Fe^{3-}(CN)_6$ as a dominant canonical form. In 1935, Van Vleck compared Pauling's approach with the crystal field model of Penney and Schlapp and Mulliken's molecular orbital method.

In many manganous and ferric compounds, including, for example, the sulphates (weak field complexes) the ligand fields are sufficiently strong to destroy the

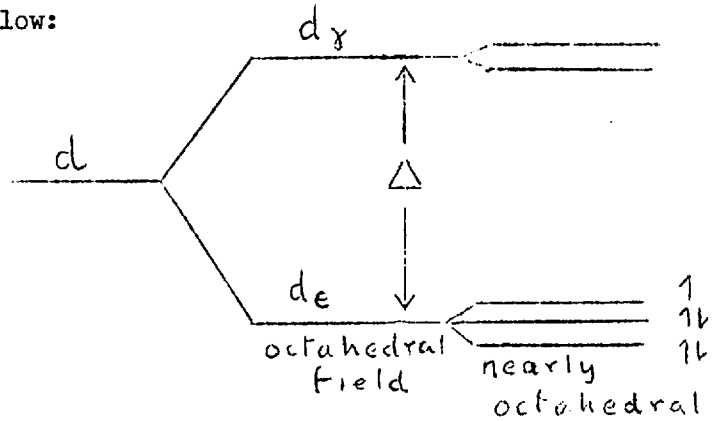
free-ion spin-orbit coupling, so that the magnetic moment is given by,

$$\mu_{eff} = \left\{ L(L + 1) + 4S(S + 1) \right\}^{\frac{1}{2}} \quad \text{B.M.}$$

In the iron group complexes, however, the ground state is $^6S_{5/2}$, having zero orbital moment, so that the resulting moment is given by the spin-only formula,

$$\mu_{eff} = \left\{ 4S(S + 1) \right\}^{\frac{1}{2}} \quad \text{B.M.}$$

In the cyanide complex, the electrostatic ligand field is sufficiently large to destroy the Russell-Saunders coupling completely, giving the Stark pattern shown below:



Thus, the five d electrons in the ferricyanide ion are accommodated in the lower triplet as the octahedral field splitting, Δ, is large enough to cause the breakdown of Hund's rule (maximum spin multiplicity lowest). It is interesting to note the significance of the state $d^5\ ^6S$ in terms of this splitting diagram. Usually, Russell-Saunders coupling involves collective quantization in such a way as to prevent any simple interpretation in terms of the above one-electron diagram (see, for example, the correlation diagram, figure 4.3). However, when the spin quantum number equals half the number of electrons, as in $d^5\ ^6S$, the spins are all mutually parallel. Such an alignment is possible only if each

each electron has its own 'private' orbital. Hence, a state of the configuration d^5 with $S = {}^5/_2$ involves one electron in each of the five levels of the figure. This distribution has an invariant significance (one to a state) independent of the axis of space quantization. Hence, the state is an S state and is reflected in the high magnetic isotropy of manganous and ferric sulphates, for example. In the ferricyanide case, however, the five electrons are distributed among the d_ϵ triplet: true cubic symmetry is achieved only if the three components are populated equally. Hence, $K_3Fe(CN)_6$ exhibits a large magnetic anisotropy. Howard (1935) published a quantitative treatment in which, assuming a small rhombic distortion of the cyanide octahedron, the calculated principal magnetic susceptibilities which agreed with Jackson's measurements to within 10%. He also showed that the orbital contribution to the total magnetic moment is considerable, explaining why the observed susceptibility is almost twice that predicted by the spin-only formula for one unpaired electron. This early success of ligand field theory appeared to solve the problem of potassium ferricyanide.

* * *

6.2 Recent studies

More recently, research has been concerned, using the techniques of magnetic susceptibility and electron spin resonance, to correlate more accurately the magnetic behaviour of complex ions with spin-orbit coupling, distortion and electron delocalization parameters. To this end, the bulk susceptibility of $K_3Fe(CN)_6$ has been measured several times, the most accurate and recent results,

of Figgis (1960), being given in detail in section 6.3. The experimental curve of μ_{eff} versus temperature was fitted by empirical adjustment of the parameters k, v, Δ, λ. The delocalization factor, k, defines the fraction, (1 - k), of time which the t_{2g} electrons spend on the ligand atoms where they do not contribute to the orbital angular momentum of the ion: Δ is defined as the separation between the orbital levels of $^2T_2$ created by an axial ligand field component in the absence of spin-orbit coupling: λ is the spin-orbit coupling constant for the d^5 configuration: and $v = \Delta/\lambda$. The curve of best fit gave the values for the parameters k, v, Δ, λ as 0.8, 0, 0, -400, respectively. The values of k and v may be compared with those obtained from the electron spin resonance studies by Bleaney and O'Brien (1956) in which k = 0.87 and v = -0.5. Of course, such methods cannot take the place of a detailed study which includes measurement of magnetic anisotropy, electron spin resonance g-values and a single crystal X-ray structure analysis. While this was a sufficient raison d'etre for the present work, another problem had arisen.

In 1955, Stephenson and Morrow reported a detailed investigation of the heat capacities of potassium ferricyanide and cobalticyanide over the temperature range 15-300°K. A gradual transition was found in potassium ferricyanide, with a maximum occuring in the heat capacity at about 131°K. The heat capacity of potassium cobalticyanide is normal, suggesting to the authors that the ferricyanide transition is magnetic in nature, the two structures being crystallographically isomorphous. The entropy associated with the transition was found by graphical integration to be 0.9 ± 0.2 cal. $deg.^{-1} mole^{-1}$, and it was suggested

that the effect derived from magnetic interactions between the ferricyanide ions.

Previously, Guha (1950) had remeasured the paramagnetic anisotropies of potassium ferricyanide using Krishnan's technique (section 4.7). There was general agreement between his and Jackson's earlier measurements (using Finke's method) but this did not extend to the details. In particular, Guha found that one anisotropy reached a maximum at about 120°K, falling off rapidly at lower temperatures.

The possibility of a connection between Guha's magnetic measurements and Stephenson and Morrow's heat capacities prompted Ristau, Ruckpaul and Shoffa (1958) to re-measure the anisotropies of $K_3Fe(CN)_6$ once more, this time taking measurements at 2° intervals over the range 80°-300°K where Guha had worked at 20° intervals. They confirmed the anisotropy maximum reported by Guha, finding it to occur at 126°K. Much more remarkable, however, was the discovery of a very sharp maximum in one principal susceptibility matched by an equally sharp minimum in another, of approximately equal, very large, magnitudes, both at 126°K. That no indication of this anomaly had been found in any previous Gouy measurements was due, the authors suggested, to the two effects being opposite in sense and, quantitatively, nearly equal. To test this, they also re-measured the powder susceptibility of the compound over the same range at the same 2° intervals and, at 126°K, found a small discontinuity in the plot of $\overline{\chi}$ versus temperature.

As a preliminary to our main line of investigation, namely the correlation of structural with ligand field parameters, we attempted, therefore, to

reproduce the reported anomalies in the magnetic behaviour of potassium ferricyanide.

* * *

6.3 Magnetic results

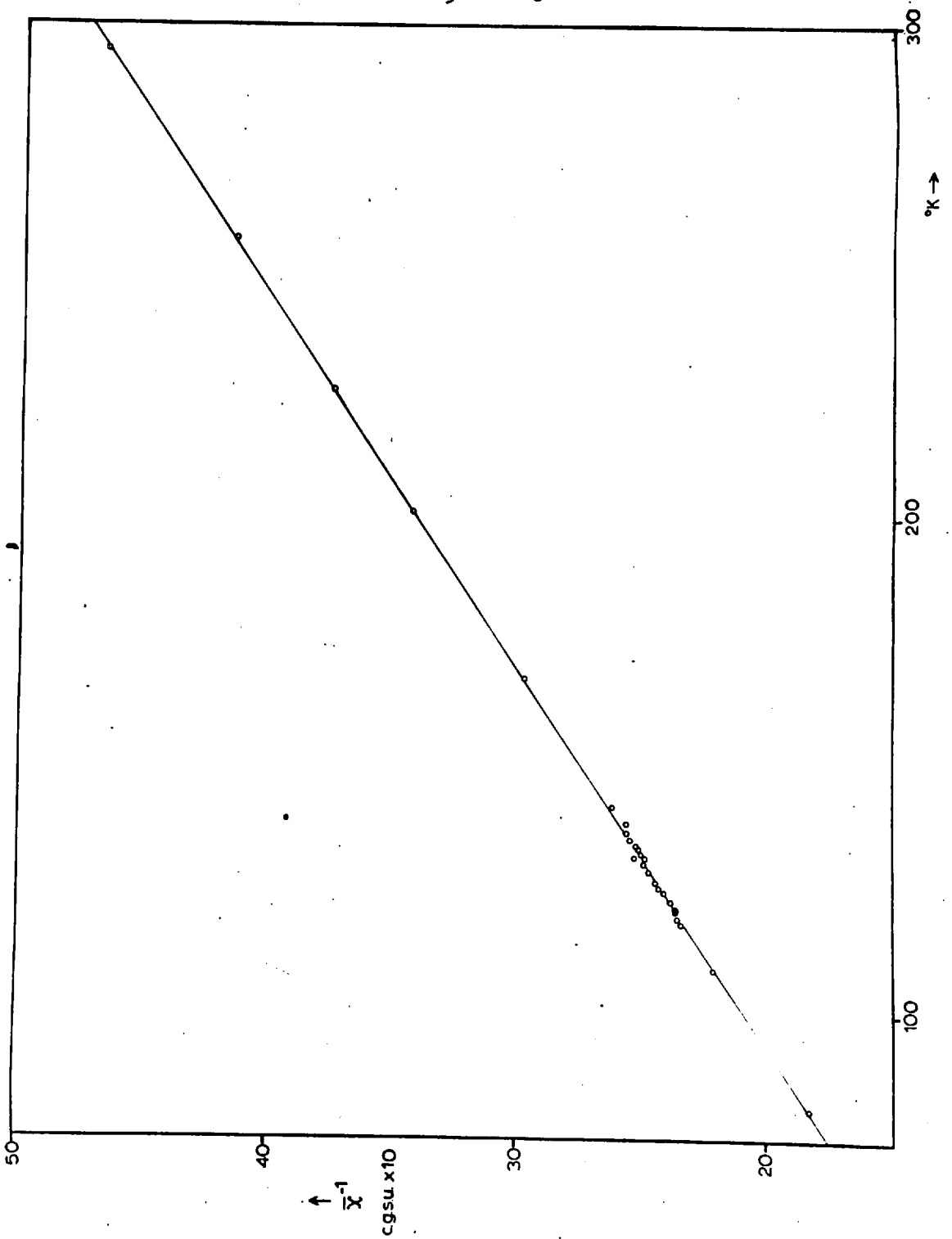
The temperature dependence of the powder susceptibility of potassium ferricyanide has been determined very carefully by Figgis (loc.cit) with particular attention to the temperature range 120°-140°K. His results are summarized in Table 6.1 and shown graphically in Figure 6.1.

Table 6.1 $K_3Fe(CN)_6$ - Paramagnetic bulk susceptibilities

°K	$\bar{\chi}_{Fe}$	°K	$\bar{\chi}_{Fe}$
81.0	5486	131.1	3953
108.6	4533	131.7	4000
117.9	4274	132.7	3984
119.0	4246	133.5	3968
120.4	4237	134.8	3932
120.8	4236	136.2	3906
122.5	4198	138.0	3903
124.1	4149	141.4	3817
125.2	4115	167.5	3361
126.3	4093	201.3	2920
128.3	4049	225.8	2670
129.9	4016	256.5	2408
131.0	4022	295.0	2137

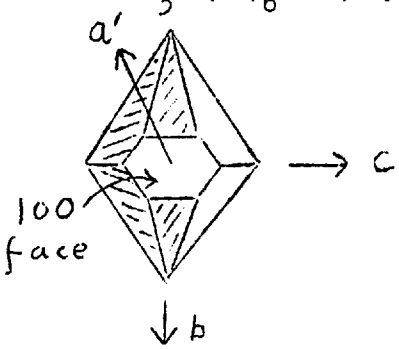
The absence of any discontinuity around 126°K is immediately apparent from the figure, the relative accuracy of these results being ± 0.5% : an estimated maximum error of ± 2% in the absolute values is due to the usual packing

Figure 6.1 The Curie-Weiss behaviour of the bulk susceptibility of $K_3Fe(CN)_6$



inconsistencies inherent in the Gouy powder method. Secondly, the inverse susceptibility is seen to vary linearly with temperature over the range, the Weiss constant, θ, being $\pm 2^{\circ}$. The effective magnetic moment is 2.25 $\pm$ 0.03 B.M.

The magnetic anisotropies have been measured over the same temperature range, 80-300°K, suspending crystals along the 'a′', 'b' and 'c' axes in turn, corresponding to the anisotropies $\Delta\chi_{a'}$, $\Delta\chi_{b}$ and $\Delta\chi_{c}$, respectively. Crystals of about 2.3 mm. diameter and weighing 10-25 mgm. were grown from aqueous solutions of A.R. $K_3Fe(CN)_6$ and, typically, had the habit shown below:-



a′ is perpendicular to both c and b

The angle ψ (section 4.6), determined by suspending the crystal along the 'b' axis, was found by Guha (loc.cit.) to be sensibly 90° throughout the temperature range. The relative magnitudes of χ_a, χ_b, and χ_c were determined by noting the orientation of the crystals, suspended along each axis, in the magnetic field, giving:-

$$\chi_a > \chi_b > \chi_c$$

The results of measurements, which were carried out on several crystals, are summarized in Table 6.2 and plotted in Figure 6.2. Readings were taken at frequent temperature intervals, as close as $\frac{1}{2}^{\circ}$ in the region 120-140°K. Again, the maximum in $\Delta\chi_c$ at 130°K confirms the results of previous investigations

Table 6.2 $K_3Fe(CN)_6$ - Crystal paramagnetic anisotropies

A Crystals suspended along 'c'

°K	$\Delta\chi_c$ c.g.s.u. ($\times 10^{-6}$)	°K	$\Delta\chi_c$ c.g.s.u. ($\times 10^{-6}$)	°K	$\Delta\chi_c$ c.g.s.u. ($\times 10^{-6}$)
89.4	188	129.8	471	187.4	261
97.4	257	133.3	455	200.7	229
111.6	338	135.3	447	222.5	186
120.3	400	149.9	384	244.9	152
122.7	428	168.5	318	271.5	1120
126.4	446	185.6	267		

B Crystals suspended along 'b'

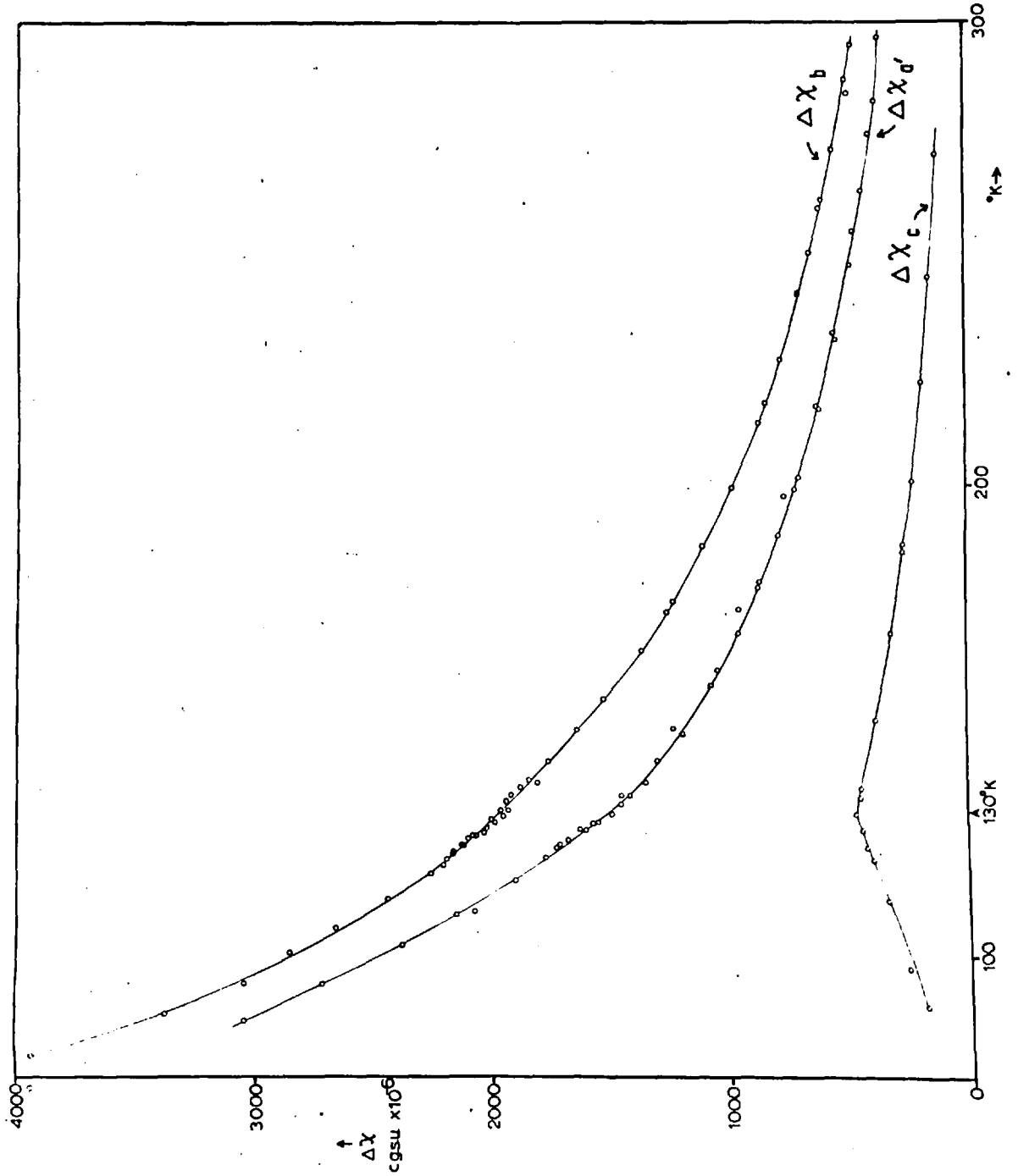
°K	$\Delta\chi_b$ c.g.s.u. ($\times 10^{-6}$)	°K	$\Delta\chi_b$ c.g.s.u. ($\times 10^{-6}$)	°K	$\Delta\chi_b$ c.g.s.u. ($\times 10^{-6}$)
79.6	3938	126.5	2039	173.2	1265
88.4	3379	127.4	2028	187.2	1111
94.6	3040	128.4	1990	199.7	988
101.2	2850	129.0	2003	213.7	874
106.4	2660	129.7	1957	218.2	846
112.5	2439	131.0	1965	227.4	780
118.0	2260	131.0	1934	241.3	706
119.8	2202	132.8	1941	250.1	658
120.9	2190	134.2	1910	259.9	615
122.1	2152	135.8	1881	261.5	607
122.4	2161	136.8	1811	272.5	560
123.8	2128	137.4	1849	284.5	495
123.9	2121	141.3	1765	287.5	506
125.1	2102	148.0	1641	295.0	477
125.8	2085	154.6	1532		
125.9	2075	165.0	1372		

Table 6.2 (continued)

C Crystals suspended along 'a'

^{o}K	$\Delta\chi_{a'}$ c.g.s.u. ($\times 10^{-6}$)	^{o}K	$\Delta\chi_{a'}$ c.g.s.u. ($\times 10^{-6}$)	^{o}K	$\Delta\chi_{a'}$ c.g.s.u. ($\times 10^{-6}$)
86.6	3045	130.0	1492	189.3	790
94.4	2715	132.0	1455	197.7	764
102.7	2380	132.2	1412	199.1	725
109.1	2150	133.7	1420	201.6	704
109.9	2170	133.8	1455	216.5	615
112.5	1900	136.7	1353	217.1	625
116.4	1901	141.2	1309	231.6	543
118.1	1743	147.0	1198	233.0	553
121.0	1771	148.4	1238	247.6	482
123.0	1728	155.1	1034	254.9	472
123.7	1715	157.3	1075	263.5	433
124.7	1680	160.6	1050	275.6	409
126.6	1630	168.4	956	282.7	378
126.6	1605	173.6	955	296.5	363
128.1	1575	178.2	871		
128.3	1551	179.1	870		

Figure 6.2 $K_3Fe(CN)_6$ - the temperature dependence of the principal crystal magnetic anisotropies.



but there is no evidence at all of any other anomalies.

We wish to correlate these experimental anisotropies with the ligand field parameters discussed earlier. The next steps, therefore, are to calculate the principal crystal susceptibilities χ_a, χ_b, χ_c and hence the principal molecular susceptibilities, K_1, K_2 and K_3. For the first step, we require knowledge only of the unit cell symmetry, which has been reported by Barkhator and Zhdanov (1942) as monoclinic: for the second, we need to know the direction cosines of the cyanide octahedra with respect to the 'a', 'b' and 'c' axes - these being obtained from an accurate X-ray structural analysis. A survey of the literature revealed, however, that not only was the structure of potassium ferricyanide not solved but that even the symmetry and space group were the subjects of some controversy.

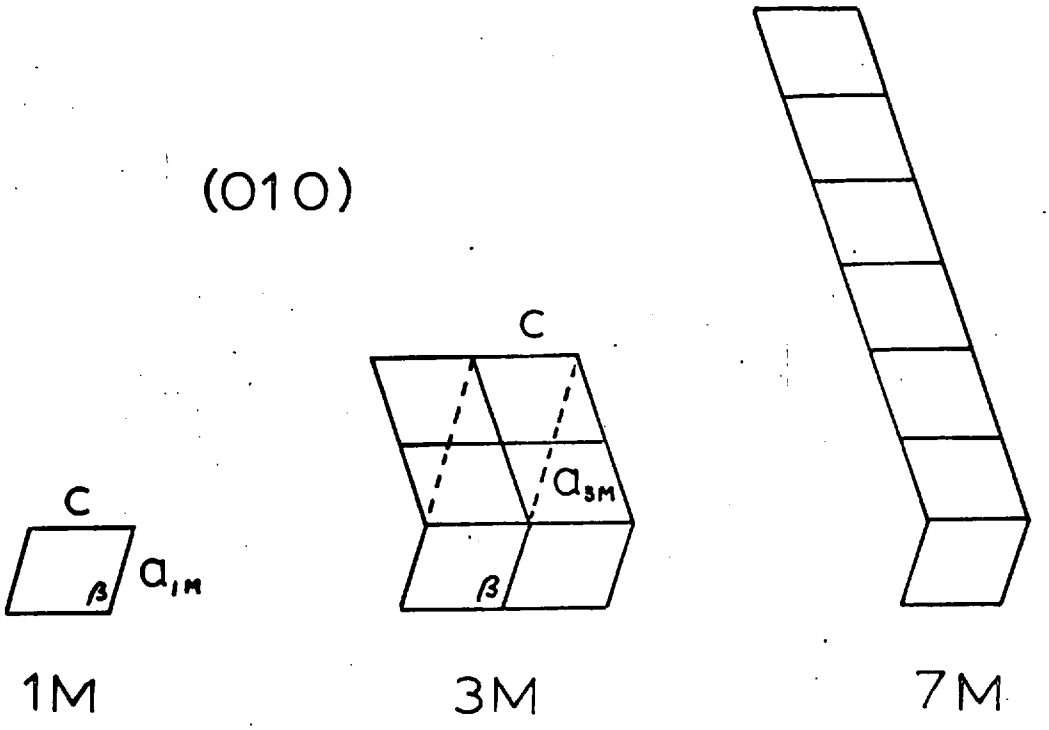
* * *

6.4 Crystallographic survey

Potassium ferricyanide has been known to exhibit many forms of twinning for a long time and the literature on the subject shows a considerably confused situation. Kohn and Townes (1961) have reviewed the work on potassium ferricyanide and on several closely isomorphous compounds; $K_3Cr(CN)_6$, $K_3Mn(CN)_6$, $K_3Ir(CN)_6$, $Rb_3Fe(CN)_6$ and $K_3Co(CN)_6$. The unit cell symmetries of these compounds have been reported variously as monoclinic $P2_1/c$ ($\beta \approx 90^\circ$), monoclinic $P2_1/c$ ($\beta \approx 107^\circ$) and orthorhombic Pnca. Kohn and Townes report a detailed investigation of the symmetries displayed by crystals of potassium cobalticyanide,

which they describe as a series of four polytypes. Figure 6.3 illustrates the 1 M (one layer monoclinic), 2 Or (2 layer orthorhombic), 3 M and 7 M (3 and 7 layer monoclinic) polytypes which were observed. Although the effect is one of cell twinning rather than of the more usual crystal twinning, many crystals also displayed surface striations parallel to the trace of (100) on both prism and pyramid faces, being manifest of a lamellar structure parallel to (100). In polarized light, all crystals viewed on (100) showed extinction parallel to the traces of (010) and (001) as required, but, in addition, even monoclinic crystals viewed on the major prism face demonstrated extinction pseudo-parallel to the trace of (100), thus behaving optically pseudo-orthorhombic. It is this last effect which has been mainly responsible for the confusion and inaccurate pseudo-orthorhombic cells reported. The effect is clearly demonstrated by the $\{h0\ell\}$ Weissenberg photograph of $K_3Fe(CN)_6$ reproduced in Figure 6.4: it shows almost perfect mm symmetry typical of an orthorhombic zone, although the $\{h1\ell\}$ net of the same crystal has monoclinic symmetry with reciprocal axes corresponding to those marked in the figure. Other crystals, however, have orthorhombic $\{h1\ell\}$ nets. Thus, while $K_3Fe(CN)_6$ may not exhibit exactly the same polytype as $K_3Co(CN)_6$, a similar situation is apparent.

A partial structural analysis was first attempted by Bakhator and Zhdanov (1942) who used the basic 1 M unit cell. Working with reflections from the $\{hk0\}$ zone only, they reported $^x/a$ and $^y/b$ co-ordinates for all atoms, which Curry and Runciman (1959) used as a starting point for a neutron diffraction study of $K_3Fe(CN)_3$ - again, for the $\{hk0\}$ zone only. These authors were



(Eight different stacking sequences)

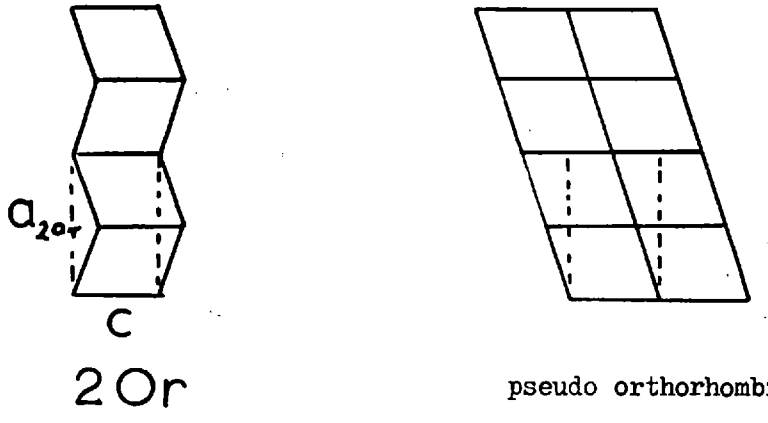


Figure 6.3 Polytypes of potassium cobalticyanide (after Kohn and Townes, 1961)

Figure 6.4 $K_3Fe(CN)_6$ - Weissenberg $\{h0\ell\}$ net showing pseudo orthorhombicity



particularly concerned to identify, positively, carbon and nitrogen atoms and were able to conclude that the substance contained Fe-C rather than Fe-N bonds. The final reliability factor, R_{hk0}, was 0.124. The last difference Fourier synthesis suggested that the temperature factors of the iron and (special) potassium atoms would be represented better anisotropically (but see also section 6.6) although this may have been an indication of some disorder. Okaya and Pepinsky (1956) noted in the 2 Or polytype of $K_3Co(CN)_6$ some one-dimensional disorder in the form of diffuse streaks between ℓ odd reflections parallel to a with integral k indices.

With this background, we set out to obtain accurate structural parameters for $K_3Fe(CN)_6$ at room and low (95°K) temperatures.

* * *

6.5 The structure of $K_3Fe(CN)_6$ at 300°K

Crystals of about 0.2 mm. diameter were grown from aqueous solutions of the A.R. $K_3Fe(CN)_6$. From Weissenberg photographs (MoKα radiation) the unit cell, assuming 1 M symmetry, was determined as,

$a = 7.06$ Å ; $b = 10.38$ Å ; $c = 8.40$ Å ; $\beta = 107°20'$

Some 325 visually estimated reflexions were collected from Weissenberg $\{h0\ell\}$, $\{hk0\}$ and $\{0k\ell\}$ photographs, being scaled together initially by common reflexions and later by calculated structure factors.

Although some three dimensional data revealed the presence of superlattice effects, it was decided to work initially with complete two-dimensional data only,

using the simple 1 M system: how inadequate a description of disorder this strategy was, would be apparent at the end of the analysis. Curry and Runcinan (loc.cit) had calculated two sets of cyanide z-coordinates from their $\{hk0\}$ analysis, which we now used as starting models for two separate analyses. With isotropic temperature factors of 3.0 for K and Fe, 4.0 for C and 4.5 for N, the reliability factors, R, were ~ 0.30. Several cycles of least squares refinement, adjusting all positional and isotropic thermal parameters reduced the R factor for one model to ~ 0.21, while bringing virtually no improvement to the other, which was therefore discarded. Although we had now determined the correct orientation of the cyanide octahedra, isotropic refinement would not reduce R further. Careful examination of observed and calculated structure factors revealed no systematic anomalies in either the $\{hK0\}$ or $\{h0\ell\}$ zones, but showed that, in the $\{0k\ell\}$ data, calculated structure factors of reflexions with k odd were grossly different from the observed amplitudes. It appeared from the literature, that the only parameter which had not been properly established was the z-coordinate of the potassium ion at the general (e) equipoints, this being given by Barkhatov and Zhdanov (loc.cit.) as $z \approx \frac{1}{8}$. The correct co-ordinate is, however, $z \approx \frac{3}{8}$, as the following discussion shows.

The form of the structure factor for spacegroup $P2_1/c$ is:-

$k + \ell = 2n \quad : \quad A = 4\cos 2\pi(hx + \ell z)\cos 2\pi ky \quad ; \quad B = 0$

$k + \ell = 2n + 1 \quad : \quad A = -4\sin 2\pi(hx + \ell z)\sin 2\pi ky \quad ; \quad B = 0$

The co-ordinates of the (general) potassium ion are,

$x \approx \frac{1}{2}\ , \ y \approx 0.23\ , \ z \approx \frac{1}{8}$

$x \approx \frac{1}{2}\ , \ y \approx 0.23 \quad z \approx \frac{3}{8}$

Let us consider the contribution of this aton to the diffraction maxima,

(a) for the $\{hk0\}$ zone:

No differences in z-coordinates can be detected in a projection down the z-axis.

(b) for the $\{h0\ell\}$ zone.

k = 0, therefore,

$\ell = 2n$: $A = 4\cos 2\pi(hx + \ell z)$

$\ell = 2n + 1$: $A = 0$ - reflexions absent

that is, for $\ell = 2n$:

$A = 4(\cos 2\pi hx \cos 2\pi \ell z - \sin 2\pi hx \sin 2\pi \ell z)$

but as $x \approx \frac{1}{2}$, $\sin 2\pi hx \approx 0$,

$A = 4 \cos 2\pi hx \cos 2\pi \ell z$

Now $\cos 2\pi \ell z \approx \cos \frac{\ell\pi}{4}$ or $\cos \frac{3\ell\pi}{4}$ which are numerically equal but different in sign only if $\ell = 2n + 1$. As reflexions with ℓ odd are systematically absent, all $\{h0\ell\}$ intensities are independent of the difference between the two z-coordinates.

(c) for the $\{0k\ell\}$ zone.

h = 0, therefore,

$k + \ell = 2n$: $A = 4\cos 2\pi \ell z \cos 2\pi ky$

$k + \ell = 2n + 1$: $A = -4\sin 2\pi \ell z \sin 2\pi ky$

Now $\cos 2\pi \ell z \approx \cos \frac{\ell\pi}{4}$ or $\cos \frac{3\ell\pi}{4}$ as above, and

$\sin 2\pi \ell z \approx \sin \frac{\ell\pi}{4}$ or $\sin \frac{3\ell\pi}{4}$

These functions are again numerically equal for the different z-values, but,

(i) for $k + \ell = 2n$

k and ℓ even : same sign

k and ℓ odd : opposite sign

(ii) for $k + \ell = 2n + 1$

k even, ℓ odd : same sign

k odd , ℓ even : sign change

Hence, the potassium ion contribution for the two z-coordinates are always equal numerically but different in sign if h is zero and k is odd. When the diffraction contributions are added to those from other atoms, the numerical values of these k-odd structure factors will also be different for the two positions.

With the new potassium position ($z \approx \frac{3}{8}$), the R factor reduced to 0.16 and, after eight further least squares cycles, adjusting anisotropic temperature factors, convergence was reached at R = 0.092. Table 6.3 lists final observed and calculated structure factors for the two-dimensional room temperature analysis. The final atomic positional and thermal parameters are given in Tables 6.4 and 6.5 respectively.

Figures 6.5 a, b, c illustrate the packing projection down the three principal crystal axes. The structure consists of layers of ferricyanide octahedra with potassium ions (special positions, k2), parallel to (100), interleaved with layers of potassium ions (general positions, k1). The layers are seen edge-on in Figures 6.5(a) and (c) and from above in 6.5(b). The potassium ions in special positions are in essentially octahedral holes, as can be seen most readily in Figure 6.5(b), while the 'general' potassiums are at the centres of

			$\lvert F_o \rvert$	F_c
0	0	0	3902	3448
0	0	2	797	671
0	0	4	2732	2472
0	0	6	2190	2085
0	0	8	1141	1170
0	0	10	751	974
0	0	-12	1213	1409
0	0	-10	547	493
0	0	-8	3041	2823
0	0	-6	5978	6864
0	0	-4	3564	3570
0	0	-2	2142	2222
0	0	0	3904	3854
0	0	2	1006	892
0	0	4	410	407
0	0	6	844	841
0	0	8	967	962
0	0	10	333	365
0	0	-12	967	933
0	0	-10	3693	3386
0	0	-8	3145	2959
0	0	-6	735	788
0	0	-4	5014	5407
0	0	-2	3916	3882
0	0	0	2928	2705
0	0	2	1269	1072
0	0	4	698	726
0	0	6	2012	2024
0	0	8	669	632
0	0	10	1631	1773
0	0	-12	949	881
0	0	-10	520	602
0	0	-8	2897	2582
0	0	-6	3838	3749
0	0	-4	2986	2653
0	0	-2	1448	1391
0	0	0	3579	3391
0	0	2	1847	1708
0	0	4	476	532
0	0	6	908	1017
0	0	8	1269	1278
0	0	10	2223	2034
0	0	-12	949	984
0	0	-10	1284	1140
0	0	-8	1395	1279
0	0	-6	4418	4367
0	0	-4	2394	2189
0	0	-2	378	-387
0	0	0	1926	1861
0	0	2	1395	1506
0	0	4	821	988
0	0	6	929	1197
0	0	8	433	450
0	0	10	628	650
0	0	-12	3683	3503
0	0	-10	2347	2220
0	0	-8	2138	2029
0	0	-6	2282	2144
0	0	-4	751	840
0	0	-2	433	785
0	0	0	644	851
0	0	2	1867	1939
0	0	4	1974	1666
0	0	6	2138	2025
0	0	8	3325	3168
0	0	10	886	833
0	0	-12	698	603
0	0	-10	698	664
0	0	-8	987	888
0	0	-6	773	902
0	0	-4	669	725
0	0	-2	1935	1832
0	0	0	2265	2081
0	0	2	880	873
0	0	4	2284	2090
0	0	6	1436	1454
0	0	8	333	385
0	0	10	581	616
0	0	-12	1409	1411
0	0	-10	698	898
0	0	-8	698	614
0	0	-6	1224	1102
0	0	-4	1255	1078
0	0	-2	1060	1075
0	0	0	278	488
0	0	2	698	882
0	0	4	698	609
0	0	6	1299	1347
0	0	8	1005	1085
0	0	10	944	701
0	0	-12	831	934
0	0	-10	939	851
0	0	-8	581	812
0	0	-6	698	600
0	0	-4	1255	1284
0	0	-2	804	777
0	0	0	1086	1181
0	0	2	791	-793
0	0	4	1321	1082
0	0	6	1174	1140
0	0	8	778	-820
0	0	10	401	-504
0	0	-12	1578	1537
0	0	-10	869	808
0	0	-8	802	-858
0	0	-6	405	-524
0	0	-4	918	928
0	0	-2	959	-918
0	0	0	3015	3448

			$\lvert F_o \rvert$	F_c
0	0	2	1309	1294
0	0	4	3467	-3458
0	0	6	1547	1601
0	0	8	797	782
0	0	10	2210	2868
0	0	-12	744	-900
0	0	-10	1911	2078
0	0	-8	655	961
0	0	-6	1395	1027
0	0	-4	542	565
0	0	-2	1147	1145
0	0	0	450	-458
0	0	2	539	582
0	0	4	528	565
0	0	6	1097	-1008
0	0	8	872	-900
0	0	10	1472	1502
0	0	-12	1293	-1277
0	0	-10	450	-505
0	0	-8	589	842
0	0	-6	455	-02
0	0	-4	254	488
0	0	-2	725	671
0	0	0	673	-559
0	0	2	3856	3973
0	0	4	1145	898
0	0	6	1156	970
0	0	8	2049	3065
0	0	10	547	-517
0	0	-12	1412	1342
0	0	-10	577	-341
0	0	-8	1102	1159
0	0	-6	320	100
0	0	-4	931	1044
0	0	-2	1157	910
0	0	0	1176	1171
0	0	2	894	850
0	0	4	701	-707
0	0	6	680	771
0	0	8	760	690
0	0	10	2593	2473
0	0	-12	1868	-1866
0	0	-10	2046	2070
0	0	-8	1860	1797
0	0	-6	1426	1439
0	0	-4	572	-410
0	0	-2	1469	1366
0	0	0	957	876
0	0	2	1216	1024
0	0	4	405	-371
0	0	6	1143	1088
0	0	8	880	835
0	0	10	597	589
0	0	-12	651	666
0	0	-10	1015	819
0	0	-8	505	-479
0	0	-6	2013	2085
0	0	-4	411	-314
0	0	-2	411	410
0	0	0	2147	1988
0	0	2	859	889
0	0	4	1182	1160
0	0	6	601	665
0	0	8	791	710
0	0	10	944	629
0	0	-12	1132	1170
0	0	-10	770	650
0	0	-8	1389	1334
0	0	-6	510	-440
0	0	-4	944	945
0	0	-2	881	588
0	0	0	788	858
0	0	2	2054	2768
0	0	4	4908	5295
0	0	6	1703	1034
0	0	8	883	855
0	0	10	1188	1134
0	0	-12	725	797
0	0	-10	491	374
0	0	-8	515	540
0	0	-6	924	903
0	0	-4	69	40
0	0	-2	5890	6312
0	0	0	3850	3970
0	0	2	1000	1415
0	0	4	1253	1241
0	0	6	3592	3777
0	0	8	330	241
0	0	10	1120	1130
0	0	-12	491	-415
0	0	-10	1155	1197
0	0	-8	69	-50
0	0	-6	979	1056
0	0	-4	330	-277
0	0	-2	817	497
0	0	0	515	650
0	0	2	380	335
0	0	4	2783	2823
0	0	6	1044	-1239
0	0	8	69	-98
0	0	10	431	501
0	0	-12	470	494
0	0	-10	4235	4501
0	0	-8	588	520
0	0	-6	2437	2471
0	0	-4	2221	2431
0	0	-2	312	193
0	0	0	1215	1291

			$\lvert F_o \rvert$	F_c
2	11	0	98	120
2	12	0	923	778
2	13	0	318	-393
2	14	0	994	868
2	15	0	471	524
2	16	0	196	431
3	0	0	947	-418
3	1	0	870	-845
3	2	0	5317	5000
3	3	0	1395	-1240
3	4	0	99	104
3	5	0	99	14
3	6	0	2719	2078
3	7	0	367	-198
3	8	0	1585	1500
3	9	0	374	400
3	10	0	1715	1781
3	11	0	919	1085
3	13	0	99	47
3	14	0	507	587
3	16	0	422	508
4	0	0	4396	4307
4	1	0	910	899
4	2	0	972	910
4	3	0	410	-279
4	4	0	3437	3287
4	6	0	421	485
4	7	0	711	-813
4	8	0	2000	1808
4	9	0	340	-154
4	10	0	1040	1059
4	12	0	741	709
4	14	0	589	723
4	15	0	69	248
4	16	0	386	322
5	0	0	809	821
5	1	0	98	60
5	2	0	2935	3010
5	3	0	69	-70
5	4	0	1446	1492
5	5	0	399	-176
5	6	0	1789	1958
5	8	0	954	940
5	10	0	721	640
5	12	0	329	504
5	14	0	444	387
5	16	0	422	556
6	0	0	3120	3108
6	1	0	69	-141
6	2	0	791	747
6	3	0	69	19
6	4	0	2187	2266
6	5	0	98	-122
6	6	0	422	436
6	7	0	698	598
6	8	0	967	1045
6	9	0	69	171
6	10	0	524	575
6	12	0	519	510
6	13	0	120	-53
6	14	0	529	578
6	16	0	190	298
7	0	0	585	538
7	2	0	2215	2133
7	3	0	640	628
7	4	0	326	237
7	5	0	208	282
7	6	0	1270	1303
7	7	0	495	502
7	8	0	481	487
7	10	0	847	832
7	12	0	350	-297
7	13	0	581	651
7	14	0	324	404
8	0	0	1157	1078
8	1	0	340	333
8	2	0	98	137
8	3	0	330	152
8	4	0	1104	1257
8	6	0	830	835
8	8	0	921	979
8	10	0	515	447
8	12	0	510	451
8	14	0	308	381
8	16	0	316	182
9	1	0	308	-97
9	2	0	1012	1045
9	3	0	405	-324
9	4	0	580	562
9	5	0	129	-101
9	6	0	583	578
9	8	0	317	540
9	10	0	428	528
9	12	0	392	525
10	0	0	1136	1304
10	2	0	139	254
10	3	0	98	-113
10	4	0	618	857
10	6	0	79	175
10	8	0	374	465
10	10	0	361	384
11	2	0	921	745
11	4	0	405	509
11	11	0	335	94
11	0	0	149	477
11	4	0	343	476
12	0	0	454	783
12	2	0	224	41

Table 6.3 Observed and calculated structure factors at 300°K

Table 6.4 $K_3Fe(CN)_6$ - Atomic co-ordinates at $\sim 300^{\circ}K$

Atom	x/a	y/b	z/c
K1	0.4982	0.2271	0.3743
K2	0	0	$\frac{1}{2}$
Fe	0	0	0
C1	0.1185	0.1677	0.0309
C2	0.1830	-0.0503	0.2055
C3	0.1845	-0.0552	-0.1091
N1	0.1953	0.2594	0.0488
N2	0.3040	-0.0791	0.3304
N3	0.2782	-0.0914	-0.1897

Table 6.5 $K_3Fe(CN)_6$ - Atomic Debye factors at $\sim 300^{\circ}K$

$$T = 2^{-(b_{11}h^2 + b_{22}k^2 + b_{33}l^2 + b_{23}kl + b_{13}hl + b_{12}hk)}$$

Atom	b_{11}	b_{22}	b_{33}	b_{23}	b_{13}	b_{12}
K1	0.0183	0.0100	0.0099	0.0004	0.0063	0.0036
K2	0.0108	0.0053	0.0092	-0.0013	0.0082	0.0011
Fe	0.0138	0.0062	0.0060	0.0001	0.0055	-0.0006
C1	0.0354	0.0068	0.0119	0.0007	0.0207	-0.0014
C2	0.0151	0.0091	0.0043	0.0007	-0.0024	0.0032
C3	0.0187	0.0077	0.0082	-0.0017	0.0122	0.0034
N1	0.0218	0.0158	0.0235	0.0317	0.0173	-0.0145
N2	0.0106	0.0113	0.0111	-0.0020	0.0025	-0.0060
N3	0.0363	0.0114	0.0363	0.0105	0.0092	-0.0018

Figure 6.5 (a) $K_3Fe(CN)_6$ - The crystal structure projected down 'c'

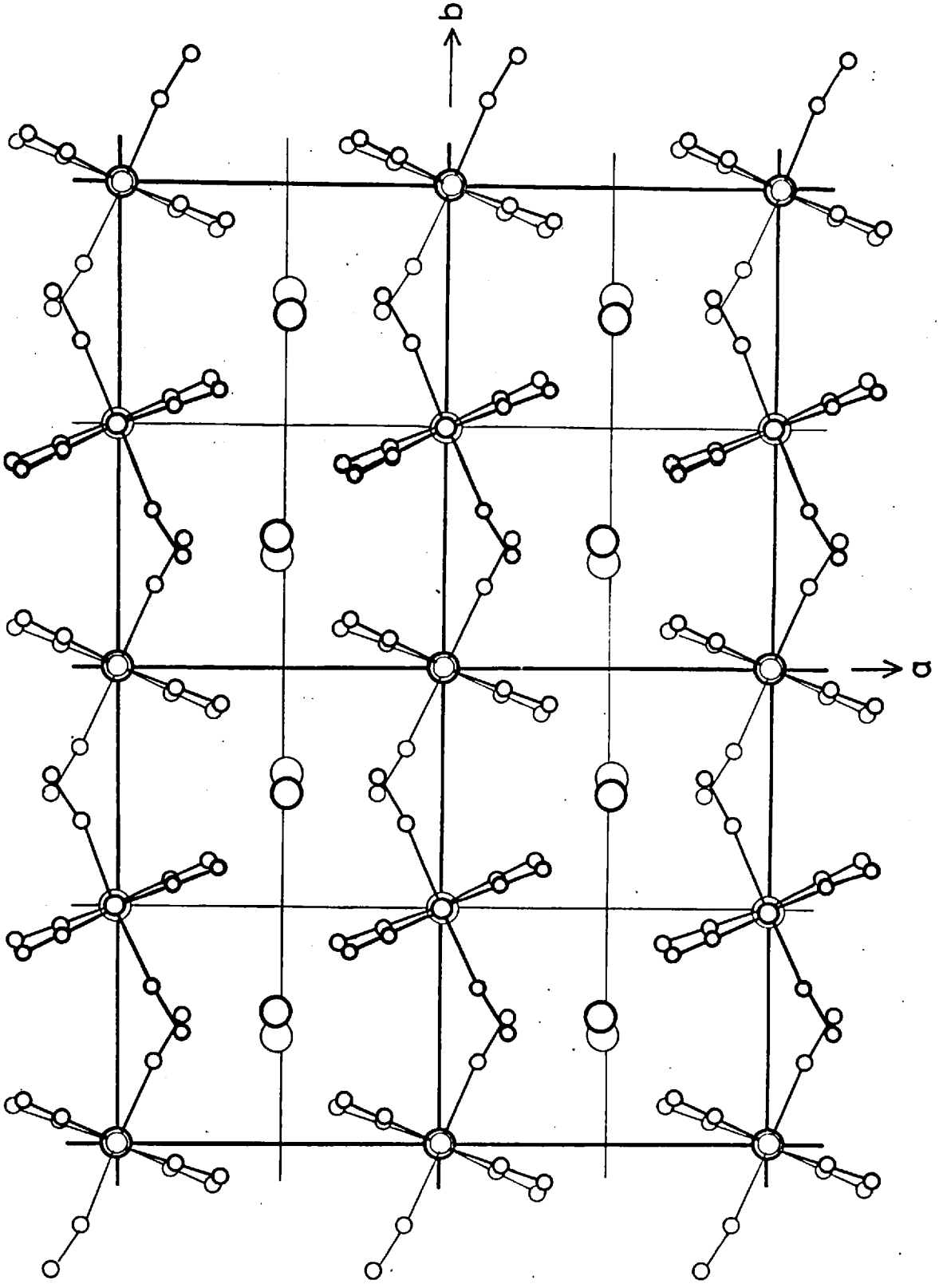


Figure 6.5 (b) Projection down 'a'

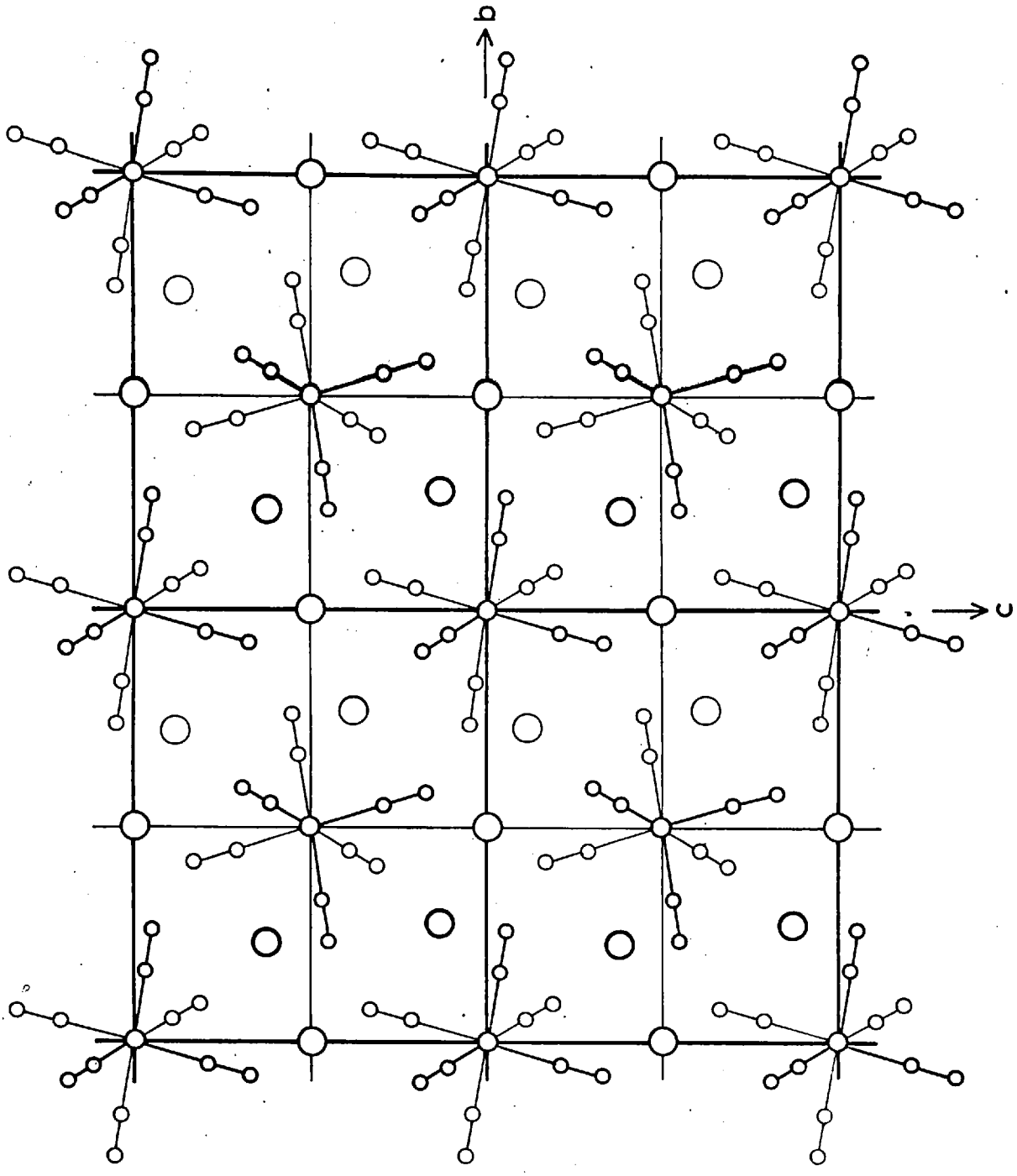
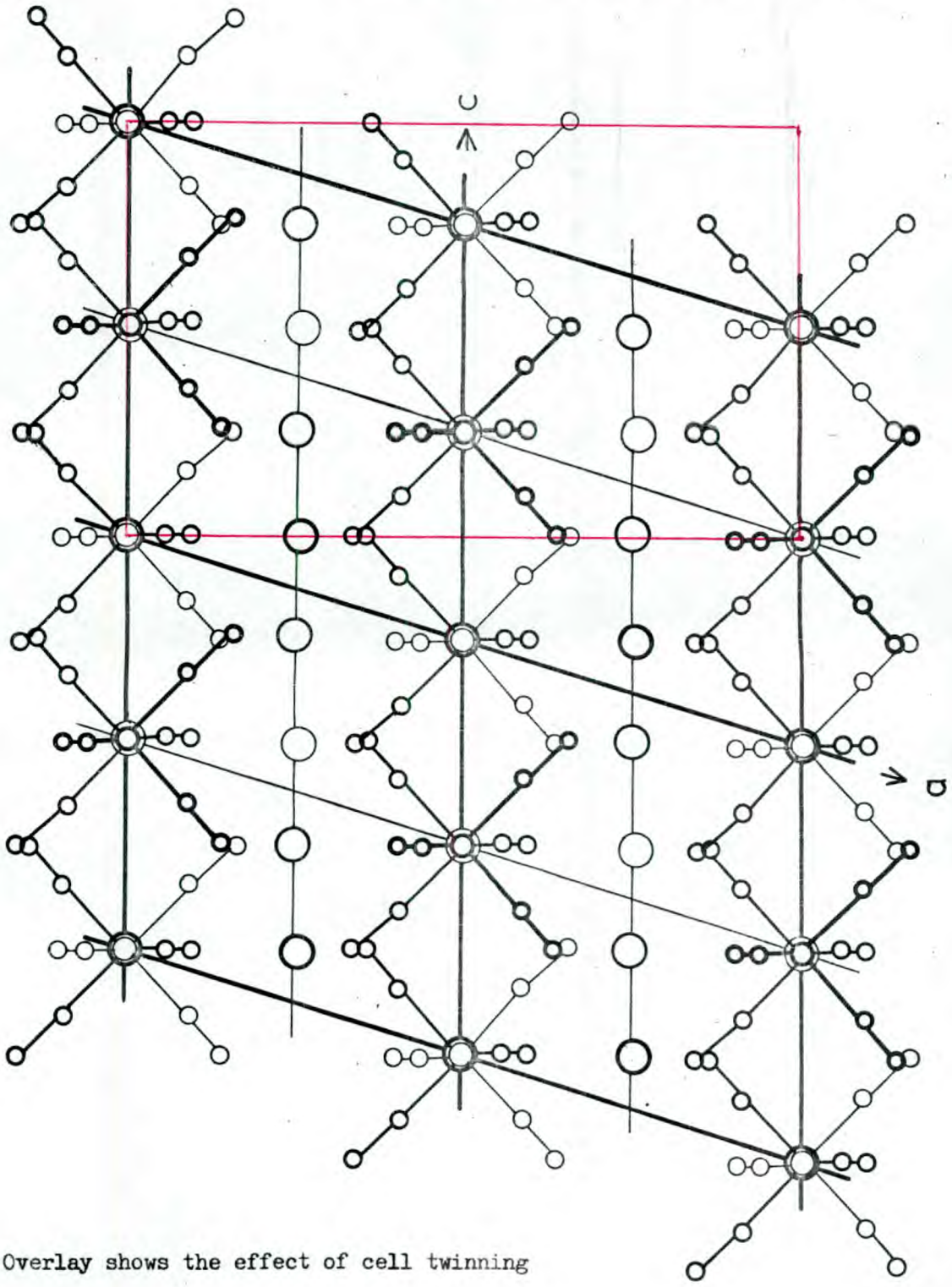
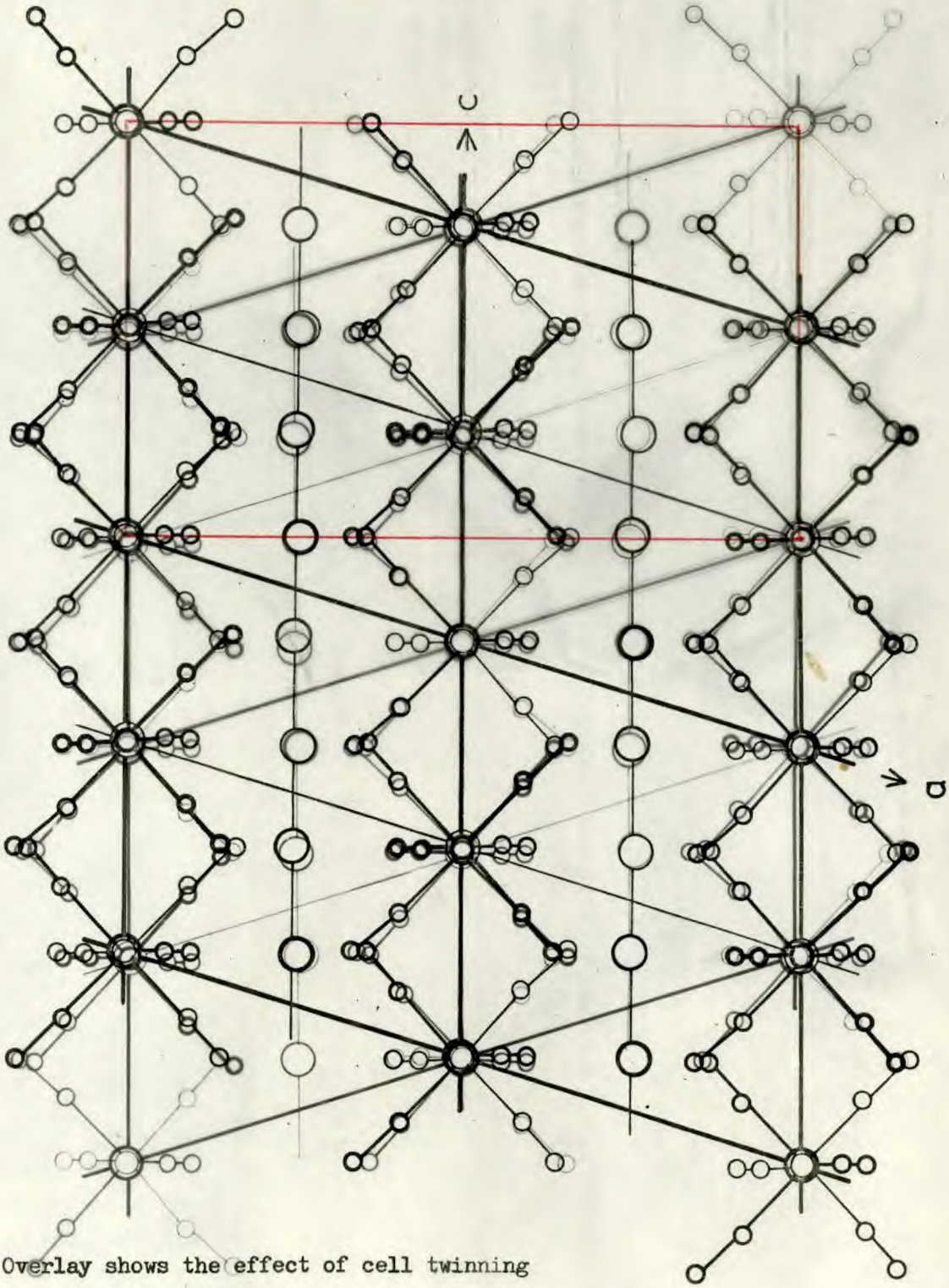


Figure 6.5(c) Projection down 'b', showing four 1M unit cells. The pseudo-orthorhombic cell is outlined in red.



Overlay shows the effect of cell twinning

Figure 6.5(c) Projection down 'b', showing four 1M unit cells. The pseudo-orthorhombic cell is outlined in red.



Overlay shows the effect of cell twinning

trigonal antiprisms (Figure 6.5(a)). Table 6.6 lists the shortest contacts with the potassium ions, forming their co-ordination spheres: next-nearest neighbours are also tabulated.

Figure 6.5(c) clearly shows the pseudo-orthorhombic nature of the crystals. The red rectangle shows how all the atoms may be very closely described by an orthorhombic unit cell projection. Further, the overlay, which represents cell twinning in the form of the polytypes shown in Figure 6.3, shows again how exact is the overlap of all atoms in this projection - it is hardly surprising that the $\{h0\ell\}$ Weissenberg photograph (Figure 6.4) showed such perfect mm symmetry! In fact, the $\{h0\ell\}$ data were collected from a crystal having orthorhombic symmetry in $\{h1\ell\}$ also, and this must result in larger b_{33} thermal parameters, in particular.

A discussion of the octahedron geometry is left until section 6.7.

* * *

6.6 The structure of $K_3Fe(CN)_6$ at $\sim 95^{\circ}K$

For similar reasons to those described in the previous section, work has so far been concerned only with two-dimensional data. Complete Weissenberg data from $\{h0\ell\}$, $\{hk0\}$ and $\{0k\ell\}$ zones were collected from three crystals, while several other crystals were examined briefly. The crystals were cooled by a continuous stream of cold nitrogen vapour, whose temperature was separately determined as 95°-$100^{\circ}K$. The unit cell dimensions have, as yet, only been determined approximately: they are,

Table 6.6 $K_3Fe(CN)_6$ - Non-bonded interactions with potassium ions (300°K)

A Closest neighbours around K1 (general position) in trigonal bipyramidal array.

Vector, K1 →		Å
N1	(x , y , z)	2.94
N1	(x , $\frac{1}{2}$ - y, $\frac{1}{2}$ + z)	2.94
N2	(1 - x, -y , 1 - z)	2.90
N3	(1 - x, -y , -z)	2.89
N2	(1 - x, $\frac{1}{2}$ + y, $\frac{1}{2}$ - z)	3.22
N3	(1 - x, $\frac{1}{2}$ + y, $\frac{1}{2}$ - z)	3.25

B Closest neighbours around K2 (special position) in octahedral array.

Vector, K2 →		Å
N1	(x , $\frac{1}{2}$ - y, $\frac{1}{2}$ + z)	2.82
N1	(-x ,$-\frac{1}{2}$ + y, $\frac{1}{2}$ - z)	2.82
N2	(x , y , z)	3.02
N2	(-x , -y , 1 - z)	3.02
N3	(x , y , 1 + z)	2.91
N3	(-x , -y , -z)	2.91

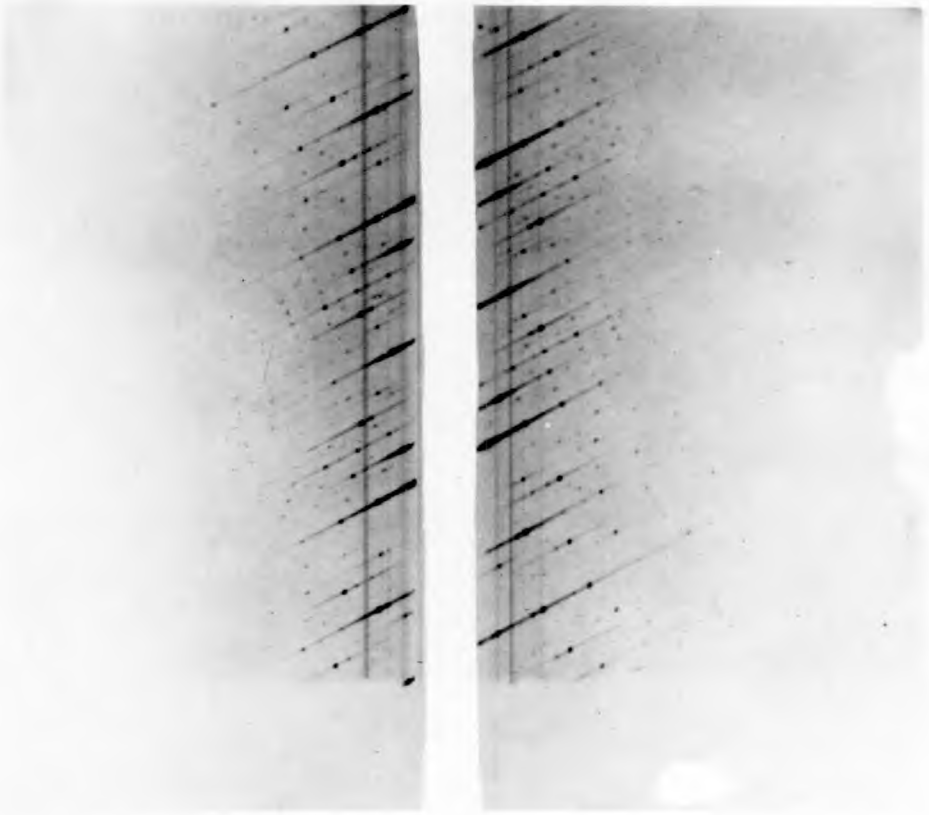
C Next-nearest neighbours around K1 and K2 at less than 4 Å

Vector, K1 →		Å	Vector, K2 →		Å
C1	(x , y , z ,)	3.35	C1	(x , $\frac{1}{2}$ - y, $\frac{1}{2}$ + z)	3.54
C1	(x , $\frac{1}{2}$ - y, $\frac{1}{2}$ + z,)	3.50	C1	(-x ,$-\frac{1}{2}$ + y, $\frac{1}{2}$ - z)	3.54
C2	(x , y , z ,)	3.65	C2	(x , y , z)	3.16
C2	(1 - x, $\frac{1}{2}$ + y, $\frac{1}{2}$ - z,)	3.43	C2	(-x , -y , 1 - z)	3.16
C3	(1 - x, $\frac{1}{2}$ + y, $\frac{1}{2}$ - z,)	3.37	C3	(x , y , 1 + z)	3.20
N2	(x , y , z ,)	3.44	C3	(-x , -y , -z)	3.20

$a = 7.07$ Å ; $6 = 10.46$ Å ; $c = 8.41$ Å ; $\beta = 107^{\circ}20$

Much of the analysis centres around an interesting phenonenon. Figure 6.6 shows prints taken from Weissenberg $\{hk0\}$ photographs taken at 95°K and 300°K from the same crystal. There are twice as many reflexions at low temperatures, approximately half of which lie on 'extra' layer lines parallel to b*, clearly indicating or doubling of the a cell edge. The change is quite reversible, but unfortunately perhaps, the effect is not observed for all crystals. An effect like this could be explained by atoms, say the potassium ions, lying in one minimum of a double potential energy well, in such a way as to be resolvable when the atomic vibrations are small but not when they are large: this sort of explanation seemed more likely in view of the reversibility of the change, and of the fact that the reflexions common to all photographs (i.e. h even) followed similar patterns and, in particular, agreed well with those from crystals not showing the effect at all. At first, therefore, the photographs were indexed for the small (undoubled) unit cell, omitting all of the 'extra' $\{hk0\}$ reflexions, giving 302 intensities in all.

With the final positions from the room-temperature analysis and isotropic temperature factors of 2.0 and 3.0 for heavy and light atoms respectively, the initial R factor was 0.16. Ten least squares cycles, adjusting positional and anisotropic thermal parameters for all atoms, reduced R to 0.077, when convergence was complete. This low value of R appeared to justify the strategy of omitting half of the observed $\{hk0\}$ reflexions. The final observed and calculated structure factors are collected in Table 6.7 while positional and



95°K

Figure 6.6 Doubling of the 'a' cell dimension



300°K

			$\lvert F_o \rvert$	F_c
2	0	0	2994	2726
3	0	0	821	-598
8	0	0	1032	1505
10	0	0	2572	2391
12	0	0	806	654
14	0	0	819	682
2	1	0	1447	-1462
1	1	0	709	-504
4	1	0	904	1032
8	1	0	597	485
0	2	0	1545	1675
2	2	0	382	-160
4	2	0	819	747
6	2	0	3210	3273
8	2	0	766	504
7	2	0	2832	2773
9	2	0	1585	1409
11	2	0	1637	1417
13	2	0	1033	1021
2	3	0	409	455
3	3	0	1350	-1208
7	3	0	1130	1038
9	3	0	647	-450
11	3	0	868	813
1	4	0	1380	1422
2	4	0	409	-475
4	4	0	3406	3496
5	4	0	1433	1360
6	4	0	2576	2658
8	4	0	1796	1697
10	4	0	1525	1440
12	4	0	1149	1045
1	5	0	1184	1120
2	5	0	738	600
8	5	0	597	760
1	6	0	3341	3789
2	6	0	2161	2096
3	6	0	2723	2706
4	6	0	0	155
5	6	0	2077	2271
7	6	0	1784	1856
8	6	0	1063	944
9	6	0	1598	1420
11	6	0	891	818
2	7	0	647	697
3	7	0	501	472
4	7	0	752	-536
6	7	0	900	907
7	7	0	738	893
0	8	0	2706	2810
1	8	0	960	884
2	8	0	2417	2436
3	8	0	1176	952
4	8	0	1995	1804
5	8	0	806	750
6	8	0	1326	1446
7	8	0	480	515
8	8	0	1262	1248
9	8	0	480	460
10	8	0	752	767
12	8	0	831	733
4	9	0	434	454
9	9	0	614	474
0	10	0	766	719
1	10	0	1193	1214
2	10	0	1339	961
3	10	0	1730	1733
4	10	0	880	832
5	10	0	819	708
8	10	0	522	485
7	10	0	1013	1135
8	10	0	670	734
9	10	0	738	830
3	11	0	480	432
9	11	0	597	599
0	12	0	1043	940
1	12	0	809	698
2	12	0	831	753
4	12	0	738	884
5	12	0	434	497
9	12	0	879	810
7	12	0	647	717
8	12	0	647	680
1	13	0	924	907
0	14	0	560	560
1	14	0	647	692
2	14	0	947	1005
3	14	0	383	351
4	14	0	879	870
5	14	0	382	301
6	14	0	383	300
0	0	1	4040	3400
1	0	1	2498	2003
2	0	1	2498	2452
3	0	1	1742	1304
4	0	1	1093	1072
5	0	1	1893	1782
6	0	1	1408	1410
10	0	1	770	777
12	0	1	850	940
0	4	1	915	1739
0	7	1	1072	1188
0	9	1	738	-528
0	11	1	914	371
1	1	2	1043	1100
1	2	2	1416	1378
1	3	2	3244	-3448
1	4	2	4062	3654
1	5	2	880	790
1	6	2	2923	2723
1	7	2	914	-613
1	8	2	1802	1982
1	9	2	560	638
1	10	2	560	941
1	11	2	779	749
2	1	3	383	-418
2	3	3	383	-559
2	4	3	383	370
2	5	3	831	1232
2	6	3	914	-733
2	7	3	679	-535
2	9	3	614	423
2	11	3	614	-418
2	1	4	560	-523
2	2	4	4053	4183
2	3	4	1112	1225
2	4	4	880	833
2	6	4	3236	3052
2	8	4	779	936
2	10	4	1043	1267
2	12	4	831	809
2	5	5	480	757
2	1	6	2306	-2100
2	2	6	2288	2270
2	3	6	2288	2100
2	4	6	1245	1838
2	5	6	480	-668
2	6	6	1270	1302
2	7	6	915	1052
2	8	6	1043	1004
2	10	6	915	1133
2	12	6	728	732
2	1	8	383	-467
2	2	8	383	508
2	4	8	2274	2237
2	6	8	738	747
2	8	8	1073	1258
2	9	9	614	-414
2	1	10	831	921
2	2	10	1409	1561
2	3	10	480	-637
2	4	10	915	1057
2	5	10	880	797
2	6	10	831	914
2	8	12	1324	1585
2	6	12	1073	1135
3	0	0	2749	2720
4	0	0	4733	4704
4	0	0	3864	3839
8	0	0	1418	1505
10	0	0	2021	2291
1	0	2	5297	5498
2	0	2	2447	2528
3	0	2	1119	1143
4	0	2	2221	2286
6	0	2	2109	2208
7	0	2	731	722
8	0	2	1469	1274
9	0	2	1559	1511
10	0	2	915	1085
11	0	2	579	445
1	0	4	3221	3406
2	0	4	926	954
3	0	4	1119	1088
4	0	4	457	-503
5	0	4	2009	2715
6	0	4	522	500
7	0	4	1570	1561
9	0	4	1591	1705
1	0	6	4037	3982
2	0	6	1778	1770
3	0	6	2611	2675
4	0	6	947	1007
5	0	6	3773	3755
6	0	6	457	-553
7	0	6	2561	2705
8	0	6	560	532
9	0	6	1930	2010
11	0	6	1094	1804
12	0	6	611	611
0	0	6	1012	1002
1	0	6	779	855
2	0	6	647	670
3	0	6	2021	1981
4	0	6	2122	2144
5	0	6	800	856
6	0	6	839	837
7	0	6	808	818
8	0	6	915	810
9	0	6	631	680
10	0	6	614	615
1	0	-6	2930	3075
2	0	-6	3006	3050
3	0	-6	2909	2701
4	0	-6	752	851
5	0	-6	647	600
6	0	-6	2041	2046
7	0	-6	2237	2297
8	0	-6	700	873
9	0	-6	819	792
10	0	-6	856	840
11	0	-6	904	901
12	0	-6	663	705
13	0	-6	614	708
0	0	8	2426	2452
1	0	8	434	400
2	0	8	2404	2360
3	0	8	351	-141
4	0	8	2072	2039
6	0	8	1403	1418
8	0	8	1170	1139
1	0	-8	458	398
8	0	-8	3058	3733
3	0	-8	458	459
4	0	-8	2477	2405
5	0	-8	409	394
6	0	-8	2451	2471
8	0	-8	2161	2074
10	0	-8	1447	1548
12	0	-8	1334	1296
0	0	10	1184	1203
1	0	10	856	914
2	0	10	971	939
3	0	10	892	804
4	0	10	579	559
5	0	10	960	1000
6	0	10	766	815
1	0	-10	1605	1608
2	0	-10	1211	1188
3	0	-10	1230	1100
4	0	-10	1675	1584
5	0	-10	1170	1313
5	0	6	0	-10
7	0	-10	942	894
8	0	-10	892	900
9	0	-10	541	585
10	0	-10	1002	998
11	0	-10	868	914
12	0	-10	522	583
1	0	12	1578	1579
3	0	12	1497	1527
5	0	12	679	707
7	0	12	856	903
1	0	-12	1205	1272
2	0	-12	354	342
3	0	-12	2641	2446
4	0	-12	354	410
5	0	-12	1294	1318
7	0	-12	1579	1547
9	0	-12	1041	1060
11	0	-12	663	811
12	0	-12	971	1014
0	0	14	663	771
1	0	14	611	678
2	0	14	560	570
4	0	14	458	568
1	0	-14	570	587
3	0	-14	970	806
1	0	-14	811	837
4	0	-14	904	792
6	0	-14	960	882
1	0	-14	611	620
7	0	-14	694	558
8	0	-14	552	496
9	0	-14	560	677
11	0	-14	647	552
12	0	-14	458	500
0	0	16	960	790
2	0	16	647	735
4	0	16	914	811
1	0	-16	1082	1056
3	0	-16	1158	1005
5	0	-16	1081	1012
8	0	-16	904	907
11	0	-16	705	760
12	0	-16	736	722

Table 6.7 $K_3Fe(CN)_6$ – Observed and calculated structure factors at 95°K

thermal parameters are given in Tables 6.8 and 6.9, respectively. The geometry of the ferricyanide octahedron is discussed in detail in the next section. The co-ordination of the potassium ions is summarized in Table 6.10 and may be compared with values given in Table 6.6.

We were now concerned to account for the extra $\{hk0\}$ reflexions and began by examining the effect of disordering the potassium ions in general positions, thus being able to maintain the same spacegroup. This was done by chosing two sites about 0.3 Å apart, differing only in their y-coordinates, in such a way as to repeat at every other (small) unit cell along the a direction. Disordering of the two sites was examined in various proportions - 50:50, 70:30, 90:10 etc. - but it soon became apparent that the observed extra intensities were far too strong to be explained by disordering the potassium ions alone. There were other arguments to support this.

An examination of the temperature factors in Table 6.9 shows a very inconsistent pattern, especially for the heavy atoms whose parameters are generally the more accurately determined in an X-ray analysis. The temperature factors b_{11}, b_{22} and b_{12} for Fe, b_{12} for K2 (special) and b_{22} for K1 (general) all seem large, suggesting that disorder affects all of these atoms. Further, difference $\{hk0\}$ Fourier maps calculated from the small cell analysis above and from variously signed complete $\{hk0\}$ data, showed similar features around the K (special) and Fe positions (these are superimposed in this projection as is illustrated in Figure 6.5) It is interesting to note that similar features, though less pronounced, were noticed in the neutron diffraction study of Curry

Table 6.8 $K_3Fe(CN)_6$ - Atomic co-ordinates at $\sim 95^{\circ}K$

Atom	x/a	y/b	z/c
K1	0.4980	0.2303	0.3745
K2	0	0	$\frac{1}{2}$
Fe	0	0	0
C1	0.1250	0.1737	0.0309
C2	0.1861	-0.0523	0.2080
C3	0.1874	-0.0508	-0.1148
N1	0.1998	0.2680	0.0502
N2	0.3080	-0.0771	0.3319
N3	0.2866	-0.0935	-0.1858

Table 6.9 $K_3Fe(CN)_6$ - Atomic Debye factors at $\sim 95^{\circ}K$

$$T = 2^{-(b_{11}h^2 + b_{22}k^2 + b_{33}l^2 + b_{23}kl + b_{13}hl + b_{12}kh)}$$

Atom	b_{11}	b_{22}	b_{33}	b_{23}	b_{13}	b_{12}
K1	0.0062	0.0104	0.0055	0.0048	0.0038	-0.0041
K2	0.0063	0.0039	0.0061	0.0052	0.0052	-0.0116
Fe	0.0117	0.0116	0.0038	-0.0059	0.0054	-0.0151
C1	0.0044	0.0274	0.0084	0.0234	0.0010	-0.0168
C2	0.0082	0.0170	0.0056	-0.0066	0.0044	-0.0220
C3	0.0101	0.0115	0.0077	0.0179	0.0098	-0.0026
N1	0.0045	0.0110	0.0139	0.0035	0.0014	0.0025
N2	0.0043	0.0130	0.0069	0.0095	0.0003	-0.0033
N3	0.0113	0.0119	0.0290	-0.0292	0.0046	-0.0168

Table 6.10 $K_3Fe(CN)_6$ - Non-bonded interaction with potassium ions (95°K)

A Closest neighbours around K1 (general position) in trigonal bipyramidal array

	Vector, K1 →	Å
N1	(x , y , z)	2.93
N1	(x , $\frac{1}{2}$ - y, $\frac{1}{2}$ + z)	2.92
N2	(1 - x, -y , 1 - z)	2.92
N3	(1 - x, -y , -z)	2.89
N2	(1 - x, $\frac{1}{2}$ + y, $\frac{1}{2}$ - z)	3.22
N3	(1 - x, $\frac{1}{2}$ + y, $\frac{1}{2}$ - z)	3.19

B Closest neighbours around K2 (special position) in octahedral array

	Vector, K2 →	Å
N1	(x , $\frac{1}{2}$ - y, $\frac{1}{2}$ + z)	2.78
N1	(-x , $-\frac{1}{2}$ + y, $\frac{1}{2}$ - z)	2.78
N2	(x , y , z)	3.04
N2	(-x , -y , 1 - z)	3.04
N3	(x , y , 1 + z)	2.97
N3	(-x , -y , -z)	2.97

C Next-nearest neighbours around K1 and K2 at less than 4 Å

	Vector, K1 →	Å		Vector, K2 →	Å
C1	(x , y , z)	3.33	C1	(x , $\frac{1}{2}$ - y, $\frac{1}{2}$ + z)	3.52
C1	(x , $\frac{1}{2}$ - y, $\frac{1}{2}$ + z)	3.43	C1	(-x , $-\frac{1}{2}$ + y, $\frac{1}{2}$ - z)	3.52
C2	(x , y , z)	3.70	C2	(x , y , z)	3.16
C2	(1 - x, $\frac{1}{2}$ + y, $\frac{1}{2}$ - z)	3.40	C2	(-x , -y , 1 - z)	3.16
C3	(1 - x, $\frac{1}{2}$ + y, $\frac{1}{2}$ - z)	3.40	C3	(x , y , 1 + z)	3.15
N2	(x , y , z)	3.46	C3	(-x , -y , -z)	3.15

and Runciman (loc.cit.): it was suggested, there, that the features might be due to the effects of anisotropic vibrations, which, to some extent at least, may be correct.

Taken together, the difference Fourier maps and the thermal parameters in Table 6.9 suggest that better co-ordinates for the Fe atom may be $x \approx +0.02$ Å, $y \approx -0.03$ Å, with concomitant adjustment of the positions of the cyanide groups. It is likely that the potassium atoms co-ordinates also need similar adjustment. All this may be achieved in many ways, which fall broadly into two classes: (a) disordering of monoclinic unit cells and (b) disordering within an orthorhombic system, perhaps in such a way that the low temperature form of $K_3Fe(CN)_6$ is rigorously orthorhombic. One serious objection to the last possibility is the fact that the superlattice effect is not observed with all crystals: this suggests that we are dealing with a disordering effect rather than a true phase change. So far, we have studied disordered models of both types but have not reduced R below 0.30. As the solution of this problem may be protracted, it seemed worth while to present this interim report with some tentative conclusions, which will now be described.

* * *

6.7 The geometries of the ferricyanide octahedron

The bond lengths and angles in the octahedron at $\sim 300^{\circ}K$ and $\sim 95^{\circ}K$ are compared in Table 6.11. These is a close parallel between the two sets of parameters which have been derived from the two independent sets of data from

Table 6.11 $K_3Fe(CN)_6$ - Geometries of the ferricyanide octahedron at $\sim 300^{\circ}K$ and $\sim 95^{\circ}K$

A. Bond lengths

Bond	$\sim 300^{\circ}K$ Å	$\sim 95^{\circ}K$ Å
Fe - C1	1.92	2.00
Fe - C2	1.89	1.92
Fe - C3	1.89	1.93
C1 - N1	1.08	1.11
C2 - N2	1.18	1.16
C3 - N3	1.14	1.14

B. Bond angles

Angle	$\sim 300^{\circ}K$ degrees	$\sim 95^{\circ}K$ degrees
C1 - Fe - C2	89	89
C2 - Fe - C3	89	89
C3 - Fe - C1	90	88
Fe - C1 - N1	176	178
Fe - C2 - N2	177	175
Fe - C3 - N3	172	172

several different crystals. The results seem to be characterised by a tetragonal distortion of the octahedra along the bonds Fe-Cl-Ni. Before considering any implications of such a distortion, it is necessary to establish some level of significance for the values quoted in Table 6.11.

We must comment, firstly, on the unit cell dimensions. The values given above are all slightly greater at 95°K than at 300°K : if these results are significant, they could only be accounted for by assuming that a phase change had occurred at some intermediate temperature, which is, of course, possible. However, no significance can be attached to the cell dimensions quoted, as they were obtained from intensity photographs only. A careful measurement of the high-angle splitting of the Kα doublets at room and low temperatures is presently in progress.

Also, the bond lengths have not been corrected for librational effects (Cruickshank, loc.cit.), a correction which will result in slight increases in bond lengths, most particularly at the higher temperature.

In addition to these two factors, which can be allowed for, there is the, as yet unknown, correction for any systematic errors introduced by ignoring disorder effects. When the disorder mechanism has been fully established a suitable adjustment of the bond lengths can be applied. Although we anticipate that such a correction would be small, in view of the low R factors reached, we have not felt justified in quoting estimated standard deviations for the atomic parameters, for, being calculated assuming random data errors, these would be somewhat meaningless.

Qualitatively, however, the octahedron does appear to be distorted tetragonally, as both, independent, analyses indicate. The agreement between the two analyses could, of course, be due in part to similar disorder effects being ignored in both models. In view of the low R factors, however, and of the relatively small inconsistencies in the temperature factors discussed above, it seems unlikely that this alone could account for the qualitative agreement of the two octahedron geometries.

* * *

6.8 Correlation of the magnetic and structural properties of $K_3Fe(CN)_6$

In view of the possible errors discussed above, no quantitative attempt has yet been made to correlate the structural and magnetic properties of potassium ferricyanide. A qualitative investigation, however, is revealing.

If we consider the tetragonal distortion of the ferricyanide octahedron along Fe-Cl-Nl as established, we can describe the principal molecular paramagnetic susceptibilities by $K_{||}$ and $K_{\perp}$, parallel and perpendicular to the axial distortion, We would then expect that the larger crystal magnetic anisotropies would be associated with a large component of $K_{||}$ lying in the plane of the magnetic field. Thus, with Figure 6.5(a) in mind, we would expect $\Delta\chi_c$, the anisotropy closely related to $|\chi_a - \chi_b|$, to be large, because $K_{||}$ (Fe-Cl-Nl) lies close to the ab plane: in fact, $\Delta\chi_c$ is found to be the smallest anisotropy. Similarly $\Delta\chi_a$, and $\Delta\chi_b$, which are the anisotropies closely associated with the projections in Figures 6.5(b) and (c) respectively, should be small;

this can be seen most easily in Figure 6.5(c) which shows that $K_{||}$ is nearly perpendicular to the ac net. Experimentally, however, it is found that $\Delta\chi_a$, and $\Delta\chi_b$ are the larger anisotropies. Thus, an interpretation of the magnetic properties of the ferricyanide crystal solely in terms of non-interacting tetragonally-distorted octahedra is completely at variance with experimental fact.

The contradiction can be explained, however, if we can assume a significant super exchange effect parallel to the c axis. A possible mechanism for this is summarized in Figure 6.7. The 'special' potassium ions are co-ordinated octahedrally by nitrogen atoms as described previously: more significant is the proximity of four carbon atoms - as may be seen from Tables 6.6 and 6.10. Thus the π-electron clouds of the cyanide groups are very favourably disposed to overlap with the K^+ ion as Figure 6.7 illustrates. Normally, antiferromagnetic exchange through a five-atom non-bonded bridge would be expected to be very small, and we may indeed expect that such interactions perpendicular to the c axis, as represented in figure, would be small. By contrast, the situation parallel to c seems very favourable - particularly in view of the nature of the high-field cyanide ligands which make much use of their π- and π^*- orbitals in 'back-bonding'. Indeed, this is one justification for an electron-delocalization parameter, k, of 0.87, representing the proportion of time spent by the metal t_{2g} electrons on the ligand atoms. Thus, the cyanide ligands may be regarded, to some extent at least, as an extension of the direct sphere of influence of the metal electrons. Interaction between ferricyanide octahedra

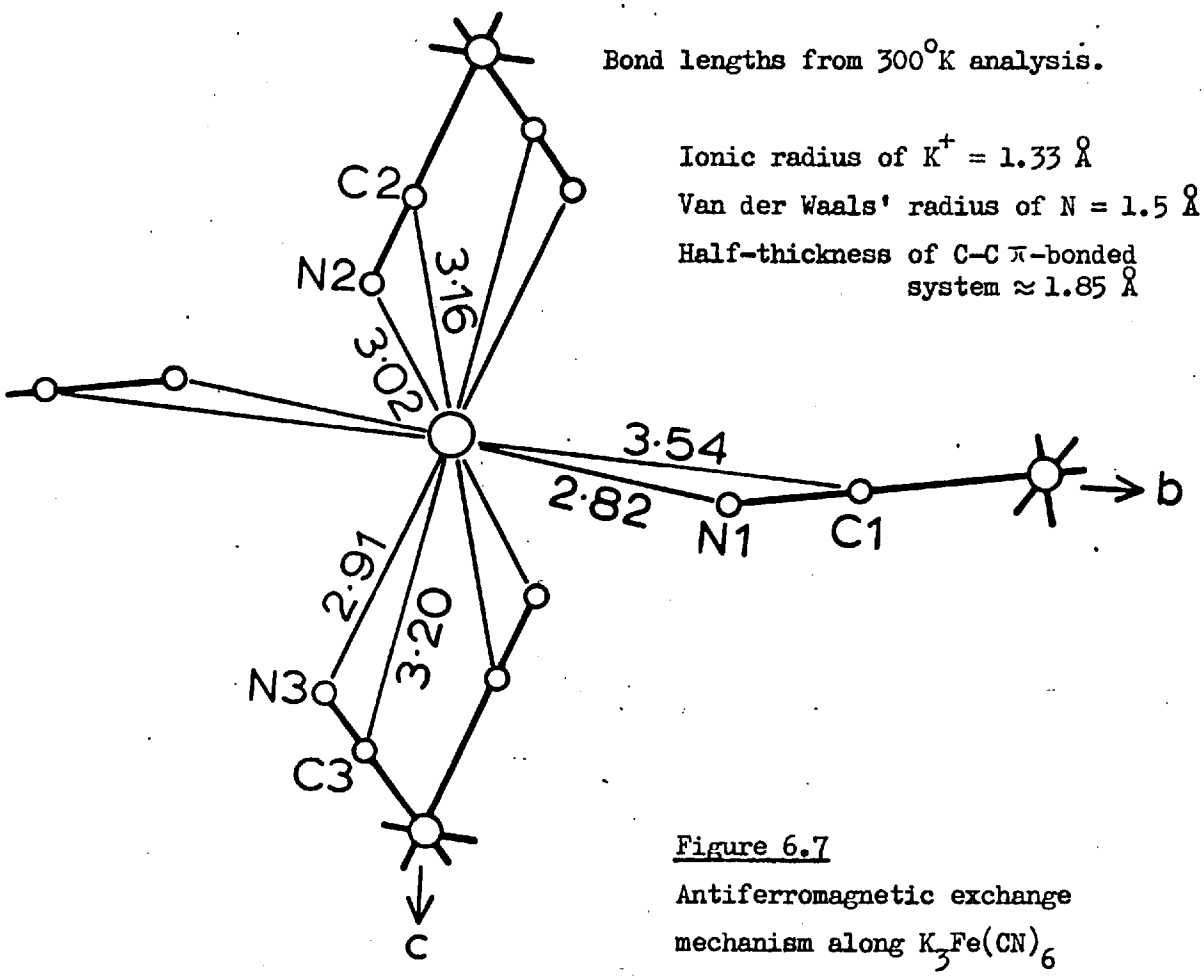
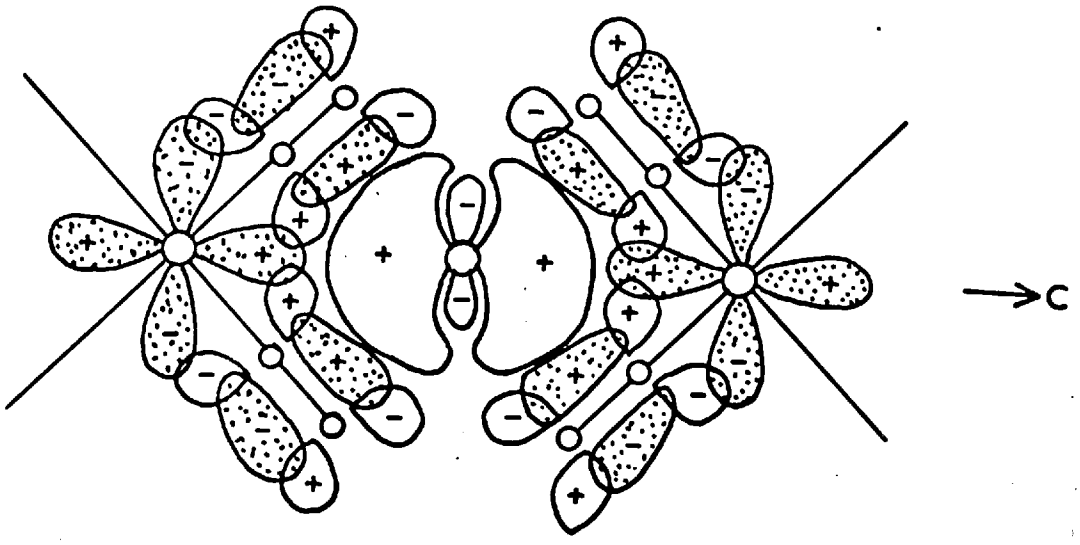


Figure 6.7
Antiferromagnetic exchange mechanism along $K_3Fe(CN)_6$ chains parallel to c



vis a potassium ion is, then, not so very different from that shown in various binary compounds. Although the 3d orbitals lie energetically close to the 4s orbital in this region of the Periodic Table and can be sterically well disposed on account of the near-octahedral co-ordination of the potassium ion, it seems unlikely that they could play more than a minor role in the exchange mechanism because of their unfavourable symmetry. When hybridized with the 4s orbital, however, they could satisfy all the necessary conditions. Perhaps the most likely hybrid orbital is a $3d_{z^2}$ 4s and, following Coates (1962), this is illustrated in Figure 6.7. If we suppose that such super-exchange is significant, the observed anisotropies are readily explicable. Exchange parallel to *c* will reduce the magnitude of the susceptibility in that direction relative to that along *a* or *b*, resulting in larger anisotropies $\Delta\chi_b$ and $\Delta\chi_{a'}$, respectively. Further, the relative magnitudes $\chi_a > \chi_c$; $\chi_b > \chi_c$ agree with the observed order $\chi_a > \chi_b > \chi_c$. The relatively low value for $\Delta\chi_c$ presumably results in part from an 'averaging-out' of various strong and weak exchange and tetragonal distortion effects and also, perhaps, as a result of the distortion being less important than has been previously supposed. To ascertain the importance of the antiferromagnetic *vis à vis* distortion effects, it may be very useful to measure the crystal anisotropies of magnetically dilute crystals, a most suitable diluent being potassium cobalticyanide.

Some support is lent to the idea that antiferromagnetism is important by the specific heat transition reported by Stephenson and Morrow (*loc. cit.*) who assumed that it was magnetic in origin. They had argued that the total magnetic

entropy to be expected at low temperatures is $R \log 2 = 1.38$ cal.deg.$^{-1}$mole^{-1}, there being two spin states of the molecule. The observed entropy of transition was 0.9 ± 0.2 cal. deg.$^{-1}$mole^{-1}, suggesting that about 0.5 cal.deg.$^{-1}$mole^{-1} would be lost below 15°K. The specific heat transition, which is gradual, may well correspond to a gradual increase in the magnetic ordering around 131°K. This should result in an increase in the anisotropies $\Delta\chi_a$, and $\Delta\chi_b$ at that temperature, as these most directly involve the c direction. In fact, $\Delta\chi_a$, does exhibit a fairly sudden increase below this temperature, but any increase in $\Delta\chi_b$ is slight. As an algebraic consequence, so to speak, the increase in $\Delta\chi_a$, must be matched by an equivalent decrease in $\Delta\chi_c$: it appears that this decrease is sufficiently large to counter-act the Boltzman effect (increasing susceptibility with falling temperature) resulting in a maximum in the $\Delta\chi_c$ versus T curve. Finally, it does not appear possible to explain the anomalies reported by Ristau, Ruckpaul and Shoffa (loc.cit.) which we have been quite unable to reproduce.

The qualitative proposals outlined above are presently being tested by further, quantitative work and are, as yet therefore, somewhat tentative. If proved correct, the solution of the ferricyanide problem will have furnished an instructuve example of the part antiferromagnetic exchange can play in crystals of simple inorganic complexes.

* * *

CONCLUSION

At the outset of the work described in Chapters 2 and 3 we hoped to determine the stereochemistries of the two complexes involved and we have described how the structure proposed for the hydride from n.m.r spectroscopy was confirmed while that suggested for a cyclobutadiene compound turned out to entail the cyclopentadienone ligand. While such positive results were satisfactory in themselves, more interesting discoveries had arisen, showing that both of these molecules were prototypes, so to speak, of two novel organometallic bonding mechanisms. The cyclopentadienone complex structure shows how a transition metal bonds to these cyclic ligands by σ- and π - bonds to an extent depending partly upon the nature of the ring substituents. Further, both molecular structures solved here have shown how the bonding of the cyclopentadienyl ring to the metal may not be perfectly symmetrical as had been previously supposed. In both bonding schemes, we have emphasized how the proposed bonding is intermediate between extreme forms and how different substituent groups on the cyclopentadienone ring or on the metal may cause the molecule to adopt an electronic distribution closer to one or other of these extremes. Both analyses, taken in conjunction with the structures of analagous compounds, show how even an unsophisticated molecular orbital approach to the bonding mechanism may improve on a valence bond description.

In the second part we have shown how structural data, much of which was

not already available, may be correlated with single crystal paramagnetic anisotropy. In the case of the cobaltous complexes even a qualitative correlation of the tetrahedral distortions with the observed magnetic anisotropies was sufficient to indicate that the sign of the distortion in Cs_3CoCl_5 reported earlier must be incorrect; our subsequent X-ray analysis confirmed this prediction. Quantitative calculations showed that the electron delocalization parameters of the metal t_{2g} electrons were approximately 0.9 in each case and allowed an order-of-magnitude estimate of anisotropic magnetic exchange in the chlorides. In Chapter 6 the problem of potassium ferricyanide has been described. This compound has long been a key example in magnetochemistry and while the structural work and interpretation of the magnetic anomaly are not yet complete we can now visualize a mechanism to correlate these physical properties which suggests that the behaviour may be explained by a superexchange mechanism.

* * *

REFERENCES

Books

Beurger, M.J. 'Crystal Structure Analysis'. Wiley (1960).

Beurger, M.J. 'Vector Space'. Wiley (1959).

Condon, E.U. and Shortley, G.H. 'The Theory of Atomic Spectra'. C.U.P. (1953).

Hertzberg, G. 'Atomic Spectra and Atomic Structure'. Blackie (1937).

Lewis, J. and Wilkins, R.G. 'Modern Coordination Chemistry'. Interscience (1959)

Lipson, H. and Cochran, W. 'The Crystalline State'. Vol. III Bell (1953).

Pauling, L. 'Nature of the Chemical Bond'. O.U.P. (1960)

Van Vleck, J.H. 'Theory of Electric and Magnetic susceptibilities' O.U.P. (1932)

Papers

Allegra, G.and Ganis, P. Lincei. Rend. Sc. fis mat e nat. 33 , 438, (1962)

Bailey, N.A., Gerloch, M. and Mason, R. Nature 201 , 72, (1964)

Bailey, N.A. and Mason, R. (1963) In preparation.

Ballhausen, C.J. Dan. Mat. Fys. Med. 4 , 29, (1954)

Ballhausen, C.J. and Dahl, J.P. Acta Chem. Scand. 15 , 1333, (1961)

Barkhatov, V. and Zdhanov, H. Acta Phys.-chim U.R.S.S. 16 , 43, (1942)

Bennett, M.J., Churchill, M.R., Gerloch, M. and Mason, R. Nature, 1318, (1964)

Bennett, M.J., Gerloch, M., McCleverty, J.A. and Mason, R. Proc. Chem. Soc. 357, (1962)

Bennett, M.J. and Mason, R. Proc. Chem. Soc. 273, (1963)

Bethe, H. Ann. Phys. 3 , 133, (1929)

Bishop, E.O., Down, J.L., Emtage, P.R., Richards, R.E. and Wilkinson, G. J. Chem. Soc. 2484, (1959)

Boston, J.L., Sharp, D.W.A. and Wilkinson, G. J. Chem. Soc. 3488, (1962)

Bowers, K.D. and Owen, J. Rep. Prog. Phys. 18 , 304, (1955)

Brown, M. (1963) Private communication.

Churchill, M.R. and Mason, R. (I) Proc. Chem. Soc. 112, (1963)

Churchill, M.R. and Mason, R. (II) Proc. Chem. Soc. 365, (1963)

Cooke, A.H., Lazenby, R., McKim, F.R., Owen, J., and Wolf, W.P. Proc. Roy. Soc. A250 , 97, (1959)

Cotton, F.A. J. Amer. Chem. Soc. 80 , 4425, (1958)

Cotton, F.A., Goodgame, D.M.L. and Goodgame, M. J. Amer. Chem. Soc. 83 , 4690, (1961)

Cox, E.G., Cruickshank, D.W.J. and Smith, J.A.S. Nature 175 , 766, (1955)

Craig, D.P., Heffernan, M.L., Mason, R. and Paddock, N.L. J. Chem. Soc. 1376, (1961)

Curry, N.A. and Runciman, W.A. Acta Cryst. 12 , 674, (1959)

Dahl, L.F. and Smith, D.L. J. Amer. Chem. Soc. 83 , 752, (1961)

Dahl, L.F. and Wei, C.H. Inorg. Chem. 2 , 713, (1963)

Dickens, B. and Lipscomb, W.N. J. Chem. Phys. 37 , 2084, (1962)

Edwards, J., Kington, G.L. and Mason, R. Trans. Farad. Soc. 56 , 660, (1960)

Figgis, B.N. Trans. Farad. Soc. 56 , 1553 (3 papers) (1960)

Figgis, B.N. and Nyholm, R.S. J. Chem. Soc. 331, (1959)

Figgis, B.N., Gerloch, M. and Mason, R. Proc. Roy. Soc. (1964) in press.

Figgis, B.N., Gerloch, M. and Mason, R. Acta Cryst. (1963) in press

Fritz, H.P., Hristidu, Y., Hummel, H. and Schneider, R. Z. Naturforsch. 15b, 419, (1959)

Gerloch, M. and Mason, R. Proc. Roy. Soc. (1964) in press

Green, M.L.H., McCleverty, J.A., Pratt, L. and Wilkinson, G. J. Chem. Soc. 4854, (1961)

Green, M.L.H., Pratt, L. and Wilkinson, G. J. Chem. Soc. 3916, (1958)

Griffiths, J.H.E., Owen, J., Park, J.G. and Partridge, M.F. Proc. Roy. Soc. A250 , 84, (1959)

Griffith, J.S. in 'Theory of Transition Metal Ions'. C.U.P. (1961)

Guha, B.C. Proc. Roy. Soc. A206 , 353, (1951)

Harris, J.F., Harder, R.J. and Sausen, G.N. J. Org. Chem. 25 , 633, (1960)

Howard, B.J. J. Chem. Phys. 3 , 813, (1935)

Ibers, J.A. and LaPlaca, S.J. J. Amer. Chem. Soc. 85 , 3501, (1963)

Jackson. L.C. Proc. Roy. Soc. A140 , 695, (1933)

Kamimura, H. Phys. Rev. 128 , 1077, (1960)

Kohn, J.A. and Townes, W.D. Acta Cryst. 14 , 617, (1961)

Krishnan, K.S. and Banerjee, S. Phil. Trans. 234 , 265, (1934)

Krishnan, K.S. and Banerjee, S. Phil. Trans. 235A , 343, (1935)

Krishnan, K.S. and Lonsdale, K. Proc. Roy. Soc. 156 , 597, (1936)

Krishnan, K.S. and Mookherji, A. Phys. Rev. 54 , 533, (1938)

Krishnan, K.S. and Mookherji, A. Phil. Trans. 237 , 135, (1938)

McDonald, T.R.R. Acta Cryst. 9 , 162. (1956)

Miejer, O.H.E. and Gernitsen, H.J. Phys. Rev. 100 , 742, (1955)

Natta, G., Corradini, P. and Bassi, I.W. J. Amer. Chem. Soc. 80 , 755, (1958)

Pauling, L. Phys. Rev. 36 , 430, (1930)

Penney, W.G. and Schlapp, R. Phys. Rev. 41 , 666, (1932)

Porai-Koshits, M.A. Trudy Inst. Krist., Akad. Nauk. U.S.S.R. 10 , 117, (1954)

Powell, H.M. and Wells, A.F. J. Chem. Soc. 359, (1935)

Randic, M. J. Chem. Phys. 36 , 2094, (1962)

Ristau, Ruckraul and Shoffa J.E.T.P. 7 , 64, (1958)

Sparks, R.A. 'Computing Methods in X-ray Crystal Analysis' 4 , 170, (1961)

Stephenson, C.C. and Morrow, J.C. J. Amer. Chem. Soc. 77 , 275, (1955)

Stevens, R.M., Kern, C.W. and Lipscomb, W.N. J. Chem. Phys. 37 , 279, (1962)

Sutor, J. Acta Crystal. 16 , 97, (1963)

Tanabe, Y. and Sugamo, S. J. Phys. Soc. Japan, 13 , 880 (1958)

Van Vleck, J.H. Disc. Farad. Soc. 26 , 96, (1958)

Zdhanov, G.S. and Zvonkova, K.V. Zhur. fiz. khim. 24 , 1339, (1950)

* * *